US Belle II Project
Technical Design Report

Principal Investigators:

D. M. Asner[†], J. E. Fast, J. C. Hall, M. Schram, G. Tatishvili, L. S. Wood
Pacific Northwest National Laboratory, Richland, Washington 99352

R. A. Briere
Carnegie Mellon University, Pittsburgh, Pennsylvania 15213

K. Kinoshita, A. J. Schwartz
University of Cincinnati, Cincinnati, Ohio 45221-0011

T. E. Browder, K. Nishimura[‡], S. E. Vahsen, G. Varner
University of Hawaii, Honolulu, Hawaii 96822

A. Vossen
Indiana University, Bloomington, Indiana 47408

D. Joffe
Kennesaw State University, Kennesaw, Georgia 30144

T. K. Pedlar
Luther College, Decorah, Iowa 52101

L. Cremaldi, R. Kroeger, D. Summers
University of Mississippi, University, Mississippi 38677

I. Danko, V. Savinov
University of Pittsburgh, Pittsburgh, Pennsylvania 15260

R. Godang, M. Jenkins
University of South Alabama, Mobile, Alabama 36688

M. V. Purohit, C. Rosenfeld
University of South Carolina, Columbia, South Carolina 29208

L. Piilonen
Virginia Polytechnic Institute and State University, Blacksburg, Virginia 24061-0435

G. Bonvicini, D. Cinabro
Wayne State University, Detroit, Michigan 48202

December 1, 2013

[†]Contact:david.asner@pnnl.gov
[‡]Current position at SLAC

1 Executive Summary

1.1 Introduction

Since the end of operations of the B-factory at SLAC in 2008, the U.S. does not have a facility capable of making precision measurements of the properties of B meson and other heavy quarks and leptons. Precision measurements are part of the Intensity Frontier of the particle physics road map developed by the Particle Physics Project Prioritization Panel (P5), a subpanel of the High Energy Physics Advisory Panel. The P5 roadmap points out that at the Intensity Frontier scientific opportunities exist in the measurement of rare process to indirectly probe for scientific discoveries at and beyond the energy range of the Large Hadron Collider (LHC). A new detector at a next generation B-factory could resolve puzzles discovered by the previous generation of experiments, discriminate among new physics identified at the LHC, or even discover evidence for new phenomena inaccessible to the LHC. There are two planned facilities, one in Italy and another in Japan, to pursue this research.

The US Department of Energy, Office of Science, Office of High Energy Physics (HEP) has issued a Mission Need Statement, "Mission Need Statement for a Next Generation B Factory Detector Systems." In that Mission Need Statement two possible development paths are called out. Option A is the upgrade of the current Belle detector at KEK in Tsukuba, Japan. Option B is joining the SuperB effort in Italy.

Option A - *following the KEK roadmap, the KEKB accelerator will be upgraded in 3-4 years to reach an initial target luminosity of* $8 \times 10^{35} cm^{-2} s^{-1}$ *(about 10x the current data rate of the current accelerator complex). The US participated in the present detector and in the subsequent data analysis. The US would continue its participation by taking key roles in the upgrade of the present Belle detector to match the planned upgrade in accelerator capabilities.*

Option B - *SuperB is the initiative by the Italian HEP community and its national labs to build a high luminosity B factory and associated detector. The US would contribute components and expertise for the construction of a new dedicated detector. The possibility also exists to contribute existing SLAC accelerator components and expertise at minimal to no expense to the US program and possibly modest contributions of some new components. In fact the reuse of these components will save on the cost of disposing of them.*

Option A, the US Belle II, was selected with approval of CD-1 on September 18, 2012.

1.2 Science Case

A next-generation B-factory will complement the exploration of New Physics beyond the Standard Model currently being carried out at the energy frontier by the experiments at the LHC. These energy frontier experiments provide a direct probe of the TeV mass scale, whereas high-precision measurements of rare decays and CP violation in heavy quarks and leptons provide a unique probe of new physics at these and even higher mass scales through the effects of new particles in higher order processes. The nature of the effects observed in

these high precision measurements are complementary to the direct searches at the energy frontier and can provide important insights into the specific nature of the New Physics that is anticipated to be observed at the LHC.

1.3 Technical Performance

The US Belle II Project is subsidiary to the Japanese-led Belle II detector upgrade. The Belle II upgrade will replace the inner tracking systems and particle identification (PID) systems of the existing Belle detector as well as the endcap and inner layers of the barrel K_L/muon systems (KLM). The US Belle II Project scope is to provide elements of the barrel PID system, an imaging Time of Propagation (iTOP) detector, and barrel KLM systems and electronics for these systems as well as for the endcap KLM replacement system that will be provided by other collaborators. In addition, the US will provide components for the SuperKEKB commissioning detector that will be used to evaluate beam background around the interaction point concurrently with the roll-in of the Belle II detector. The Japanese are responsible for final system integration and, while the US groups anticipate a significant role in this phase of the Belle II upgrade, this is not part of the scope of the US Belle II Project. The completion criteria for the US Belle II Level 2 elements are described in the US Belle II Project Execution Plan.

1.4 Cost and Schedule

The Total Project Cost is currently estimated at $15.00 million with $12.81M base and $2.19M contingency. The project duration is expected to be three years and will largely be executed over a two year period to meet the overall Belle II upgrade schedule requirements.

1.5 Acquisition Strategy

The contractor for acquisition of US Belle II will be the Pacific Northwest National Laboratory operated by Battelle for the US Department of Energy under contract DE-AC05-76RL01830. Details may be found in the Acquisition Strategy for the US Belle II project.

2 Acronym List

ADR	Advanced detector research
ALD	Atomic layer deposition
ANITA	Antarctic Impulsive Transient Antenna experiment
ANL	Argonne National Laboratory
APD	Avalanche photodiode
ASIC	Application-specific integrated circuit
BEAST	Belle commissioning detector
BGO	Bismuth germanate
BLAB	Buffered LABRADOR
CDC	Central drift chamber
CERN	European Organization for Nuclear Research
CESR	Cornell Electron Storage Ring
CFD	Constant fraction discriminator
CKM	Cabbibo-Kobayashi-Maskawa (parameters)
CLEO	High energy physics experiment at CESR
CMM	Coordinate measurement machines
CMS	Compact muon solenoid (CERN experiment)
COPPER	COmmon Pipelined Platform for Electronics Readout
CP	Charge parity
DAQ	Data acquisition
DEPFET	Depleted field effect transistor
DIRC	Detection of Internally Reflected Čerenkov light (PID detector for Babar experiment)
DOE	US Department of Energy
ECL	Electromagnetic calorimeter
EM	Electromagnetic
ES&H	Environmental Safety and Health (PNNL program)
FCNC	Flavor-changing neutral currents
FEB	Front-end Board
FEE	Front-end (readout) electronics
FINESSE	Front-end Instrumentation Entity for Sub-detector Specific Electronics
FNAL	Fermi National Accelerator Laboratory
FPGA	Field-programmable gate array
FTE	Full-time equivalent
FTSW	Trigger/Timing distribution board
GAPD	Geiger mode avalanche photo-diode
GSIM	GEANT-3-based Monte Carlo simulation

HEP	High Energy Physics
HER	High-energy ring
HSLB	High Speed Link Board
ILC	International Linear Collider
INGRID	Interactive Neutrino GRID detector
IP	Interaction Point
IRS	iTOP Readout ASIC
IRS3B	The 3B version of the IRS ASIC
ISM	Integrated Safety Management (PNNL program)
ITEP	Institute for Theoretical and Experimental Physics (Moscow, Russia)
iTOP	Imaging time of propagation
KEK	High energy physics laboratory, Tsukuba, Japan
KLM	K_L/muon detector
KM	Kobayashi and Maskawa
LABRADOR	Large Analog Bandwidth Recorder and Digitizer with Ordered Readout ASIC
LAPPD	Large Area Picosecond Photo Detector
LER	Low-energy ring
LHC	Large Hadron Collider
MAPMT	Mult-anode PMT
M&O	Management & Operations
MC	Monte Carlo (simulation)
MCP	Micro-channel plate
Micro-TPC	Micro time projection chamber
MIE	Major item of equipment
MoU	Memorandum of understanding
MPPC	Multi-pixel photon counter
NEPA	National Environmental Policy Act (of the US DOE)
NICADD	Northern Illinois Center for Accelerator and Detector Development
NSF	National Science Foundation
NTUHEP Group	National Taiwan University High Energy Physics Group
P5	Particle Physics Project Prioritization Panel
PCB	Printed circuit board
PDF	Probablility density function
PEP-II	Electron-positron collider at SLAC
PID	Particle identification
PMT	Photo-multiplier tube

PNNL	Pacific Northwest National Laboratory
PNSO	DOE's Pacific Northwest Site Office
POPOP	1,4-bis(5-Phenyloxazole-2-yl)benzene
PPEP	Preliminary Project Execution Plan
PPO	2,5-biphenyloxazole
PQAP	Project-Specific Quality Assurance Program (PNNL program)
PXD	Pixel detector
QA	Quality Assurance
QCS	Final focus quadrupole magnet
R&D	Research and development
RF	Radio frequency
RFI	Request for information
RFP	Request for proposal
RICH	Ring imaging cherenkov (detector)
RPC	Resistive plate counters
SalSA	Saltdome Shower Array (astroparticle physics neutrino detector)
SC	US Department of Energy's Office of Science
SLAC	Stanford Linear Accelerator Laboratory
SNR	Signal-to-noise ratio
SOW	Statement of work
SRM	Subdetector readout modules
STUD	SalSA transient UHF digitizer
SVD	Silicon vertex detector
TARGET	KLM Readout ASIC
TDC	Time to digital converter
TOF	Time-of-flight
TOP	Time-of-propagation
TPC	Total project cost
TPC	Time projection chamber
TTS	Transit time spread
UHF	Ultra-high frequency
US	United States
WBS	Work breakdown structure
WLS	Wavelength shifting fiber

Contents

1 Executive Summary **i**

1.1 Introduction i

1.2 Science Case i

1.3 Technical Performance ii

1.4 Cost and Schedule ii

1.5 Acquisition Strategy ii

2 Acronym List **iii**

3 US Belle II Project Overview **1**

3.1 Introduction 1

3.2 Goals and mission 2

3.3 Connection to full Belle II SuperKEKB upgrade 2

3.4 Analysis of Alternatives 4

3.5 Project Schedule 5

3.6 Cost Estimate 6

3.7 Funding Requirements 6

3.7.1 Participating Institutions and US-Japan Contributions 6

3.8 Risk Assessment and Mitigation 7

3.9 Acquisition Strategy 9

4 Science Case **9**

5 Technical Description **12**

5.1 Imaging Time-of-Propagation Detector 13

5.1.1 US Role in the iTOP Detector 13

5.1.2 iTOP Detector Motivation 13

5.1.3 iTOP Detector Description - US Contributions 13

5.1.4 Quartz Acceptance Testing Plans 15

5.1.5 Expected performance 17

5.1.6 Beam Test Results 22

5.1.7 Beam-related Backgrounds 30
5.1.8 US Belle II Project Scope for the iTOP 34
5.2 Readout Systems for the Belle II Upgrade 34
5.2.1 Fast Timing with Waveform Sampling 34
5.2.2 US Role in Belle II Readout Systems 35
5.2.3 US Belle II Project scope for the Readout Systems 44
5.3 Upgrade of the K_L/muon System 44
5.3.1 US Role in the KLM System Upgrade 44
5.3.2 RPC Performance Limitation 45
5.3.3 KLM Upgrade Strategy 46
5.3.4 Barrel KLM Modules 48
5.3.5 Scintillator extrusions 49
5.3.6 Wavelength-shifting fibers 52
5.3.7 Photosensors 55
5.3.8 Module assembly 56
5.3.9 Pre- and post-shipment tests 59
5.3.10 US Belle II Project scope for the Barrel KLM Upgrade 60
5.4 SuperKEKB Commissioning Detector 60
5.4.1 US Role in a Background Commissioning Detector 60
5.4.2 Commissioning Detector Motivation 61
5.4.3 KEKB Commissioning Experience 61
5.4.4 SuperKEKB Commissioning Plan 62
5.4.5 Beam Background Sources at SuperKEKB 65
5.4.6 Planned Measurements During SuperKEKB Commissioning 68
5.4.7 Commissioning Detector Description and US Contributions 68
5.4.8 Commissioning Detector Design Overview 69
5.4.9 Commissioning Detector Dose Monitor 71
5.4.10 Commissioning Detector micro-TPCs 73
5.4.11 Commissioning Detector Description - Non-US Contributions 79
5.4.12 US Belle II Project scope for the Commissioning Detector 79

6 Environment, Safety, and Health **80**

7 Quality Assurance and Quality Control **81**

A Quartz Specifications **85**

A.1 Overview 85

A.2 Material 85

A.3 Bar Specifications 85

A.4 Prisms Specifications 87

A.5 Mirror Specifications 88

B Quartz Acceptance Test Plan **94**

B.1 Overview 94

B.2 Acceptance Testing at the Manufacturers 94

B.3 Testing Bars at KEK 95

B.3.1 Chip inspection 95

B.3.2 Bulk transmittance and surface reflectivity 96

B.3.3 Other tests: optical interfaces after gluing 97

B.3.4 Testing and assembly schedule 98

B.4 Testing Mirrors at Cincinnati 98

B.4.1 Transmittance and reflectance 99

B.4.2 Focal length (radius of curvature) 100

B.5 Testing Prisms at Cincinnati 100

B.5.1 Transmittance 102

B.5.2 Angle of tilted face 102

B.6 Battelles Quality Assurance Requirements 103

B.6.1 Source Inspection (cl QA-178 – May 2003) 103

B.6.2 Certificate of Conformance (cl QA-180 - April 2011) 103

B.6.3 Test Report: Inspection Data (cl QA-191 – April 2008) 104

B.6.4 Contractor Nonconformance Report (cl 360 – May 2009) 104

C KLM Technical Drawings **105**

D SuperKEKB Commissioning Detector **108**

D.1 VXD Group Plans and Requirements 108

D.1.1 Introduction 108

D.1.2 VXD proposal for BEAST II 109

D.1.3 BEAST II PXD 112

D.2 Commissioning Detector Luminosity Monitoring Device 112

D.3 micro-TPC Simulation & Design Optimization 115

D.3.1 Simulation framework 120

D.3.2 Design optimization 122

D.3.3 Rates and Detection efficiency 135

D.4 Older Simulation Studies 141

D.4.1 Beam Background Dose Estimates 141

D.4.2 Commissioning Detector: Neutron Simulations 141

D.4.3 Commissioning Detector: Micro-TPC Simulations 141

E WBS Dictionary **152**

3 US Belle II Project Overview

3.1 Introduction

The mission of the Department of Energy (DOE) Office of Science (SC) is to advance basic research and the instruments of science that are the foundations for DOE's applied missions, a base for U.S. technology innovation, and a source for remarkable insights into our physical and biological world and the nature of matter and energy. Within SC, the High Energy Physics mission includes understanding how our universe works at its most fundamental level. This is done by discovering the most elementary constituents of matter and energy, exploring the basic nature of space and time itself, and probing the interactions between them. These fundamental ideas are at the heart of physics and hence all of the physical sciences. To enable these discoveries, HEP supports theoretical and experimental research in both elementary particle physics and fundamental accelerator science and technology.

The Belle II experiment is part of a broad-based search for new physics. The LHC, which is now operating with high luminosity at a center of mass energy of 7 TeV, is designed to search for new physics at the *energy* frontier. Its high center-of-mass energy may allow it to produce heavy, as-yet-undiscovered particles such as Higgs bosons and supersymmetric partners of quarks and leptons or new particles linked to extra dimensions. The SuperKEKB/Belle II facility searches for new physics by colliding very high *intensity* particle beams, i.e., by precisely measuring and comparing with theory a number of observables that are difficult or unfeasible to measure at the energy frontier. In the past, measurements of processes involving internal loops have given access to high mass scales before accelerators were available to directly probe these scales. To continue this paradigm-shifting pursuit of flavor physics, about two orders of magnitude more data is now needed.

The Mission Need Statement for the Next Generation B Factory Detector Systems was signed by John Kogut, Program Manager, Office of High Energy Physics on July 8, 2011, Frederick Borcherding, Program Manager, Office of High Energy Physics on July 8, 2011, Daniel Lehman, Director, Office of Project Assessment on July 10, 2011, and Michael Procario, Acting Associate Director, Office of High Energy Physics, Office of Science, Department of Energy on July 28, 2011; and Critical Decision 0 (CD-0) was approved on August 29, 2011. Critical Decision 1 (CD-1), Approve Alternative Selection and Cost Range for the US Belle II Project was approved by James Siegrist, Associate Director, Office of High Energy Physics, Office of Science, Department of Energy on September 18, 2012. In addition, CD-3A Approval for Start of Long Lead Procurements, was approved by James Siegrist, Associate Director, Office of High Energy Physics, Office of Science, Department of Energy on November 8, 2012, authorizing procurements for the KLM system.

The US Belle II Project will provide essential systems for the Belle II detector upgrade being carried out at the KEK laboratory in Tsukuba, Japan. The upgrade of the Belle detector and the KEKB accelerator to Belle II and SuperKEKB are being managed by the KEK laboratory with significant contributions to the Belle II detector being provided by international collaborators. The US Belle II contributions will be in the particle identification

systems ($K^{\pm}, \pi^{\pm}, K_L, \mu$), electronics for these systems, and a commissioning detector system. These systems have been selected based on impact to the Belle II physics program, prior US contributions to the original Belle detector, and the expertise and capabilities of the US collaborating institutions.

3.2 Goals and mission

The goal of the US Belle II Project is to provide detector systems to the Belle II/SuperKEKB physics program that are commensurate in scope and cost with the US participation in Belle II and that will provide high impact towards accomplishing the physics goals of the experiment. The US groups are currently about 12% of the Belle II collaboration and are anticipated to continue to grow to become ∼15% of the Belle II collaboration by the start of operations in 2015. The US groups have identified the particle identification systems and related advanced electronics systems as the critical Belle II detector systems that deliver high impact to the physics, are of appropriate scale for the US contribution, and are aligned with previous US involvement and the expertise of the US groups.

Good separation between pions and kaons has proven crucial for studying rare B decays in which backgrounds from other processes can mask the signal. For example, the process $B^0 \to \rho^0\gamma$, with a branching fraction of 8×10^{-7}, can be easily overwhelmed by background from the process $B^0 \to K^{*0}\gamma$, which has a branching of 4×10^{-5} (50 times larger). Without good kaon rejection, identifying the $B^0 \to \rho^0\gamma$ signal would be unfeasible. Efficient muon identification is required for the precision determination of the quark mixing matrix and for searching for new phenomena with lepton number and lepton flavor violating processes.

In addition, the US groups will contribute to the commissioning detector which will be installed inside the outer detector systems of Belle II to evaluate the radiation and beam backgrounds from the accelerator as it is commissioned. The US groups provided the original "BEAST" system used during commissioning of KEKB prior to the installation of the Belle inner detectors. This is a critical system that serves the dual purpose of shielding the calorimeter while measuring backgrounds from the accelerator during commissioning. The safety of the inner detectors during Belle II operation depends upon the understanding of backgrounds from the accelerator.

3.3 Connection to full Belle II SuperKEKB upgrade

An elevation view of the Belle II detector is shown in the upper half of Fig. 1. For comparison, the current Belle detector is shown in the lower half. The new detector will re-use many of the existing Belle components. However, the high luminosity will be accompanied by much higher occupancy and radiation levels than those in the present Belle detector, and new detector components will be built to address this. The new detector is designed to be able to handle backgrounds 20 times higher than those in Belle while giving improved performance.

For inner vertexing, pixels based on depleted field effect transistors (DEPFETs) will be

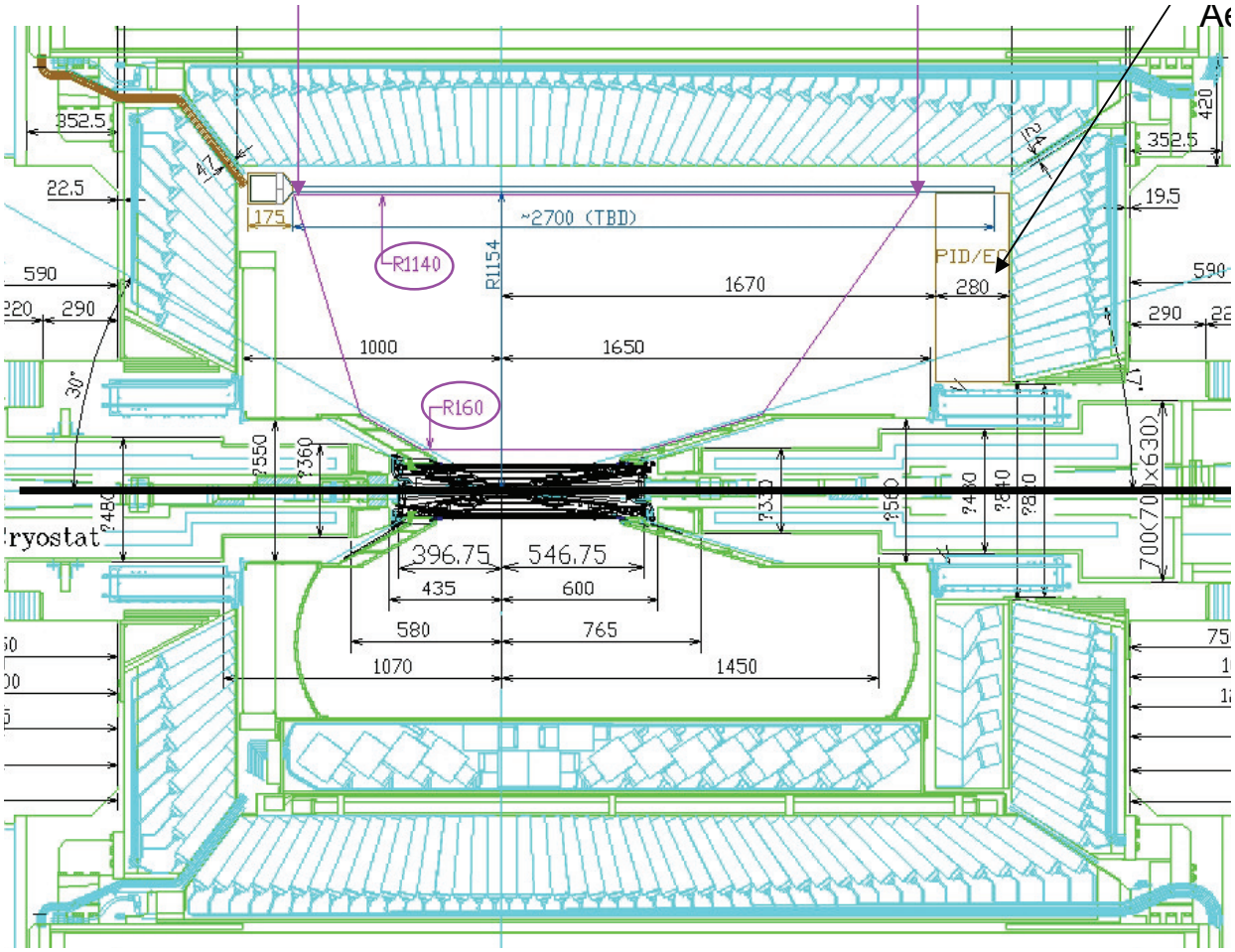

Figure 1: *Two-dimensional CAD drawing showing the proposed Belle II detector in the upper half and the original Belle detector in the lower half.*

used. These devices, which were originally developed for inner vertexing at the ILC, will be adapted to SuperKEKB factory conditions. In test beams these devices achieved intrinsic resolutions of $\sim 2\mu m$. Assuming 22.5μm $\times$22.5μm pixels with a 10μs integration time, the expected occupancy will be $\sim$0.5% at SuperKEKB.

The pixels will be followed by a silicon strip tracker with four layers that extend out to r $\sim$16 cm. Since the current occupancy from beam background in the innermost silicon layer is $\sim$10%, the new silicon strips require a new high speed pipelined readout chip. They will use a readout based on the APV25 chip originally developed for the CMS experiment at the LHC. A new drift chamber with smaller cells using a helium-based gas mixture will extend from the silicon tracker to the barrel particle ID.

Excellent particle identification is needed to distinguish kaons and pions in the 1-4 GeV momentum range with high efficiency and resolution. This will by achieved in the barrel

region by measuring internally reflected Čerenkov light radiated in quartz bars, and in the forward endcap region by an aerogel RICH (Ring Imaging CHerenkov) detector. The barrel detector is similar to the BaBar DIRC (Detection of Internally Reflected Cherenkov light) detector but will have three notable improvements: *(a)* it precisely measures the propogation time of photons; *(b)* it employs a spherical mirror to focus parallel photons (thus reducing smearing from the bar thickness); and *(c)* it uses micro-channel-plate phototubes with fine segmentation to measure photon hit positions with very good x and y position resolution. Because the photon time measurement plays an important role, this type of detector is referred to as a "time-of-propagation" (TOP) or "imaging time-of-propagation" (iTOP) counter.

The CsI(Tl) crystals of the electromagnetic calorimeter will be re-used. However, the readout electronics will be replaced with pipelined waveform sampling. The forward endcap crystals will also use improved electronics. Extensive tests of the new waveform sampling electronics as well as pure CsI crystals have been done.

The barrel K_L/muon system will be modified to run with scintillators in the innermost layers and improved electronics for all resistive plate counters (RPC) layers. In the endcap region, scintillator-based counters will handle the high background rates. The light from the scintillation strips will be collected by embedded wavelength-shifting fibers and read out by Geiger mode avalanche photo-diodes (GAPDs). Fast waveform sampling electronics similar to that used for the iTOP will also be used for the K_L/muon system.

All readout electronics will be pipelined. A new high speed DAQ has been designed. The computing demands will be comparable to LHC experiments and will require extensive use of Grid and Cloud computing.

3.4 Analysis of Alternatives

The alternatives for the Next Generation B Factory Detector Systems were reviewed at the Comparative Review of Intensity Frontier Projects August 10-12, 2010. The review panel report strongly endorsed the Belle II at SuperKEKB proposal. This merit panel pointed out that the Belle II proposal is an upgrade to an existing facility with little civil construction involved; and KEK has a strong track-record of delivering accelerator projects on schedule. In addition, the upgrade is underway, with the majority of the funding already approved by the Japanese government. The commitment of the Japanese government to the project has been reinforced by the approval of significant additional funding in Japan Fiscal Year (JFY) 2012 that was authorized after the March 2011 earthquake and Tsunami. The panel also pointed out that historically there has been strong US participation in the Belle program.

"The SuperKEKB proponents also have a very strong history of producing interesting and important physics results on the Belle experiment. For more than a decade, these groups have been playing a key role in the Belle experiment."

Further, the reviewers found the Belle II proposal to be very cost-effective and a "good value" for the investment.

Within the US Belle II Project, several alternatives covering a broad range of scope and cost have been considered. These alternatives are constrained by existing commitments by other Belle II collaborating institutions and the need to have the US funding availability matched to the detector system schedule and required delivery to meet the overall Belle II Upgrade schedule. A low-cost option (∼$5M) was considered, but the scope in this option was marginal in terms of physics impact (partial delivery of the PID system, for instance) and there is no clear funding mechanism within the greater Belle II upgrade project to deliver the remaining scope required to complete the systems that would be only partially furnished by the US in this option. At the other end of the spectrum, a >$20M option was considered that would replace the entire barrel K_L/muon system, including the endcap K_L/muon system scintillator replacement, and the scope presented in this Conceptual Design Report. The replacement of the other layers of the barrel K_L/muon system, while providing an additional margin of safety against radiation damage and background rate limitations, was not found to be compelling at this time based on estimates of lifetime from the existing Belle endcap systems (which have experienced significant radiation dose over their lifetimes) and the anticipated backgrounds that are expected to be dominated by Touschek (intra-bunch) scattering. The schedule for the endcap K_L/muon system replacement was not compatible with the funding authorization process in the US and that scope was moved to Russian collaborators.

3.5 Project Schedule

Below is shown the preliminary schedule for Critical Decisions for the US Belle II Project. Following the methodology outlined by DOE Order 413.3B, a tailored and phased approach has been applied to the US Belle II schedule. Because the US Belle II design is well advanced, critical decisions CD-2 and CD-3 will be combined.

Table 1: Preliminary Schedule for US Belle II Project

Critical Decision	Description	Estimated Approval Dates
CD-0	Mission Need Approval	Aug 2011 (actual)
CD-1	Preliminary Baseline Range Approval	Sep 2012 (actual)
CD-3A	Long Lead Procurement Approval (KLM Modules)	Nov 2012 (actual)
CD-2/3	Performance Baseline and Start of Construction Approval	Mar 2014
CD-4	Project Completion	Jun 2016

3.6 Cost Estimate

The US Belle II Project is a Major Item of Equipment (MIE). The Total Project Cost is $15.00 million with $12.81M base and $2.19M contingency. The Total Project Cost, broken down to level 2 WBS elements as shown in Table 2 below, includes design, hardware procurement, project management, safety and health, quality assurance, assembly of subsystem elements, delivery of subsystems to KEK, and acceptance testing. This is the baseline cost being requested for approval at CD-2.

Table 2: Project cost estimate at WBS level 2.

WBS	Description	Cost Estimate (M$)
1.1	Project Integration and Support	1.39
1.2	Imaging Time-of-Propogation Optics	7.63
1.3	Readout Systems	3.20
1.4	KLM Systems	0.19
1.5	Commissioning Detectors	0.40
	Contingency	2.19
	US Belle II Total Project Costs	**15.00** (including contingency)

3.7 Funding Requirements

A three year construction schedule is proposed for the US Belle II Project so that delivery of the detector systems is matched to the overall Belle II schedule being managed by the Belle II Project Manager at KEK. In order to meet this schedule, the funds will need to be made available predominantly over the first two years of the project. Table 3 presents the funding profile with contingency.

Table 3: Projected US Belle II Funding Profile (M$) including contingency

	FY12	FY13	FY14	FY15
Total Project Costs	0.65	5.00	6.00	2.35

3.7.1 Participating Institutions and US-Japan Contributions

A number of US institutions, members of the Belle II Collaboration, are responsible for the deliverables of the scope of the US Belle II Project. These US institutes have expertise

Detector System	US Institute(s)
iTOP (Optics)	Cincinnati, Hawaii, Luther, PNNL*
Readout Systems	Hawaii*, Indiana, PNNL, Pittsburgh, South Carolina, VPI, Wayne State
Barrel K_L/Muon System	South Alabama, VPI*
Commissioning Detector	Hawaii*, PNNL, Wayne State

Table 4: Contributions of US institutions to Belle II. Lead US institution is indicated by *.

and past experience in designing, constructing and delivering subsystems used in previous HEP experiments, including Belle. All of the institutes discussed here have provided written expressions of interest in contributing in specific areas of the US Belle II Project. Scientific, engineering and technical staff at these institutes will contribute to the development, design, test, and assembly of the US Belle II detector systems. The institutes have identified the numbers of full-time-equivalents (FTEs) in these categories to be made available to the project over time. All participating US Belle II institutions and their proposed contributions are listed in Table 4.

The responsibilities of US Belle II Collaborators are specified in comprehensive US Belle II Memoranda of Understanding (MoU). A multi-year MoU details the work that the Collaborator has agreed to do for the Project, and includes a list of the personnel involved and the significant milestones. In addition to the MoUs, those groups that receive DOE Project funding will do so via subcontracts from Pacific Northwest National Laboratory (PNNL). These subcontracts will have fixed periods of performance, typically one year, with clearly defined scope and resource requirements defined in a Statement of Work (SOW).

3.8 Risk Assessment and Mitigation

Proactively managing risks is an integral component of the US Belle II Project. Risk management is an ongoing activity and will be performed throughout the lifecycle of the project. The detailed project Risk Management Plan can be found in the Project Execution Plan. This section briefly describes the project's enabling assumptions and major categories of risk and presents general actions and strategies for mitigation

Project Funding Enabling Assumptions: Project execution relies on contributions from a number of sources, including via the US-Japan (Nichibei) mechanism and collaborating institution grants from DOE and National Science Foundation (NSF). All of the anticipated US-Japan funding was received in JFY11 and JFY12, retiring that important cost risk. However, risk remains associated with assumptions about availabale manpower funded by institutional grants. Since the impact of this categories of risk would be devastating to the project (in terms of delay and reduction of scope) and is beyond the control of the project manager, these risks are treated as enabling assumptions. Enabling assumptions are risks so large, no action can mitigate the consequence if the risk were to occur.

Cost and Schedule Risks: Use of fixed-price subcontracts and competition will be maximized to reduce cost risk. Schedule risk will be minimized via: realistic planning, verification of subcontractor's credit and capacity during evaluation, close surveillance of subcontractor performance, advance expediting, and incremental awards to multiple subcontractors when necessary to assure total quantity or required delivery. Quartz vendor capability and capacity was an identified risk and significant difficulties have been encountered with vendor delivery, particularly for quartz bars. In response, additional vendors with much higher capacity have been evaluated through significant prototyping activities.

Technology and Engineering Risks: Preparation of clear and concise specifications, judicious determination of subcontractor responsibility and approval of proposed lower tier sub-subcontractors, and implementation of Quality Assurance (QA) provisions will minimize technical risk. The project further minimizes technical risk by exploiting previous experience to the greatest extent possible, and minimizing exposure to single vendor failures. For example, multiple fused silica optics vendors have been identified and prototype optics procured from multiple vendors during the research and development (R&D) phase to develop capability at multiple vendors.

Project Interface Risks: The US Project deliverables must integrate with the full Belle II upgrade at KEK, the constraints of which are well understood. The responsibility for integration into Belle II rests with KEK. The scope of this project has been defined narrowly to reduce project risk due to technical difficulties experienced by non-US contributions. The risk that US elements do not readily integrate with the rest of the systems is mitigated by bi-weekly meetings of the sub-detector groups within Belle and strong US participation (including the Project Manager, Chief Scientist and Level 2 managers of the US Belle II Project) at the three annual Belle II collaborations meetings that are largely focused on the detector upgrade. Additionally, the senior US technical contributors are both Level 2 managers in the US Belle II Project and co-conveners of the corresponding international technical groups within Belle II as a whole. For the KLM system, the new elements from the US are replacing ones made by the same US group for the original Belle experiment so there is institutional knowledge of all interface issues.

Collaborator Resource Availability and Accountability Risks: The project is reliant on technical contributions from the US university collaborators on Belle II. These resources are being defined by MOUs between the project and collaborating institutions. These contributed resources have played a significant role during the conceptual design phase and there is low to moderate risk that these resources will not continue to be available during the remaining phases of the project. However the Belle II project management team believes that it is prudent to carry additional cost contingency to cover scope that may not be performed as planned under the contributed resource scope. Additionally, this risk is being mitigated by reducing the scope of key overburdened project participants.

Contracting Risks: The project will require many contracts to be executed in a timely manner. These contracts will include large procurements, sole-source procurements, contracts with universities and smaller purchases. To mitigate risks associated with procurements the project has a dedicated procurement officer and two contracts specialists have been

assigned to process all of the project requisitions. Other mitigations include conducting Request For Information (RFI) and Request for Proposal (RFP) processes ahead of funding authorization to reduce time from available funding to letting of contract, and contracts with options to allow for single RFP processes for procurements that span multiple funding allotments.

3.9 Acquisition Strategy

The DOE Pacific Northwest Site Office (PNSO) will implement the US Belle II Project under the existing Management & Operations (M&O) contract (DE-AC05-76RL01830) at the Pacific Northwest National Laboratory (PNNL). The Federal Project Director residing in the Pacific Northwest Site Office will have the ultimate responsibility to successfully execute the project. Details may be found in the Acquisition Strategy for the US Belle II project.

4 Science Case

Research in flavor physics is an essential component of the future US program in particle physics. This document discusses US participation in Belle II, a Super B factory flavor experiment to be based in Japan at the upgraded KEKB accelerator. The design luminosity of SuperKEKB is $0.8 \times 10^{36}\,\mathrm{cm}^{-2}\mathrm{s}^{-1}$[1], approximately fourty times higher than what has been achieved at the KEKB accelerator. This will allow a data sample with an integrated luminosity of 50 ab^{-1} to be accumulated. This can be compared to the 1 ab^{-1} data sample obtained over a decade of Belle running with KEKB.

Belle, together with BaBar, established the existence of large charge-parity (CP) violation (e.g., matter-antimatter asymmetry) in the b quark system in agreement with the expectation of Kobayashi and Maskawa (KM). In contrast to the kaon system (strange quarks), the observed CP violation effects for b quarks are of order one rather than 10^{-3}. This critical experimental contribution of the B factories was explicitly recognized in the 2008 Nobel Prize in Physics citation.

The B factory results show most of standard model CP violation can be explained by the single irreducible complex KM phase in the weak interaction coupling. Nevertheless, the possibility of contributions from new physics that are O(10%) of the size of the standard model contribution are not ruled out. Moreover, the matter-antimatter asymmetry of the universe cannot be explained by the KM phase alone. The standard model KM explanation of the baryon asymmetry of the universe falls short by ten orders of magnitude. This demonstrates that there must be new sources of CP violation and new heavy particles, which remain to be discovered.

The Belle II experiment is part of a broad-based search for new physics. The LHC, which is now operating with high luminosity at a center of mass energy of 7 TeV, is designed to search for new physics at the *energy* frontier, i.e., its high center-of-mass energy may

allow it to produce heavy, as-yet-undiscovered particles such as Higgs bosons and supersymmetric partners of quarks and leptons or new particles linked to extra dimensions. The SuperKEKB/Belle II facility searches for new physics using the very high luminosity of the *Intensity* frontier, i.e., by precisely measuring and comparing with theory branching fractions, angular distributions, CP asymmetries, forward-backward asymmetries, and a host of other observables that are difficult or infeasible to measure at the LHC.

At the LHC and in the future at the International Linear Collider (ILC), the particles that are responsible for the electroweak force in the Standard Model will be studied in detail. These include the W, Z^0 and the recently discovered Higgs boson. In the upcoming round of neutrino and muon experiments properties of leptons will be explored; there will be improved measurements of neutrino mixing angles and a determination of whether future neutrino CP violation experiments are feasible. However, these experiments will not explore the new physics possibilities of the flavor and heavy quark sector that will be studied at SuperKEKB/Belle II.

In the past, measurements of processes involving internal loops have given access to high mass scales before accelerators were available to directly probe these scales. For example, the suppression of $K_L \to \mu^+\mu^-$ decays allowed theorists to infer the existence of the charm quark; the charm quark mass was subsequently estimated from the observed rate of K^0-$\overline{K}^0$ oscillations. The unexpected observation of CP violation in K^0 meson decays was used to predict the existence of a third generation of quarks. The unexpected discovery of large B^0-$\overline{B}^0$ oscillations indicated that the top quark was very heavy, contrary to the theoretical prejudice at the time (and contrary to where experiments were looking). These processes, as well as the violation of CP symmetry, are quantum mechanical phenomena sensitive to very high energy scales and revolutionized thinking about extensions of the Standard Model. To continue this paradigm-shifting pursuit of flavor physics, about two orders of magnitude more data is now needed. Such a data set would reveal whether the CP violation effects observed in B decays are consistent with the Standard Model. Searching for flavor-changing neutral-currents (FCNC) with such a data set would probe a mass range of 1-100 TeV, which is mostly beyond the reach of direct searches at the LHC. If supersymmetry is discovered during future LHC operation at 14 TeV, a Super B Factory could help determine how the supersymmetry was broken [2]. To be more concrete, listed below are several big questions that can only be addressed by further study of loop processes and rare decays at a Super B factory.

Are there new CP violating phases?

Answering this question will require new measurements of time-dependent CP violation in $b \to s$ modes such as $B \to \phi K^0$ and $B \to \eta' K^0$ with a data sample of order 50 ab^{-1}. If there is new physics in $b \to d$ transitions, precise measurements of Cabibbo-Kobayashi-Maskawa (CKM) parameters in mixing and in tree processes will be required. For example, the measurement of $B_d \to J/\psi K_S$ should be consistent with measurements of V_{ub}/V_{cb} and other constraints.

New measurements of B_s properties and perhaps CP-violating asymmetries in B_s decays might be possible with long runs at the $\Upsilon(5S)$. The feasibility of B_s studies at the $\Upsilon(5S)$ has been demonstrated recently by Belle [3], which has recorded a 125 fb^{-1} data sample. Belle II can explore B_s decays with neutral particles or neutrinos in contrast to hadronic experiments.

Are there new operators with quarks enhanced by new physics?

Experimentally, it is important to measure forward-backward asymmetries $A_{FB}(q^2)$ as a function of the q^2 of the dilepton pair in $b \to sl^+l^-$ decays. Although there are now rough measurements of $A_{FB}(q^2)$ using the full statistics of the B factories and LHCb, the zero-crossing point of $A_{FB}(q^2)$ is sensitive to new physics and is an observable that will be accessible at SuperKEKB factory. In particular, measurement of inclusive processes such as $b \to s\ell^+\ell^-$ and the inclusive forward-backward asymmetry are possible only at a Super B factory. (Belle recently reported the first low-statistics measurement of this inclusive observable). Another example of this approach to new physics is measuring the rates and asymmetries in $B \to K\pi$ to a precision that can determine whether or not there are enhanced electroweak penguins [4].

Are there right-handed currents from new physics?

The experimental approach involves measurement of time-dependent CP violation in $B \to K^{*0}\gamma$ ($b \to s\gamma$) or related modes such as $B \to K_S\rho^0\gamma$ or $B \to K_S\phi\gamma$. Note that $B \to K^{*0}\gamma$ involves the reconstruction of the final state $B \to K_S\pi^0\gamma$ and precision vertexing of the pions from the K_S decay. Another interesting approach involves triple-product CP violation asymmetries in $B \to VV$ decays. Data samples with luminosity of order 50 ab^{-1} are required for either approach.

Are there flavor changing neutral currents beyond the Standard Model?

Precise measurements of $B^+ \to \tau\nu$ and $B \to D^{(*)}\tau\nu$ are sensitive to new physics contributions from charged Higgs particles (partners to the standard model neutral Higgs boson). These indirect constraints on charged Higgs mass and couplings are usually more restrictive than those obtained from direct searches at LHC collider experiments.

It is of great interest to measure $b \to s\nu\bar{\nu}$ transitions such as $B \to K^{(*)}\nu\bar{\nu}$. Belle's evidence for $B^+ \to \tau^+\nu$ is the first example of a new class of B decays with large missing energy. Extrapolations from this result indicate that the necessary sensitivity to a rare B mode with the same challenging experimental signature (a single track and missing energy) can be achieved at Belle II.

Are the FCNCs observed in B decays consistent with those in kaon decays? One particularly interesting example is $B \to \rho\gamma$, which is a $b \to d$ radiative penguin. This mode has

been observed at the B factories but detailed comparisons to theory expectations are not yet possible. In general, it is desirable to measure FCNC's with comparable accuracy in $b \to d$, $b \to s$ and $s \to d$ transitions. These will complement measurements of rare kaon modes such as $K^+ \to \pi^+ \nu\bar{\nu}$ and $K_L \to \pi^0 \nu\bar{\nu}$.

Neutrino experiments have found large mixing between the muon-neutrino and the tau-neutrino. This raises the possibility of flavor-changing processes in charged leptons such as $\tau \to \mu\gamma$. Searching for $\tau \to \mu\gamma$ at the $\mathcal{O}(10^{-8})$ level would complement $\mu \to e\gamma$ searches and $\mu \to e$ conversion experiments, as $\tau \to \mu\gamma$ may have different sensitivity to new physics.

In 2007, Belle and BaBar obtained the first evidence for D^0-$\overline{D}^0$ mixing, which had been searched for since the discovery of charm over thirty years earlier. This discovery leads to the question of whether new physics enhances CP violation in the D^0-$\overline{D}^0$ system to an observable level (i.e., observable via D^0-$\overline{D}^0$ mixing). The Standard Model predicts a negligible effect, so observing CP violation in the D^0 system would be an unambiguous sign of new physics. Finally, a Super B Factory experiment would not only measure known CKM observables with unprecedented precision, but it would also measure new observables and decay modes that could shed light on new physics. More complete reviews of the physics program possible at a Super B factory are available in Refs. [5, 6].

5 Technical Description

This section describes the technical scope of the US participation in the Belle II experiment based at KEK at the SuperKEKB accelerator. The new detector is an upgraded version of the Belle detector [1]. The Belle II upgrade will replace the inner tracking systems and PID systems of the existing Belle detector as well as the endcap and inner layers of the barrel KLM detector.

The US Belle II project scope is to provide elements of the barrel PID system, an iTOP detector (Section 5.1), the inner layers of the barrel KLM system (Section 5.3), and electronics for both these systems as well as for the endcap KLM replacement system that will be provided by other collaborators (Section 5.2). In addition, the US scope includes providing components of the SuperKEKB commissioning detector (Section 5.4) that will be used to evaluate beam background around the interaction point prior to roll-in of the Belle II detector. The Japanese are responsible for final system integration and, while the US groups anticipate a significant role in this phase of the Belle II upgrade, this is not part of the scope of the US Belle II project.

5.1 Imaging Time-of-Propagation Detector

5.1.1 US Role in the iTOP Detector

The US groups have taken a leading role in the design and simulation of high precision particle identification in the barrel region, and will furnish the optical components for an iTOP detector. These components consist of bars, spherical mirrors, and expansion prisms, all fabricated from synthetic fused silica (synthetic quartz).

5.1.2 iTOP Detector Motivation

Good separation between pions and kaons has proven crucial for studying charmless B decays in which background from $b \to s$ loop processes can be competitive with the signal. For example, the $b \to d$ penguin decay $B^0 \to \rho^0\gamma$, with a branching fraction of 8×10^{-7}, can be easily overwhelmed by background from the $b \to s$ penguin decay $B^0 \to K^{*0}\gamma$, which has a branching fraction of 4×10^{-5} (50 times larger). Without good kaon rejection, identifying a signal would be infeasible. This same argument applies to other $b \to s$ and $b \to d$ penguin processes, which are especially sensitive to new sources of flavor mixing or new types of CP violation.

The high momentum Belle particle identification detector, an aerogel-radiator-based Čerenkov counter, had a typical π/K efficiency of 85-90% and a misidentification rate of 9-10%. Such discrimination as applied to the $B^0 \to \rho^0\gamma$ sample results in the $M_{K\pi}$ distribution shown in Fig. 2, i.e., one of the pion candidates is purposely (mis)assigned the kaon mass and the two-body invariant mass calculated. Although this distribution corresponds to the final event sample after all selection criteria are applied, one observes that $B^0 \to K^{*0}\gamma$ background dominates. Even after imposing a kinematic selection $M_{K\pi} > 0.92$ GeV/c^2, the ratio of signal events to background events is only 1:1. If the kaon misidentification rate were to be reduced by a factor of two while preserving the same pion efficiency, i.e., as achieved by the BaBar DIRC detector, then the significance of the signal would be substantially improved. This is the goal of the Belle II barrel particle identification detector. Such improved performance would benefit the analysis of charmless decay modes, e.g., $B \to \rho\rho$, $B^0 \to K^+K^-$, $B^0 \to \rho\ell^+\ell^-$, etc. Many additional analyses will benefit from improved particle identification at lower momentum, e.g., full reconstruction of the "other" B meson to provide kinematic constraints and background suppression, and K identification to indicate B meson flavor.

5.1.3 iTOP Detector Description - US Contributions

The Belle II iTOP detector uses wide bars of synthetic fused silica ("quartz") to produce Čerenkov radiation that is imaged onto an array of micro-channel-plate (MCP) photomultiplier tubes (PMTs). From the pattern and timing of photon hits, the Čerenkov angle is calculated. This angle, along with the track momentum measured in the central tracker, identifies the particle as a pion, kaon, or proton. The bars of fused silica are optically pol-

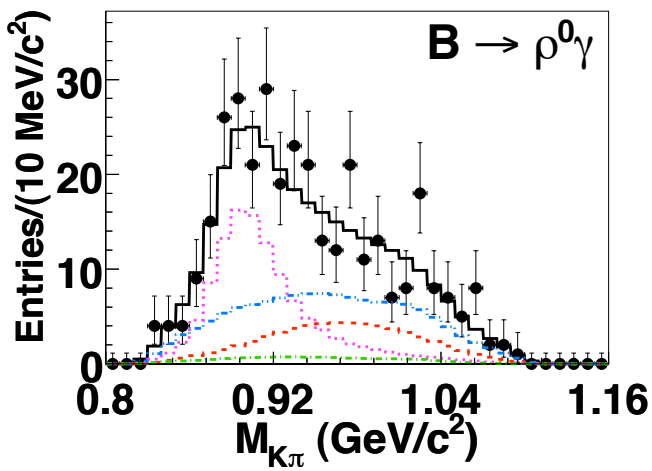

Figure 2: *$K^+\pi^-$ invariant mass spectrum of the final $B^0 \to \rho^0\gamma \to \pi^+\pi^-\gamma$ candidate sample, from Ref. [7].*

ished to have very uniform and parallel surfaces such that the Čerenkov light is transported to the end via total internal reflection with minimal loss. The timing of a photon hit is the sum of the time-of-flight (TOF) of the particle from production to when the photon was radiated in the the quartz bar plus the time-of-propagation of the Čerenkov light to the MCP-PMTs. The forward-moving light is reflected by a spherical focusing mirror such that the spread in photon hit positions on the rear MCP-PMTs due to the thickness of the bar is minimized. The focusing mirror also reduces chromatic dispersion. The remaining chromatic dispersion can be corrected for due to the precise timing of the MCP-PMTs.

The detector is positioned radially between the central tracking chamber and the electromagnetic calorimeter. There are sixteen detector modules arranged azimuthally around the beam. The geometry of one module is shown in Fig. 3. A quartz bar of cross section 2.0×45.0 cm^2 and length 2.5 m constitutes the radiator and has a spherical mirror of depth 10 cm and focal length $\sim$ 2.5 m attached at one end. The mirror reflects light back down the bar to the far end where it refracts out into a quartz "expansion prism." The prism has one rectangular face attached to the bar and the other rectangular face attached to an array of MCP-PMTs. Optical filters with a 300-350 nm wavelength cutoff in front of the PMTs may be used to further reduce chromatic dispersion. The timing of photon hits is strongly correlated with the x and y hit coordinates, and this correlation differs for kaon and pion tracks due to the difference in Čerenkov angles (i.e., photons radiated from pions and kaons of the same momentum follow slightly different trajectories in the bar). The purpose of the prism is to allow the multiple photons radiated by a track to spread out, better resolving the hit pattern and reducing hit ambiguities. Timing ambiguities occur when TOF+TOP is the same for kaon and pion tracks. This ambiguity only occurs for very specific particle kinematics.

The MCP-PMT chosen is the Hamamatsu SL-10. The technical specifications of the optical components are listed in Appendix A. Vendors have been identified both within and outside the US that can fabricate these components. Contracts for preproduction prototype

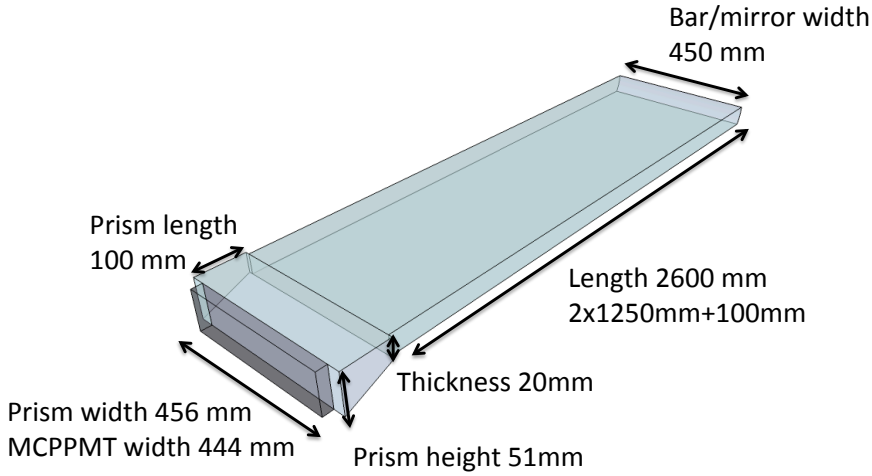

Figure 3: *Geometry of an iTOP module. A focusing mirror is attached to the forward end of a quartz bar and focuses Čerenkov photons onto micro-channel-plate phototubes (MCP-PMTs) located at the backward end of the bar. There are 16 such assemblies in light-tight boxes arranged azimuthally around the beamline.*

bars have placed with Aperture Optical Sciences Inc. (Durham, CT), which operates in partnership with Okamoto Optics (Yokohama, Japan), and Zygo (Middlefield, CT). AOS/OOW are producing 4 prototype bars and Zygo is producing 5 in order to assess each vendor's production capacity as well as technical capability to meet the optics specifications. As of November 2013 Zygo has delivered one bar meeting specifications with additional pairs due at the end of December 2013 and February 2014. AOS/OOW are many months behind schedule and are due to deliver the first completed bar in December 2013 and the remainder of the order by the end of January 2014. ITT Exelis (Rochester, NY) has produced one prototype mirror that met the specifications. Subsequently the specifications were changed (length of mirror and radius of curvature) and ITT is producing four pre-production prototypes with the final specifications. These are due to be completed in February 2014. Cosmo Optics (Middletown, NY) produced an initial prototype prism. The overall length of the prism was out of specification. A subsequent order for 4 pre-production prototypes has been awarded to Zygo (Middlefield, CT) with delivery expected in December 2013.

5.1.4 Quartz Acceptance Testing Plans

Two types of acceptance tests will be performed for the quartz optics. The first type will be performed by the manufacturer and will verify the mechanical and optical specifications contracted for: physical dimensions, flatness and r.m.s. roughness of all surfaces, the parallelism and perpendicularity of relevant faces, and the total surface area of scratches and digs (chips). The results of these tests will be compiled in a metrology report that will be submitted to the contracting lab (PNNL) for review and approval upon completion of the tests. These tests will be performed with large aperture interferometers and high precision

coordinate measurement machines (CMM). Should the results of these tests be unsatisfactory, an optical component may be rejected until it can be brought into specificication, e.g., with additional re-work. The mechanical and optical specifications of bars, mirrors, and prisms to be validated by the manufacturers are listed in Appendix A.

The second type of acceptance testing will be performed by Belle II physicists at KEK and at the University of Cincinnati. The quartz bars will be tested at KEK while the mirrors and prisms will be tested at Cincinnati. These tests will focus on optical properties. Specifically, for the bars measurements will be made of:

- the bulk transmission of the fused silica substrate, and
- the coefficient of total internal reflection.

For the mirrors measurements will be made of:

- the bulk transmission of the fused silica substrate;
- the reflectivity of the mirrored face;
- the radius of curvature and the x-y-z position of the focal point; and
- the amount of astigmatism, if any.

For the prisms measurements will be made of:

- the bulk transmission of the fused silica substrate; and
- the angle of the tilted face.

These tests would be time-consuming and expensive for the manufacturers to perform, but they are needed to demonstrate that the optical components will perform satisfactorily within an iTOP module. Some results of our measurements, e.g., the precise positions of the mirror focal points, and the precise angle of the tilted faces of the prisms, will be input into our reconstruction software to improve the π/K performance of the iTOP. They will also be input into our Monte Carlo simulation code to improve the accuracy of efficiency calculations.

In addition, all optics will be carefully inspected for chips along the edges. Such chips can arise during manufacturing, during handling, and during shipping. At KEK an automatic scanning system has been developed based on a camera mounted on a translation stage and dedicated software. This system will be used to photograph all bar edges, recognize chips and surface imperfections, and document the locations and sizes of such imperfections. Further details of the above acceptance testing procedures are given in Appendix B.

5.1.5 Expected performance

The expected performance in terms of separation between pions and kaons has been studied with Monte Carlo (MC) simulation. The results are now based on GEANT4 simulations within the BASF2 (Belle Analysis Software Framework) framework. There are separate simulations for the summer 2013 beam test with the LEPS spectrometer at SPRING-8, which allow comparison with beam test data, and for the full Belle II detector, which enable the evaluation of physics performance. GEANT4 determines the trajectory of primary charged particles and any secondaries produced by electromagnetic and hadronic interactions of the primary particle. The threshold energy for propagation of electrons is 0.5 MeV, which is smaller than the Čerenkov radiation threshold. GEANT4 produces secondary particles from electromagnetic interactions in the bar, and carry out all optical processes for all charged particles. For the Belle II detector simulation, all intervening material is included and the effect of backsplash from interactions in the CsI(Tl) crystals is modeled.

All simulations include chromatic dispersion (variation of group velocity with wavelength), PMT transit time spread (TTS), and PMT quantum and collection efficiencies. These values are taken from measured data distributions. The effects of glue joints, wavelength filters and other interfaces in the quartz bar module are included. The GEANT4 simulation also include multiple scattering of tracks in material, delta ray production, nuclear interactions, and backsplash from the electromagnetic calorimeter.

The detector performance is quantified by obtaining separate probability density functions (PDFs) for pion and kaon tracks. These PDFs depend on track momentum, impact angle, impact position, and particle type, are calculated analytically.

Subsequently, photon hits from a given track are fit to these PDFs to calculate likelihoods $\mathcal{L}_\pi$ and $\mathcal{L}_K$, respectively. If the difference $\log \mathcal{L}_\pi - \log \mathcal{L}_K$ is positive, then the track is classified as a pion; if negative, as a kaon. These likelihood-based classifications can be compared with the known species of simulated particles to determine the fractions of correctly identified kaons and incorrectly identified pions.

To study the robustness of the iTOP, the following parameters are varied when simulating the detector performance:

- **electronics timing resolution** The electronics timing resolution is increased from the expected value of 50 ps to 100 ps and 150 ps. Performance for $B^0 \to \pi^+\pi^-$ very similar to that of Belle is achieved; performance for $B^0 \to \rho^0\gamma$ is still notably better than that of Belle.

- **t_0 start-time jitter** The start-time jitter is increased from an expected value of 25 ps to 50 ps and 100 ps. (Note that the t_0 jitter achieved in Belle was 40 ps.) Performance for $B^0 \to \pi^+\pi^-$ very similar to that of Belle is achieved; performance for $B^0 \to \rho^0\gamma$ is still notably better than that of Belle.

- **photon detection efficiency** The photon yield is reduced to 60% of the nominal value and the resulting performance is still found to be superior to that of Belle.

- **tracking uncertainty** The tracking angular uncertainty is increased from the expected value of 1.5 mrad to four times worse: 6.0 mrad. The resulting performance is still significantly better than that of Belle.

- **background level** The background (extraneous photon hits) is increased to ten times the expected value; the resulting change in performance is small.

Typical photon yields are plotted in Fig. 4; the resulting identification efficiencies and misidentification fractions are plotted in Fig. 5. To understand the impact of these efficiencies upon a physics analysis, these values are convolved with the two-dimensional $(p, \cos\theta)$ distribution of daughter tracks from physics modes such as $B^0 \to \rho^0\gamma$ and $B^0 \to K^{*0}\gamma$. This provides the signal efficiency and background contamination expected when analyzing these decays. The resulting values for two signal modes of interest, $B^0 \to \pi^+\pi^-$ and $B^0 \to \rho^0\gamma$, are listed in Table 5 for a variety of conditions. In almost all cases the values obtained are significantly better than the performance achieved with the Belle aerogel-based particle identification detector.

To understand the impact of optical components with imperfect geometry Monte Carlo studies are performed to evaluate iTOP performance as parameters are varied beyond the specified tolerances described in Appendix A. Establishing the performance derivative with respect to each specification will identify what specifications can be relaxed if the supplier has trouble meeting them.

To date the iTOP performance has been evaluated for the following list of specifications:

1. length, width, thickness of quartz bar
2. kink at the bar-bar glue joint
3. parallelism of large quartz bar faces
4. parallelism of long quartz bar faces
5. perpendicularity of large face to long face of quartz bar
6. surface roughness of large faces and long faces of quartz bar
7. position of center of mirror
8. mirror tilt axis
9. mirror focal length

Performance is evaluated by considering photon yield, efficiency and fake rate for 1,2,3, and 4 GeV kaons and pions in 14 bins of polar angle utilizing the PDF for the *ideal* geometry. In some cases PDFs were generated for the imperfect geometry to check whether the performance can be recovered if the imperfect geometry is known accurately. In general, the iTOP performance is robust for imperfect geometries outside specified tolerances. In addition, lost

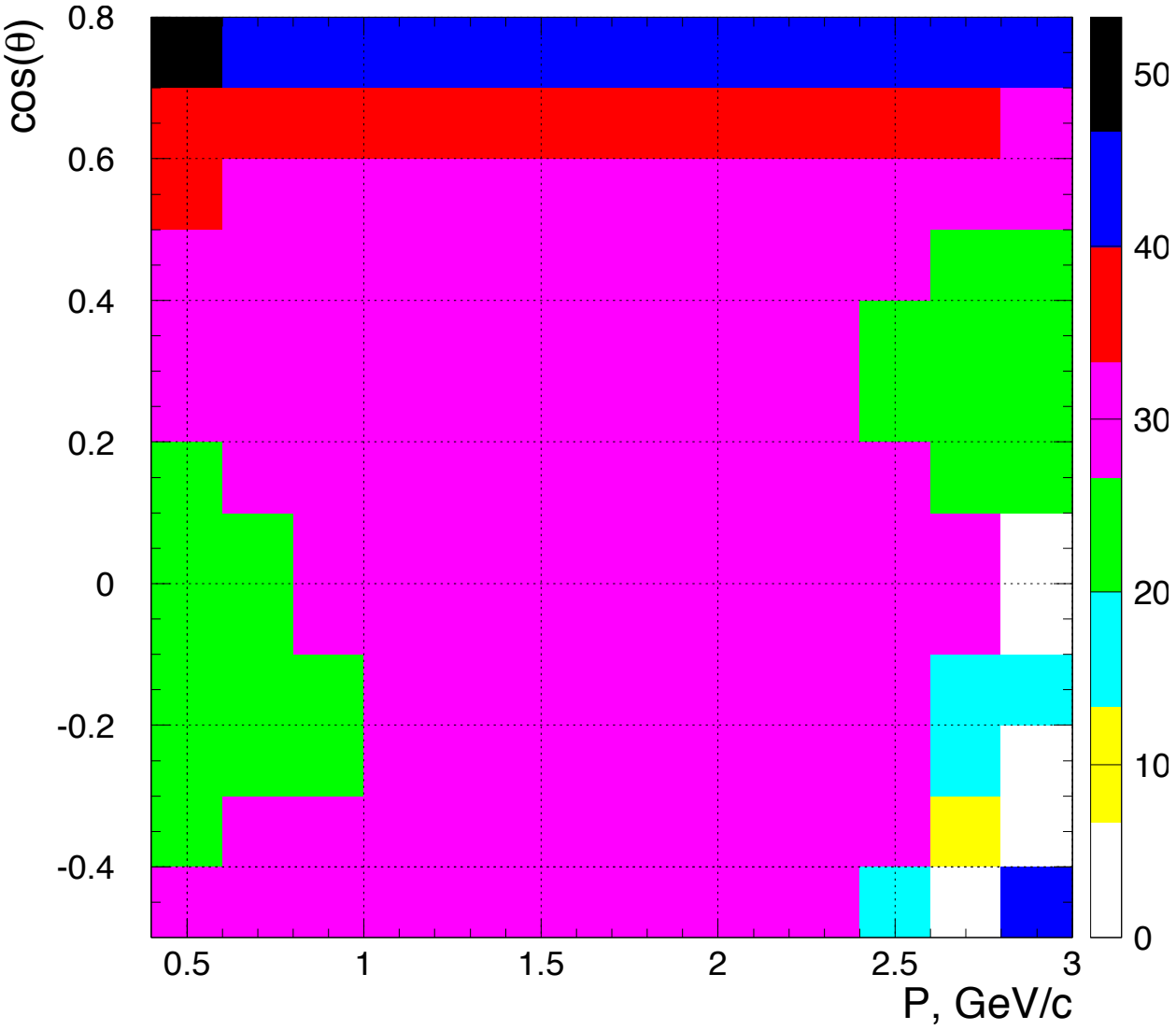

Figure 4: *Simulation results showing mean photon yields as a function of track momentum and the cosine of the track polar angle for tracks.*

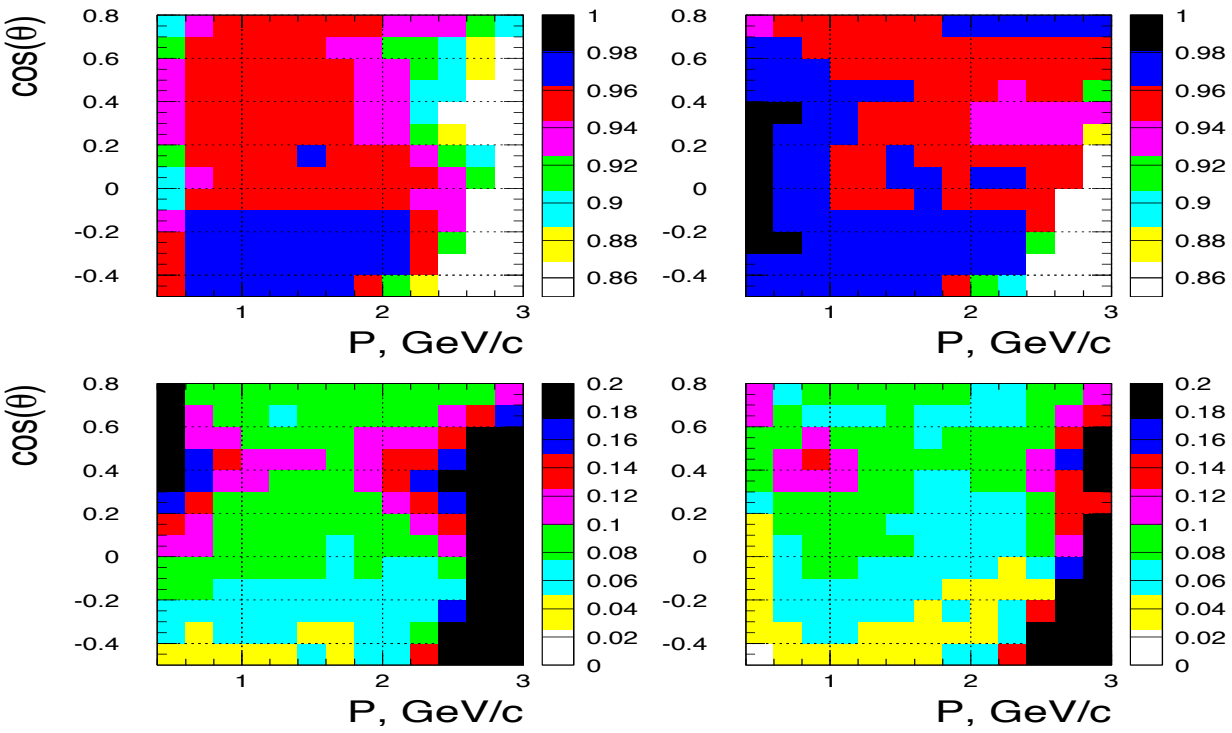

Figure 5: *Simulation results for iTOP only (left) and iTOP+dE/dx (right) showing pion identification efficiencies (top) and kaon misidentification fractions (bottom), as a function of track momentum and the cosine of the track polar angle.*

Parameter Condition	$B^0 \to \pi^+\pi^-$ Efficiency (%)	$B^0 \to K^+\pi^-$ Fake rate (%)	$B^0 \to \rho^0\gamma$ Efficiency (%)	$B^0 \to K^{*0}\gamma$ Fake rate (%)
Baseline Performance t resolution (50ps) t_0 jitter (25ps)	90.4 ± 0.3	7.1 ± 0.3	96.7 ± 0.2	4.7 ± 0.3
t resolution (100ps)	89.2 ± 0.3	9.1 ± 0.4	96.5 ± 0.2	5.3 ± 0.2
t resolution (150ps)	86.7 ± 0.3	11.9 ± 0.4	96.1 ± 0.2	5.8 ± 0.2
t_0 jitter (50ps)	88.8 ± 0.3	8.0 ± 0.4	96.3 ± 0.2	4.9 ± 0.2
t_0 jitter (100ps)	83.8 ± 0.3	14.4 ± 0.5	95.5 ± 0.2	7.4 ± 0.2
(t resolution=50ps)				
1a. Photon yield × 0.60	86.5 ± 0.3	9.3 ± 0.4	93.7 ± 0.2	6.57 ± 0.3
2a. 10 × background	90.4 ± 0.4	6.8 ± 0.3	97.4 ± 0.2	3.78 ± 0.3
3a. $\sigma_\theta = 6.0$ mrad	82.9 ± 0.3	12.4 ± 0.4	95.9 ± 0.2	5.43 ± 0.3
4a. t_0 jitter = 50 ps	88.8 ± 0.3	8.0 ± 0.4	97.3 ± 0.2	3.89 ± 0.3
1a. + 2a.	86.2 ± 0.4	9.4 ± 0.4	93.7 ± 0.2	7.50 ± 0.3
3a. + 4a.	81.6 ± 0.3	14.3 ± 0.4	95.2 ± 0.2	6.41 ± 0.3
(t resolution=100ps)				
1b. Photon yield × 0.60	84.3 ± 0.3	12.1 ± 0.4	93.3 ± 0.2	7.83 ± 0.4
2b. 10 × background	88.2 ± 0.4	8.4 ± 0.4	97.0 ± 0.2	4.25 ± 0.3
3b. $\sigma_\theta = 6.0$ mrad	82.3 ± 0.3	13.8 ± 0.4	95.6 ± 0.2	5.55 ± 0.3
4b. t_0 jitter = 50 ps	87.1 ± 0.3	10.4 ± 0.4	96.2 ± 0.2	4.68 ± 0.3
1b. + 2b.	83.9 ± 0.5	11.8 ± 0.4	93.3 ± 0.2	8.10 ± 0.3
3b. + 4b.	81.2 ± 0.3	14.6 ± 0.5	95.6 ± 0.2	6.61 ± 0.3
(t resolution=150ps)				
1c. Photon yield × 0.60	80.9 ± 0.3	15.6 ± 0.5	93.2 ± 0.2	8.80 ± 0.4
2c. 10 × background	86.7 ± 0.4	12.1 ± 0.4	96.0 ± 0.2	5.40 ± 0.3
3c. $\sigma_\theta = 6.0$ mrad	80.9 ± 0.3	15.7 ± 0.5	95.2 ± 0.2	6.68 ± 0.3
4c. t_0 jitter = 50 ps	85.7 ± 0.3	12.1 ± 0.4	96.4 ± 0.2	4.92 ± 0.3
1c. + 2c.	81.1 ± 0.5	15.5 ± 0.5	95.6 ± 0.2	8.82 ± 0.4
3c. + 4c.	80.5 ± 0.4	16.7 ± 0.5	95.7 ± 0.2	6.81 ± 0.3

Table 5: *Simulation results based on BASF2. The signal efficiencies are from $B^0 \to \pi^+\pi^-$ (left) and $B^0 \to \rho^0(\pi^+\pi^-)\gamma$ (right). The backgrounds are from $B^0 \to K^+\pi^-$ (left) and $B^0 \to K^{*0}(K^+\pi^-)\gamma$ (right). For baseline value, t resolution = 50 ps and t_0 jitter = 25 ps. The uncertainty is the statistical error only.*

performance is recovered when the PDF evaluated with the appropriate imperfect geometry is used. Two examples are illustrated below.

Parallelism of large quartz bar faces The large faces of the 1.25 m quartz bars are specified to be parallel within 4 arc seconds, which corresponds to 24 micron runout over 1.25 m length of the quartz bar. The impact on kaon efficiency of a ± 300 micron deviation from the ideal geometry evaluated with the ideal PDFs is shown in Fig. 6. Substantial performance degradation is observed for higher momentum tracks. Regenerating the PDF for the imperfect geometry fully recovers the iTOP performance as shown in Fig. 7.

Position of mirror center The center of curvature of the mirror is specified to a precision of ± 1 mm. The impact on ± 5mm variation for 1 GeV and 2 GeV tracks is shown in Fig. 8. Some performance degradation is observed for 2 GeV tracks using the ideal geometry. The impact of ± 5mm variation on kaon efficiency and pion fake rate for 4 GeV tracks is shown in Fig. 9. Substantial performance degradation is observed using the PDF for the ideal geometry. Regenerating the PDF for the imperfect geometry substantially recovers the iTOP performance.

5.1.6 Beam Test Results

Four beam tests have been performed to date with different prototype quartz modules; results from all tests are described below.

CERN Beam Test

In 2010, two bars and a mirror were epoxied together to make a prototype module of length 1.85 m and width 40 cm. This module was tested in a 120 GeV/c pion beam at CERN in November 2010. For this test, photon hits were recorded with nine Hamamatsu SL-10 MCP-PMTs with a 1×4 anode configuration. Data was taken with the beam normal to the bar as well as tilted at 60° with respect to the beam, to better mimic track trajectories expected in Belle II. Photon hit multiplicities (Fig. 10) and the photon hit time distributions (Fig. 11) demonstrated reasonable agreement with MC simulation.

Fermilab Beam Test

In 2011, two bars, a prism, and a mirror were epoxied together to create a 2.98 m-long, 45 cm wide module, which was tested in a 120 GeV/c proton beam at the Fermilab Test Beam Facility. For this test, data was recorded with the radiator both normal to the beam and also tilted at a polar angle of 60° to the beam. This module was intended to be close to the baseline design for Belle II; the only differences are *a)* the expansion prism was 10 mm narrower than nominal and did not have a tilted face; and *b)* the mirror focal length was 3.5 m instead of 2.5 m. Waveforms were recorded with 20 Hamamatsu SL-10 MCP-PMTs having 4×4 anode configuration connected to an early prototype of the final front-end electronics board stack.

2012 LEPS Beam Test The bar used at Fermilab was taken to LEPS in October 2012 for

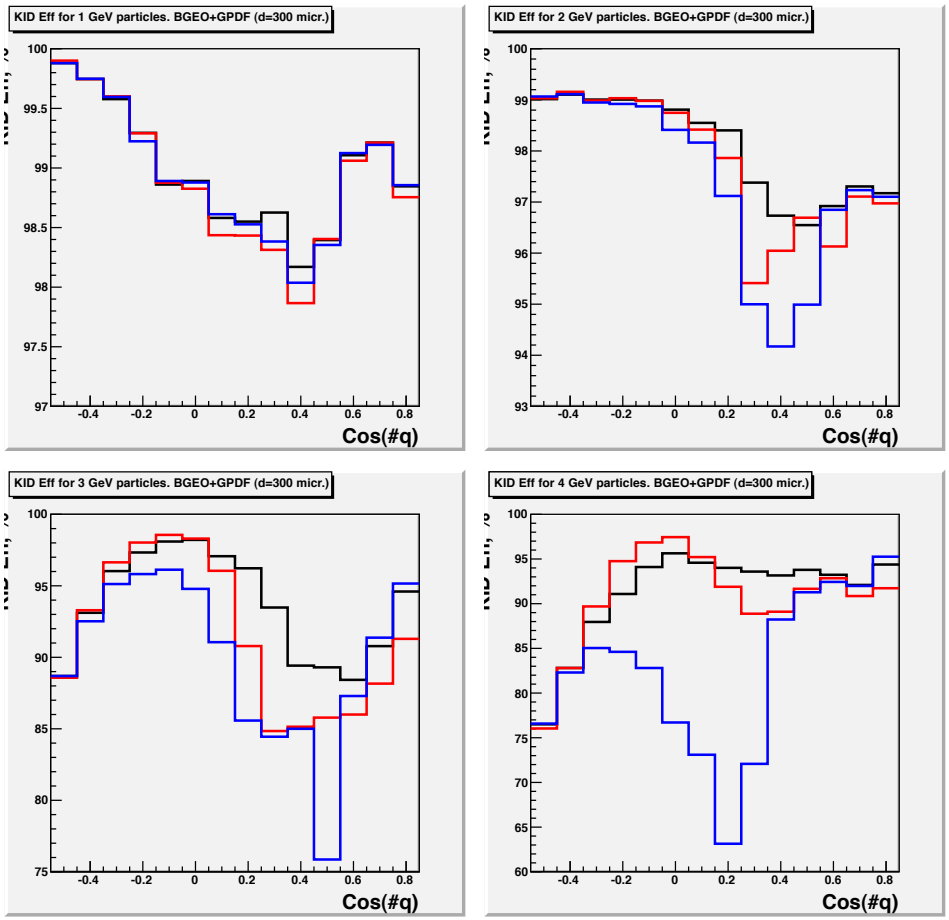

Figure 6: *Simulation results showing kaon efficiency versus polar angle for 1 GeV/c (top-left), 2 GeV/c (top-right), 3 GeV/c (bottom-left), and 4 GeV/c (bottom-right) tracks. The iTOP performance with ideal geometry (black) and with the large faces of a quartz bar deviating from parallel by +/− (red/blue) 300 microns (>10× the 24 micron specification) are evaluated using the PDF for the ideal geometry. Substantial performance degradation is observed.*

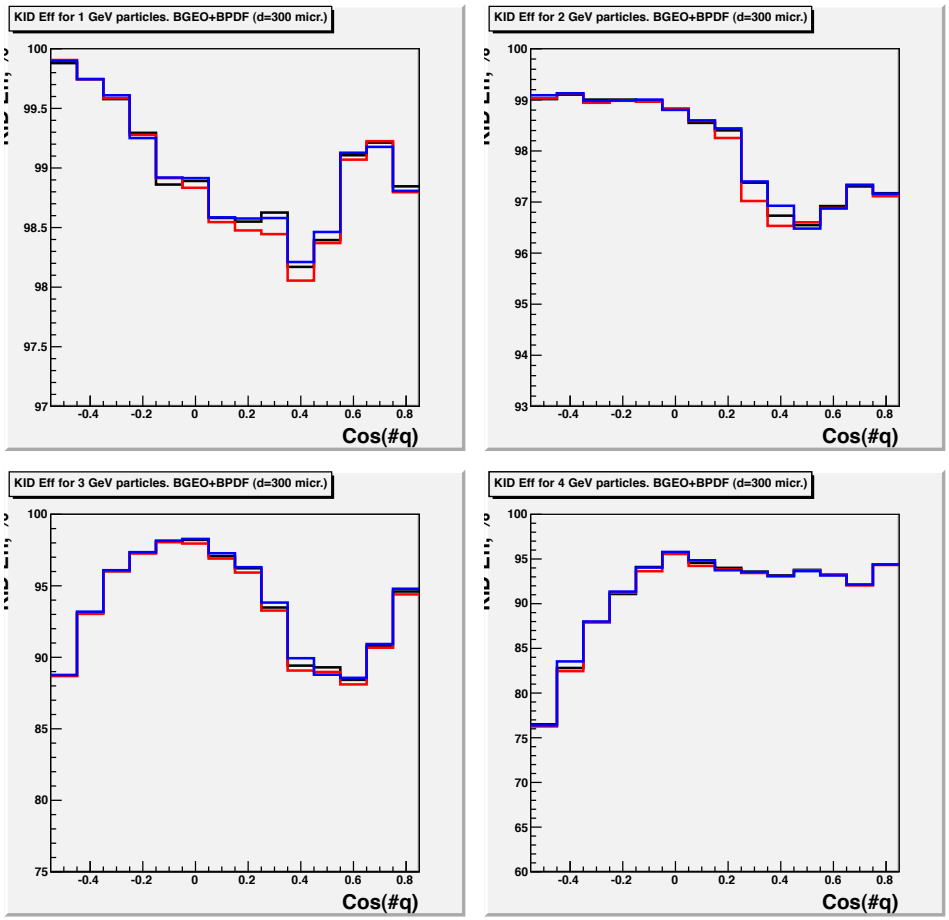

Figure 7: *Simulation results showing kaon efficiency versus polar angle for 1 GeV/c (top-left), 2 GeV/c (top-right), 3 GeV/c (bottom-left), and 4 GeV/c (bottom-right) tracks. The iTOP performance with ideal geometry (black) and with the large faces of a quartz bar deviating from parallel by +/− (red/blue) 300 microns (>10× the 24 micron specification) are evaluated using the regenerated PDF for the imperfect geometry. No performance degradation is observed.*

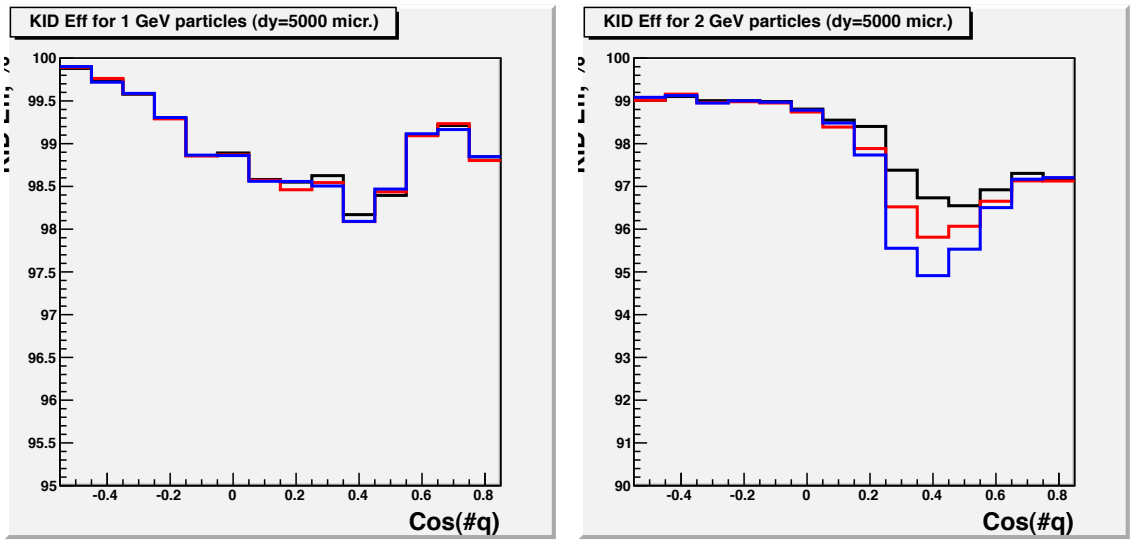

Figure 8: *Simulation results showing efficiency for 1 GeV (left) and 2 GeV (right) tracks versus polar angle. The performance of the perfect mirror (black) and mirror with center shifted by +/-5 mm vertically (red/blue) - five times the 1 mm specification - are evaluated using the PDF for the ideal geometry (top). Some performance degradation is observed for 2 GeV tracks. Performance is nearly fully recovered when the PDF regenerated for the imperfect geometry is used.*

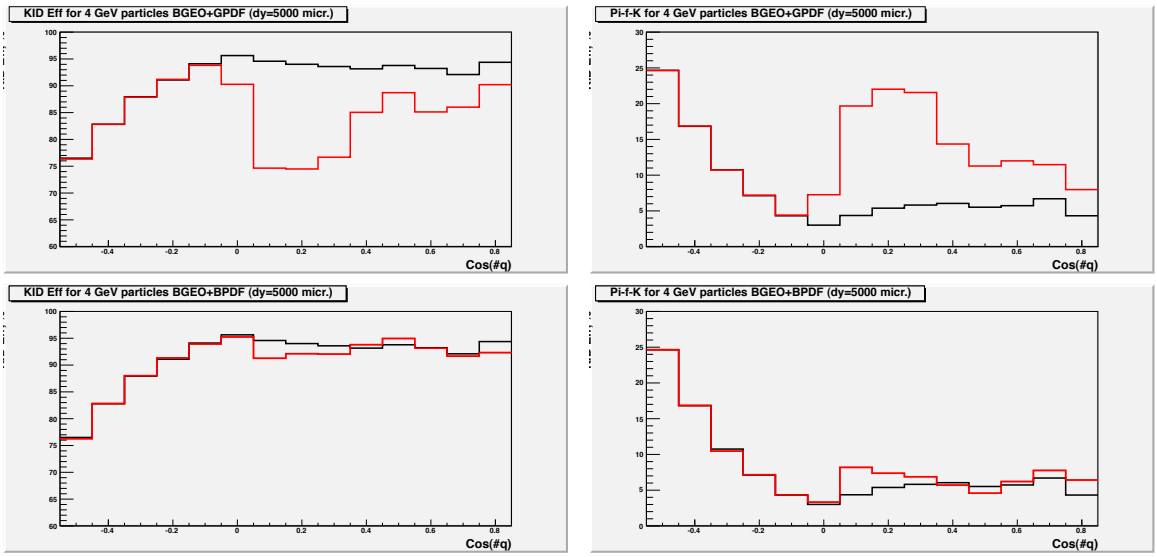

Figure 9: *Simulation results showing (left) kaon efficiency and (right) pion-fakes-kaon rate for 4 GeV tracks versus polar angle. The performance of the perfect mirror (black) and mirror with center shifted by 5 mm vertically (red) - five times the 1 mm specification - are evaluated using the PDF for the ideal geometry (top). Substantial performance degradation is observed. Performance is nearly fully recovered when the PDF regenerated for the imperfect geometry is used (bottom).*

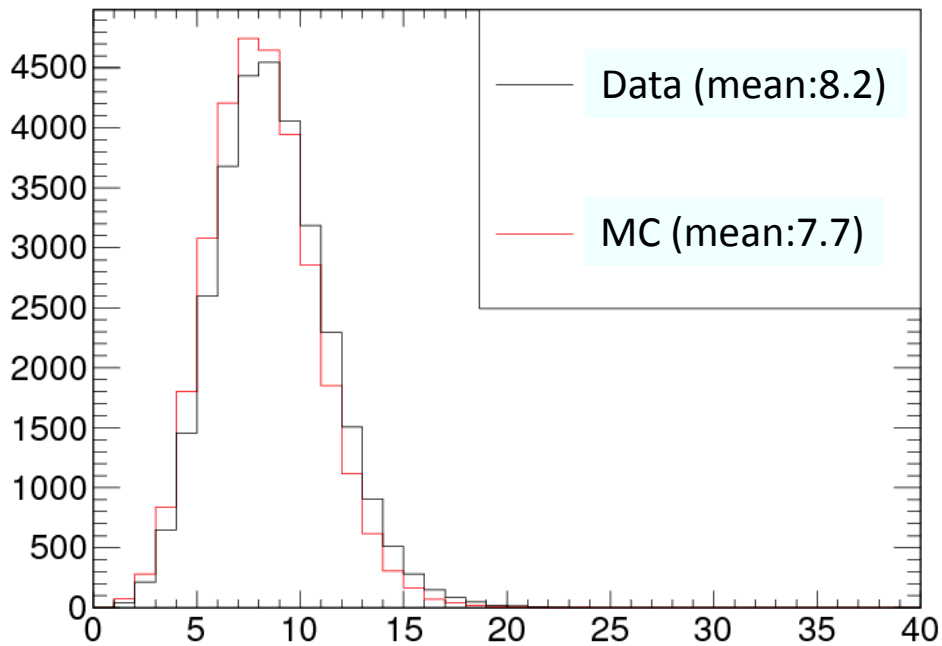

Figure 10: *CERN beamtest results: photon hit multiplicity distributon. The black histogram shows the data, and the red histogram shows the distribution from MC simulation. There is reasonable agreement between the two.*

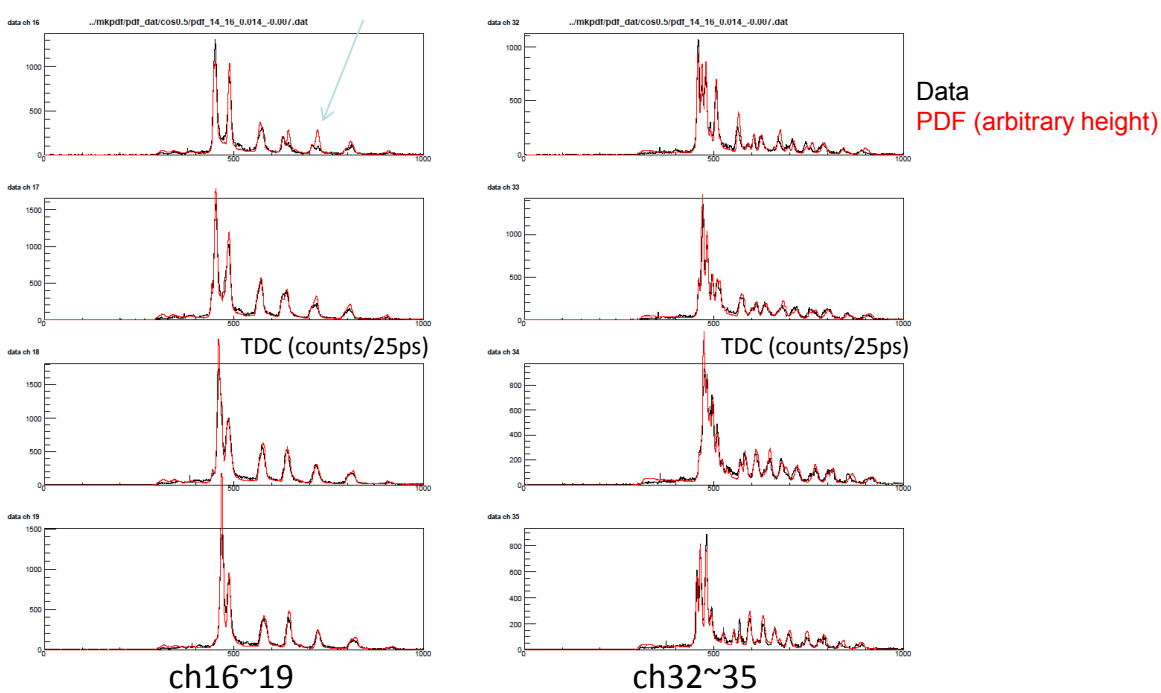

Figure 11: *CERN beamtest results: photon TDC hit time distribution for data (black) and MC simulation (red) for the four channels of two different PMTs. There is reasonable agreement between the data and MC.*

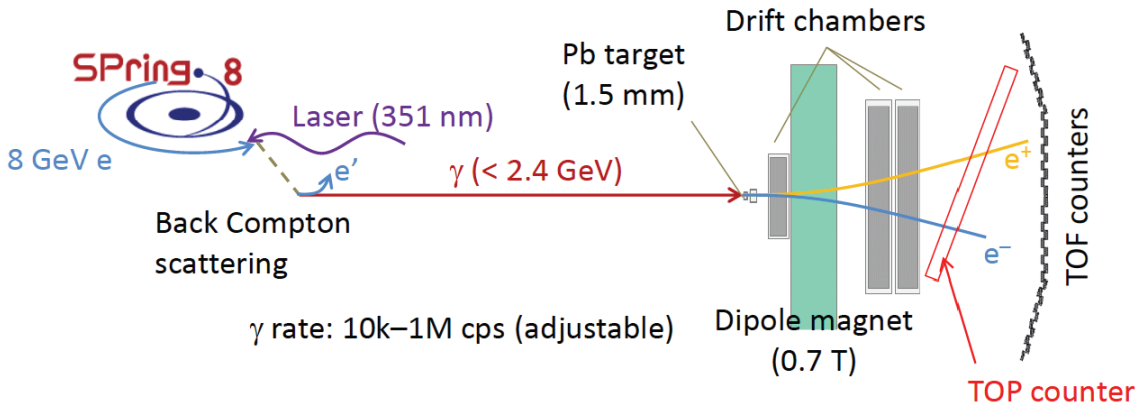

Figure 12: *The LEPS apparatus. Backward Compton scattering of UV laser photons off the 8 GeV electrons in the SPring-8 synchrotron rign produced ∼2.1 GeV photons, which then generated electron/positron pairs in a Pb target.*

a week long test. For this test, the 4×4 pixelated SL-10 MCP-PMTs were readout with 4×4 constant fraction discriminator electronics and CAEN TDC's. Although there were clear x vs t correlations visible in the data, the interpretation of results was hampered by optical coupling problems for many PMT's and severe cross-talk in the CFD electronics, which could not be removed in off-line analysis.

2013 LEPS Beam Test

In June 2013, two bars, a prism, and a mirror were assembed to create a 2.6 m-long, 45 cm wide module with a full compliment of 32 SL-10 MCP-PMTs having 4×4 anode configuration for a total of 512 readout channels. This module was tested at the Laser Electron Photon Experiment (LEPS) facility at SPring-8 with a 2.1 GeV positron beam (Fig. 12). The module was tested in the following three configurations: beam centered and normal to the quartz, beam centered and $cos\theta$=0.4 (∼64°), and beam 20 cm above the center with $cos\theta$=0.3 (∼72.5°).

This beam test was designated as a "vertical slice" test, where data would be taken from initial particle to raw data storage with as many components as possible matching the Belle II iTOP baseline design. Other than the quartz module already described, components included MCP-PMTs in the final configuration, front-end readout electronics based on the IRS3B ASIC for fast timing and waveform readout, the Belle II standard FTSW-based trigger and distributed clock, and a standard Belle II COPPER-2 pipelined back-end electronics crate for simultaneous data collection from all front-end modules. Timing and trigger signals were made available to the FTSW by the LEPS facility. Pulser and laser data was taken as well as beam data, and used to calibrate the channels. Uneven laser illumination (provided by a fiber optic cable at a corner of the quartz bar at the opposite end from the readout electronics) meant that some channels were not easily calibrated, and are visible as blank vertical lines in the ring image in Fig. 13. In addition, poor optical coupling on some PMTs

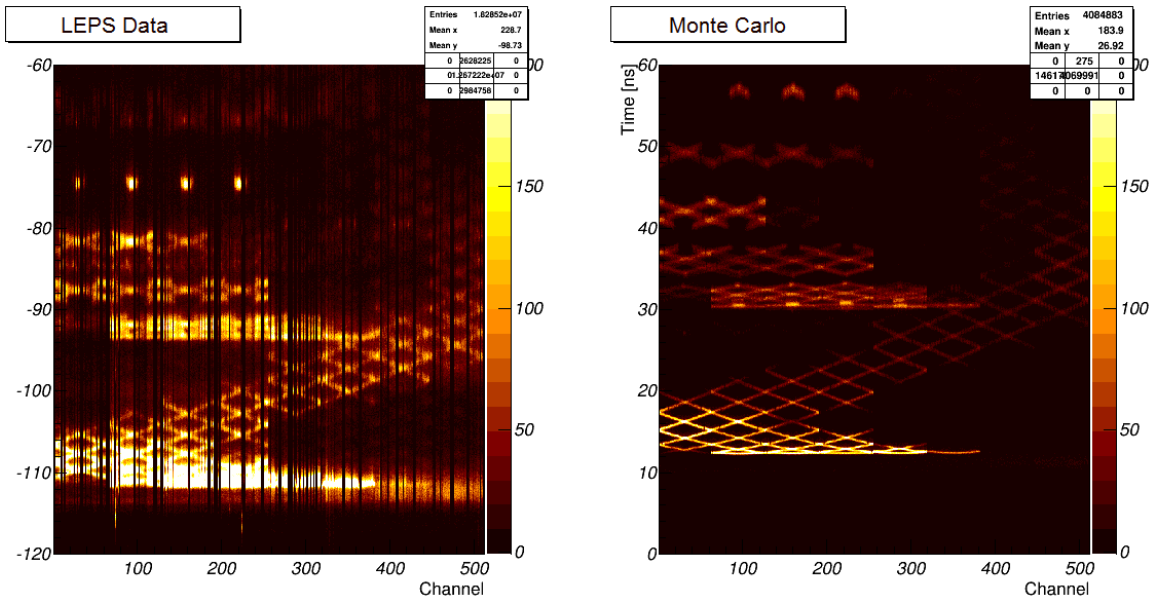

Figure 13: *Ring image for beam at normal incidence for the LEPS beam test. Actual data is at left; MC simulation results at right. Blank vertical lines in the data plot correspond to uncalibrated channels due to uneven laser illumination.*

affected light collection in some regions of the readout.

Once the channels were calibrated, results appeared reasonably well-matched to the MC simulations in time; however variations were present in signal amplitude. Further investigation of these differences is in progress, as can be seen in Fig. 16, where various processes missing from the MC simulation tools (such as cross-talk, quartz bulk transmittance and surface reflectance, and PMT subsurface reflections), have been identified as contributors to the amplitude differences. Work to include these parameters in the BASF2 GEANT4 MC simulations is underway.

Background photons are also visible in the ring images. These are due to various processes, such as gammas not converted in the Pb target or delta rays producing their own Čerenkov photons. These background photons may appear either in-time or out-of-time with the positron beam, depending on their source. Ring images from simulations of these processes are shown in Fig. 14.

Alignment optimization studies are also currently underway, where LEPS data ring images are compared to those generated by simulation to better identify quartz module alignments for the various orientations. The simulation is scanned across the beam variables y, z, θ, and ϕ, then the resulting simulated image is matched to the beam data image by adjusting the time offset until a maximum log likelilhood is reached. From these results, the overall best fit is obtained. Figure 15 displays a range of log likelihood values for the y-ϕ and z-θ planes.

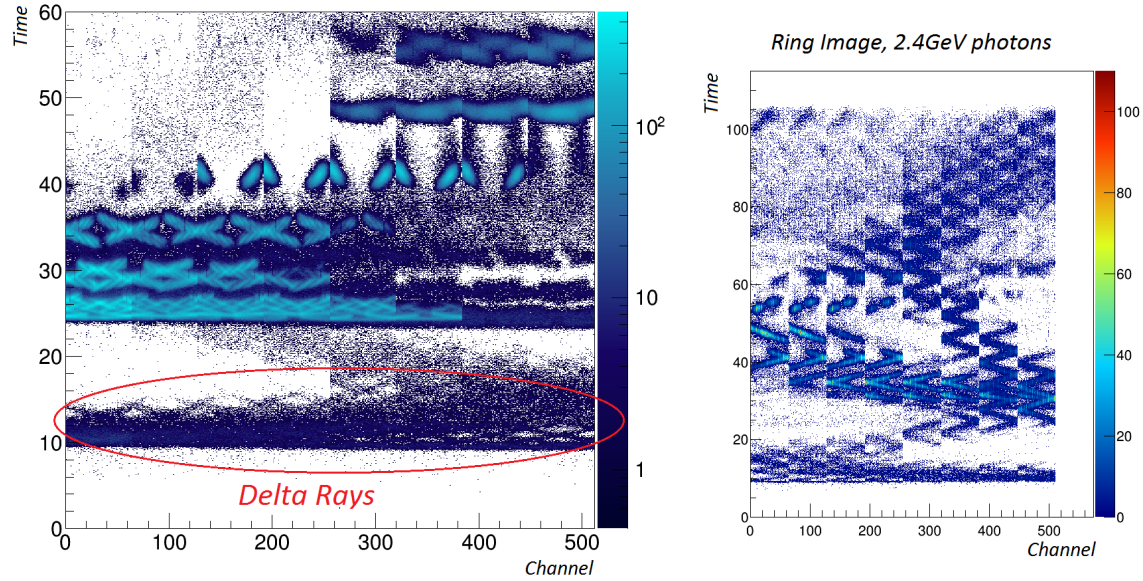

Figure 14: *Simulations of the delta ray and beam photon background processes. The ring image generated by delta rays is indicated at left, while the ring image from 2.4 GeV photons that do not interact in the Pb target is at right. Note that the delta rays will be in-time with the positron beam, while the gamma ring images will be out-of-time.*

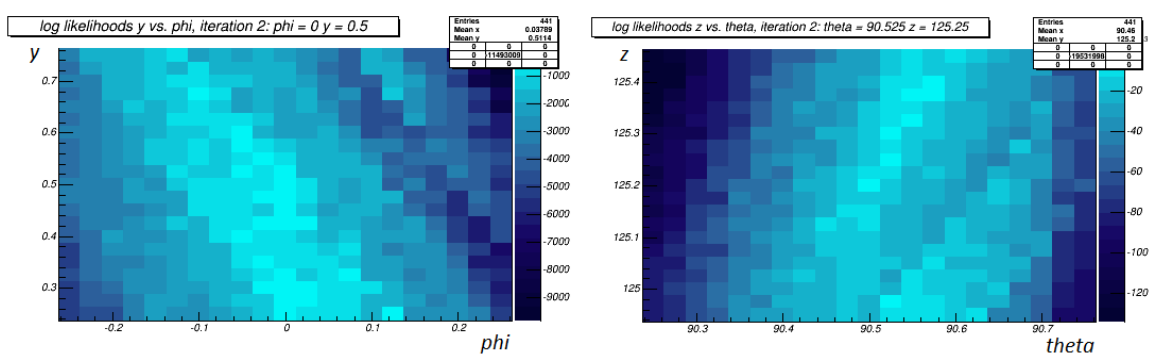

Figure 15: *Alignment studies for the LEPS experiment. Simulated ring images are compared to actual beam data and the overall log likelihood of the match is plotted.*

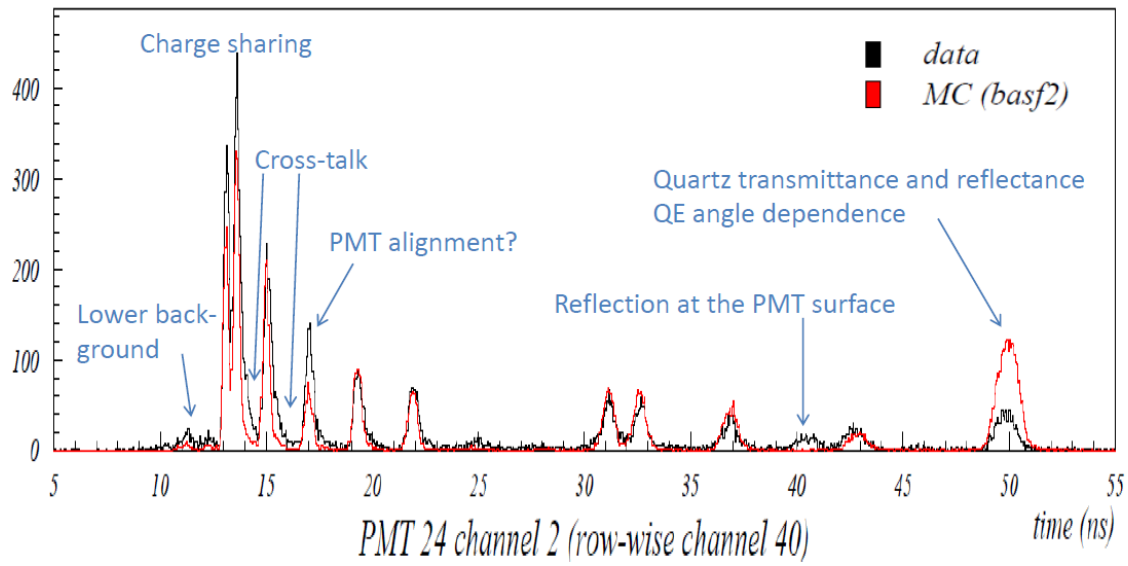

Figure 16: *Time distribution of photons for a single MCP-PMT channel from the LEPS beam test, compared with MC results. Known differences between data and MC are identified. [note that this is from CFD electronics]*

Analysis of the overall photon peak resolution, combined with knowledge that the iTOP physics (including the effect of dispersion) produces a minimum timing resolution of 120 ps, demonstrates that the readout electronics used at LEPS achieved 100 ps resolution (see Fig. 17). These results match pulser and laser lab measurements of the electronics, where overall electronics timing resolution was found to be 95 ps. This is further confirmed by comparing timing widths of all peaks in a ring image as in Fig. 18, where beam test data and MC are in good agreement.

5.1.7 Beam-related Backgrounds

Beam-related backgrounds in the iTOP are being studied using BASF2 based GEANT-4 simulations. Six separate background sources are considered: radiative Bhabha's, Touschek losses and Coulomb scattering, each from both the high-energy ring (HER) and low-energy ring (LER). The resulting neutron flux through the radiator bars and PMTs is satisfactory, but the photoelectron rates at the MCP-PMTs are prohibitively high for the conventional type of multi-alkali MCP-PMTs planned for Belle II. After a large integrated charge is accumulated, the efficiency of the PMTs begins to degrade rapidly. Operation at lower than nominal gain (5×10^5), may extend the lifetime by a factor of ~ 2.

During the last two years, Hamamatsu had adopted the atomic layer deposition (ALD) technique developed at Argonne National Laboratory (ANL) in the LAPPD R&D project for use in its MCP-PMTs. Hamamatsu's ALD-type MCP-PMTs appear to tolerate an integrated charge of ~ 10 C/m^2 with no degradation in performance.

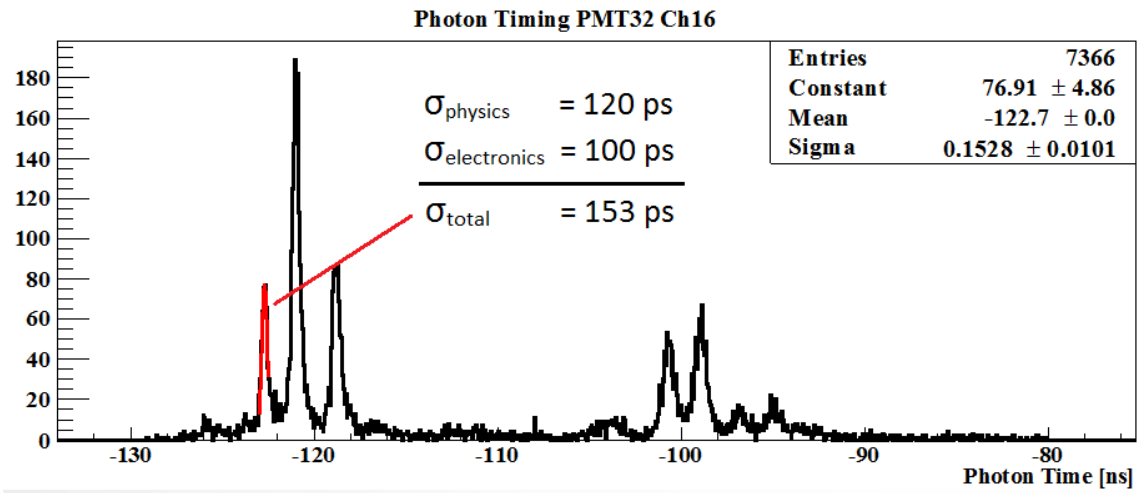

Figure 17: *Typical initial peak timing resolution measurement for the LEPS beam test. Note that a timing resolution measurement of 153 ps, combined with a known iTOP physics resolution of 120 ps, implies that the timing resolution contribution due to the electronics is on order of 100 ps.*

Without any magnet shielding and with the current beam lattice design, these rates are in excess of 10 MHz per PMT for all azimuthal angles. This value corresponds to an integrated charge of about 20 C/cm^2 in 50 ab^{-1} of data, and the SL-10 PMT can tolerate only about 1.5 C/cm^2. Most of this rate is due to radiative Bhabha's from the HER, and this background can be substantially reduced by shielding the final focus quadrupoles with several centimeters of tungsten. It is found from simulation that adding 3 cm of tungsten around these magnets reduces the radiative Bhabha background by one order of magnitude. However, about 1 MHz/PMT of Touschek background still remains, after extensive efforts to collimate this background around the LER ring. These results are summarized in Fig. 19, which shows the photoelectron rate at the PMTs as a function of azimuthal angle. The remaining background corresponds to an integrated charge of about 2 C/cm^2 during the Belle II experiment, which is also too high for conventional MCP-PMTs operating at nominal gain.

Once the superior performance of ALD-type MCP-PMTs was established, Belle II switched its production at Hamamatsu. By the time MCP-PMT production is complete, 50% of the iTOP PMTs will be of the ALD type. These ALD type PMTs will be used for the partial installation of TOP modules and initial running of Belle II. It may be possible for Nagoya University and KEK, who are responsible for MCP-PMT production to exchange the conventional PMTs for ALD-type PMTs for the completion of TOP installation.

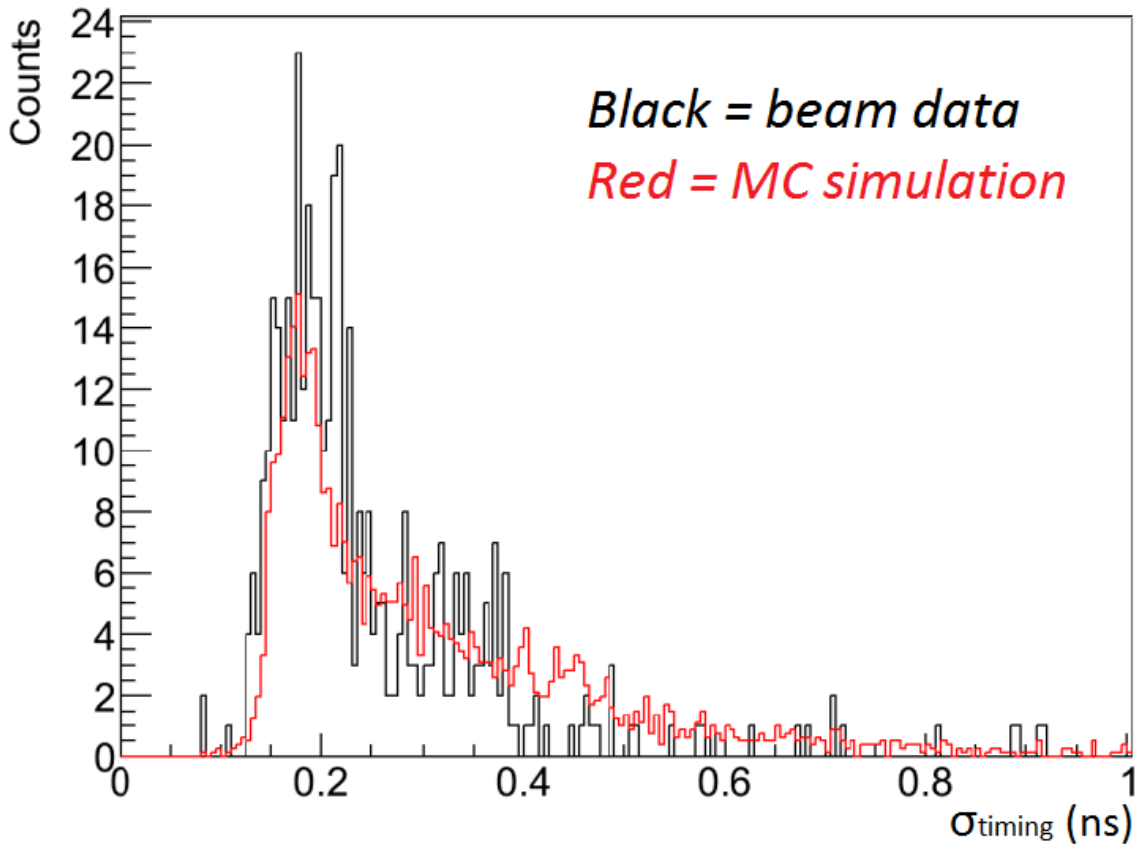

Figure 18: *Distribution of timing widths for all peaks in ring images compared to MC results where 100 ps contribution due to electronics has been added. Data and MC are in good agreement.*

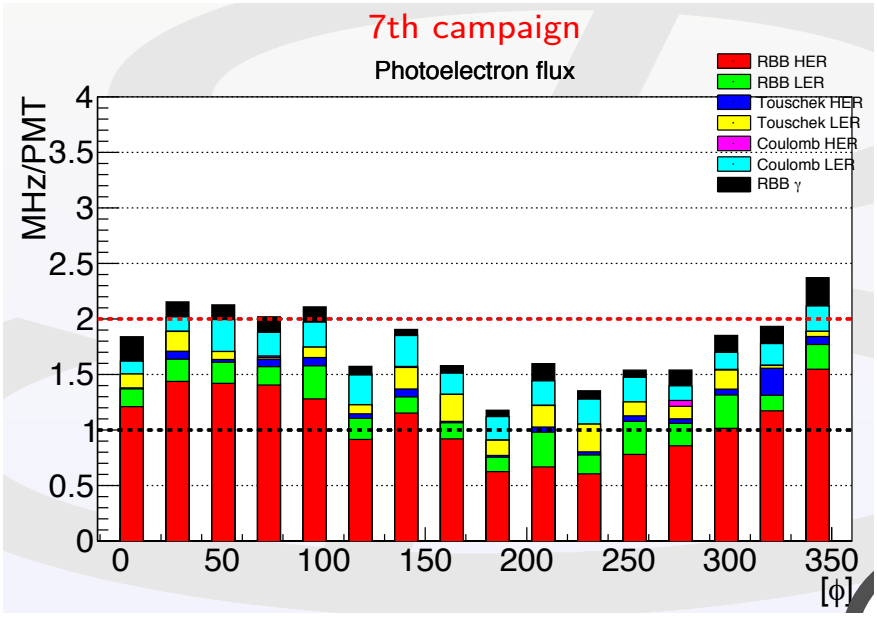

Figure 19: *Photo-electron rates from GEANT-4-based study of beam-related backgrounds. Six background sources are considered: Bhabha, Touschek, and Coulomb scattering, from both the HER and LER. The maximum tolerable rate is 1 MHz per PMT for conventional MCP-PMTs operating at nominal gain. Operation at lower than nominal gain may extend the lifetime by a factor of* ~ 2.

5.1.8 US Belle II Project Scope for the iTOP

The US Belle II Project has defined the requirements for the fused silica optics, and will procure the optical components along with suitable metrology services to perform quality assurance on the components, deliver the components to KEK, and perform acceptance tests. The US is also providing engineering support related to the module integration as both the optics and electronics for the iTOP are being provided by the US and hence the mechanical infrastructure and interfaces to these elements are most efficiently addressed by US collaborators.

The final assembly, testing, integration, installation and commissioning of the iTOP system is a Japanese responsibility. It is anticipated that significant US resources will contribute to those activities, but that these would be funded outside of the US Belle II Project. A separate resource-loaded work breakdown structure (WBS) has been created to capture that scope of work and to provide the appropriate linkages between the US Belle II Project effort and the integration effort, which must draw on the same resources and personnel, and in some cases occur in parallel.This delineation was chosen so that the completion of the US Belle II Project would not rely on contributions to the iTOP being provided by non-US institutions, e.g., Nagoya University, which will provide the MCP-PMTs, assembly fixtures, and bar boxes to house the optical assemblies.

5.2 Readout Systems for the Belle II Upgrade

5.2.1 Fast Timing with Waveform Sampling

Upgrade of the barrel PID device for the Belle II detector relies on precision time recording of individual Čerenkov photon signals. This places severe demands on the transit time performance of photodetectors that need to operate in a 1.5 T magnetic field, as well as on the precision with which photo-electron signals are recorded. A key to tackling this latter challenge in a compact and cost-effect package is the development of a low-power, GHz-bandwidth, high-performance waveform-recording [8, 9, 10] ASICs (Application Specific Integrated Circuits). In contrast to previous GHz-rate sampling devices, such as the ATWD [11], having GHz analog input bandwidth exploits the full benefit of GHz sampling. Such waveform sampling has been successfully flown twice on the ANITA long duration balloon payload [12, 13], where excellent timing performance (30 ps) provided sub-degree pointing resolution to an in-ice transmitter located more than 100 km away. Subsequently, this "oscilloscope on a chip" technology (see Fig. 20) has been adopted for readout of two Belle II sub-detectors.

This readout development is well-aligned with recent improvements in high-density, high precision timing photodetectors. Initial studies of integrated single-photon, high-precision timing devices were initiated as part of previous DOE Advance Detector Research (ADR) awards [14, 15]. Integration of sampling and digitization ASICs with both traditional vacuum-based (Micro-Channel Plate, Hybrid Photo-Diode) and solid state (Geiger-mode

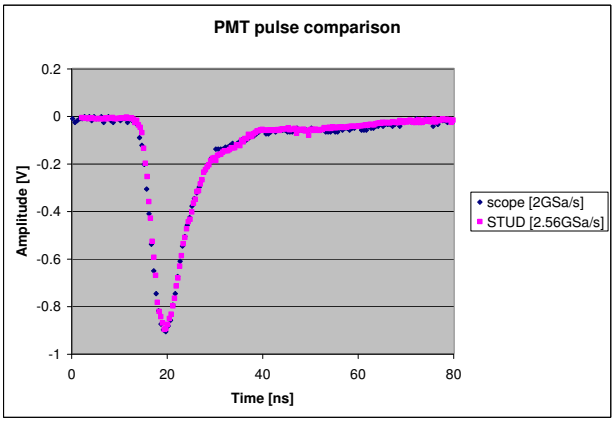

Figure 20: *Recording of a fast Belle fine-mesh Photo-Multiplier Tube (PMT) signal with a high-speed digital oscilloscope and a prototype sampling ASIC (SalSA Transient UHF Digitizer [STUD]).*

APD) photodetectors has been achieved. This integration promises lower cost, higher photon detection efficiency, and improved transit-time-spread performance.

5.2.2 US Role in Belle II Readout Systems

Subsequently detector readout systems were designed for the barrel iTOP particle identification detector and the endcap K_L/muon detector that take advantage of this enhanced technology. The high bandwidth and sampling rate, combined with the deep buffer depth, provide important performance advantages over previous Belle readout systems. The ASICs for the iTOP and K_L/muon systems are designated the IRS and TARGET, respectively. Though the specifications of the two ASICs differ slightly, both are descended from a first single-channel prototype of the buffered LABRADOR chip [16], a die photograph of which is shown in Fig. 21. This ASIC demonstrated excellent performance during testing and characterization. Sampling rates of over 5 GSa/s were measured, and single samples could be recorded with over 1.4 V dynamic range and 1.4 mV of noise; this corresponds to 10 real bits per sample. This prototype ASIC was used to instrument a 16-channel readout system that was tested with a prototype focusing DIRC detector at SLAC [17], where excellent beamtest results were obtained [18]. Moreover, a great benefit of the waveform digitizing technique was the ability to examine noise in the experiment in-situ, in real time. This study ultimately revealed why the timing resolution of the standard Constant Fraction Discriminator (CFD) electronics suffered significantly relative to test bench results. A 140 MHz radio-frequency (RF) signal was omnipresent and degrading the performance of these standard electronics. By having the raw waveforms the noise source can be digitally filtered and significantly improve the timing performance of this ASIC-based readout. This is a concrete example where having access to the waveforms has a significant advantage over standard CFD+TDC techniques. Further testing of this ASIC indicated that in the case where effects of photodetector

and time jitter could be removed by digitizing identical signals on two separate ASICs, 10 ps or better timing resolution could be obtained [19]. A later study using a slower sampling ASIC measuring pulses from two separate MCP-PMTs was able to obtain roughly 40 ps resolution [20], as shown in Fig. 22.

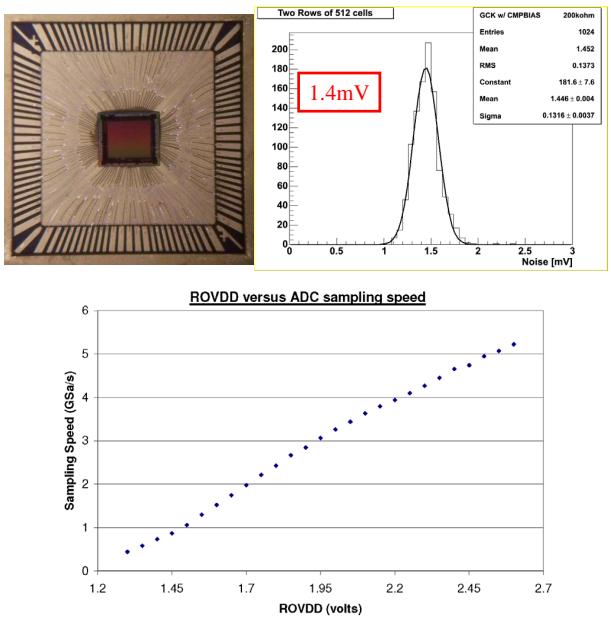

Figure 21: *Upper left, a die photograph of the first prototype buffered LABRADOR ASIC (3mm x 3mm), a single-channel demonstrator with 65,536 storage cells fabricated in the TSMC 0.25μm process [16]. At right and below are the measured noise and adjustable sampling speed, respectively.*

In order to build a feasible large-scale system, it is necessary to process, sparsify and collect the data generated by the devices mentioned above. Towards this goal, Hawaii has been collaborating with colleagues in Japan and China on the *Belle2link* [21] fiber-optic based upgrade of the data acquisition platform, named COPPER [22]. The High Speed Link Board (HSLB) is a generic FINESSE card [23] that will be utilized by most Belle II subdetectors to accept fiber-optic data from SRMs and transmit it to the DAQ system through the COPPER system. However, systems based on high speed waveform sampling may require more signal processing resources than an HSLB can provide. As such, a set of custom FINESSE cards are being developed. Prototypes developed at Hawaii utilize commercial DSPs to provide waveform feature extraction capability, and work is underway at PNNL to create the next revision of these FINESSE cards that replace the DSPs with the latest commercial SoC devices that integrate programmable logic and microprocessors into a single device. This new architecture is presented in Fig. 23, where prototypes of each of the components shown have been fabricated and large scale system performance tests have been carried out. Another potential solution under study is moving the signal processing upstream by adding additional FPGAs to the SRMs, which would allow use of the

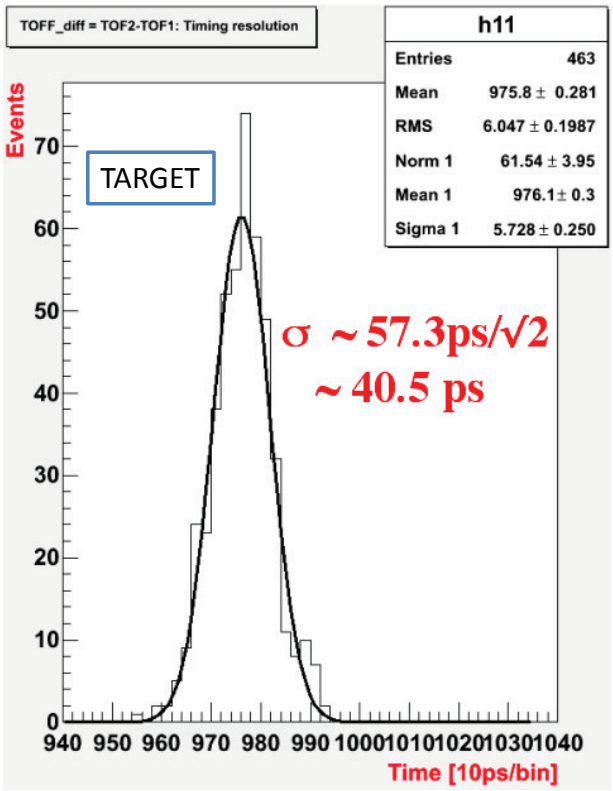

Figure 22: *Demonstration of the timing resolution obtained with a first-generation TARGET ASIC recording MCP-PMT signals. Since the plotted distribution represents the measured time difference between a pair of tubes, the single channel value is better by the statistical error [20].*

common HSLB interface on COPPER instead of custom FINESSE designs. Investigation of the requirements and merits of this solution is underway, but the analysis firmware design for the FPGAs is identical in either case.

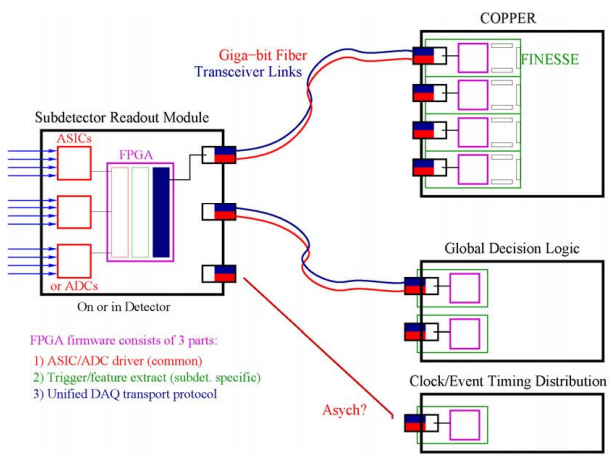

Figure 23: *Block diagram of the upgrade Belle II Trigger and DAQ system. Optical fiber links are used to convey trigger and front-end digitized data, significantly reducing the cable infrastructure of the upgraded Belle detector, as well as improving signal recording fidelity.*

Particle-identification Detector Readout: The barrel PID detector is composed of 16 barrel staves, each of which has an optical imaging plane viewed by a 2 row by 16 column array of Hamamatsu SL-10 micro-channel plate photomultipliers of 10 μm pore size. As each MCP-PMT has 16 anodes, a total of 512 channels of precision timing readout are required for each iTOP module, corresponding to 8,192 total subdetector channels.

Four DAQ and four trigger fiber-optic links (8x MCP-PMTs/fiber link) are used to read out each of the 16 barrel PID modules. A total subdetector count of 8,192 channels are instrumented with 1,024 IRS ASICs, 64 Subdetector Readout Module (SRM) fiber optic links, 32 FINESSE cards and 8 COPPER modules. A photograph of one of the integrated photodetector readout modules is shown in Fig. 24.

These modules have been used to digitize waveforms from SL-10 MCP-PMTs both in bench and beam tests. Example digitized signals are shown in Fig. 25. These test results are being used to improve techniques for calibration and waveform analysis, which will ultimately be implemented as real-time feature extraction on FINESSE cards.

Based upon detailed simulation studies, PID performance does not degrade significantly until single-photon timing resolutions are above 100 ps. This sets the threshold specification for electronics acceptance. Timing resolutions obtained from the existing prototype electronics modules currently safely meet this requirement, with measurements of roughly 25-40 ps for fixed-amplitude pulses from a pulse generator, and $\sim$ 60 ps for SL-10 signals obtained during single-photon laser testing, with the ranges reflecting varying conditions of temperature and signal-to-noise (SNR) ratio. These results are shown in Fig. 26.

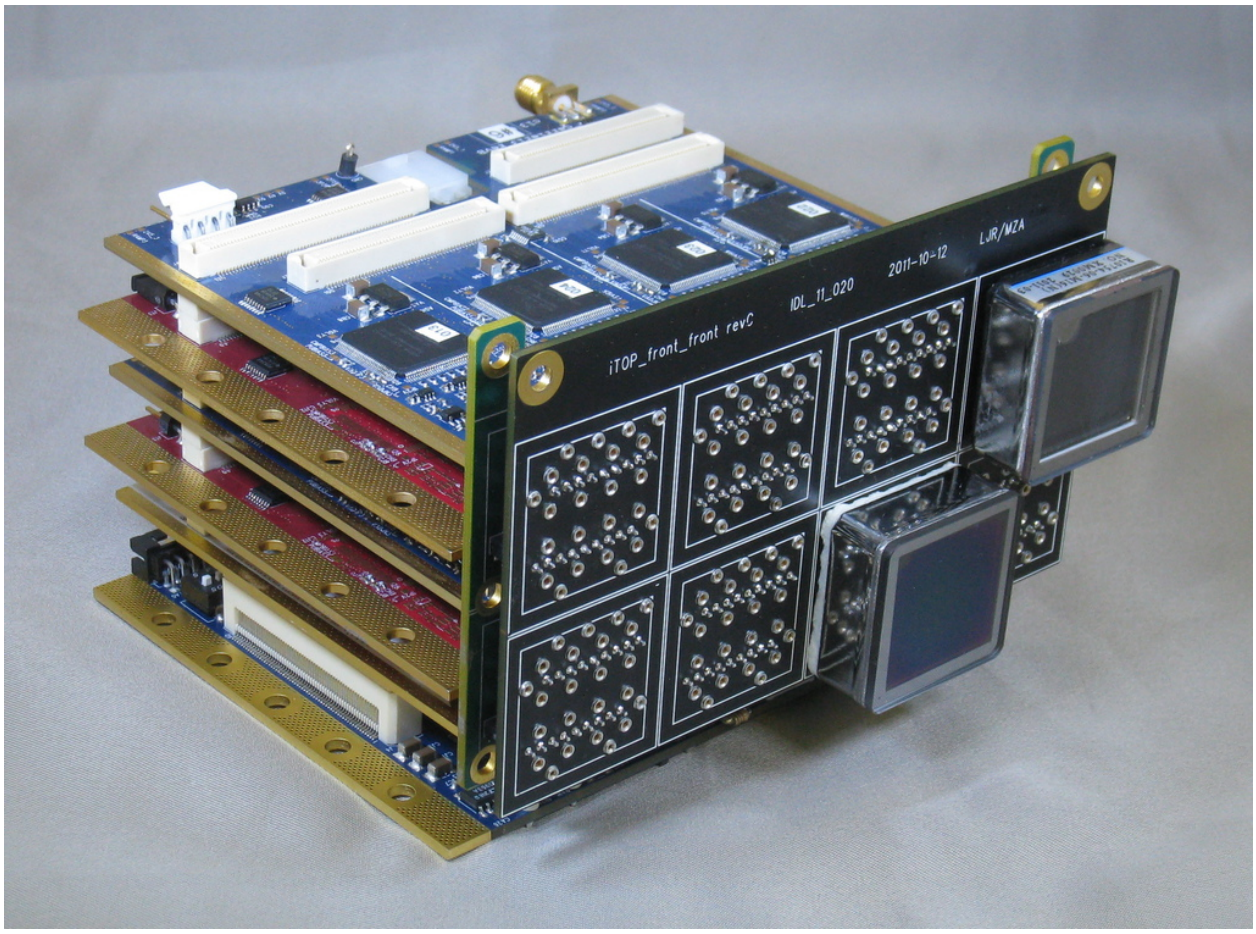

Figure 24: *Photograph of an integrated readout module. Eight 16-anode SL-10 MCP-PMTs are read out from a single "board stack" module, which contains 16 IRS ASICs, four per carrier card (upper four boards, colored red and blue).*

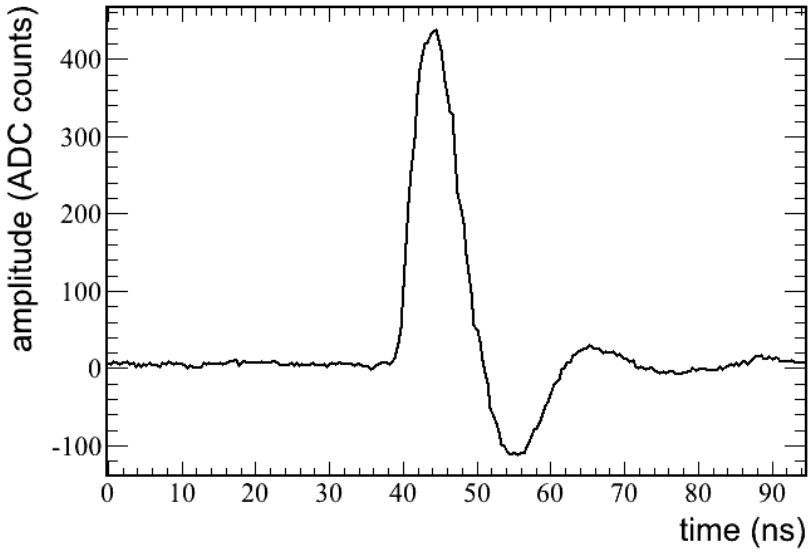

Figure 25: *Example of a shaped and digitized SL-10 signal obtained with a prototype iTOP SRM. The time base is approximated by assuming equally spaced samples at a nominal sampling rate of 2.7 GSa/s.*

The ultimately achievable timing resolution depends on a variety of factors, from jitter in common clock distribution to ASIC time-base performance and the algorithms used to extract time for candidate pulses. Next revision ASICs and SRMs include features to improve time-base stability, operate at higher sampling rates, and increase SNR by raising the available dynamic range and simultaneously reducing digitization noise. The expected result of these improvements leads to our design specification of 35 ps timing resolution. Due to environmental noise and other factors beyond our control, our objective specification is 50 ps for the electronics only.

The results of these test studies are being used to make improvements to the iTOP ASICs, printed circuit boards (PCBs), firmware, and calibration/analysis algorithms. A final IRS variant has been designed, based upon feedback from earlier bench and beam tests. A pre-production prototype run will be undertaken in the next calendar year based upon this ASIC and the final board stack configuration.

K_L/Muon Detector Readout: For the Belle II upgrade, the RPCs in the endcap and the first two layers of the barrel will be replaced with scintillators with embedded wavelength shifting fibers and solid state photodetector readout. Initial tests of these proposed optical sensors with prototype waveform sampling electronics have demonstrated excellent single and multi-photon peak resolution. The rest of the architecture needed for the scintillator/fiber KLM readout is almost identical to the RPC KLM readout. Due to the difficulty of accessing the KLM modules, only amplifiers will be installed inside the detector modules, and the readout electronics will be mounted just outside. These 16,800 channels of scintillator readout are instrumented with 1,120 TARGET ASICs on 112 SRMs and read

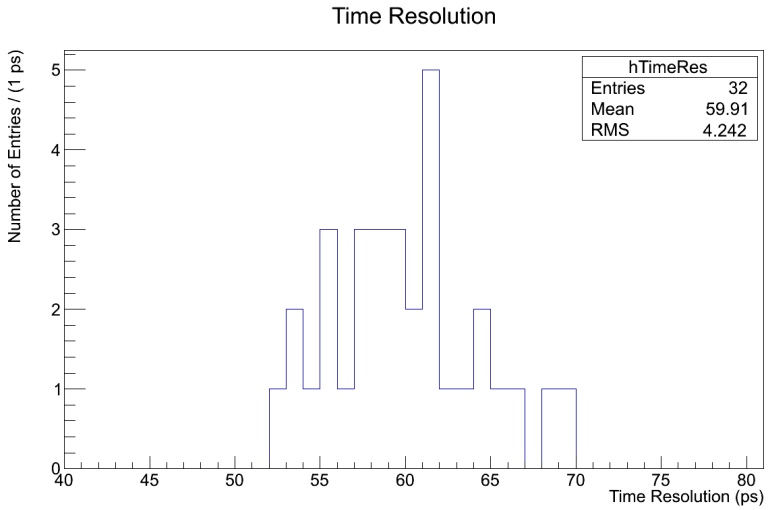

Figure 26: *Ensemble of post-calibration timing resolutions for single photo-electron laser signals from an SL-10, digitized by prototype front-end electronics based on the IRS ASIC. Each entry in the histogram corresponds to a timing resolution from a specific IRS ASIC.*

out by 28 FINESSE cards and 7 COPPER modules. A prototype KLM SRM is shown in Fig. 27. As with the IRS ASIC, a pre-production prototype design of the TARGET ASIC has been designed and will be integrated into pre-production readout modules early in the next calendar year.

Although the RPCs in the barrel region will be retained (with exception of the first couple of layers, which will be replaced with plastic scintillator as described in Section 5.3), their readout will be upgraded. Given the large signal amplitude and only modest time resolution required, no front-end ASIC is needed. Rather, the signals are discriminated using a commercial, low-cost comparator and time-encoded by the field programmable gate array (FPGA) in Fig. 23, with again the rest of the readout infrastructure being common.

Each RPC superlayer will be served by one Front-End Board (FEB) which has one connector each for both groups of 48 channels of the superlayer with opposite polarity. Since the inner two superlayers of the RPC system will be replaced with scintillators, the system will consist of 13 FEBs per crate to serve one RPC octant. There are 16 octants in the system which are correspondingly served by 16 crates which will be reused from the previous system. The analog signal cables that are already installed will also remain in place. The FEB will have a sensitivity of better than 4 mV to the incoming signals and thresholds up to 100 mV can be set for each individual channel via a 7 bit DAC. Using two times the Belle II clock, time to digital conversation will have a resolution of about 4 ns. The TDC will be implemented using a Spartan-6 FPGA and all FEB in a crate will transfer timestamps to a concentrator board in the same crate using a fast point-to-point connection via the backplane of the crate. The current FEB and concentrator board conceptual designs are shown in Fig. 28. Signals from the FEBs are processed on the concentrator board in a Virtex-6 FPGA using coincidences between r- and ϕ- planes to suppress background.

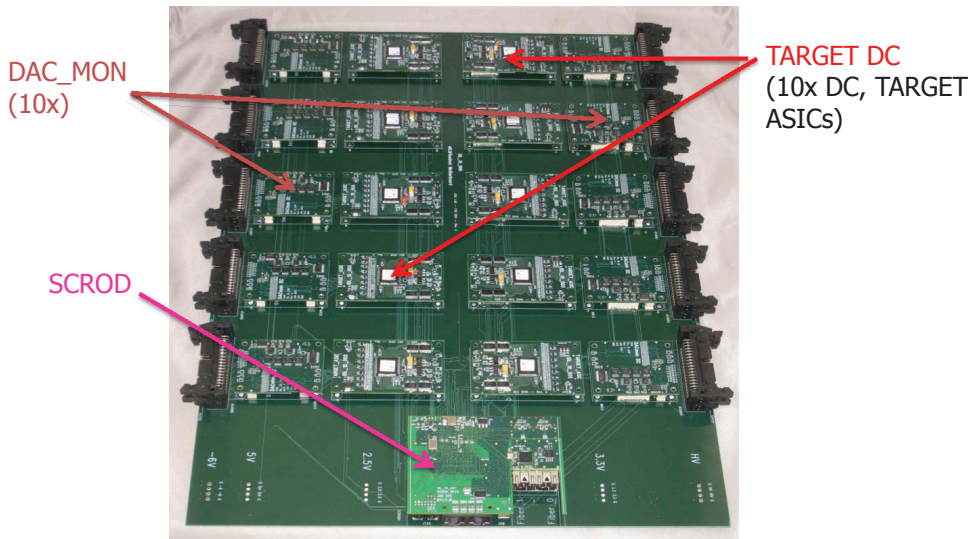

Figure 27: *Photograph of a KLM Subdetector Readout Module (SRM). In the endcap each module read out a KLM layer quadrant, consisting of 150 scintillator strips, arrayed as 75 in x and 75 in y. Each TARGET reads out a group of 15 strips and provides trigger primitives. Control and readout is provided by a SCROD digital controller board that is common to both iTOP and KLM readout. To allow ease of deployment the module will be repackaged as a 9U card, which requires moving connectors and merging the DAC control (DAC_MON) and TARGET ASIC daughtercards, a prototype of which is under test now.*

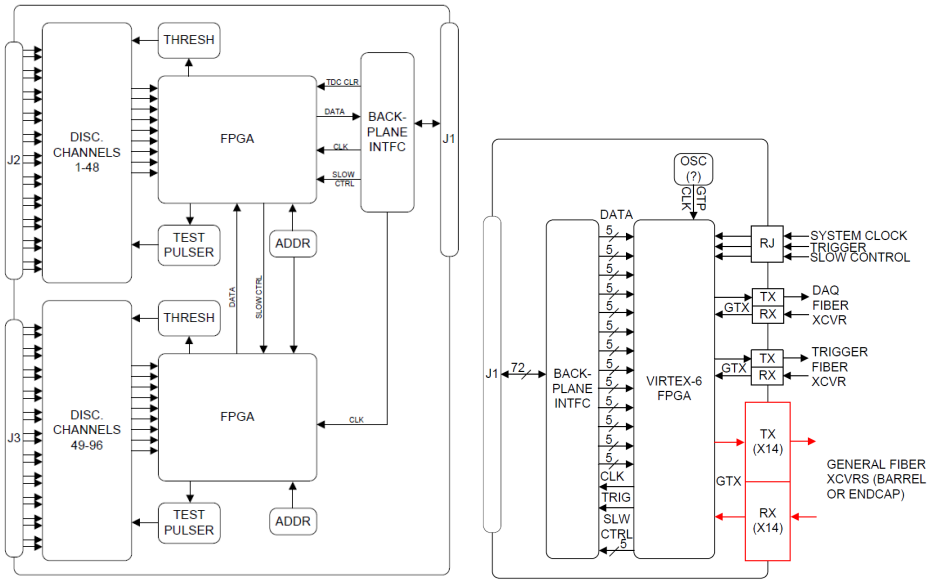

Figure 28: BKLM RPC FEB (left) and Concentrator board (right) conceptual designs. The concentrator board has additional fiber inputs for the scintillator layers of the barrel and endcap.

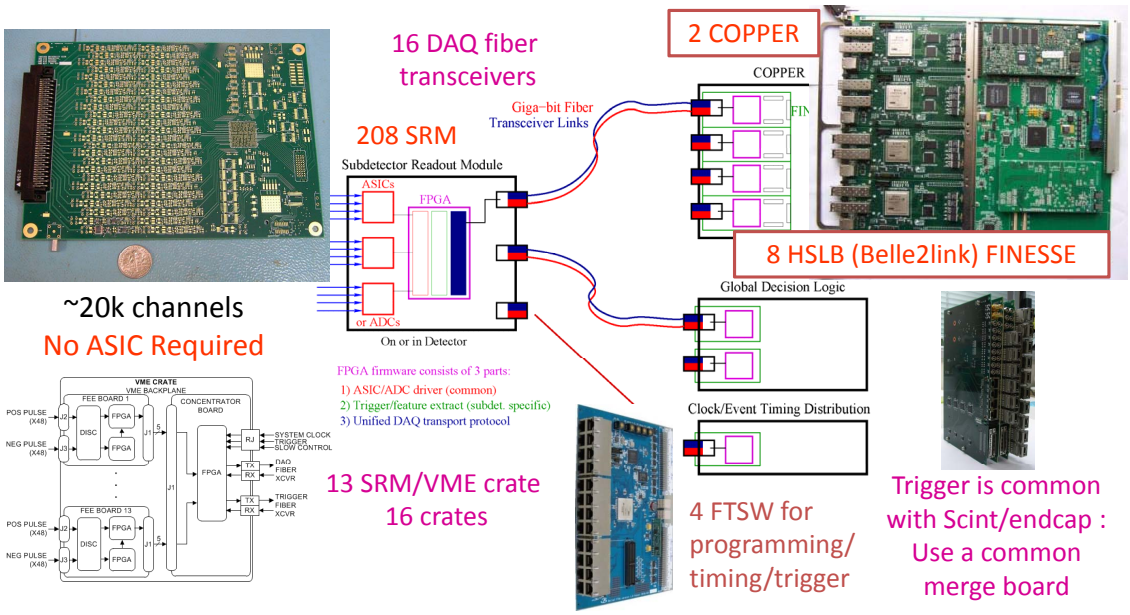

Figure 29: *Overview of the KLM RPC-based readout system, with each of the major components within the Belle II DAQ architecture indicated. Due to the digital nature of the output signal from the RPC detectors, no waveform sampling ASIC is used. On-chamber discriminator outputs are time-stamped with FPGA-based TDCs on the SRMs, 13 of which are located in a single crate and read-out over the VME backplane to the data concentrator card, which provides the Belle2link and trigger interfaces.*

The FPGA will also handle the communication with the Trigger and DAQ system. From simulation it was estimated that the latency through FEB and concentrator board to the trigger link output will be less than 1.5 μs. In addition it was decided that the concentrator board will also be used for the scintillator layers in the barrel and endcap. Therefore an FPGA is used with sufficient transceivers to connect fiber links from these detectors. The barrel scintillator layers will be read out by the concentrator board that is also reading out the RPC layers in the same octant. The endcap layers will be read out separately requiring a second FPGA design which will be related to the design for the barrel.

A Time-to-Digital Conversion algorithm inside the FPGA records the times of individual threshold crossings with nanosecond-level precision. Given the relatively low hit-rate in the barrel, one DAQ and one trigger fiber link per on-detector readout crate will be used. A crate services each detector octant, at both detector ends, for a total of 16 crates. Each crate communicates over the *Belle2link* to 2 COPPER backend readout modules.

5.2.3 US Belle II Project scope for the Readout Systems

The US Belle II Project scope includes the design, fabrication, testing, delivery to KEK, and acceptance testing of the readout systems for the iTOP and the KLM detector systems.

Integration of the readout systems into the iTOP and KLM detector systems, as well as installation and operation of the system during commissioning of the Belle II detector is outside the scope of the US Belle II Project. It is anticipated that significant US resources will contribute to those activities, but that these would be funded outside of the US Belle II Project. A separate resource loaded WBS has been created to capture that scope of work and to provide the appropriate linkages between the US Belle II Project effort and the integration and commissioning effort which must draw on the same resources and personnel and in some cases occur in parallel. This delineation was chosen so that the completion of the US Belle II Project is not reliant on the contributions to the iTOP and KLM detector systems being provided by other institutions or tied to the schedule of the SuperKEKB accelerator.

5.3 Upgrade of the K_L/muon System

5.3.1 US Role in the KLM System Upgrade

The KLM system upgrade is separated into two parts: the endcaps and the barrel. The endcap upgrade is being managed by the Institute for Theoretical and Experimental Physics (ITEP) in Moscow. Virginia Tech is leading the effort to upgrade the barrel. Virginia Tech designed, built and commissioned the RPC-based barrel KLM system for the Belle detector, and therefore has the requisite knowledge and experience to do so again for the replacement of the two innermost barrel detector layers with a scintillator-based design.

Virginia Tech will also manage the effort to commission the unified high voltage system that is common to both the barrel and the endcaps.

5.3.2 RPC Performance Limitation

The resistive plate counters used in the Belle KLM (K_L meson and muon detector) are rate-limited due to the very high resistivity ($\sim 10^{12}\,\Omega\cdot\mathrm{cm}$) of the glass electrodes: it takes several milliseconds for the gas-gap electric field to recover in the vicinity of a streamer discharge. These discharges are most often initiated by stray neutrons that arise from photoproduction in the beamline structures following Touschek scattering in a positron beam bunch or radiative Bhabha scattering (Fig. 30). In the innermost layers, some discharges are also induced by the tails of electromagnetic showers that leak out of the calorimeter.

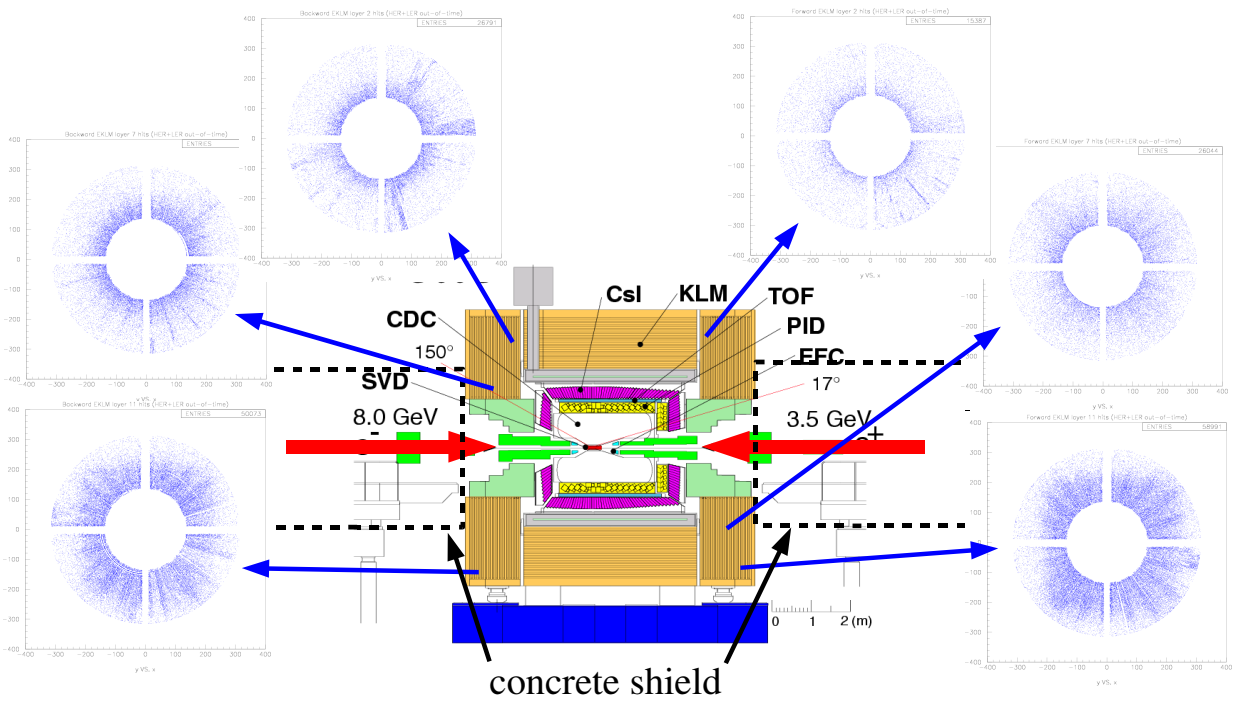

Figure 30: *Background hits in three typical superlayers of the backward (left) and forward (right) endcap KLM with $I_{e^+} = 1.5\,\mathrm{A}$ and $I_{e^-} = 1.0\,\mathrm{A}$. The hits in the outermost layers delineate the rectangular concrete shield that surrounds the beam lines, within which the exposure to neutrons is highest.*

Extrapolations from Belle/KEKB operating conditions to the Belle II/SuperKEKB environment have concluded that the dominant background in the barrel KLM is expected to be from neutrons associated with the beams (Touschek scattering in the positron beam, spent electrons striking beamline structures, radiative Bhabha scattering, and the like) with a neutron flux of $\mathcal{O}(1\,\mathrm{kHz/cm^2})$ in the innermost barrel detector layer, as determined from detailed simulations of these processes in the Belle II software framework BASF2 using the most up-to-date detector and beamline geometry that includes all background-mitigating structures and materials. The neutrons are typically quite soft and tend to peak in the forward direction (Fig. 31). Table 6 lists for each barrel KLM layer the incident neutron flux as well as the expected hit rate per unit area and the efficiency of the RPCs. The RPC

hit rate is determined by the fraction (1 in 140) of neutrons that initiate a discharge in an RPC. The efficiency of the RPCs as a function of the ambient hit rate is then calculated from the Belle measurements in Fig. 5.3.2, where the barrel RPCs exhibit an efficiency drop with ambient hit rate of $-0.05/(\mathrm{Hz/cm}^2)$. In the hybrid configuration, the neutron flux is suppressed by a factor of four in RPC layer 2 due to absorption in the plastic in layers 0 and 1. (The neutron flux appears elevated in the scintillator layers, but this is an artifact due to multiple counting from inelastic scattering in the plastic.)

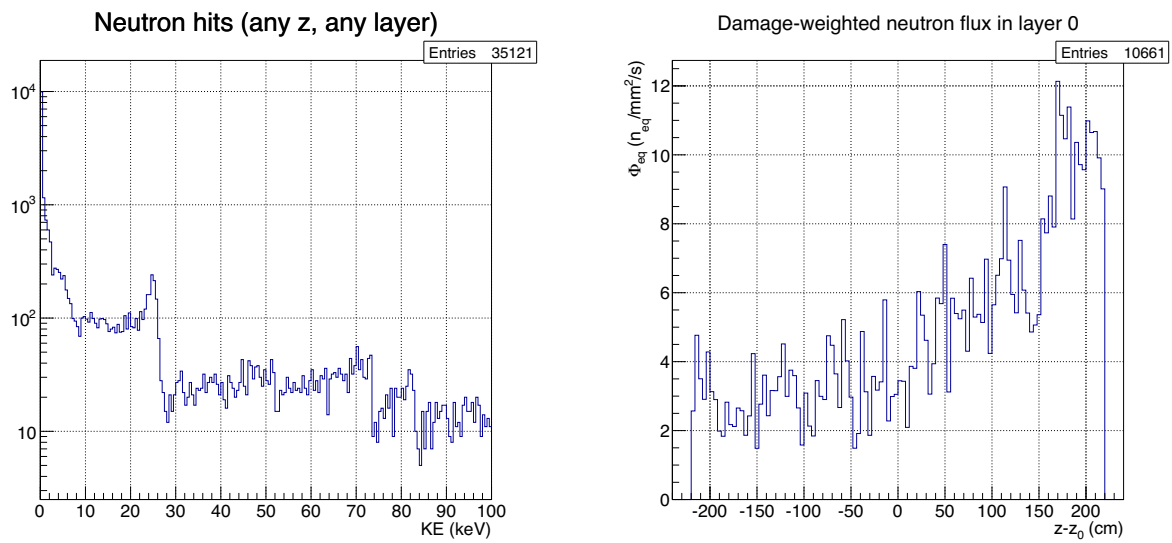

Figure 31: *Left: Kinetic energy of background neutrons originating from beam interactions. Right: Damage-weighted neutron flux entering the barrel KLM as a function of axial position (where $z_0 = 47$ cm is the location of the e^+e^- interaction point).*

5.3.3 KLM Upgrade Strategy

The endcap RPCs and the innermost two layers of the barrel RPCs are replaced with a scintillator-based design that will provide comparable—or better—information for muon tracking and K_L meson detection. The scintillators can operate efficiently at background rates at least two orders of magnitude larger than those in Belle, well above the rates expected at the SuperKEKB design luminosity.

There is no marked difference in these performance measures between RPCs and scintillators. However, the scintillators have a physics advantage over RPCs for K_L mesons in two respects: they permit a rough energy measurement of the K_L hadronic shower's energy and they allow the relaxation of the minimum requirement for the K_L definition from two detector layers to one, thereby increasing the K_L detection efficiency without an appreciable increase in the K_L fake rate. The muon detection efficiency and hadron fake rate measured by the RPCs are illustrated in Fig. 33, while the K_L meson detection efficiency and angular resolution expected with scintillators in the endcap KLM are shown in Fig. 34.

	Belle configuration			Belle II Hybrid configuration		
Layer	Neutron flux (Hz/cm^2)	Hit rate (Hz/cm^2)	Efficiency	Neutron flux (Hz/cm^2)	Hit rate (Hz/cm^2)	Efficiency
0	1974	14.2	0.13	13743	—	1.00
1	1418	10.2	0.39	4275	—	1.00
2	890	6.4	0.62	264	1.9	0.90
3	500	3.6	0.78	139	1.0	0.94
4	306	2.2	0.86	134	0.6	0.96
5	181	1.3	0.91	85	0.2	0.98
6	111	0.8	0.94	59	0.2	0.98
7	67	0.5	0.97	25	0.2	0.98
8	36	0.3	0.98	18	0.1	0.99
9	18	0.1	0.99	14	0.1	0.99
10	10	0.1	0.99	8	0.1	0.99
11	8	0.1	0.99	4	0.0	0.99
12	5	0.0	0.99	3	0.0	0.99
13	2	0.0	0.99	3	0.0	0.99
14	2	0.0	0.99	3	0.0	0.99

Table 6: *Neutron flux, hit rate per unit area, and RPC efficiency in each layer of the barrel KLM from simulation of beam-induced neutron backgrounds at the SuperKEKB design luminosity. The Belle configuration has RPCs in each layer, while the Belle II Hybrid configuration replaces the RPCs in the two innermost layers with scintillators and neutron-absorbing sheets.*

The decision to replace only the two innermost layers of the barrel KLM with scintillators is based on three considerations. (1) The physics performance (measured by muon identification and K_L detection, which depend on the detector efficiency) is uncompromised relative to that of a full replacement. According to Table 6, the detection efficiency of each layer of the barrel KLM in this hybrid configuration is 90% (in layer 2) or higher at the design luminosity. (2) The cost of the full replacement (including new sensors and electronics) is more than an order of magnitude higher than that of the hybrid configuration. (3) The logistical difficulty in replacing RPCs with scintillators is much greater for layers 2–14. The structural bracing (steel kites and radial bars) at each end of the barrel would have to be removed temporarily during the replacement operation for these outer layers and more of the services for the inner detectors would have to be dismantled temporarily during the full barrel KLM upgrade.

Nevertheless, after a few years of operation, it might be necessary to replace the remaining barrel RPCs with scintillators, perhaps due to intolerably high backgrounds and/or the end of the "natural" lifetime of the RPCs (which have shown no signs of aging over the past

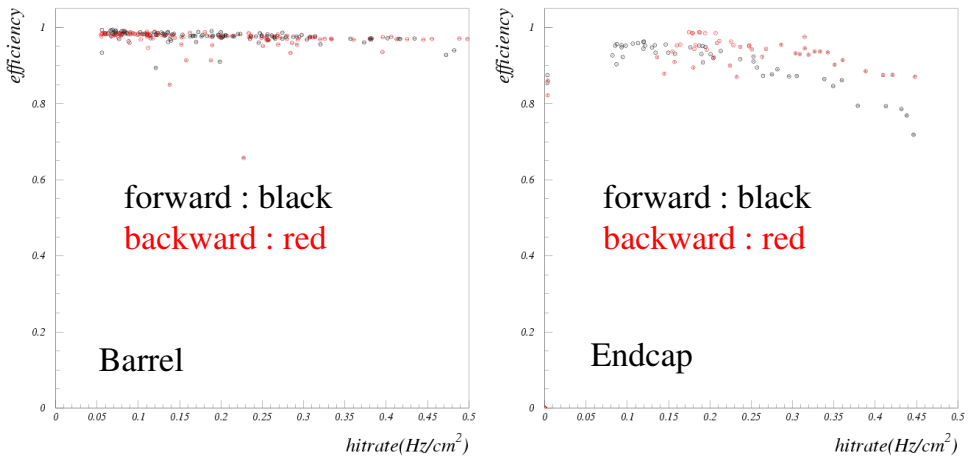

Figure 32: *Dependence of RPC superlayer efficiency on ambient hit rate (left for barrel, right for endcap).*

decade of operation). This upgrade would be a major disruption that involves the rollout of the Belle II detector and the temporary dismantling of the SuperKEKB accelerator near the interaction point, so it could be considered only in conjunction with a six-month shutdown for an anticipated replacement or upgrade of the vertexing detectors. This full barrel KLM upgrade would have to be fully planned and executed well in advance (by at least two years) of the installation time so that the newly fabricated detector modules would be stored in the detector hall and available for installation at the start of the extended shutdown.

5.3.4 Barrel KLM Modules

Two rectangular detector modules are placed in each octant of the Belle II barrel KLM (Fig 35). Within each module, two orthogonal layers of scintillator strips are placed inside an aluminum frame made of extruded U-channels. The module dimensions and strip counts are given in Table 5.3.4. The module is enclosed by a protective aluminum sheath. There is almost no magnetic field within each barrel module since the interleaved iron plates of the barrel yoke confine the solenoid's return field to their unsaturated interior.

Photons from each scintillator strip (Fig. 36) are collected by an embedded wavelength-shifting optical fiber and detected by a Multi-Pixel Photon Counter (MPPC)—an avalanche photodiode operated in Geiger mode (Fig. 37). The MPPC, which is immune to a magnetic field of up to 1.5 T, is glued directly to the scintillator strip at one end of the WLS fiber. The fiber's other end is mirrored. No intermediary clear optical fibers are used. the detector module, with 15 channels per card and a voltage gain of roughly 10, provide power at ~ 70 V to each MPPC (externally tunable per MPPC) and deliver the preamplified MPPC signal to the front-end readout electronics (FEE; see Fig. 27) mounted on the periphery of the magnet yoke. For each detector module, seven pairs of twist-n-flat ribbon cables, each between 6

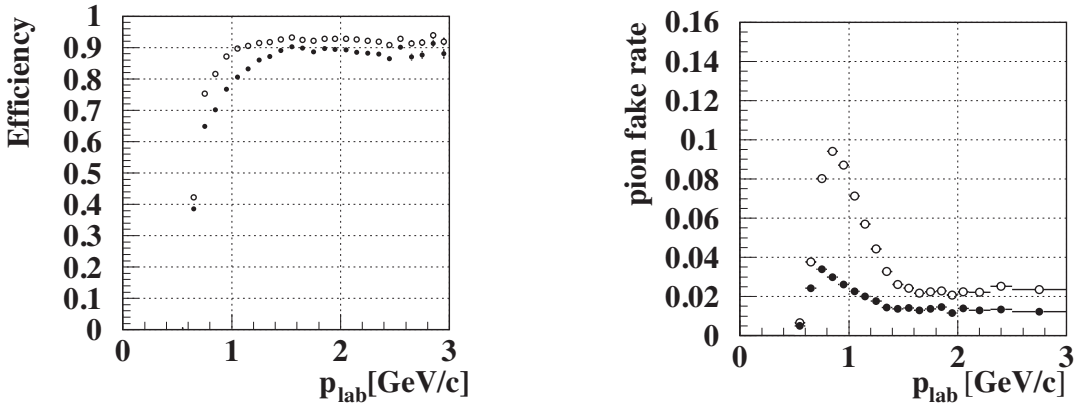

Figure 33: *Muon identification efficiency (left) and pion fake rate (right) in* $e^+e^- \to e^+e^-\mu^+\mu^-$ *events in the Belle RPCs for a loose (open circles) and tight (solid circles) definition of a muon.*

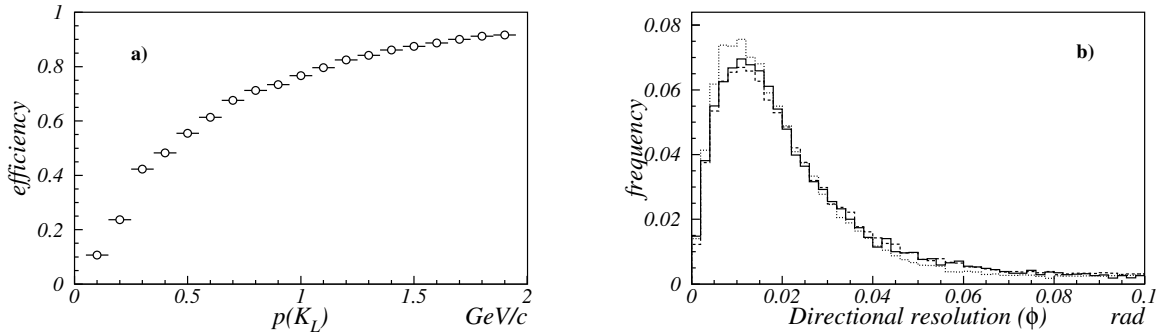

Figure 34: *K_L identification efficiency (left) and directional resolution (right) expected in the endcap KLM instrumented with scintillators.*

and 18 meters long, run between the module's service panel and the external FEE card; one cable in each pair carries power from the FEE to the MPPCs while the other cable carries signals from the MPPCs to the FEE.

5.3.5 Scintillator extrusions

Individual scintillator strips are co-extruded with a TiO_2 reflective coating and a central 2.5-mm diameter bore into which the 1.2-mm diameter WLS fiber is placed. The extruded strips are cut to length during the manufacturing process.

The extrusions are performed at the FNAL-NICADD facility[24] at Fermilab, jointly operated by Fermilab and the Northern Illinois Center for Accelerator and Detector Development at Northern Illinois University. The die for this extrusion already exists, and is similar to the one illustrated in Fig. 38 (which produces a co-extruded $1.9 \times 1.5\,\mathrm{cm}^2$ scintillator strip with a central bore).

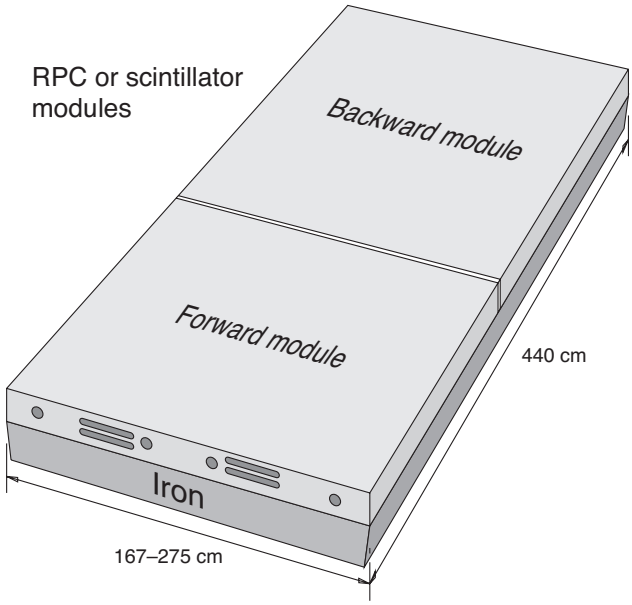

Figure 35: *Isometric view of one octant layer of the barrel KLM, showing the two detector modules. The forward module is along the $+z$ axis in the Belle II coordinate frame; the e^+e^- interaction point at $z = 0$ is about 47 cm into the backward module, measured from the intermodule boundary.*

Our scintillator strips are nearly identical to those produced at NICADD in 2007–2008 for the T2K experiment's INGRID neutrino beam monitor[25] at J-PARC in Japan. The scintillating material consists of polystyrene (Dow Styron 663 W) doped with PPO (1% by weight) and POPOP (0.03% by weight). The white reflective coating consists of 15% TiO_2 (rutile) in polystyrene. In addition to its reflective property, this rugged coating enables the direct epoxying of each strip to the polystyrene substrate to form a strip layer.

In the NICADD production facility, polystyrene pellets are dried in a nitrogen atmosphere and then conveyed to a gravimetric feeder. The dopant mixture enters via a separate gravimetric feeder that is precisely and reliably surrogated to the pellet feeder to deliver a constant mixing ratio. A twin-screw extruder melts and mixes the pellets and dopants. Polystyrene and TiO_2 pellets are fed into a separate co-extruder to form the reflective coating. The continuously extruded hot strip enters a cooling tank, where it is formed into its final shape, then cools more in water and air. The strips are then cut to length.

The NICADD facility operates at a nominal rate of 75 kg/h. A higher extrusion rate of up to 100 kg/h is possible, but increases the challenge of cooling down the extruded material. At the nominal rate, the 3700 kg of raw material, including production waste, needed for the barrel KLM upgrade will require 50 hours of production. This is inflated to 200 hours to include preparation time, production, quality control, and down time.

Quality Assurance and Quality Control procedures are already established at the production facility to check the cross-sectional dimensions and the light yield. Using a short

Standard-size modules

Layer	Module Count	Height (mm)	z Length (mm)	ϕ Width (mm)	# of z Strips (Cards)	# of ϕ Strips (Cards)
0	16	37.7	2211.1	1541.8	54 (4)	37 (3)
1	16	37.7	2211.1	1715.8	54 (4)	42 (3)

Chimney-sector modules

Layer	Module Count	Height (mm)	z Length (mm)	ϕ Width (mm)	# of z Strips (Cards)	# of ϕ Strips (Cards)
0	2	37.7	1581.1	1541.8	38 (3)	37 (3)
1	2	37.7	1581.1	1715.8	38 (3)	42 (3)

Table 7: *Dimensions and strip (preamplifier-carrier) counts for the scintillator modules in the innermost layers of the barrel KLM. The two chimney-sector modules are shortened by 630 mm along the length (z) to accommodate the solenoid's liquid helium chimney.*

(15 cm) QC sample that is cut once every 20 meters or so, the dimensions are checked with a caliper and the light yield is tested with a calibrated radioactive source.

After delivery to Virginia Tech, the scintillators are unpacked and sorted by length. At this time, each scintillator's central bore is cleaned mechanically using a pipe cleaner-like device to gently scrub away residue that condensed on the inner surface during the extrusion–cooling process.

The specifications for the extruded scintillators are:

- Cross-section: (40.0 ± 0.1) mm base and (10.6 ± 0.1) mm height, including the TiO_2 coating
- Length uniformity: 5% tolerance at NICADD, to be cut to 1% tolerance later
- TiO_2 thickness: $(300 \pm 50)\,\mu$m on the top and bottom surfaces and $(150 \pm {}^{50}_{0})\,\mu$m on the sides
- Light output uniformity: 5% variation, measured to within 1%.
- Light output stability: assumed decrease of no more than 3% per year for at least 10 years (based on historical performance).
- Attenuation length: 5 cm or longer with the TiO_2 coating.

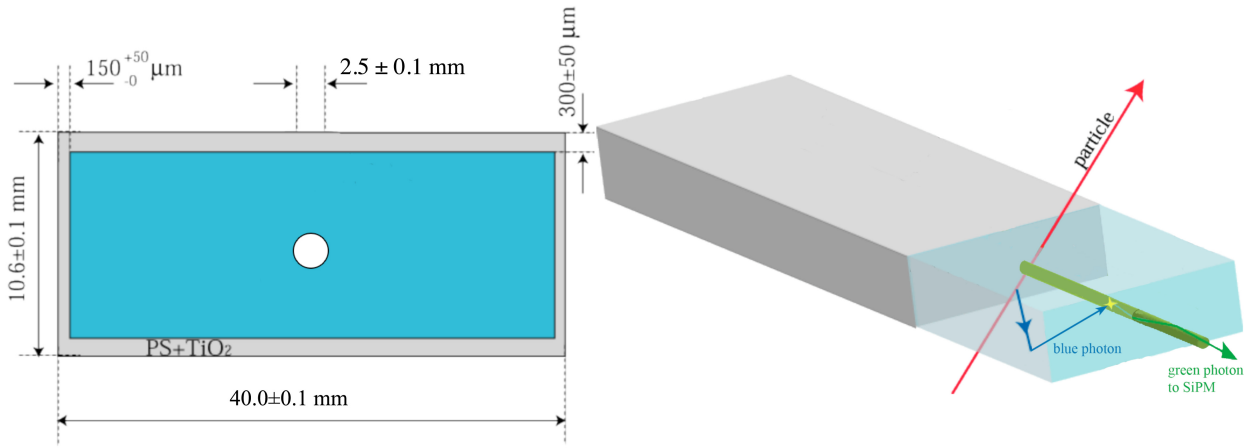

Figure 36: *Cross section of one extruded scintillator strip with an embedded WLS fiber.*

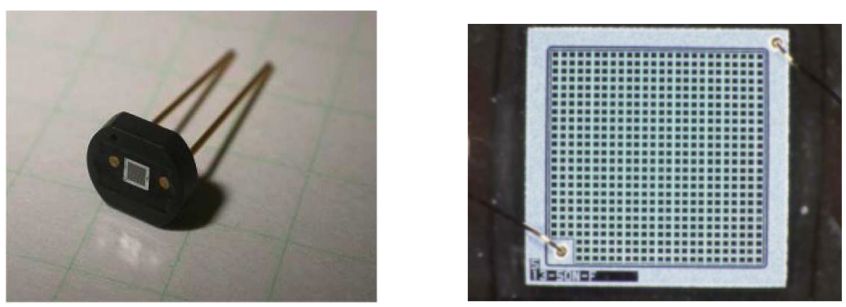

Figure 37: *Left: Hamamatsu S10362-13-050C MPPC. Right: Closeup of the active surface, showing 667 pixels, each* $50 \times 50\,\mu m^2$ *in area, in a* 26×26*-pixel array.*

5.3.6 Wavelength-shifting fibers

Belle II has selected Kuraray Y11(200)MSJ wavelength-shifting plastic scintillating fiber to extract the signals from the barrel (and endcap) KLM scintillators. These are polystyrene-core fibers ($n = 1.59$) doped with Y-11 blue-to-green wavelength-shifting dye at 200 ppm (Fig. 39). Each fiber has two coaxial claddings: an inner layer of polymethylmethacrylate ($n = 1.49$) and an outer layer of fluorinated polymer ($n = 1.42$), each with a radial thickness of $39\,\mu$m. The numerical aperture is 0.72 and the trapping efficiency is 5.4%. The S-type fiber to be used is mechanically stronger against cracking during handling (bending, for example) but at the cost of $\sim 10\%$ shorter attenuation length (~ 6.8 m for our fiber). The minimum bending diameter for our 1.2 mm diameter fibers is 0.24 m; however, our fibers are installed with no bend.

Each fiber is cut to length (with a few centimeters of excess) from the spool and then inspected for surface defects. One end is immediately polished and then epoxied into a custom noryl ferrule (part of a fiber-MPPC holder produced by ITEP and delivered to

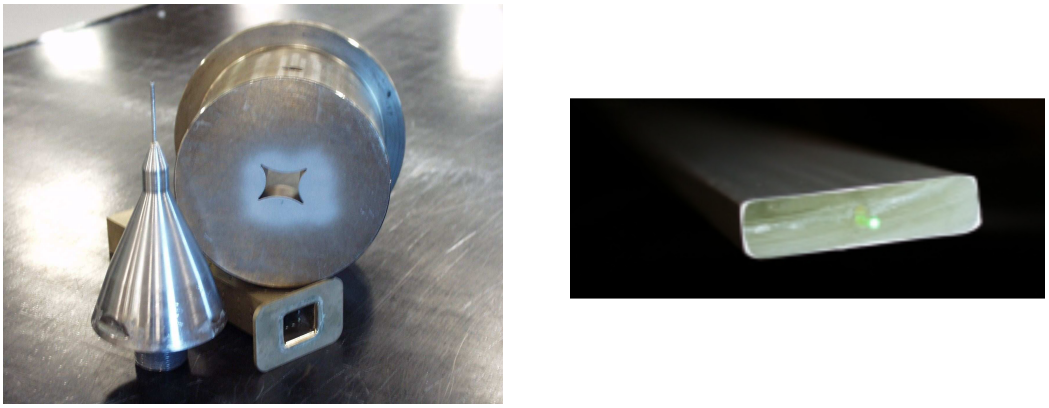

Figure 38: *Left: Extrusion die for* $1.9 \times 1.5\,\mathrm{cm}^2$ *scintillator. Right:* $4.0 \times 1.0\,\mathrm{cm}^2$ *extrusion with WLS fiber.*

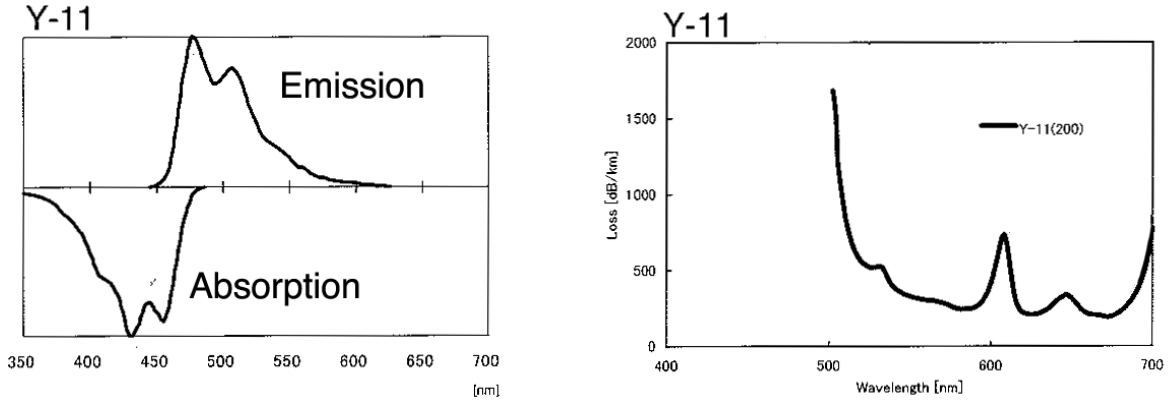

Figure 39: *Left: Y11 WLS fiber absorption and emission curves. Right: Y11(200 ppm) WLS fiber attenuation (for non-S-type fiber).*

Virginia Tech). Figure 40 shows one end of the fiber epoxied to the ferrule half of this custom-made coupler. The fiber is positioned so that $200\,\mu$m protrudes beyond the coupler surface. This increases by 40% the fraction of light delivered to the photosensor that is housed in the other half of the coupler as shown in Fig. 41. After the fiber is inserted into the scintillator strip's central bore and the noryl holder is epoxied to the end of the strip, the fiber's far end is cut to the strip's length, polished, and mirrored using Silvershine (an aluminum-loaded pigment provided by ITEP). This is much cheaper and simpler to do than the treatment applied in INGRID and Minerνa (ice-polishing, aluminum sputtering, coating with epoxy) and has been demonstrated to be equally effective in bench tests at ITEP and Virginia Tech. Finally, the MPPC, in its mating coupler, is attached to the fiber's ferrule (Fig. 42).

The WLS fiber is inserted into the strip's central bore without any optical gel. In our R&D studies with Bicron 630, the gel's viscosity was too high to permit the reliable filling of the

bore without air bubbles and/or damage to the WLS fiber during its insertion. Nevertheless, the light delivered to the photosensor in this "dry-insertion" configuration is well above the quality-acceptance threshold (specified by the number of fired MPPC pixels).

Each strip-fiber-MPPC assembly is then inserted into a cosmic ray test stand, wherein the light yields for cosmic rays passing through the near and far ends are measured after tuning the MPPC operating voltage to its optimal point in the range of 70.5–71.5 V. If the absolute light yields (measured in number of fired MPPC pixels) or the far/near ratio are below the acceptance thresholds, the strip-fiber-MPPC assembly is culled. If the MPPC's intrinsic noise rate at its optimal operating voltage is too high, it is replaced with another MPPC. The accepted strip-fiber-MPPC assemblies are stacked in a holding rack, sorted by length.

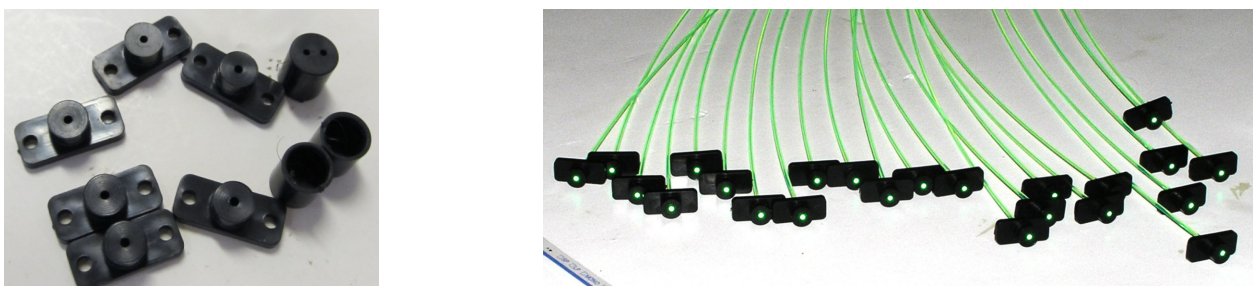

Figure 40: *Left: Fiber-to-MPPC ferrules and couplers. Right: WLS fibers epoxied to ferrules.*

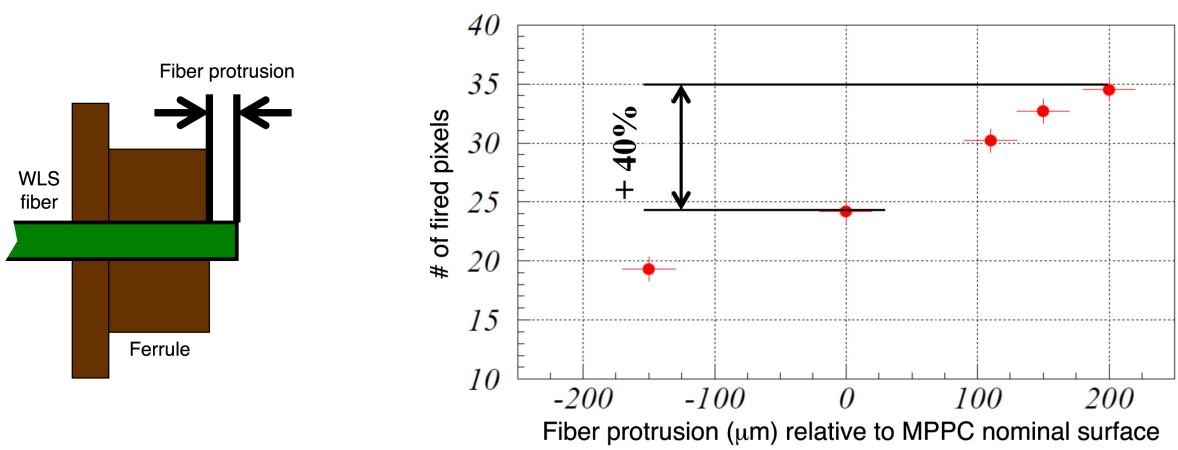

Figure 41: *Left: Schematic of WLS fiber protrusion beyond ferrule surface. Right: Light collection by MPPC vs protrusion distance.*

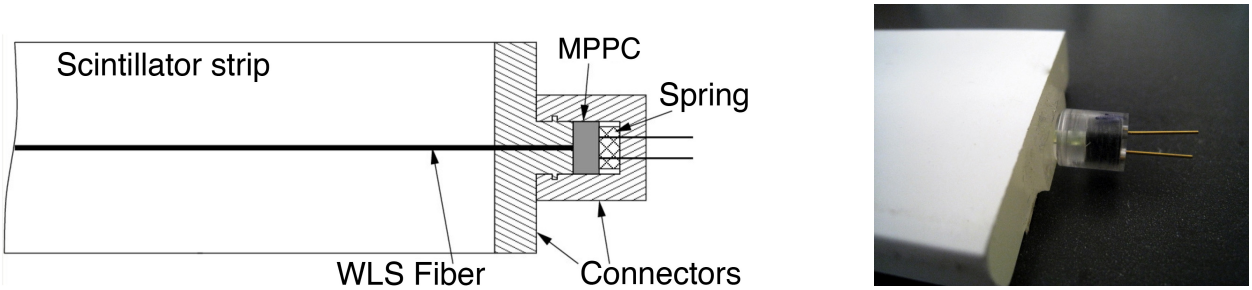

Figure 42: *Left: Detail of the scintillator-fiber-MPPC connection. The fiber's ferrule is the left half of the connector; the MPPC's housing is on the right. Right: Completed assembly (with translucent coupler).*

5.3.7 Photosensors

The photosensor that mates to each WLS fiber is the Hamamatsu S10362-13-050C MPPC (Fig. 37). This custom-area device was adapted for the INGRID beam monitor by Hamamatsu from a catalog MPPC. It has 667 50 μm-pitch pixels in an active area of $1.3 \times 1.3\,\mathrm{mm}^2$, which is well matched to the 1.2-mm outer diameter of our Kuraray WLS fiber. As was mentioned in the previous section, about 40% more light is collected by the MPPC if the WLS fiber protrudes by 200 μm beyond the mating surface between the fiber's ferrule and the MPPC's housing. The MPPC's sensitive surface is protected by a waterproof transparent silicone resin; this layer has a meniscus that dips about 200 μm below the front face of the MPPC case (Fig. 43). The fiber protrusion allows more of the exiting light cone to be captured on the MPPC's sensitive surface.

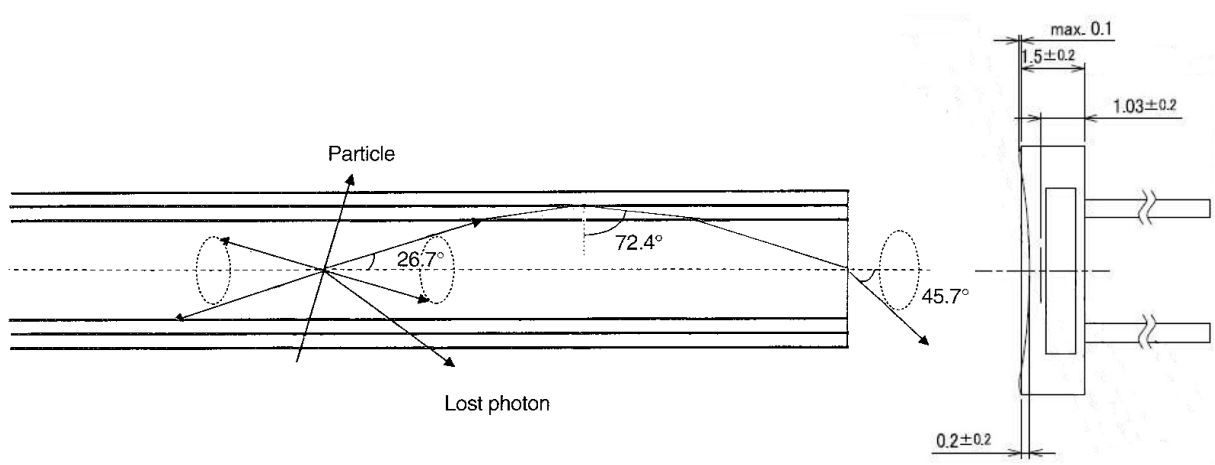

Figure 43: *Detail of the light cone illuminating the MPPC. Left: envelope of the trapped light as it exits the fiber end. Right: Side view of the MPPC surface, showing the meniscus in the protective window.*

The radiation hardness of the MPPC, measured at ITEP using a proton beam, corresponds to an expected lifetime of 25 years or more in the barrel KLM environment. Neutron radiation increases the random single-pixel noise but does not generate correlated multi-pixel background (Fig. 44). The same figure shows that the detection efficiency for a minimum-ionizing particle that passes through the far end of the scintillator bar suffers a 3% loss over ten years for a signal threshold fixed at 7.5 fired MPPC pixels if the baseline shift due to the single-pixel firings is ignored. *This efficiency loss can be mitigated effectively in the FEE ASIC by measuring the pulse height relative to the local baseline.* The noise rate of $\sim 10\,\mathrm{kHz}$ after ten equivalent years of irradiation (for a 7.5-pixel threshold) is an order or magnitude lower than the expected neutron background rate of $\sim 90\,\mathrm{kHz}$ per scintillator. Figure 45 shows that a signal with a very modest 10 fired pixels is clearly visible in both the virgin and irradiated photosensor above the background that has occasional or frequent single-pixel random pulses superimposed.

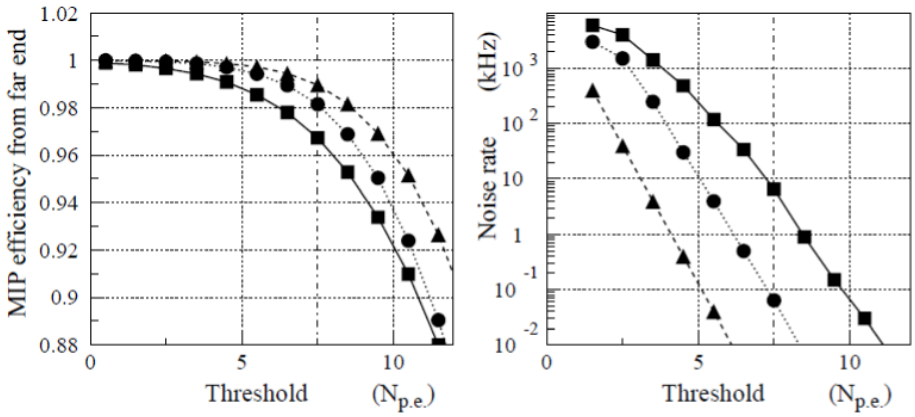

Figure 44: *Left: MPPC detection efficiency vs minimum number of fired pixels for a signal corresponding to a muon passing through the far end of the scintillator. Right: random noise rate as a function of the minimum number of fired pixels for a signal. In both figures, the triangles represent virgin MPPCs while the circles (squares) represent irradiated MPPCs corresponding to a five (ten) year dose in Belle II.*

The MPPC is powered by the A1510 module made by CAEN. This module can supply up to 100 Volts to each of 12 independent floating-ground channels. The nominal operating voltage of the MPPC is 70 V with a permissible range of 60–80 V. The 10 mA current capacity of each A1510 channel is sufficient to power all of the MPPCs in one barrel (or endcap) detector module.

5.3.8 Module assembly

The four unique sizes for the 36 modules are listed in Table 5.3.4. The module frame is assembled from four extruded aluminum U-channels joined to form the perimeter. The

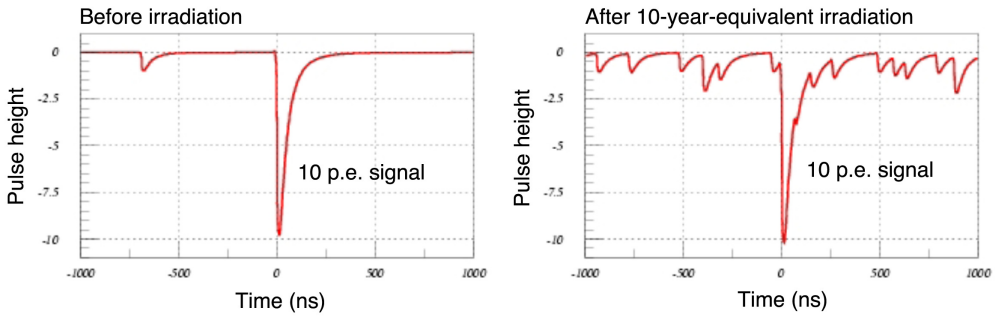

Figure 45: *Left: MPPC signal (10 fired pixels) for a virgin sensor. Right: MPPC signal (10 fired pixels) and random noise for an irradiated sensor.*

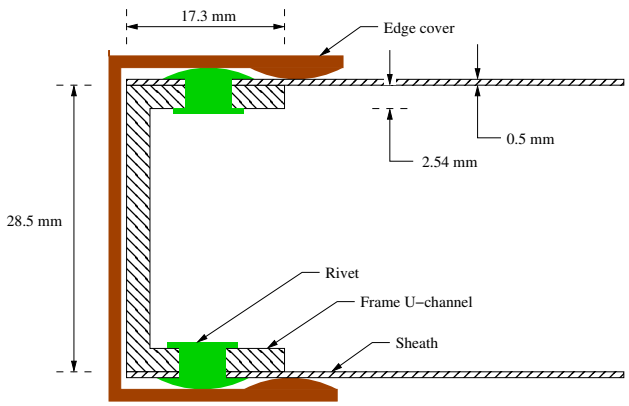

Figure 46: *Detail showing the frame, sheath and side-edge cover along the module perimeter.*

frames are cut to length and prepared for assembly in the Virginia Tech machine shop. The module is enclosed in protective aluminum sheathing riveted to the U-channels; the seams between adjacent sheaths are taped together. Opaque aluminized tape is applied at all joints after the module has been assembled. An extruded PVC edge cover, taken from the corresponding barrel RPC module that this module will replace, is then fitted along the perimeter sides (but not ends) to protect the rivets. Figure 46 shows this geometry.

With the empty aluminum frame on the assembly table, one aluminum sheath is riveted to the frame and then the frame is flipped over so that this sheath is in contact with the table surface. A $1/4''$-thick polystyrene surface (cut from two $48''x96''$ sheets) is placed inside the frame on the aluminum sheath. The preamplifier-carrier cards, each loaded with quality-accepted preamplifiers, are bolted to the interior of this frame along two sides using nylon bolts for electrical isolation. Ribbon cables (two per carrier card) are connected to the

Figure 47: *Detail showing the routing of the power and signal ribbon cables at the modules front-panel access ports. Some preamplifier-MPPC connections can be seen as well.*

carriers; some of these cables are laid immediately into slots that were pre-cut in the bottom polystyrene surface and routed out the frame's front-panel slots while the remaining cables are folded temporarily over and outside the frame.

The long scintillator strips (parallel to the Belle II z axis and beamline) are epoxied to the bottom polystyrene surface. The short orthogonal strips are then epoxied to the first layer of strips. The two-wire pigtails from each preamplifier are then soldered to the corresponding MPPC leads. The ribbon cables that had been folded outside the frame are now routed over the second scintillator-strip surface to the front-panel slots. The ribbon cables, protruding from three slots at the front panel (Fig. 47), are cut to length. Connectors are attached to each one, along with identifying labels that distinguish clearly between the MPPC-power and preamplified-output cables.

Each scintillator-fiber-MPPC-preamplifier assembly is subjected to an *in situ* cosmic ray quality assurance test to verify that it meets performance specifications. At this stage, only the preamplifier-carrier, preamplifier, or MPPC can be removed and replaced easily.

After all of the scintillator assemblies have passed this test, a second 3/16″-thick polystyrene sheet is epoxied to the second strip layer. Finally, an aluminum sheath is riveted to the frame and tape is applied along the perimeter to seal the detector module. Figure 48 shows the assembled module just after the placement of part of the top polystyrene filler sheet.

Figure 48: *Assembled barrel KLM module after placement of part of the top polystyrene filler sheet and before encasing the module in its aluminum sheath.*

5.3.9 Pre- and post-shipment tests

A second cosmic ray test of each channel in the assembled module is performed while it is still on the assembly table. If any anomalies are detected here, the top aluminum sheath is removed, the bad channel's MPPC or preamplifier is replaced and retested, and the sheath and light-tight tape are reapplied. After this, the module is lifted and rotated using an overhead crane and placed in the vertical orientation into the shipping crate. As each module is added to this crate, wooden interior framing is added to firmly hold the module and avoid movement within the crate.

The crate is trucked by Nippon Express from Virginia Tech to Seattle for shipment to Yokohama, after which it is trucked to KEK. The shipping crate is fitted with exterior and interior accelerometers (which trip if the crate's acceleration exceeds a pre-set threshold). A redundant battery-powered recording accelerometer is also mounted inside the crate to provide a history during shipment.

Upon arrival at KEK, the modules are extracted one by one from the shipping crate for post-shipment testing. Each module in the crate is connected in turn to a replica of the test setup used at Virginia Tech so that each channel's performance is remeasured with cosmic rays. This takes about 4 hours per module. Any underperforming or dead channels are repaired by replacing the MPPC, the preamplifier, the carrier card, or the external ribbon-cable connector.

Just before installation of a detector module into the magnet yoke, each channel is tested once more in a self-triggered mode to verify proper operation. This takes about 1.5 hours per module. (After installation, the self-triggered test is repeated. When the final FEE boards become available in late 2013 or early 2014, the post-installation cosmic ray test will be performed, using the layer-0 detector module as the trigger for the layer-1 module and vice versa in a given forward or backward octant.)

The cosmic-ray and self-triggered validations of each module's channels in the post-shipment pre-installation tests signal the final acceptance of the module for this Project. The validation of all modules signals the completion of the Barrel KLM Upgrade part of this Project.

5.3.10 US Belle II Project scope for the Barrel KLM Upgrade

The US Belle II Project scope includes the design, procurement, fabrication, testing, and delivery to KEK of the 36 scintillator modules. Four of these are commissioning spares; 32 are installed in layers 0 and 1 of the barrel KLM system.

Installation and commissioning of these modules at KEK, including integration with the front-end readout electronics and the Belle II data acquisition and triggering systems, are outside the scope of the US Belle II project. It is anticipated that significant US resources will contribute to these activities, but that these would be funded outside of the US Belle II project. A separate resource-loaded work breakdown structure (WBS) has been created to capture these activities and to provide the appropriate linkages between the US Belle II Project effort and the subsequent installation, commissioning, and integration effort that will draw on the same resources and personnel. This delineation was chosen so that the completion of the US Belle II Project is not reliant on the contributions being provided by other institutions nor tied to the schedule of the SuperKEKB accelerator.

5.4 SuperKEKB Commissioning Detector

5.4.1 US Role in a Background Commissioning Detector

The US Belle II groups play a lead role in the design, construction, and operation of the SuperKEKB commissioning detector (also affectionately known as BEAST II within the Belle II collaboration), which will characterize beam-induced backgrounds near the interaction point (IP), starting in January 2015. The commissioning detector is needed to prevent

radiation damage to the Belle II detector, to provide feedback to the accelerator during commissioning, and to improve our simulation of beam induced backgrounds. All of these issues will be more important in Belle II than in Belle due not only to the increased beam current, but also the more extreme beam conditions. Both are needed for the increased luminosity. The proposed work on the commissioning detector will be a natural continuation of our role during KEKB beam commissioning in 1997 and 1998, and allow the US groups to take a leadership role during a critical phase of the experiment, while requiring only modest investment in equipment and manpower. This is made possible by leveraging the historical involvement and technical expertise on radiation monitoring, gas/pixel tracking detectors, mechanical structures, and DAQ electronics in the US groups.

5.4.2 Commissioning Detector Motivation

Experience with KEKB, as well as PEP-II [28], has shown that during beam commissioning and vacuum scrubbing, it is critical to measure the particle and x-ray backgrounds near the interaction point in detail. Such measurements are needed to provide real-time measurements of luminosity and background levels to the accelerator group, to ensure a sufficiently low radiation level before the final detector is installed, and to tune the simulation of beam-related backgrounds that affect physics measurements in the Belle II detector. Due to higher beam currents, smaller beam sizes and higher luminosity, beam-related backgrounds will be larger in Belle II than experienced in Belle. Due to the innovative nano-beam scheme employed by SuperKEKB, the relative contribution of different background components (e.g., beam-gas interactions, Touschek scattering, and synchrotron radiation) will also differ from that in KEKB. There are large uncertainties in the levels predicted by simulation, so that direct, *in situ* measurements of these backgrounds are required.

5.4.3 KEKB Commissioning Experience

The Hawaii group led the KEKB commissioning detector effort in 1997 and 1998. The group provided the mechanical structure, drift tubes, and DAQ electronics for the BEAST (Beam Exorcism for A STable experiment) commissioning detector, shown in Fig. 49, and led installation and operation of this detector at KEK. BEAST detected the first KEKB beam in December 1998, the first Bhabhas, provided important feedback during the subsequent accelerator commissioning, and provided data needed for tuning the simulation of beam-induced backgrounds in the Belle detector.

Detailed x-ray and neutron measurements were lacking in BEAST, but are clearly needed here: an unexpected synchrotron radiation component, due to a steering magnet that had not been simulated, burned a hole into the first Belle beampipe. During the initial KEKB operation there was also larger radiation damage to the first Belle silicon strip detector than expected, requiring early replacement of that detector system. Neutrons from beam backgrounds produced unexpectedly large backgrounds in the Belle KLM detector endcaps, increasing their dead time and decreasing their efficiency. Scaling to Belle II conditions, it

was concluded that the resulting KLM performance losses would become unacceptable, which motivates the program of replacement of all the endcap KLM glass RPCs and the inner two layers of the barrel KLM with a scintillator-based design. This illustrates the significance of neutron backgrounds, and the importance of understanding their production. Neutrons were also an important unexpected background in the BaBar DIRC detector; PEP-II experience shows that they are difficult to measure precisely.

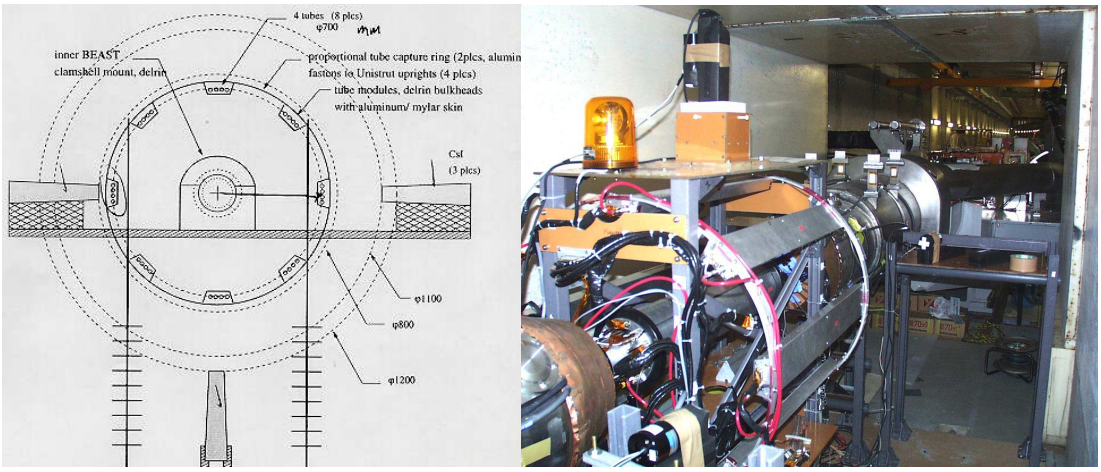

Figure 49: *Technical drawing (left) and photo (right) of the original KEKB beam commissioning detector, BEAST.*

5.4.4 SuperKEKB Commissioning Plan

Recently the Belle II group and the SuperKEKB accelerator group reached a consensus on the commissioning scenario of SuperKEKB. The commissioning will be performed in three stages.

Phase 1

From January 2015 to May 2015, the machine commissioning will be done without the final focus quadrupole magnets (QCS's) and without the Belle II detector. Instead, as shown in figures 51 and 50, a concrete shield will surround the area that will later become the interaction region. The main goals in this period are to complete the basic machine commissioning including the commissioning of each accelerator component and to perform sufficient vacuum scrubbing before the Belle II detector is rolled in. Although no beam-collision are planned for this phase, the plan is to carry out preliminary machine studies on beam dynamics issues essential for reaching high luminosity, such as low-emittance tuning. It is expected that the stored beam currents will reach $\sim 0.5 - 1$ A in this phase. Tuning the beam feedback system for suppressing beam instability to allow increased beam currents will

be of critical importance. The Belle II group has requested vacuum scrubbing with $\sim 0.5-1$ A for at least one month in total should be done. During Phase 1, the commissioning of the damping ring for the positron beam will also be done.

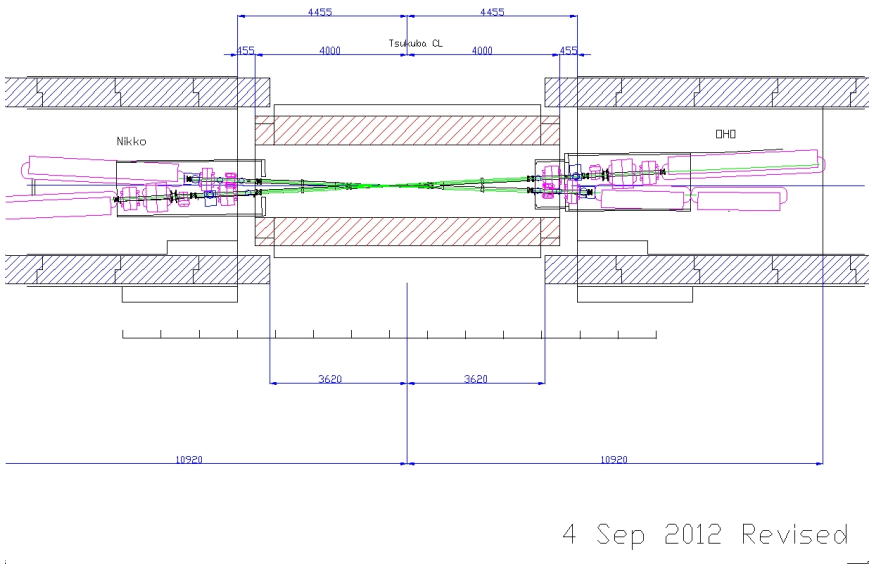

Figure 50: *Interaction region during commissioning phase 1, top view.*

Phase 2

From February 2016 to June 2016, the accelerator commissioning will be continued with QCS magnets installed and the Belle II detector rolled in. Although the vertex detector will not be installed in this phase, the machine conditions will be the same as in the final stage, from the viewpoint of the accelerator tuning, and the full luminosity tuning will be done. The target luminosity at the end of this phase is $1 \times 10^{34}\mathrm{cm}^{-2}\mathrm{s}^{-1}$. Machine tuning in this phase includes optics tuning, beam collision tuning with the nano-beam scheme and tuning and study of detector beam background. As for optics tuning, the continuous orbit correction during beam operation, tuning of squeezing the beta functions at the IP (low-beta tuning) and tuning on the low vertical emittance (low-emittance tuning) are important. Among them, low-beta tuning is essential in SuperKEKB as the achievable luminosity depends largely on the minimum value of the vertical beta functions at the IP. Squeezing the beta functions at the IP is difficult and it may take several years to attain the design values. As for beam collision tuning, the orbit feedback system to maintain optimum beam collisions and the beam tuning for suppressing beam-blowup due to the beam-beam effects are important. In SuperKEKB, much faster orbit feedback than in KEKBis needed, since the luminosity is much more sensitive to the motion of QCS's. As for detector beam background, a realistic detector beam background will be studied before installation of the vertex detector. At SuperKEKB, the dominant sources of detector beam backgrounds, described in more detail

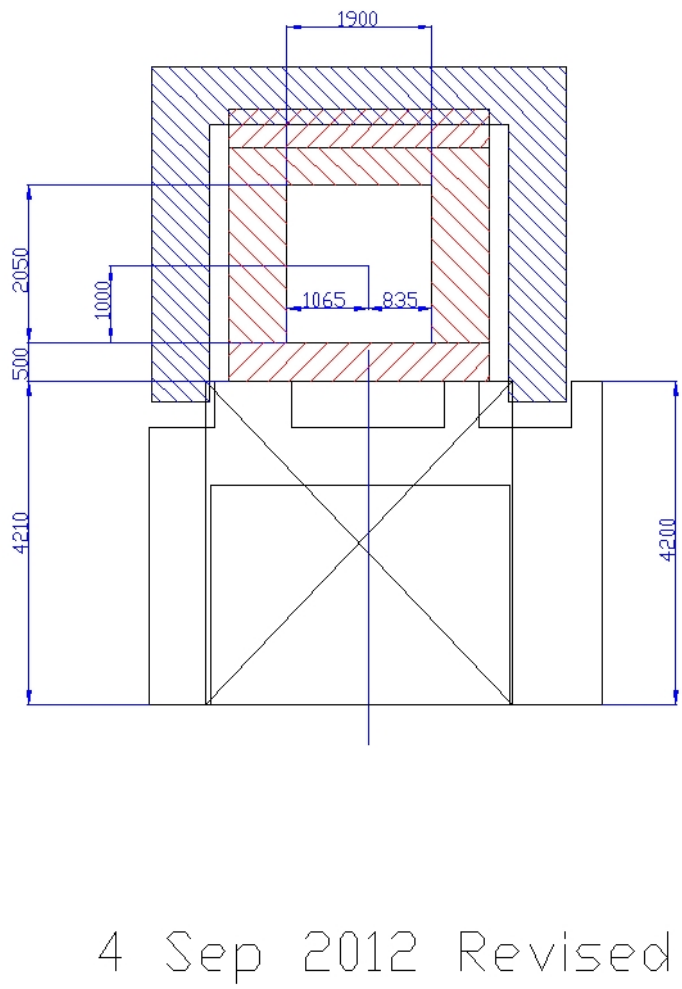

Figure 51: *Interaction region during commissioning phase 1, r/ϕ-view of concrete shield.*

in the next section, are expected to be the Touschek effect, beam-gas Coulomb scattering, and radiative Bhabha scattering. The beam backgrounds from the Touschek effect and beam-gas Coulomb are very sensitive to the IP beta functions. Since design values of the IP beta functions will not be reached in this phase, some extrapolation is required to estimate the ultimate beam background with the design machine parameters based on the study in this phase. The beam background from the radiative Bhabha process is not very sensitive to the IP beta functions so that the extrapolation to the design luminosity should be relatively straightforward. An example of machine parameters corresponding to a target luminosity of $1 \times 10^{34}\text{cm}^{-2}\text{s}^{-1}$ is: $\sim$ 1A beam currents and $\sim$ 2.4mm vertical beta function, which is 8 times larger than the design, and a vertical beam-beam parameter of $\sim$ 0.025.

Another important goal of this phase is to validate the simulation of beam induced backgrounds at the SuperKEKB Belle II interaction region. It should be clear that the

background has many components and a vigorous program of machine studies is planned to test predictions of the simulation and understand each of the mechanisms that lead to the beam induced backgrounds. Components of BEAST II will be reconfigured in this stage to not only give feed back to the machine group as they tune the machine for luminosity, but also support the background validation and extrapolation effort to be sure that the full Belle II detector can be operated with full beam current and the beams with high luminosity generating parameters.

Phase 3

In the third step (Phase 3) starting from October 2016, the full beam commissioning with the full Belle II detector will be done. At a some point in this phase, the physics experiment will start after some detector tuning, if needed.

Alternative Commissioning Scenario

The scenario described above for Phase 2 is called the baseline scenario. In addition, there is another backup scenario where the commissioning in Phase 2 will be done with QCS's and without the Belle II detector. It would be necessary to execute this scenario if there are unexpected problems such as a delay in SuperKEKb or Belle II construction.

5.4.5 Beam Background Sources at SuperKEKB

Many background sources are projected at SuperKEKB. These include the Touschek effect, Beam-gas Scattering, Synchrotron radiation, Radiative Bhabha process, two-photon process, and beam-beam effect. These are discussed below.

- Touschek effect

  The Touschek effect is intra-bunch scattering[33]. Coulomb scattering between two particles in a same beam bunch changes their energy from that of overall beam bunch. One gets more and the other has less energy than the bunch aveage. The scattering rate of the Touschek effect is proportional to the inverse beam size, third power of the beam energy, the number of bunches, and second power of the bunch current.

  Touschek-scattered particles get lost from the beam if they hit the beam pipe while they propagate around the ring. If their loss position is close to the detector, particles in the generated shower can reach the detector. Undesired hits generated by these background showers deteriorate the detector's resolution, and radiation from the showers damage detector electronics. At SuperKEKB, simple extrapolation, based on machine parameters, predicts that Touschek background will increase by factor of $\sim$20 compared to that observed in KEKB.

To reduce Touschek background, horizontal and vertical movable collimators will be installed. The movable collimators located all around the ring can stop particles being lost from the beam far from the detector. The horizontal collimators are located at local maximums of the horizontal beta function or the dispersion. Those located just before the interaction region are most critical to minimize the beam loss rate near the detector. The nearest collimator is only 18 m upstream of the IP for LER. Touschek background can be reduced effectively by collimating the beam horizontally on both inner and outer sides, and thus the collimators in SuperKEKB do this in contrast to KEKB where horizontal collimation was only done on the inner side.

A vertical collimator in the LER, which was originally installed to reduce the Beam-gas Coulomb scattering background, discussed in the next subsection, also stops vertically oscillating Touschek scattered particles. This is done at the Fuji-area, which is opposite side from the IP in the ring, where the LER beam orbit is vertically bent to pass under the HER ring.

- Beam-gas scattering

  The second important background source is beam-gas scattering by the residual gas atoms. Coulomb scattering changes the direction of the beam particle, and bremsstrahlung scattering decrease the energy of the beam particles. The rate of the beam-gas scattering is proportional to the vacuum level and the beam current. At SuperKEKB, the beam currents will be $\sim$2 times higher than that of KEKB, and the vacuum level, except for the interaction region, will be the same level as KEKB. Therefore the same order of magnitude is expected, perhaps a few times higher, beam-gas background as in the past[32]. However, our latest background simulations reveals that the Coulomb scattering rate is higher by a factor of $\sim$100 than that of KEKB, due to a smaller IR beam pipe aperture and larger vertical beta function. Beam-gas scattered particles are lost hitting the beam pipe inner wall while they propagate around the ring, similar to Touschek-scattered particles. The countermeasures used for Touschek background, movable collimators and the heavy-metal shield, are also effective at reducing beam-gas background. The vertical movable collimator is essential to reduce Coulomb scattering background. Transverse Mode Coupling (TMC) instability caused by the vertical collimator will be carefully examined since the vertical beta function is larger than the horizontal beta function. Details are explained in [34].

- Synchrotron radiation

  The third important background source is synchrotron radiation (SR) emitted from the beam. Since the SR power is proportional to the beam energy squared and magnetic field squared, the HER beam is the main source of this type of background. The energy of SR is a few keV to tens of keV, x-rays. At the first stage of Belle, the inner layer SVD was severely damaged by x-rays with E $\sim$ 2keV from the HER. To absorb synchrotron radiation before they reach the inner detectors, PXD and SVD, the inner surface of the Beryllium beam pipe are coated a thin layer of gold. Also the shape of IR beam pipe is designed such that no SR hits it directly.

- Radiative Bhabha process

  Photons from the radiative Bhabha process propagate along the beam axis direction and interact with the iron of the magnets. In these interactions, neutrons are copiously produced via the giant photo-nuclear resonance mechanism. These neutrons are the main background source for the outermost detector, the K_L and muon detector (KLM) instrumented in the return yoke of the spectrometer. The rate of neutron production by the radiative Bhabha events is proportional to the luminosity, which is 40 times higher than that of KEKB. Therefore the SuperKEKB-Belle II interaction region includes additional neutron shielding to absorb these neutrons.

  Both electron and positron energies decrease after the radiative Bhabha process. If the shared QCS magnets for incoming and outgoing beams is employed as in KEKB, the scattered particles are over-bent by the QCS magnets. The particles then hit the wall of magnets and electromagnetic showers are generated. In the SuperKEKB case, two separate quadrupole magnets are used and both orbits for incoming and outgoing beams are centered in the Q-magnets. Thus, it is expected that the radiative Bhabha background due to over-bent electrons and positrons will be small and only a limited fraction of them will have large enough energy loss (ΔE) such that they will be lost inside the detector. However, since the luminosity is 40 times higher, the rate of large ΔE particles are not negligible and is expected to be comparable to Touschek and Beam-gas BG after installation of collimators. Beam intrinsic angular divergence at the IP, angular diffusion by the radiative Bhabha process, bending from the solenoid field, and leaking fields of the other ring's Q magnets, especially for scattered electrons, all play roles for the radiative Bhabha background.

- Two-photon process

  The fifth background source is very low momentum electron-positron pair backgrounds produced via the two-photon process: $ee \to eeee$. In SuperKEKB, the radius of the innermost detector is less than that of KEKB since the PXD is introduced as close as possible to the IP. The two-photon background rate increases roughly as $1/r^2$. Simulations and machine studies at KEKB in 2010 have shown that the two-photon BG rate on the PXD is less than our requirement.

- Beam-beam background

  A beam bunch interacts with the electric field of the other bunch when they collide at the IP. Beam particles are bent by this interaction and the kick force is almost proportional to the distance from the center of the bunch at $x/\sigma << 1$. Beam-beam interaction results in non-Gaussian beam tails, therefore it can increase the background rate from synchrotron radiation as the tails explore higher focusing fields than the core. Our backround simulation study, which is CPU intensive due to a non-linear beam-beam forces, predicts that the non-Gaussian tail is significant only in the vertical, and the synchrotron background is not affected much.

5.4.6 Planned Measurements During SuperKEKB Commissioning

The BEAST group is currently planning the following measurements:

Phase 1, Vacuum scrubbing phase:

- Measuring beam gas backgrounds in order to extrapolate background condition to the target vacuum level
- Measuring backgrounds during injection and background rate during "normal" running and time profile of backgrounds for both LER and HER

Phase 2, Belle without VXD:

- Measuring beam gas backgrounds in order to extrapolate background condition to the target vacuum level
- Measure the SR hit rate in the area of the PXD sensors to get expectations for PXD operatining condition, and decide a beam abort setting for the VXD. If significantly larger SR background than expected is found, the beam pipe inner structure may have to be modified in order to meet the PXD required level. This will be crucial for the safe operation of PXD during the physics run.
- Measure Touschek background by changing beam size for the same bunch current. By monitoring neutron and electromagnetic shower hits during this study, the background simulation can be validated and background conditions estimated during the physics run.
- Touschek and radiative bhabha backgrounds will be measured not only by BEAST II subsystems, but also via the CDC HV current and hit rate information from the Belle II TOP and ECL subdetectors. In particular for the TOP, the rate of background hits due to radative bhabha events may be critical for the lifetime of the MCP-PMTs used in that detector. If larger background levels than expected are measured, additional shielding will have to be installed before starting the physics run.
- Measure the effect of movable masks. In order to efficiently reduce background around the interaction region, SuperKEKB will employ movable masks. Measuring the background level as a function of mask position is useful fundamental data for optimizing the mask settings for the physics run.

5.4.7 Commissioning Detector Description and US Contributions

The US Belle II groups will design and build the following commissioning detector components: a mechanical support structure for mounting subdetectors in commissioning phase I, a PIN-diode array for monitoring radiation dose from charged particles and x-rays, and micro Time Projection Chambers for monitoring neutrons.

A range of (non-US) collaborating institutes will install other detector prototypes and subsystems on the commissioning detector, such as silicon strip and pixel detector ladders, detectors to monitor synchrotron (keV) x-rays, a BGO crystal-based luminosity monitor, and He-3 tubes for monitoring thermal neutrons.

5.4.8 Commissioning Detector Design Overview

Figures 52 and 53 show the SuperKEKB commissioning detector setup for commissioning phases I and II, respectively. The instantaneous and integrated ionizing radiation dose throughout the inner detector volume will be monitored with an array of 64 PIN diodes. Neutrons will be monitored with an array of eight micro Time Projection Chambers (micro-TPCs). Eight sets of BGO calorimeter crystals will be used for luminosity monitoring.

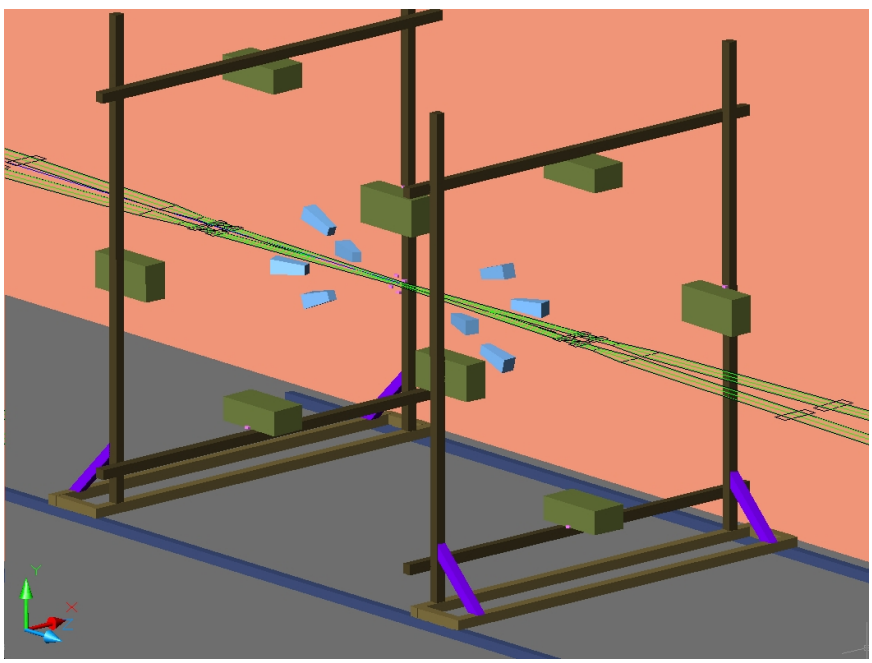

Figure 52: *Commissioning detector during phase I. BGO crystals for luminosity monitoring shown in blue, micro-TPCs for neutron monitoring shown in green.*

During commissioning phase I the different monitors will be mounted on a common mechanical structure, shown in Figure 52. As in the case of the Belle commissioning detector, BEAST (see Fig. 49), the proximity of accelerator magnets requires the use of non-magnetic materials such as fiberglass-based "Unistrut" support beams and brass connectors throughout. The most important system during this phase is the diode sytem, which will indicate when radiation levels are suffciently low that it is safe to roll in Belle II. During phase I only two of the micro-TPCs will be installed, and to operate the BGOs in analog readout mode. While the BGOs and TPCs are not critically needed during this phase, they provide complimentary information on backgrounds, and operation during phase I will allow system

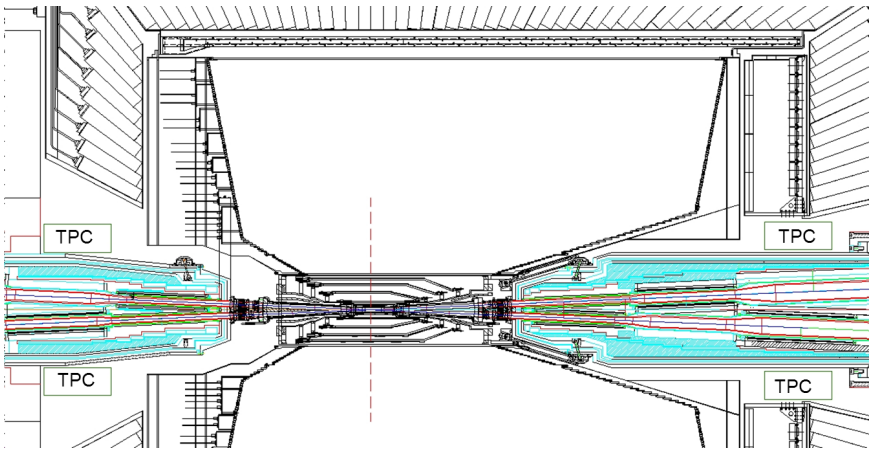

Figure 53: *Commissioning detector environment during phase II.*

tests to be performed and DAQ integration, to ensure smooth operation of all systems at the beginning of phase II.

Another motivation for having the BGO and TPC systems ready early, is the possbility of an alternate commissioning scneario. In the case the construction schedule slips, it is possible that the QCS magnets would be installed before Belle II is rolled in. In this case the accelerator will be able to produce measurable luminosity and significant beam backgrounds of all major types, and there would be plenty of space available for BEAST II susbsystems mounted on the same support structure as used during phase I. Having the BGO and TPC systems operational during the QCS-but-no-Belle-II phase would allow useful measurements of all beam background components. While this is a backup-scenario that is not part of the default schedule, our group has been charged to be ready for all possible commissioning scnearios, including this one.

During phase 2 all Belle II detectors except the vertex detectors (VXD) will have been installed, so there is little space available for BEAST systems. At that time, the PIN diodes will be installed througout the VXD volume, the BGO system will be mounted on aluminum rings inside the VXD volume, and the eight TPCs will be installed in the SVX dock space, as shown in Figure 53. This space is reserved for VXD cabling boxes, and will thus still be available. At the same time the dock space happens to be particulary suitable for measuring beam backgrounds, as a significant fraction of critical beam backgrounds that effect the PID system are generated by beam particles hitting the beam pipe wall near the z-location of the forward and backward dock spaces, with a high rate of neutrons expected to traverse the dock space. The VXD group plans for phase 2 are still under discussion. The current expectation is that they will install two prototype pixel detector (PXD) ladders, two silicon vertex detector (SVD) ladder, and a range of specialized sensors for characterizing synchrotron radiation and background rates, as described below.

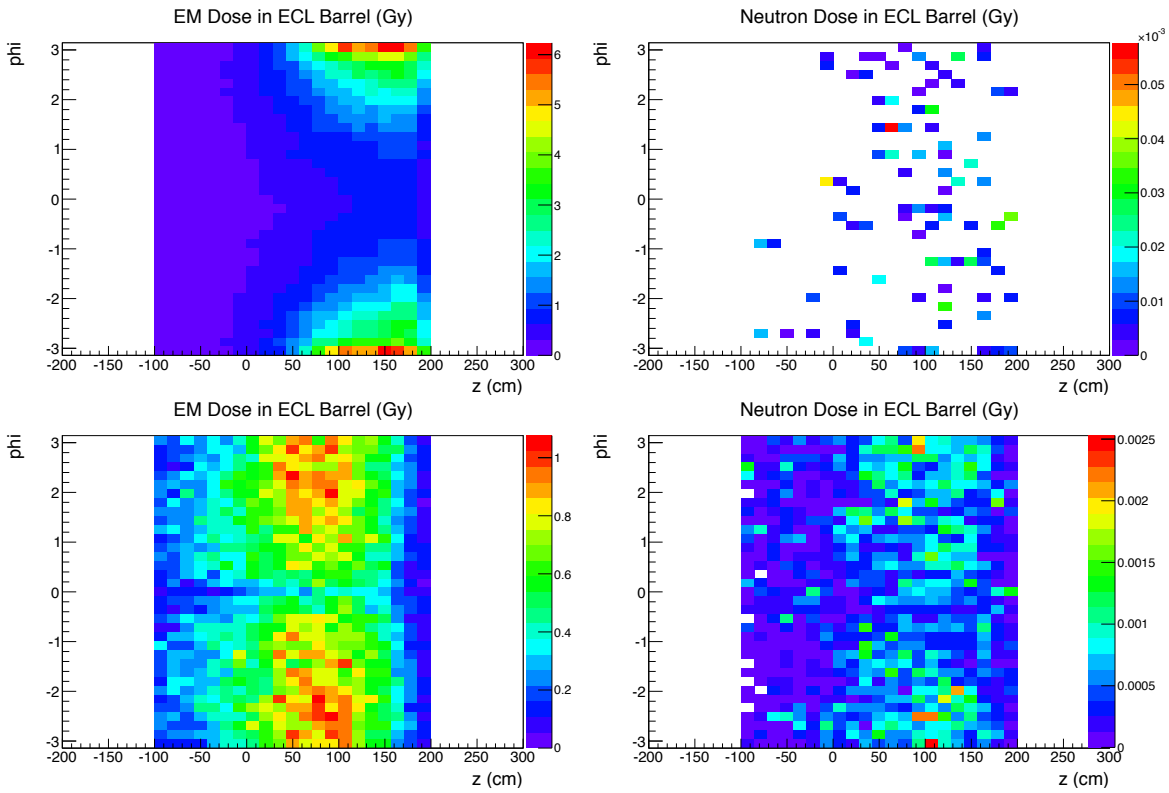

Figure 54: *Expected radiation dose in the electromagnetic calorimeter barrel from per snowmass year (10^7 seconds) of running at SuperKEKB design luminosity, extrapolated from simulating 20 μs of accelerator operation. Upper plots show radiative Bhabha events originating from the high energy electron ring (HER), while the lower plots show beam-gas Coulomb events originating from the low energy positron ring (LER).*

5.4.9 Commissioning Detector Dose Monitor

A simple, cheap, robust monitor of ionizing radiation is an array of silicon PIN diodes. Ionizing radiation effectively causes an increase in the dark current from such diodes. This current can be passively amplified and its integral is proportional to the ionizing radiation dose. Such a system was used at CLEO and CESR as a beam background monitor and beam tuning aid to minimize beam induced radiation. At CLEO half of the diodes were behind a thin layer of high-Z shielding, a layer of gold paint, and half were unshielded. X-rays from synchrotron radiation are considerably reduced on the shielded diodes while particle radiation from beam-gas scattering and radiative Bhabha events is not. Thus the difference between a shielded and unshielded diode pair gives a direct measure of the synchrotron radiation component of the dose. At CLEO and CESR this made it easy to map the location and extent of synchrotron radiation and backscattering fans caused by the beams passing through the final focusing elements and x-rays scattering off of shielding elements.

A prototype system has been demonstrated at Wayne State. It uses commercial amplifiers

from Cremat, Inc. and off the shelf PIN diodes from Siemens, see figure 55. The system returns the expected current when irradiated by a beta source of known activity. Work is going on to make the system multichannel, the commercial preamps are single channel, by sharing input power among many amplifiers.

A single diode is packaged into an aluminum block with a hole drilled out that leaves the sensitive face of the diode exposed along a long side. The leads of the diode are then attached to coax cable making for a very small, $1 \times 1 \times 2$ cm, light package that can easily be held in place with velcro straps. They are also easy to move around with minimal effort. A pair of two, one with a bare window and a second behind a high-Z layer, form the basic sensor. Four pairs, up, down, inside ring, outside ring, form a basic measuring unit at a single location along the beam line. The plan is to manufacture eight such units for a total of 64 diodes.

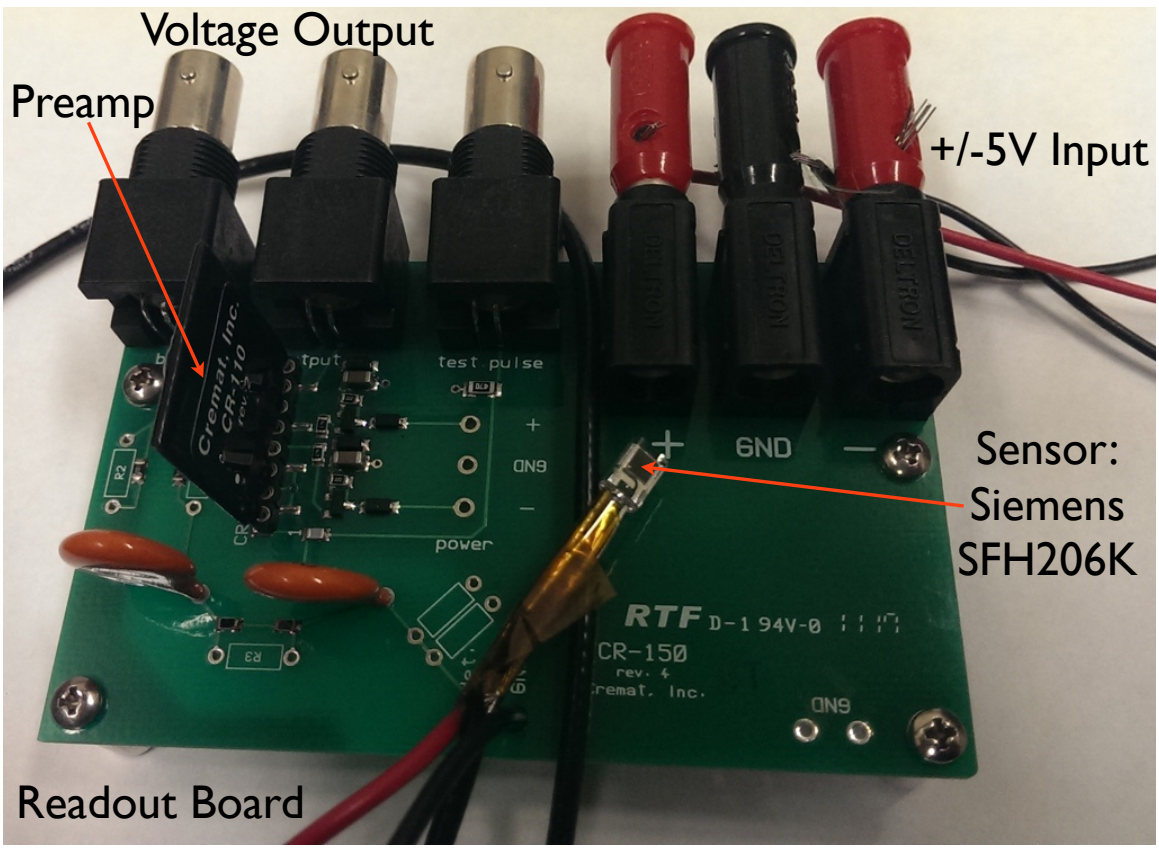

Figure 55: *Photo of PIN diode and prototype single channel readout board.*

During commissioning phase I a flexible system is desired can be moved around in response to improving beam vacuum, changing beam conditions, and for machine studies. Also it is desirable to have two units of diodes to accompany the TPC's to correlate the TPC measurements with the ionizing dose seen by the diodes. The remaining six units would be spread along the central beam line to monitor the radiation coming from the beam line.

During commissioning phase II the diodes will move to the inner tips of the ECL, where the largest dose on the calorimeter is expected, at the inner face of the quads, primarily monitoring radiative Bhabha backgrounds, and the remaining four units in the VXD volume to monitor dosage there.

In the alternative commissioning phase with QCS magnets and without Belle II rolled in, two units remain with the TPC's while the remaining six are placed on the outside of the final focus quads. Our simulations of the beam induced backgrounds show that the most troublesome radiation is coming from the quads and the diodes will provide a direct measure and test of the simulations.

This system will provide a low resolution view of any sharp x-ray features incident on the beam pipe at the longitudinal position of a diode unit. These radiation features get broadened as they scatter out of the beam pipe, thus making a higher resolution view not useful. It is expected, based on the simulations of the backgrounds, that those diodes in the plane of the rings would see x-ray features while those out of the plane would not.

The diode signals would be brought to remote analog amplifiers on shielded co-axial cables. Keeping the amplifiers remote allows the gain to be adjusted as the dose regime changes during the scrubbing and beam tuning processes. Drawing on the CLEO and CESR experience low and high gain output will be used for monitoring and tuning during injection versus normal running giving the system robustness and flexibility. Existing KEK infrastructure will be taken advantage of to digitize the analog diode signals. Since these radiation monitors are expected to be useful in beam tuning, they will be made available in real-time to the KEKB control room.

The sensors, cables, and mounting hardware will be constructed at Wayne State using the groups in-house technical support. Members of the Wayne State group, led by Professor Cinabro, will oversee the construction, installation, and commissioning of this sub-system, and analyze the resulting data.

5.4.10 Commissioning Detector micro-TPCs

Motivation & System Overview

In order to monitor and study fast neutrons, eight gas-filled micro-TPC detectors will be constructed. Since fast neutrons scatter less than thermal neutrons, and these detectors have directional sensitivity, this may allow the isolation and direct monitoring of the neutron flux component that originates from the beam line. The directional sensitivity will also enable the monitoring of the location along the beam line where the neutrons are produced, which can be used to distinguish different beam background components, and to validate and tune the neutron component in the beam backgrounds simulation.

Fast neutrons produce heavily ionizing nuclear recoils via elastic scattering in the TPC gas volume. The typically mm-length ionization trails produced by these recoils will be measured in 3D, by employing a high-resolution TPC charge readout, based on gas electron

multipliers (GEMs) and pixel electronics [27]. This makes it possible to tag fast, MeV-scale, neutrons, and measure both the energy and direction of neutron-recoils, which is not possible with other types of detectors. At high gain settings, the gas TPCs may also be used to reconstruct minimum ionizing particle (MIP) tracks, and with thin vessel walls and appropriate positioning obtain x-ray spectra in the keV range, which would be sensitive to synchrotron light (SR) backgrounds. In that case, energy deposits from MIPs, x-rays, and neutron recoils can be distinguished via the specific ionization (dE/dx) and ionization pattern measured. While our primary goal is to optimize the TPCs for neutron detection, these additional capabilities might prove useful; it will be good to have some redundancy in our commissioning setup, where the unexpected typically does occur. The micro-TPCs will be radiation hard, up to at least 50-100 Mrad, and capable of high data rates, as they will employ pixel chips developed for the ATLAS experiment at the LHC.

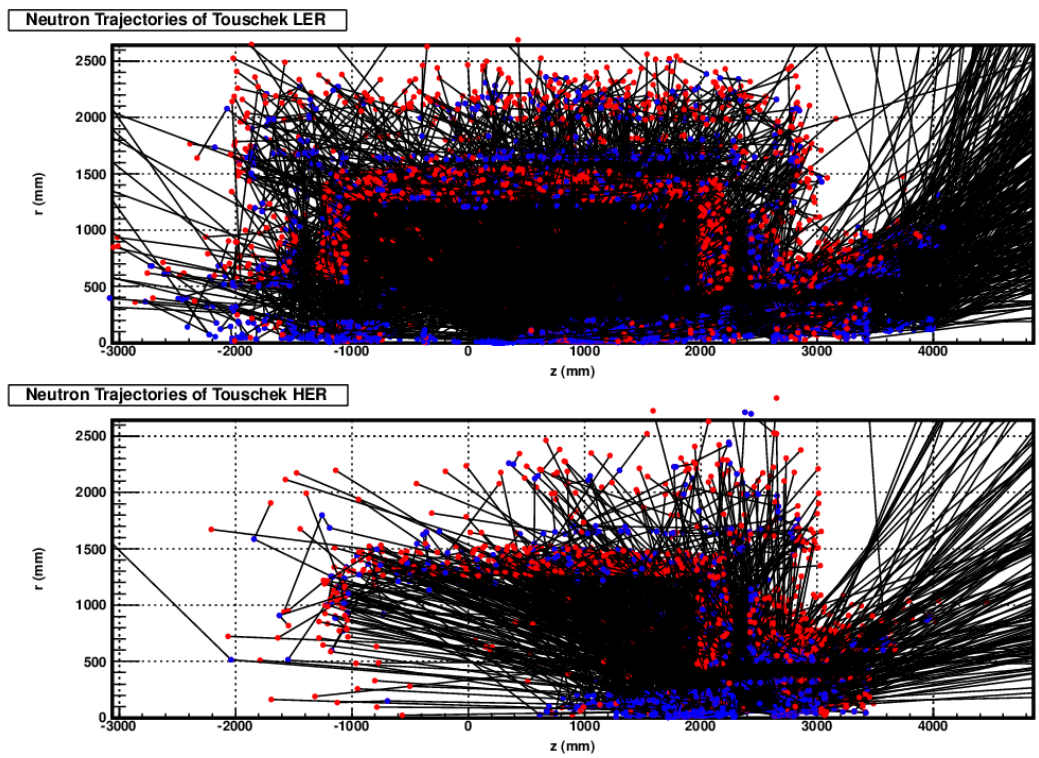

Figure 56: *GEANT production points (blue), GEANT decay points (red), and trajectories (black) of neutrons that deposit energy in the calorimeter, for Touschek backgrounds originating from the low energy ring (upper) and high energy ring (lower).*

Figure 56 shows the expected trajectories of neutrons that deposit energy in the calorimeter during commissioning phase 3, for two types of beam background. The majority of neutrons are generated near the QCS magnets, but the detailed distributions differ by background type. To monitor these neutrons in detail, the eight micro-TPCs will be positioned in the "SVX dock space" during commissioning phase 2, as shown in Figure 53. There will be four TPCs in the forward dock space, and four in the backward dock space, mounted

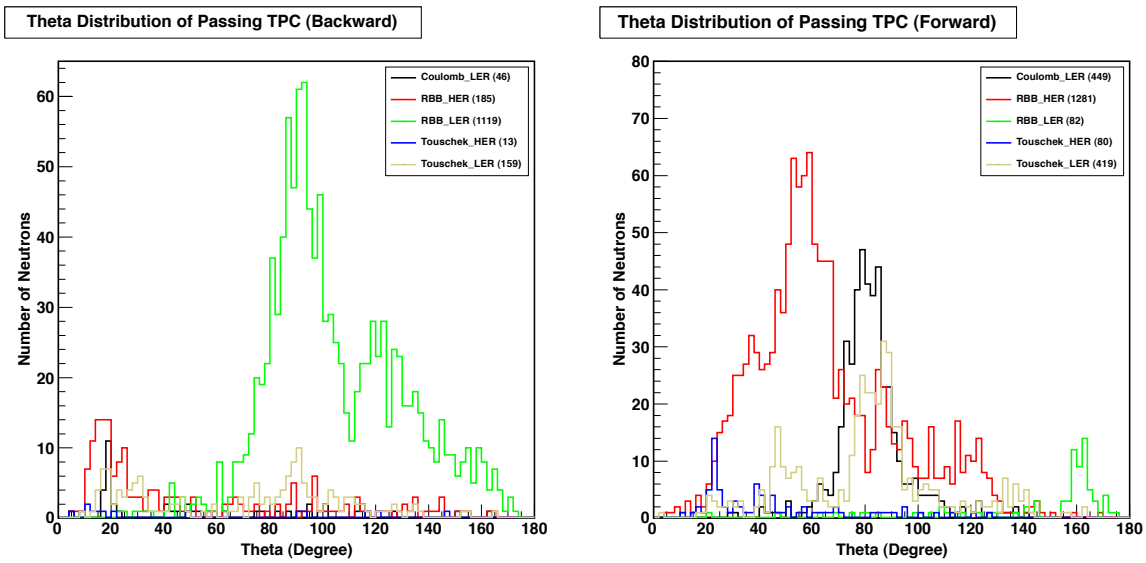

Figure 57: *Polar angle of neutrons that pass through the backward (left) and forward (right) array of micro-TPCs. The angle plotted is the polar angle of the incoming neutron direction, as seen by each micro-TPC.*

90 degrees apart in azimuthal angle, so that the ϕ-distribution of the neutrons can be measured, which is not flat as shown in Figure 54 and similar plots in the KLM system chapter. During commissioning phase 1, the installation of only two TPC prototypes is planned, so that the TPC DAQ and services can be commissioned, but most likely the final eight TPCs will not be installed at that time, since the neutron distribution will be different from the final one. There is also risk of activating the TPC vacuum vessel material, which would result in a larger rate of background event later on. If however the alternative commissioning scenario with QCS magnets and no Belle detector should occur, then all eight TPCs would be installed on the same BEAST support structure that will be used in phase I.

Figure 57 shows the polar angle distributions of only those neutrons which traverse the TPCs at the nominal position of r=70 cm, for each beam background process. (The resulting nucelar recoil distributions seen in individual TPCs are given in the Appendix.) The difference in the angular distributions, combined with the different dependence of each background process on accelerator parameters, such as beam current, luminosity, beam size, and vacuum pressure, can distinguish among and enable the measurement of the neutron production from each process during beam commissioning. The rates of neutrons traversing the TPCs are given in table 8, and are very large at design luminosity - of order 100 kHz to MHz. The fraction of neutrons that scatter elastically and lead to reconstructable recoils in the TPCs, however, is low, of order 0.1%. As a result the expected signal rate in each TPC is of order a kHz at design luminosity. As discussed above, all backgrounds except those from beam-gas are likely to be much lower during commissioning, while those from beam-gas could be much higher. The pixelated TPC image plane will be read out at 40 or 80 MHz,

	Rate in backward TPCs (MHz)	Rate in forward TPCs (MHz)
Coulomb HER	0.00	0.00
Coulomb LER	0.05	0.09
Radiative Bhabha HER	0.45	3.55
Radiative Bhabha LER	3.45	0.35
Touschek HER	0.05	0.15
Touschek LER	0.55	1.15

Table 8: *Predicted rate of neutrons traversing the backward and forward micro-TPC arrays, at design luminosity.*

which is fast enough to separate individual recoils even at the highest possible neutron rates, of order GHz, due to the low probability of elastic scattering. That scenario would motivate running in a pre-scale mode where only a fraction of the events are read out and saved.

Pre-Prototype Test Results

The University of Hawaii group is already developing TPCs for fast neutron detection [30][31], so that relatively modest resources are needed to adapt them to the commissioning detector. During the last two years, the group constructed two micro-TPC pre-prototypes, and performed detailed performance measurements using $HeCO_2$ gas. The results of these measurements have successfully demonstrated directional detection of fast neutrons with the target gas to be used in the commissioning detector, as shown in Figures 59 and 60. Key results from this test campaign are summarized in table 9, and show that the proposed micro-TPC technology can satisfy all Key Performance Parameters (KPPs) previously developed for the DOE Critical Decision 1 (CD-1) review.

Final Prototype Design and Construction

The construction of two final prototypes, with the larger mechanical dimensions needed in the commissioning detector is underway. The main differences between the pre-prototypes used for testing, and the final micro-TPCs are the pixel chip version (FE-I3 in pre-prototype, FE-I4 in final version) and the drift length (5cm in pre-prototype, 20cm in final detector). The effect of a longer drift length is mainly to increase diffusion, and has been included in our simulation studies. The successful operation of the newer FE-I4 pixel chip in a TPC, using a readout board designed by the Hawaii group, has already been demonstrated at LBNL. All basic building blocks of the final detector have been demonstrated.

The final micro-TPC prototype will have an active volume of 5 cm $\times$ 5 cm $\times$ 20 cm, and operate with $HeC0_2$ gas at atmospheric pressure. The longest dimension is the direction of

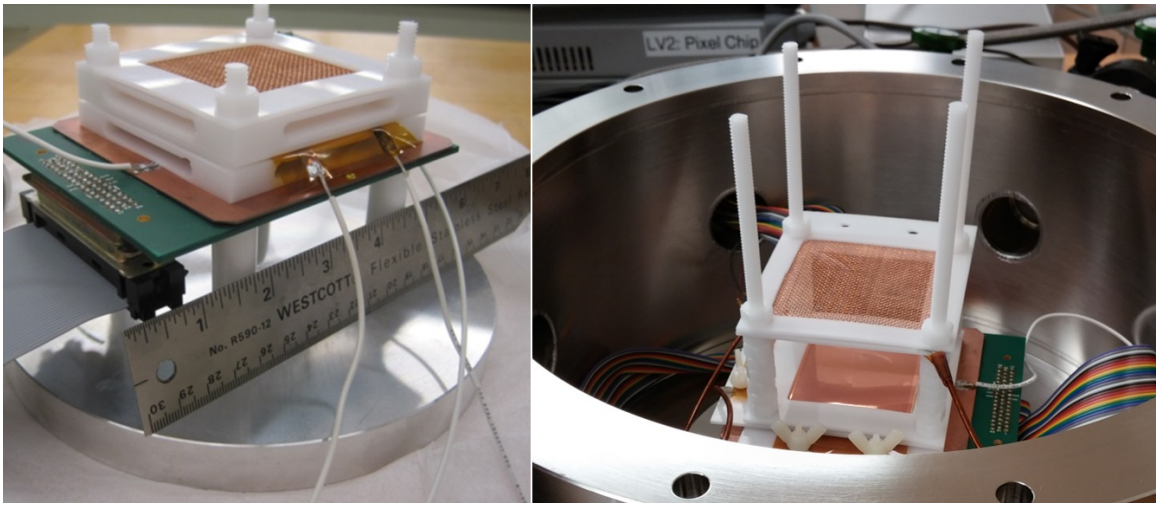

Figure 58: *Left: micro-TPC fast neutron detector pre-prototype, showing the mechanical support structure with Gas Electron Multipliers (orange, transparent foil) and Printed Circuit Board (green) with Pixel Chip installed. The sensitive volume in this detector configuration is small - an 8.6-mm "drift gap" between the GEMs and a copper mesh, which is held at a high voltage and provides a uniform electric field. Right: Larger pre-prototype with 5-cm drift gap.*

the TPC drift field, which will be parallel to the Belle II solenoid magnetic field, to minimize diffusion of drift charge. Ionization in the detector will be amplified with standard 5x5cm GEMs available from CERN. Approximately 4 cm^2 of the 5×5 cm readout plane will be instrumented with an ATLAS FE-I4 pixel chip, the rest of the area will be fed into a pulse-height analyzer, and used for gain calibration of the TPCs. The Appendix contains further details on the simulation studies that were used to optimize the TPC design. Services going to each TPC are 5V digital and analog, 20kV high voltage for the electric field cage, and gas supply. Each TPC will be self-triggering, and will be read out digitally with a SEABAS DAQ system produced by GND Co.,Ltd. of Japan. As of December 2012, the design of the pre-prototype has been completed, with more details provided in the appendix. All part have been ordered, many received, and construction is ongoing. Figure 61 shows examples

Quantity	Threshold	Objective	Specification	Measured
angular resolution (1 cm tracks)	n/a	15	5	$1-2$
energy resolution at 5.9 keV (w/o tracking)	n/a	20%	12%	10%
gain	1000	10000	20000	40000
gain stability, one week	n/a	20%	5%	$< 3\%$

Table 9: *Measured performance of micro-TPC pre-prototype, compared against Key Performance Parameter (KPP) target, object, and threshold values.*

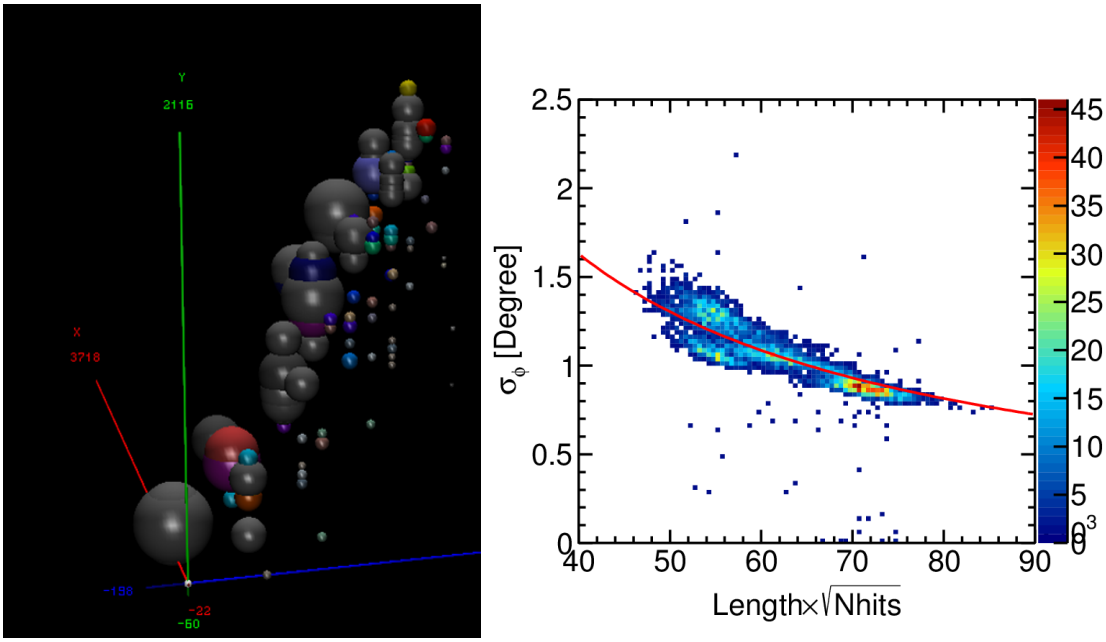

Figure 59: *Left: Helium recoil candidate event, recorded with Hawaii micro-TPC pre-prototype, operating with $HeC0_2$ gas at atmospheric pressure. The length of the track is about 4mm, which would correspond to a Helium recoil with kinetic energy of approximately 400 keV. This clearly demonstrates the ability to reconstruct such recoils in 3D. Right: Angular resolution for recoils with length of 5-mm, experimentally estimated using a Po-210 alpha source placed near the detector. The good match to the analytical prediction shows that the angular resolution is well understood from first principles, as it has the expected functional dependence on the detector.s point resolution, number of measurement points, and length of the recoil.*

of three components; the prototype vacuum vessel, a mock-up of the final field cage, and the DAQ board that will read out the FE-I4 pixel chip.

The Hawaii group will construct two full-scale micro-TPC prototypes. These will be used for detailed performance characterization with radioactive soures, studying system integration and stability issues, be subjected to a beam test, and then be installed at KEK for use during commissioning phase I. Following the beam test, another eight micro-TPCs will be constructed to be used during commissioning phase II. This phased approach will enable the incorporation of any lessons learned during the beam test in the final system and avoids the risk of radiation damage to or activation of the TPCs during phase I, when beam-gas background levels will be be severe.

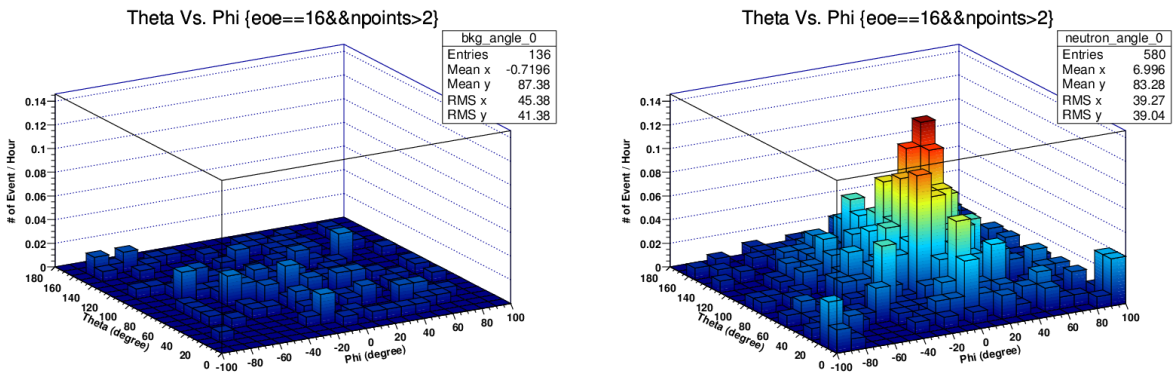

Figure 60: *Energy-weighted angular distribution of nuclear recoils observed in micro-TPC pre-prototype without (left) and with (right) a 50 μCi Cf-252 fast neutron source placed 63 cm from the detector prototype. A large excess in the energy flux is observed with the source present, and the peak of the distribution correctly point back to the neutron source location.*

5.4.11 Commissioning Detector Description - Non-US Contributions

A number of non-US institutions will be contributing to the commissioning detector effort. The National Taiwan University High Energy Physics Group (NTUHEP group) is developing a luminosity monitoring device based on Bismuth Germanate (BGO) cystals, and the pixel detector (PXD) group is planning to install two DEPFET ladders and a number of other monitors. In addition, it is anticipated that both the drift chamber (CDC) and silicon vertex detector (SVD) groups will install prototypes on the commissioning detector support structure. The University of Victoria, Canada, is planning to install He-3 thermal neutron detectors next to the micro-TPC fast neutron detectors discussed above.

5.4.12 US Belle II Project scope for the Commissioning Detector

The US Belle II Project scope includes simulation of the overall design, physics design of a shield to protect the Belle II calorimeter from radiation damage during vacuum scrubbing,

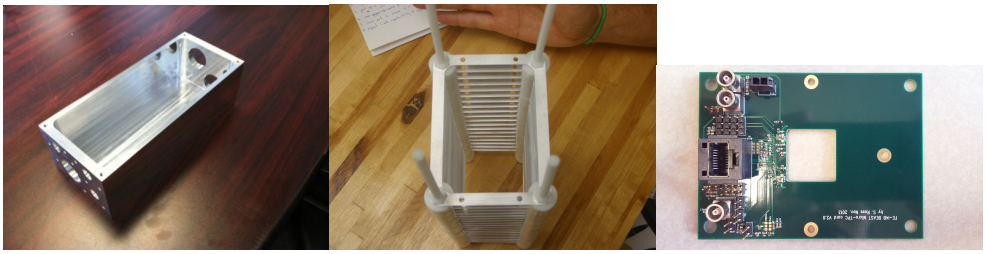

Figure 61: *Final Vacuum vessel (left), field cage mock-up (middle), and pixel DAQ baord (right) for micro-TPC final prototype.*

and design, fabrication, testing, and delivery to KEK of the support structure, the micro-TPCs and their readout electronics, and the PIN diode system for dose measurement.

Integration of other detectors into the Commissioning Detector System, such as DEPFET pixel detectors, silicon strip detectors, as well as installation and operation of the system during commissioning of the SuperKEKB accelerator is outside the scope of the US Belle II Project. It is anticipated that significant US resources will contribute to those activities, but that these would be funded outside of the US Belle II Project. A separate resource loaded work breakdown structure (WBS) has been created to capture that scope of work and to provide the appropriate linkages between the US Belle II Project effort and the integration and commissioning effort which must draw on the same resources and personnel and in some cases occur in parallel. This delineation was chosen so that the completion of the US Belle II Project is not reliant on the contributions to the commissioning detector system being provided by other institutions or tied to the schedule of the SuperKEKB accelerator.

6 Environment, Safety, and Health

The Pacific Northwest National Laboratory (PNNL) Integrated Safety Management (ISM) Program will be utilized to continually assure that functions, processes, and procedures PNNL staff use to plan and perform work enable them to understand the work scope, risks/hazards, and appropriate tailored controls so they may conduct their work safely.

The US Belle II Management Team is committed to conducting all work so that the mission can be accomplished with adequate controls in place to protect the public, the workers, and the environment. Operation of existing electron accelerators across DOE facilities has provided familiarity with the principal hazards and risks associated with them. Existing and mature programs at PNNL will be used to ensure that all aspects of the design, fabrication, and assembly and testing of the Belle II detector systems are funded under DOEs program are properly managed. Environment, safety and health (ES&H) will be integrated into all phases of planning and implementation through to the final design and production processes of U.S. Belle II by applying the ISM program.

Additional information on the hazard analysis results is available in the US Belle II Hazards Analysis Report. DOE National Environmental Policy Act (NEPA) coverage of the project is met by a categorical exclusion. Applicable ES&H expectations will be flowed down from PNNL to collaborating institutions on the U.S. Belle II Project by way of either subcontracts or Memoranda of Understanding agreements.

7 Quality Assurance and Quality Control

Quality Assurance (QA) is an integral part of effective project management and are employed throughout the design, procurement, and construction of the project. All work on the US Belle II Project are performed in compliance with the DOE approved PPEP and Project Specific Quality Assurance Program (PQAP). The PQAP establishes all applicable Quality Assurance (QA) requirements for the US Belle II project and its Integrated Project Team (IPT) members consistent with DOE Order 413.3B. The PQAP is based on the DOE adopted QA Criteria and supports the management approach and project execution processes that are used to successfully execute the project. In addition, national codes and standards are followed throughout as applicable.

The US Belle II PQAP describes how QA is integrated and implemented on the project. The PQAP establishes the QA graded approach for work performed by DOE National Laboratories, Universities, and other US Belle II participants. For essential components, quality requirements have been established for purchased, construction, lab fabrication, or for all sub contractors performing work for the project. Refer to the design and procurement documents for specific QA, testing and evaluation, and acceptance requirements.

The US Belle II Project will use the PNNL Issue Tracking System (ITS) as the central repository to track any project QA issues, deficiencies, non-conformances and related corrective actions. This use of PNNLs ITS will facilitate the ability to do tracking and trending as well as the integration of QA on the project and among US Belle II IPT members.

References

[1] K. Abe *et al.*, KEK report 04-4, hep-ex/0406071. The Belle technical design report (TDR), edited by Z. Dolezal and S. Uno, T. Abe et al., (Belle II collaboration), arXiv: 1011.0352.

[2] See for example: A. J. Schwartz, "Complementarity: Flavor Physics in the LHC Era," invited talk at the Tenth Conference on the Intersections of Particle and Nuclear Physics (CIPANP 2009), arXiv:0909.4344.

[3] R. Louvot et al. (Belle collab.), arXiv:0809.2526; J. Wicht et al. (Belle collab.) Phys. Rev. Lett 100, 121801 (2008); A. Drutskoy et al. (Belle collab.) Phys. Rev. D 76, 012002 (2007); A. Drutskoy et al. (Belle collab.) Phys. Rev. Lett. 98, 052001 (2007).

[4] S-W Lin et al. (Belle collab.), Nature 452, 332 (2008).

[5] T. E. Browder, T. Gershon, D. Pirjol, A. Soni and J. Zupan, Rev. Mod. Phys. **81**, 1887 (2009).

[6] T. E. Browder, M. Ciuchini, T. Gershon, M. Hazumi, T. Hurth, Y. Okada, and A. Stocchi, JHEP 0802: 110 (2008).

[7] N. Taniguchi *et al.* (Belle Collab.), Phys. Rev. Lett. **101**, 111801 (2008).

[8] G.S. Varner, L.L. Ruckman, R.J. Nichol, J. Nam, J. Cao, M. Wilcox and P. Gorham, "Large Analog Bandwidth Recorder and Digitizer with Ordered Readout (LABRADOR) ASIC," Nucl. Instr. Meth. **A483** (2007) 447-460.

[9] G. Varner, *et al.*, "A Giga-bit Ethernet Instrument for SalSA Experiment Readout", Nucl. Instr. Meth. **A 554** (2005) 437-443.

[10] G. Varner, *et al.*, "Monolithic Multi-channel GSa/s Transient Waveform Recorder for Measuring Radio Emissions from High Energy Particle Cascades", Proc. SPIE Int. Soc. Opt. Eng. 4858-31, 2003.

[11] S. Kleinfelder *et al.*, "GHz Waveform Sampling and Digitization Circuit Design and Implementation", IEEE Trans. Nucl. Sci. **50** 955 (2003).

[12] G.S. Varner *et al.* [ANITA Collaboration], "Detection of Ultra High Energy Neutrinos via Coherent Radio Emission," SLAC-PUB-11872, SNIC-2006-0046, Proceedings of International Symposium on Detector Development for Particle, Astroparticle and Synchrotron Radiation Experiments (SNIC 2006), Menlo Park, California, 3-6 Apr 2006, pp 0046.

[13] P. Gorham *et al.* [ANITA Collaboration], "The Antarctic Impulsive Transient Antenna Ultra-high Energy Neutrino Detector Design, Performance, and Sensitivity for 2006-2007 Balloon Flight," Astroparticle Physics **32** (2009) 10-41. arXiv:0812.1920

[14] DE-FG02-06ER41424 (PI Gary Varner)

[15] DE-FG02-08ER41571 (PI Gary Varner)

[16] G.S. Varner, L.L. Ruckman and A. Wong, "The First version Buffered Large Analog Bandwidth (BLAB1) ASIC for high luminosity collider and extensive radio neutrino detectors," Nucl. Instr. Meth. **A591** (2008) 534-545.

[17] J. Benitez *et al.*, "Development of a Focusing DIRC", Prepared for 2006 IEEE Nuclear Science Symposium, SLAC-PUB-12236.

[18] J. Benitez, D.W.G.S. Leith, G. Mazaheri, B.N. Ratcliff, J. Schwiening, J. Vavra, L. Ruckman, G.S. Varner, "Status of the Fast Focusing DIRC (fDIRC)," Nucl. Instr. Meth. **A595** (2002) 104-107.

[19] G. Varner and L. Ruckman, "Sub-10ps Monolithic and Low-power Photodetector Readout," Nucl. Instr. Meth. **A602**(2009) 438-445. [arXiv:0805.2225 [physics.ins-det]].

[20] D. Breton, E. Delagnes, J. Maalmi, K. Nishimura, L.L. Ruckman, G. Varner, J. Vavra, "High resolution timing with MCP-PMTs: a comparison of commercial constant fraction discriminator (CFD) with ASIC-based waveform readout digitizers TARGET and WaveCatcher," Nucl. Instr. Meth. **A629** (2011) 123-132.

[21] T. Higuchi *et al.*, "Belle2link Design", Draft specification v.0.3: http://www.phys.hawaii.edu/∼idlab/taskAndSchedule/local_DAQ/Belle2link-note-draft-ver0.3.doc

[22] T. Higuchi *et al.*, "Development of a PCI based Data Acquisition Platform for High Intensity Accelerator Experiments", CHEP-2003-TUGT004 (2003), hep-ex/0305088.

[23] Y. Igarashi *et al.*, "The Data Acquisition System Based on PMC Bus", CHEP-2003-TUGP009 (2003), physics/0305137.

[24] D. Beznosko *et al*, "FNAL-NICADD Extruded Scintillator", FERMILAB-CONF-04-216-E (2004).

[25] Y. Kudenko (T2K Collaboration), "The near neutrino detector for the T2K experiment," arXiv:0805.0411 (2008).

[26] J. Cohen-Tanugi *et al.*, "Optical Properties of the DIRC Fused Silica Cherenkov Radiator," Nucl. Instr. Meth. Phys. Res. A 515 (2003) 680.

[27] T. Kim, M. Freytsis, J. Button-Shafer, J. Kadyk, S. E. Vahsen and W. A. Wenzel, "Readout Of TPC Tracking Chambers With GEMs And Pixel Chip", Nucl. Instrum. Meth. **A589** (2008), 173-184

[28] R. Cizeron, A. Durand, T.L. Geld, V. Lepeltier, B. Meadows, Michael T. Ronan, S. Sen, A. Valassi, G. Wormser, "A Mini - TPC for SLAC B factory commissioning", Nucl. Instrum. Meth. **A419** (1998), 525-531

[29] K. Miuchi et al., "Performance of a micro-TPC for a time-resolved neutron PSD", Nucl. Instrum. Meth. **A517** (2003), 219-225

[30] J. Yamaoka, H. Feng, M. Garcia-Sciveres, I. Jaegle, J. Kadyk, Y. Nguyen, M. Rosen, S. Ross, T. Thorpe, S. Vahsen, "Application of Time Projection Chambers with GEMs and Pixels to WIMP Searches and Fast Neutron Detection", TIPP2011, submitted to Elsevier Physics Procedia (2011)

[31] S. E. Vahsen, H. Feng, M. Garcia-Sciveres, I. Jaegle, J. Kadyk, Y. Nguyen, M. Rosen, S. Ross, T. Thorpe, J. Yamaoka,"The Directional Dark Matter Detector", arXiv:1110.3401v1 (2011)

[32] Belle II Technical Design Report, `http://xxx.lanl.gov/ abs/1011.0352`

[33] A. Piwinski, "The touschek effect in strong focusing storage rings", Mar 1999.

[34] H. Nakayama et al, "Small-Beta Collimation at SuperKEKB to Stop Beam-Gas Scattered Particles and to Avoid Transverse Mode Coupling Instability", IPAC-2012-TUOBC02.

A Quartz Specifications

A.1 Overview

Battelle Memorial Institute, operating the Pacific Northwest National Laboratory (PNNL) for the U.S. Department of Energy (DOE), seeks to procure synthetic fused silica optics for the Imaging Time-of-Propagation (iTOP) detector, one element of the Belle-II experiment at KEK laboratory, Tsukuba, Japan.

This detector will utilize 16 long-bars having an overall length of 2.50 m (nominal). The bars will be arranged azimuthally around the beamline such that the bar lengths are aligned with the beam (z) axis. Each long-bar will be constructed from two bars of length 1.25 m (nominal) epoxied together end-to-end. The width of the bars will be 450 mm (nominal), and the bar thickness will be 20 mm (nominal). In addition to the 16 production long-bars, several prototype units will also be produced.

At one end of each long bar a prism fabricated from synthetic fused silica will be attached to guide the light from the bar to an array of photodetectors. At the other end of the long bar a spherical mirror will reflect the light back to the photodetector array. The final joining of these units into a complete optical assembly will be done on-site at KEK in Japan.

A.2 Material

The optical components shall be fabricated Corning 7980 class 0, grade F or better. As the vendor is aware, the as-cut blank material will exceed the homogeneity specification near the surfaces where subsurface damage is present that introduces large stress locally in the material. It is expected that the vendor will use appropriate grinding, polishing and etching techniques to ameliorate this subsurface damage in the course of finishing the blank to final specifications.

A.3 Bar Specifications

Dimensional tolerances can also be found in Fig. 62.

- Thickness 20.00±0.10 mm
- Width 450.00±0.15 mm
- Length 1250.00±0.50 mm

The following geometrical tolerances shall also be satisfied:

Tolerance	Specification	Comments
S1 ▱ (Datum A)	≤6.3 μm	Equal to 10 waves over full aperture of surface
S2 ▱	≤6.3 μm	Equal to 10 waves over full aperture of surface
S3 ▱ (Datum B)	≤6.3 μm	Equal to 10 waves over full aperture of surface
S4 ▱	≤6.3 μm	Equal to 10 waves over full aperture of surface
S5 ▱ (Datum C)	≤25 μm	Equal to 40 waves over full aperture of surface
S6 ▱	≤25 μm	Equal to 40 waves over full aperture of surface
S1 // S2	≤4 arcsec	4 arcsec = 24 micron runout over 1.25 m
S1 ⊥ S3	≤20 arcsec	20 arcsec = 2 micron runout over 20 mm
S1 ⊥ S4	≤20 arcsec	20 arcsec = 2 micron runout over 20 mm
S1 ⊥ S5	≤1 arcmin	1 arcmin = 6 micron runout over 20 mm
S1 ⊥ S6	≤1 arcmin	1 arcmin = 6 micron runout over 20 mm
S3 // S4	≤60 μm	60 microns = 10 arcsec over 1.25 m as projected on datum A; note that an angular specification would over-constrain perpendicularity relative to S1
S3 ⊥ S5	≤20 arcsec	20 arcsec = 44 micron runout over 0.450 m; note that this tolerance is comparable to the flatness of the surface S5
S3 ⊥ S6	≤20 arcsec	20 arcsec = 44 micron runout over 0.450 m; note that this tolerance is comparable to the flatness of the surface S6
S5 // S6	≤20 arcsec	20 arcsec = 44 micron runout over 0.450 m

Table 10: Quartz Bar Specifications

In addition to the dimensional tolerances above, there are additional optical specifications: local surface flatness, surface roughness, the area of scratches and digs, the maximum allowable edge chamfer, and the number and size of allowable chips.

- Local flatness is important for the two large faces (S1 and S2). In addition to the total surface flatness specified above, the surface flatness shall be $\leq 1.8\mu m$ (3 waves) over any 20 cm x 20 cm area.
- Surface roughness shall be ≤5 angstroms RMS for surfaces S1, S2, S3 and S4 and shall be ≤25 angstroms RMS for surfaces S5 and S6.
- All surfaces shall have ≤75 mm^2 total area of scratches and digs and any 100 mm^2 area shall have ≤3 mm^2 of scratches and digs. Surfaces S5 and S6 shall have ≤5 mm^2 total area of scratches and digs (per surface).
- All chamfers (bevels) of edges shall have face width ≤ 0.2 mm to sharp.
- Each bar shall have total area of all chips ≤ 25 mm^2. Bars should have ≤20 chips total on all edges.

- No chip should have edge length >10 mm or face width >1 mm and no more than 2 chips on a bar should have edge length >1 mm.
- Surfaces S5 and S6 (including their edges) shall have total area of all chips $\leq$10 mm^2 (per surface).

Surface	L(mm)	W(mm)	Flatness	Roughness (RMS)
S1	1250±0.50	450±0.15	10 waves, 3 waves locally	5 angstrom
S2	1250±0.50	450±0.15	10 waves, 3 waves locally	5 angstrom
S3	1250±0.50	20±0.10	10 waves	5 angstrom
S4	1250±0.50	20±0.10	10 waves	5 angstrom
S5	450±0.15	20±0.10	40 waves	25 angstrom
S6	450±0.15	20±0.10	40 waves	25 angstrom

Table 11: Quartz Bar Specifications

A.4 Prisms Specifications

Attached to the backward end of each long quartz bar will be a quartz prism (or wedge) optic. This optic will be in the shape of an extruded trapezoid where two of the angles of the trapezoid are right angles, as shown in the attached drawing. Of the six faces, one face is epoxied to the downstream face of a long quartz bar and the opposite face is joined (via a wavelength filter and an optical cookie) to two rows of Hamamatsu SL-10 phototubes, with 16 phototubes per row; the prism acts as an expansion volume from the thin bar to the thicker phototube array. Dimensional tolerances can also be found in Fig. 63.

- Thickness at bar end 20±0.10 mm
- Thickness at photodetector array end 51±0.10 mm
- Width 456±0.15 mm
- Length $100^{+0.10}_{-0.25}$ mm
- Prism angle 18.07±0.04 degrees

In addition to the dimensional tolerances above, there are additional optical specifications: local surface flatness, surface roughness, the area of scratches and digs, the maximum allowable edge chamfer, and the number and size of allowable chips.

The following geometrical tolerances shall also be satisfied:

Tolerance	Specification	Comments (e.g. driver for specification)
S1 ▱ (Datum A)	≤6.3 μm	Equal to 10 waves over full aperture of surface
S2 ▱	≤6.3 μm	Equal to 10 waves over full aperture of surface
S3 ▱ (Datum B)	≤25 μm	Equal to 40 waves over full aperture of surface
S4 ▱	≤25 μm	Equal to 40 waves over full aperture of surface
S5 ▱ (Datum C)	≤6.3 μm	Equal to 10 waves over full aperture of surface
S6 ▱	≤6.3 μm	Equal to 10 waves over full aperture of surface
S1 ∠ S2	≤60 μm	This equates to ~2.3 arcmin along the 90 mm length of the wedge or ~1/2 arcmin across 456 mm width of wedge
S1 ⊥ S3	≤25 μm	This equates to ~4.3 arcmin along the 20 mm thickness
S1 ⊥ S4	≤25 μm	This equates to ~1.7 arcmin along the 50 mm thickness
S1 ⊥ S5	≤100 μm	This equates to ~6.8 arcmin along the 50 mm thickness
S1 ⊥ S6	≤100 μm	This equates to ~6.8 arcmin along the 50 mm thickness
S3 // S4	≤20 arcsec	20 arcsec = 40 micron runout over 0.456 m
S3 ⊥ S5	≤200 μm	This equates to ~7.6 arcmin along the 90 mm length
S3 ⊥ S6	≤200 μm	This equates to ~7.6 arcmin along the 90 mm length
S5 // S6	≤200 μm	This equates to ~7.6 arcmin along the 90 mm length

Table 12: Quartz Prism Specifications

- Surface roughness shall be ≤5 angstroms RMS for surfaces S1, S2, S5 and S6 and shall be ≤25 angstroms RMS for surfaces S3 and S4.
- All surfaces shall have ≤10 mm^2 total area of scratches and digs and any 100 mm^2 area shall have ≤3 mm^2 of scratches and digs.
- All chamfers (bevels) shall have face width ≤ 0.2 mm to sharp.
- All edges shall have ≤ 10 edge chips per meter of edge length and all chips shall have a maximum edge length ≤ 3 mm. Total chip area shall be ≤ 5 mm^2.

A.5 Mirror Specifications

Attached to the forward end of each long quartz bar will be a concave spherical mirror to focus the Cerenkov light. One of the six faces will be ground and polished to a spherical surface and subsequently coated with a reflective metal such as Ag or Al. The opposite surface will be epoxied to the upstream face of a long bar. Dimensional tolerances can also be found in Fig. 64.

- Thickness 20±0.10 mm

- Width 450±0.15 mm
- Length 100±0.15 mm

The spherical surface shall have the following dimensions and tolerances

- Radius of curvature of spherical surface 6500±100 mm
- Center of curvature located coincident to surface S1 (upper surface of optic) and along the central axis of surfaces S3 and S4 to a precision of ±1 mm at the center of the spherical surface (i.e. at 6.5 meters). The mirror optical axis will define datum B.
- All mirrors will be qualified using a test plate with the aforementioned radius of curvature and center of curvature; the number of fringes between a mirror and the test plate must correspond to $\leq$ 5 waves. Vendors may recommend alternative inspection methods and such methods may be adopted with written permission from Battelle.

All faces except for that opposite the spherical surface shall have a roughness of $\leq$5 angstroms r.m.s.; the face opposite the spherical surface (S5) shall have a roughness of $\leq$ 25 angstroms r.m.s. The number of edge chips should not exceed 10 chips per linear meter, and all chips must be less than 0.5 mm in size. All chamfers shall have face width $\leq$ 0.2 mm to sharp. In addition to the dimensional tolerances above, there are additional optical specifications:

- Surface roughness shall be $\leq$5 angstroms RMS for surfaces S1, S2, S3 and S4 and shall be $\leq$25 angstroms RMS for surface S5.
- All surfaces shall have $\leq$10 mm^2 total area of scratches and digs and any 100 mm^2 area shall have $\leq$3 mm^2 of scratches and digs.
- All chamfers (bevels) shall have face width $\leq$ 0.2 mm to sharp.
- All edges shall have $\leq$ 10 edge chips per meter of edge length and all chips shall have a maximum edge length $\leq$ 3 mm. Total chip area shall be $\leq$ 5 mm^2.

The mirrored surface will reflect internal light so the aluminization will be directly on the quartz and the protective coating applied over the metal to prevent oxidization and to improve robustness for handling. Vendors should provide recommendations for the protective coating layer(s). A robust coating (for instance a polymer encapsulant) that provides protection superior to Al/SiO2 is highly desirable. The mirror surface shall have reflectivity $>$ 85% for wavelengths of 300-600 nm.

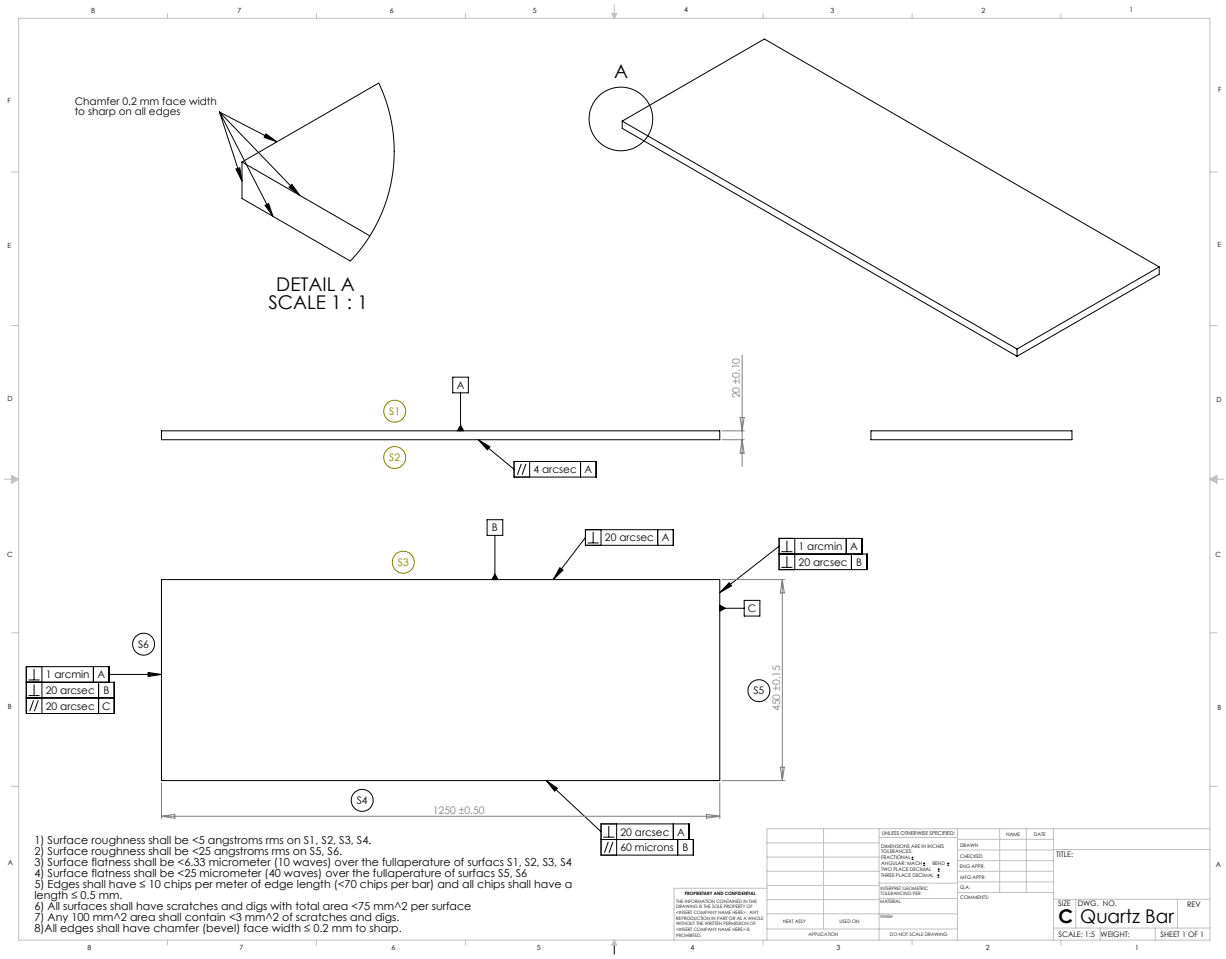

Figure 62: Quartz Bar Engineering Drawing

The following geometrical tolerances shall also be satisfied:

Tolerance	Specification	Comments (e.g. driver for specification)
S1 ▱ (Datum A)	≤6.3 μm	Equal to 10 waves over full aperture of surface
S2 ▱	≤6.3 μm	Equal to 10 waves over full aperture of surface
S3 ▱	≤6.3 μm	Equal to 10 waves over full aperture of surface
S4 ▱	≤6.3 μm	Equal to 10 waves over full aperture of surface
S5 ▱ (Datum C)	≤25 μm	Equal to 40 waves over full aperture of surface
S1 // S2	≤30 μm	This equates to ~50 arcsec along the 100 mm length of the wedge or ~14 arcsec across 450 mm width of wedge
S1 ⊥ S3	≤25 μm	This equates to ~4.3 arcmin along the 20 mm thickness
S1 ⊥ S4	≤25 μm	This equates to ~4.3 arcmin along the 20 mm thickness
S1 ⊥ S5	≤25 μm	This equates to ~4.3 arcmin along the 20 mm thickness
Datum B // S1	≤0.7 arcmin	0.7 arcmin= 20 micron runout over 100 mm, 1.3 mm over 6.5 m
S3 // Datum B	≤0.7 arcmin	0.7 arcmin= 20 micron runout over 100 mm, 1.3 mm over 6.5 m
S4 // Datum B	≤0.7 arcmin	0.7 arcmin= 20 micron runout over 100 mm, 1.3 mm over 6.5 m
S3 // S4	≤1 arcmin	1 arcmin= 29 micron runout over 100 mm
S5 ⊥ Datum B	≤20 arcsec	20 arcsec = 44 micron runout over 0.450 m

Table 13: Quartz Mirror Specifications

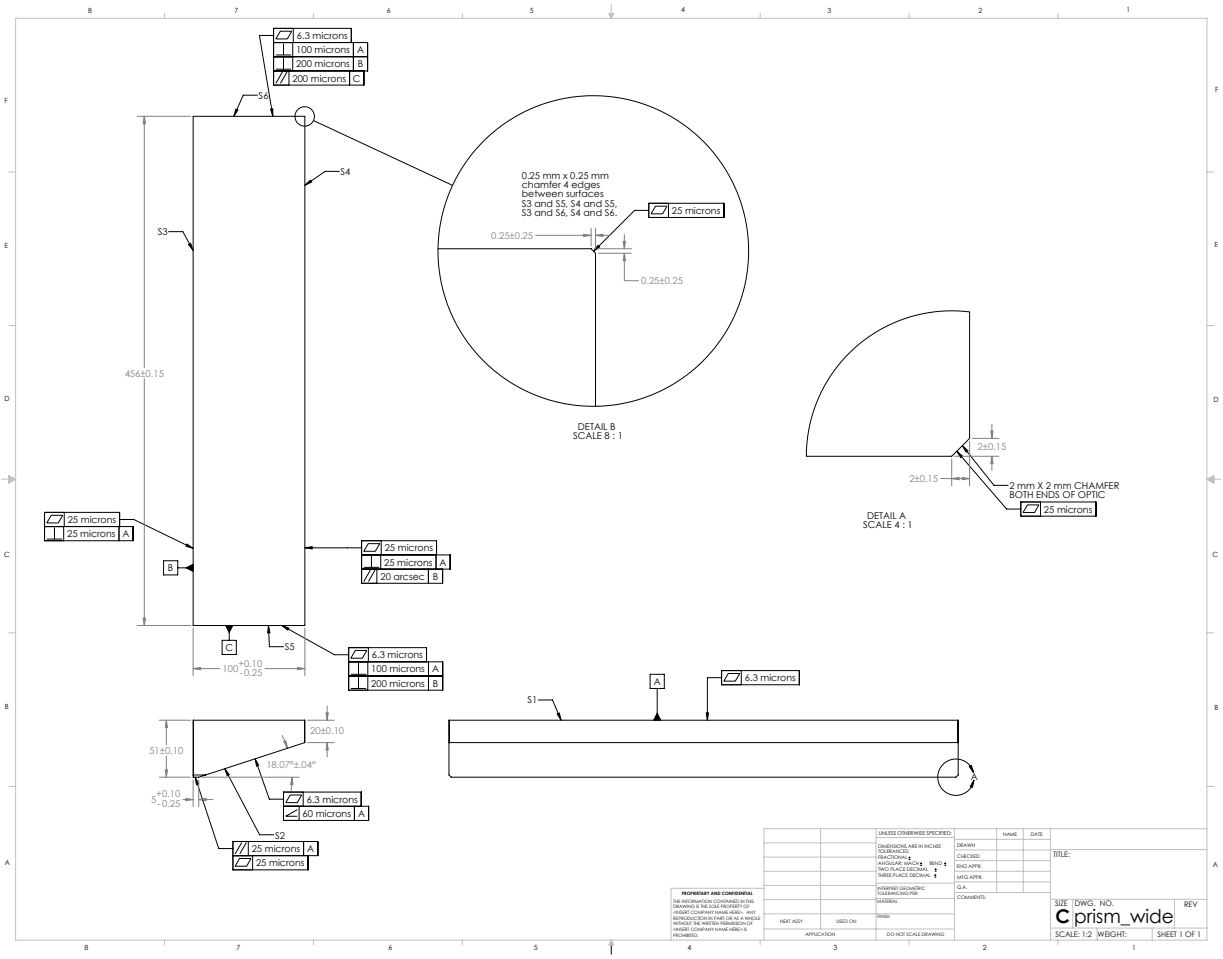

Figure 63: Quartz Prism Engineering Drawing

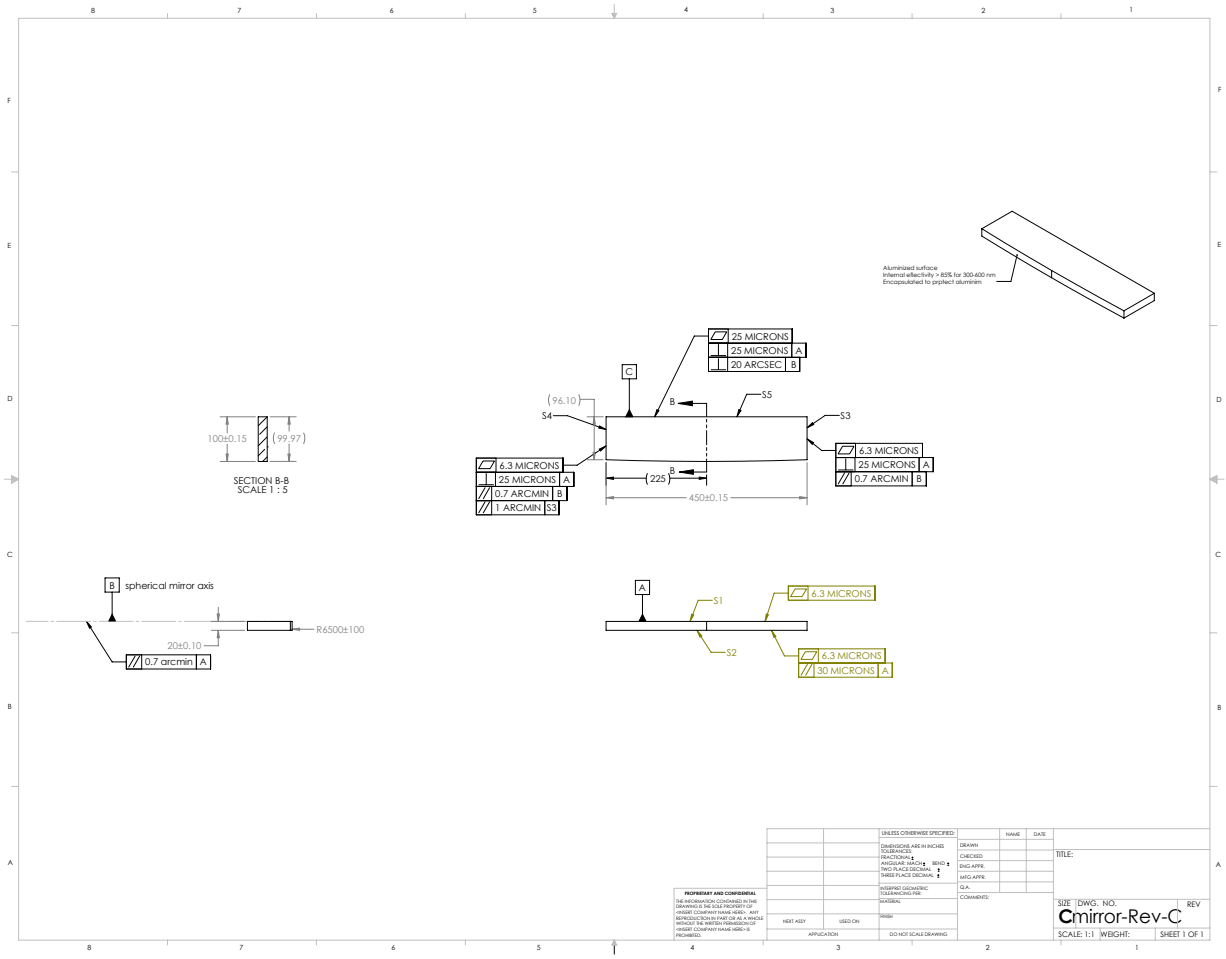

Figure 64: Quartz Mirror Engineering Drawing

B Quartz Acceptance Test Plan

B.1 Overview

To take acceptance of quartz optical components requires verification that such components were fabricated to both mechanical and optical specifications. For all optical components the majority of such verification will be performed by the manufacturer and made available to PNNL via a metrology report furnished with each completed optical component. Any failures to meet any specifications will be duly noted on these reports. In addition, the reports will contain the final physical dimensions of all optical components and a complete "scratch and digs" report noting the locations and sizes of all surface scratches, chips, and imperfections.

In addition to these metrology reports, the iTOP group will perform a complementary set of measurements to verify optical performance. These include measuring the focal length of the focusing mirrors, the tilt angle of the tilted face of the prisms, and the optical transmission of all components. These tests will be done at two locations: bars will be tested at KEK in the same clean room used to assemble the iTOP modules, and mirrors and prisms will be tested at the University of Cincinnati prior to shipping to KEK. The measurements described below have been previously performed at the University of Cincinnati, at Nagoya University, and at KEK.

B.2 Acceptance Testing at the Manufacturers

Prior to component delivery, the iTOP group will review the manufacturers' metrology report provided with the furnished optic. PNNL (as contracting agent) or other iTOP personnel may travel to a manufacturer facilities to observe and approve their acceptance tests. This requirement is included in the Quality Assurance Requirements portion of PNNLs contracts with the component suppliers. These tests will verify that all specified physical dimensions and optical requirements for surfaces (flatness, roughness, parallelism, and perpendicularity) are met. The manufacturers will mainly use large aperture interferometers, high precision Coordinate Measuring Machines (CMMs), and various magnifiers to make these measurements. Manufacturers will provide PNNL with their acceptance test plan for approval, and the metrology report furnished will specify what was inspected or measured, the result of the measurement, and whether the result satisfies the required optical/mechanical specification.

The angle of the tilted face of the prism will be measured with a CMM. This value will be checked optically with higher precision at the University of Cincinnati as described below. The mirror radius of curvature will be measured by counting fringes with a test plate; this value will also be checked optically at Cincinnati (see below).

B.3 Testing Bars at KEK

The bars will be shipped directly from the manufacturer to KEK, where they will be tested in the same cleanroom as will be used for gluing together the optics and iTOP module assembly.

B.3.1 Chip inspection

Two quartz bars are unpacked from their wooden crates outside the cleanroom. They will be enclosed in sealed plastic bags surrounded by Styrofoam. The Styrofoam "packages" can be hand-carried into the outer clean room and stored. When ready for assembly, the Styrofoam is removed in the outer clean room and a sealed bag is carried into the inner cleanroom. Here the bag is opened, cut away, and the quartz bar placed on the large optical table. The procedure is repeated with another quartz bar such that there are two bars on the table – see Fig. 65. Subsequently, seven "camera rails" are positioned around the bars as shown in Fig. 65. Two cameras are mounted on these rails, one for each quartz bar, and a chip search is commenced for both bars in parallel. For each bar the lower four edges are scanned first, then the camera is raised, and finally the upper four edges are scanned. A schematic diagram of the camera system is shown in Fig. 66.

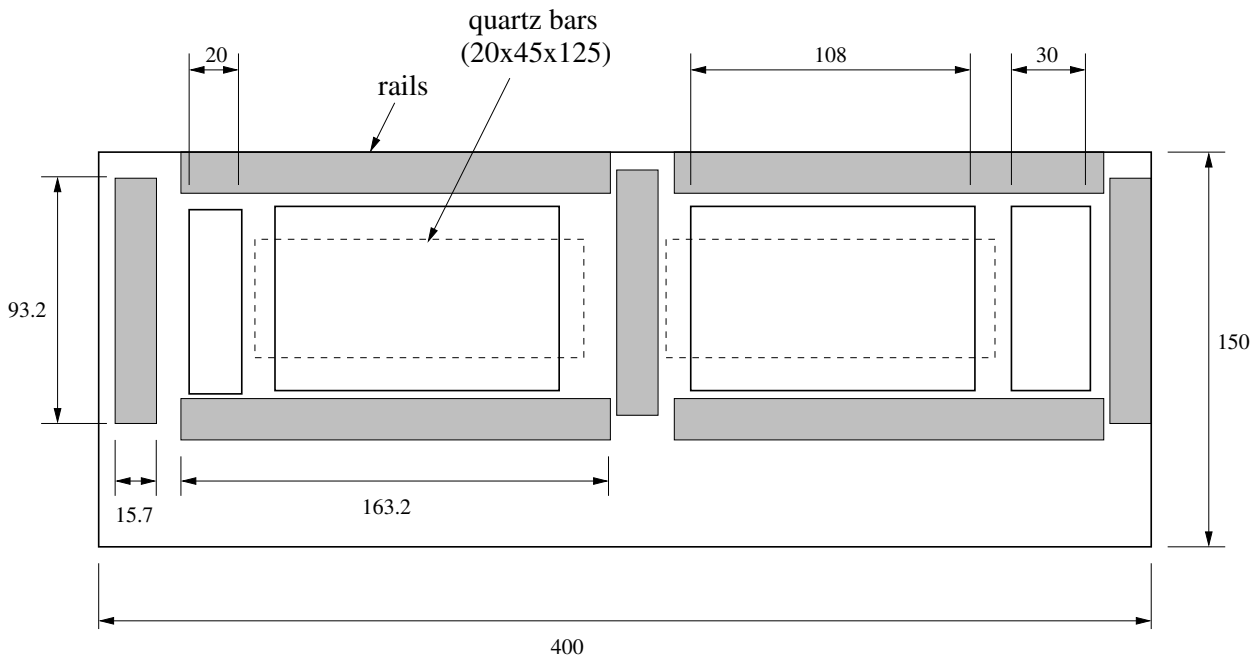

Figure 65: Plan view of the optical table as used for chip inspection. Both bars can be inspected in parallel. All dimensions are in centimeters.

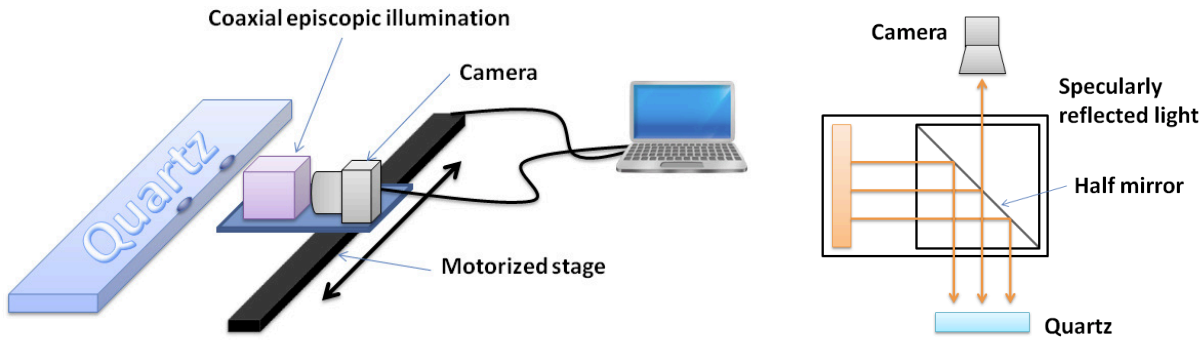

Figure 66: Schematic diagram of the camera assembly used for the chip search in bars.

B.3.2 Bulk transmittance and surface reflectivity

After the chip search is completed, the camera rails are removed and three x-y stages are positioned as shown in Fig. 67. A laser is placed to the side of the center x-y stage, a mirror is mounted on this stage, and photo-diodes are mounted on the end stages. This setup is then used to measure the bulk transmittance and surface reflectivity of the bars. Each bar will be measured in turn (sequentially) by a two-man team.

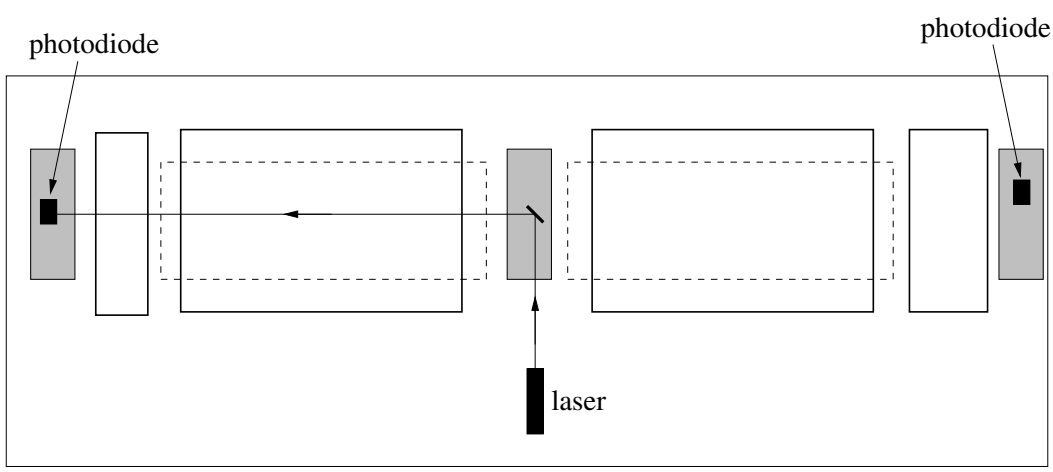

Figure 67: Plan view of the optical table as used for measurements of bulk transmission and surface reflectivity. Due to the use of only one center stage, the bars will be measured sequentially.

The setup used to measure the coefficient of total internal reflection (α) is shown in Fig. 68. A laser beam enters one end of the bar, totally internally reflects down the bar, and refracts out of the bar where the intensity (I_1) is measured by a photodiode. Comparing to the incident intensity (I_0) gives the total light loss within the bar. From this value one calculates α via the formula $(I_1 - R_1) = (I_0 - R_0) \cdot \alpha^N \cdot \exp\left(-(L/\Lambda) \cdot \sqrt{1 + (Nh/L)^2}\right)$, where Λ is the bulk attenuation of the quartz ($\gtrsim 1000\ m$), L (h) is the bar length (height),

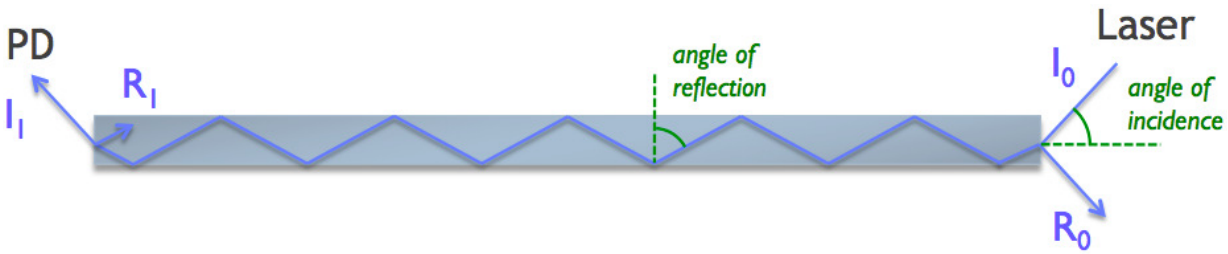

Figure 68: Schematic of method used to measure the coefficient of total internal reflectance of a quartz bar.

Incident angle (degrees)	Angle of internal reflection (degrees)	# of bounces	Internal surface reflectivity
56.0	55.7	41	**0.9993**
50.0	58.6	37	**0.9994**
45.0	61.2	33	**0.9995**
40.0	64.1	29	**0.9996**
35.0	67.0	25	**0.9995**
30.0	70.1	21	**0.9999**

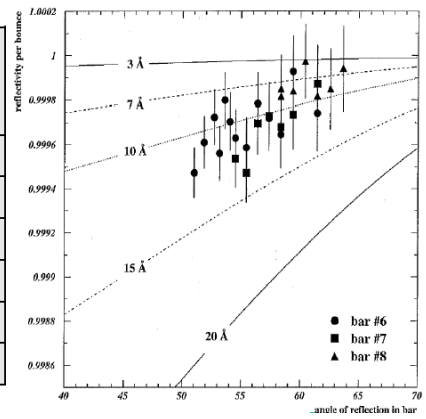

Figure 69: Measurements of the coefficient of total internal reflection for a prototype bar performed at Nagoya University. Measured values obtained at KEK and at Cincinnati (using a BaBar DIRC bar) are similar.

N is the number of light bounces within the bar, and the reflected intensities R_0 and R_1 are calculated via the Fresnel equations. This procedure is similar to that described in Ref. [26]. Results of previous measurements made at Nagoya University are plotted in Fig. 69.

B.3.3 Other tests: optical interfaces after gluing

After attaching the mirror and prism to the quartz bars, it is necessary to test these optical interfaces for high transmission. To test the mirror-bar interface, a laser beam is sent from the center x-y stage through the bar, reflected off the mirror, and back through the bar to a photo-diode also mounted on the center x-y stage (see Fig. 70). This photo-diode should have a large area such that when the beam is scanned across the face of the bar, the reflected beam remains in the photo-diode active area. The response function of this active area will have been previously mapped and thus calibrated. To test the prism-bar interface, the same beam is sent to the right through that bar and the prism and imaged onto a photo-diode mounted on the right-most x-y stage.

Assuming the mirror and prism are attached successfully with good optical coupling, the two quartz bars are then glued together. The interface between the two quartz bars is

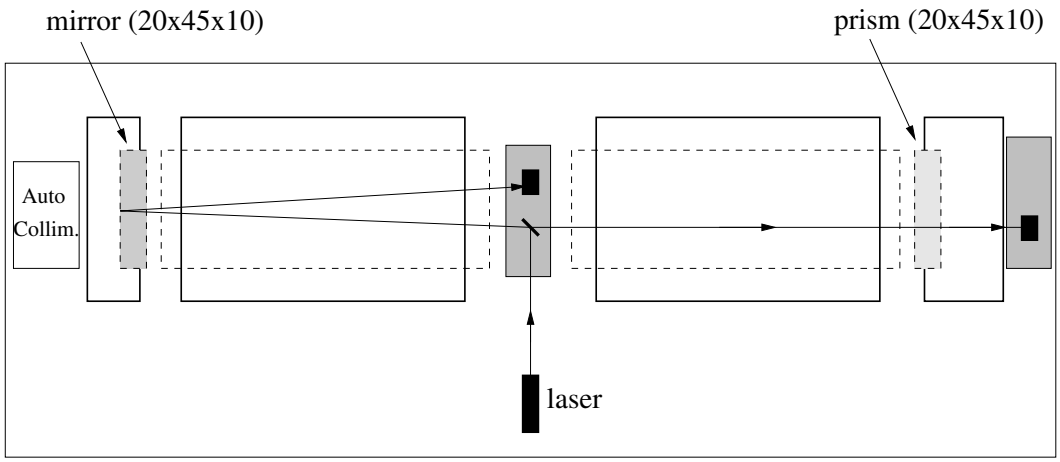

Figure 70: Plan view of the optical table as used for measurements of transmission through glue joints after the mirror and prism are attached to the bar.

subsequently tested by sending a beam from the right-most x-y stage through both bars, reflected off the mirror, and back through both bars to a large-area photo-diode mounted on the same x-y stage.

B.3.4 Testing and assembly schedule

The time required to assemble the quartz optics is estimated in Table 14. Note that this schedule assumes no failed tests for the optics and no re-work of the glue joints. The total time required is 13.5 days including contingency.

B.4 Testing Mirrors at Cincinnati

The iTOP mirrors and prisms will be fabricated by ITT Excelis and Zygo Corporation and shipped to the University of Cincinnati for testing. Components that meet specifications will be forwarded to KEK for assembly into a module. Components deemed unsatisfactory will be returned to the manufacturer for rework.

At Cincinnati a large class 1000 cleanroom with HEPA filtration and temperature/humidity control has been set up. The cleanliness of the room is monitored with a Lighthouse S3100 particle counter. This room is equipped with a 1.5m x 3m Newport optical table, a 532 nm laser, two large aperture photodiodes, several beam-splitters, a beam polarizer, a high resolution CCD camera, a high precision autocollimator, numerous high precision translation and rotation stages with robotic control, and various high precision mirrors and mounting components.

Each iTOP mirror will be inspected for surface defects (chips, scratches) and tested for bulk attenuation, reflectance, and focal aberrations. The position of the focal point will

Step	Manpower	Time (days)
Mounting 2 bars on table	4	0.5
Chip search	2	1
Bulk transmittance + surface reflectivity, bar 1	2	1
Bulk transmittance + surface reflectivity, bar 2	2	1
Alignment and gluing of mirror	2	1
Alignment and gluing of prism	2	1
Test mirror-bar interface	2	0.5
Test prism-bar interface	2	0.5
Alignment and gluing of two bars	2	1
Test bar-bar interface	2	0.5
Full cure of NOA63 bonds	1	2
Transport to other table for QBB assembly	4	0.5
Cleaning of full assembly	1	0.5
Contingency		3
Total		14.0

Table 14: Estimated time and manpower required for assembly of optical components, assuming no re-work.

be measured. The optical properties are measured using a 532 nm laser. Spherical mirrors under test will be mounted to the optics bench on a platform that can be precision translated via robotic control over 45 cm in one dimension. This allows the entire mirror surface to be mapped. For transmittance and reflectivity measurements, the beam is passed through a non-polarizing splitter. One beam is considered the test beam and the other is used as a reference for the laser output power. Two photodiodes are used to monitor the power of each beam.

B.4.1 Transmittance and reflectance

To measure transmittance, a mirror is placed in the path of the test beam and oriented so that the beam passes through the long dimension of the optic. The beam is set at normal incidence to the faces (aligned with the autocollimator) to minimize reflections. After correcting for losses at the air-quartz interfaces using the Fresnel equations, the ratio of photodiode outputs gives a measurement of the transmittance. As the path length of the beam inside the optic is known, the transmittance determines the bulk attenuation of the substrate. To measure the reflectance, the mirror is oriented to allow the test beam to reflect off the mirrored surface and the photodiode output ratio is again measured and corrected for losses at the air-quartz interface. Translating the mirror allows the reflectivity to be measured at several dozen points along the mirrored surface.

B.4.2 Focal length (radius of curvature)

To measure the focal length and focal aberrations, two methods are used. In the "two-beam" method (Fig. 71), the laser source is split into two parallel beams with fixed spatial separation. The angular alignment of the beams is achieved to within 60 micro-radians using the autocollimator. The beams have a horizontal separation of about 50 mm and a vertical separation of 15 mm. Both beams enter the mirror substrate normal to the surface and are brought to a focal point by the mirror. The CCD camera is mounted near the focal point on a pair of orthogonal 250 mm robotic translation stages. A third manual translation stage allows for vertical adjustment of the CCD. The trajectory of a reflected beam is found by scanning the CCD across the table with the other beam blocked, at two different distances from the spherical mirror. Once the trajectory of the outgoing beam is determined, the other beam is unblocked and the CCD camera is translated in x-y along the trajectory of the first beam. During this translation, the image of the second beam comes into view and passes through the image of the first beam; see Fig. 72. The positions of the CCD that in turn minimize the horizontal and vertical RMS of the beam image correspond to the tangential and sagittal focal planes, respectively. These positions are corrected for an apparent decrease in focal length due to refraction of the beams out of the mirror substrate. The mean value of these positions gives a measure of the focal length of the mirror, and the difference indicates the astigmatism of the mirror. The process is repeated for several beam input positions over the mirror surface. The resulting distributions of tangential and sagittal focal point positions indicates the degree of spherical aberration of the mirror.

These results can be checked using a "one-beam" method, in which a single beam is incident on the mirror and the trajectory of the reflected beam determined as described above. The mirror is then translated and the measurement repeated. From the resulting set of trajectories of input and reflected beams, the mirror radius of curvature can be fitted for. As a check of these procedures, the focal length of a spherical telescope mirror of known focal length was measured, 609.60 mm. The result obtained was $f = 612 \pm 8$ mm, where the error is dominated by the precision of alignment. As a further check, the radius of curvature of a prototype iTOP spherical mirror manufactured by ITT was measured, the vendor contracted to furnish all 16 iTOP mirrors. The results obtained was $r = 4955.9 \pm 7.3$ mm, in excellent agreement with ITT's own measured value of 4960 mm.

B.5 Testing Prisms at Cincinnati

Similar to the mirror inspection, each prism will be visually inspected for chips and scratches. The prisms will then be tested for transmittance, and the tilt angle of the tilted surface will be measured.

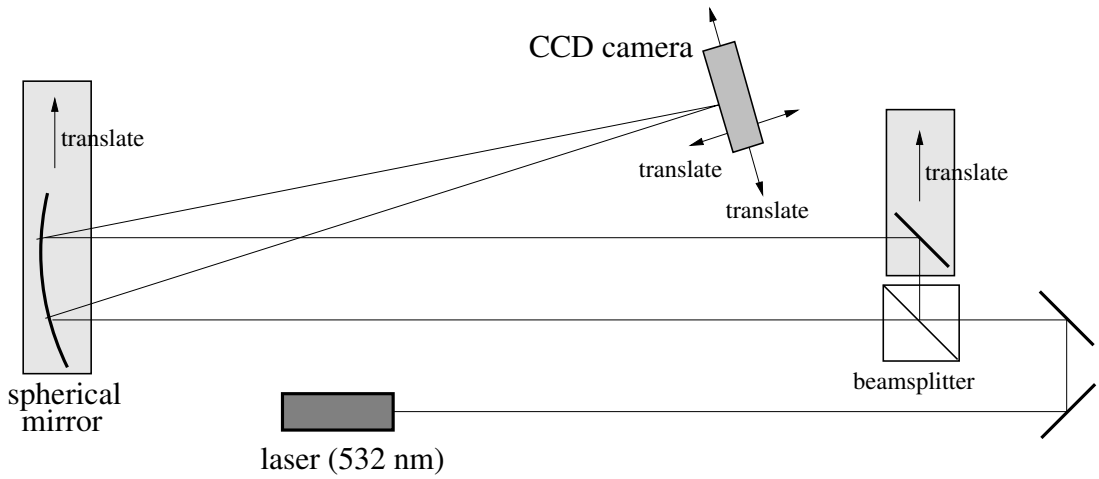

Figure 71: The laboratory configuration used to measure focal length.

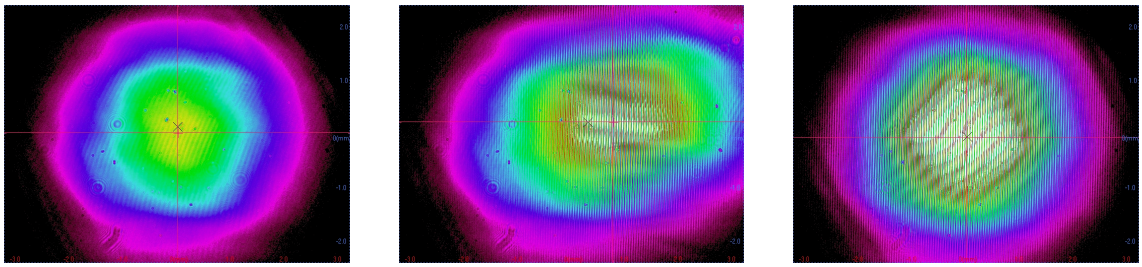

Figure 72: Left: a single reflected beam centered on the CCD. Middle: two beams, unfocused, imaged on the CCD. The CCD is translated until the overall image RMS in x and y is minimized. Right: both beams at the tangential focal point.

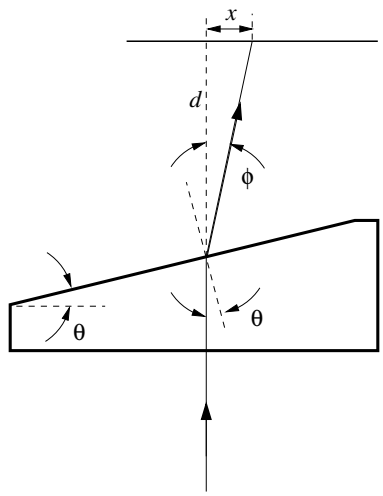

Figure 73: Set up used to measure the angle of the tilted face of the prism. A laser beam is incident normal to the non-tilted face of the prism.

B.5.1 Transmittance

The transmittance measurement is similar to that of the mirror. The test prism is placed in the path of the test beam and oriented so that the beam passes through the long dimension of the optic. The beam is at normal incidence to the faces (aligned with the autocollimator) to minimize reflections. The ratio of the two photodiode outputs gives a measurement of the transmittance, which is then corrected for losses at the air-quartz interfaces using the known polarization of the beam and the Fresnel equations. As the path length of the beam inside the optic is known, the transmittance determines the bulk attenuation of the substrate.

B.5.2 Angle of tilted face

The tilt angle of the titled face of the prism is measured as shown in Fig. 73. The beam enters the prism at normal incidence (aligned with the autocollimator), passes through the prism, and refracts out of the prism through the tilted face. The position x of the beam on an imaging surface placed a distance d behind the prism gives the tilt angle according to $\tan\theta = (x/d)/\left[n_{\mathrm{qtz}}\sqrt{1+(x/d)^2}-1\right]$. The accuracy of this value is given by $\delta\theta = \cos\phi(n\cos\phi-1)/(1+n^2-2n\cos\phi)\times(\delta x/d)$, where $\tan\phi = x/d$. For a nominal tilt angle of $\theta = 18.07°$, the angle $\phi = 8.90°$. Thus for $d = 20$ cm and $\delta x = 5$ μm (as determined by the accuracy of the Newport ILS translation stage upon which the CCD camera is mounted), $\delta\theta = 9.1$ arcseconds. This is an order of magnitude better than the manufacturing tolerance of 144 arcseconds.

B.6 Battelles Quality Assurance Requirements

The following paragraphs will be contained in the contracts established between Battelle Memorial Institute Pacific Northwest Division and the vendors providing bars, mirrors, and prisms. These requirements flow down to subcontractors the vendor uses.

B.6.1 Source Inspection (cl QA-178 – May 2003)

Contractor shall give Battelle ten (10) calendar days advance written notice of the date, time, and place the acceptance test and/or inspection is scheduled to be performed. Contractor shall in no event perform any such operation, inspection, or test prior to the date specified in its notice or change the date, time, or place specified therein without Battelle's prior written approval. Battelle's authorized representative may, but is not required to, be present. In the event said representative witnesses an operation, inspection, or test performed by Contractor or conducts an inspection, surveillance, or test on Battelle's behalf, Contractor shall be provided documentary evidence to such effect.

B.6.2 Certificate of Conformance (cl QA-180 - April 2011)

The Contractor shall submit a Certificate of Conformance containing the following:

1. nomenclature and part number
2. contract requirements met, including reference to codes, standards, specification (including revision status).

Each report shall be legible, reproducible, and contain, in addition to any other requirements as specified by this contract, the following:

1. The contract number
2. A clear identification of the supplies covered, including, but not limited to, the use of serial, lot, batch, heat, or mill number
3. The data and title of the person signing

Unless otherwise specified, Contractor shall deliver all documents required by this contract to the Battelle Contracts Representative. A document is not delivered until it is received by Battelle. Battelle shall have the right to reject, as not in conformity with the requirements of this contract, any supplies or services for which all required reports, procedures, or certifications are not delivered.

B.6.3 Test Report: Inspection Data (cl QA-191 – April 2008)

Contractor shall submit an Inspection Data Report(s) of actual inspection results, specifying what was inspected, the characteristics inspected, and the acceptance criteria, all as required by this contract. Each report shall be legible, reproducible, and contain, in addition to any other requirements as specified by this contract, the following:

1. The contract number
2. A clear identification of the supplies covered, including, but not limited to, the use of serial, lot, batch, heat, or mill numbers
3. The date and title of the person signing

Unless otherwise specified, Contractor shall mail all documents required by this contract to be delivered to the Battelle Contracts Representative, Battelle, PO Box 999, Richland, Washington 99352. Submission of a certification constitutes Contractor's express warranty that the identified supplies conform to all of the requirements of this contract. A document is not delivered until it is received by Battelle. Battelle shall have the right to reject, as not in conformity with the requirements of this contract, any supplies or services for which all required reports, procedures or certifications are not delivered. Contractor's failure to deliver such documents, or delivery of deficient documents, shall be deemed a failure to make delivery within the meaning of the Default clause of this contract.

B.6.4 Contractor Nonconformance Report (cl 360 – May 2009)

Contractor is required to report to the Battelle Contracts Representative any nonconformance or deviation from Battelle's technical requirements. To comply with the reporting requirements the Contractor shall complete Battelle's Contractor Nonconformance Report (CNCR) which is available at www.pnl.gov/contracts/documents. The completed CNCR shall be submitted by the Contractor to the Battelle Contracts Representative to request Battelle to accept a deliverable not meeting all of Battelle's technical requirements. The decision whether to accept or reject such a request shall be within Battelle's sole discretion, and the Contractor shall not proceed in accordance with the requested deviation or present for inspection or acceptance any product produced in accordance with such deviation, unless and until Battelle's written approval on the CNCR is received by the Contractor. Battelle's rights and remedies provided in this clause are in addition to any and all other rights and remedies that Battelle may have under Federal or State law.

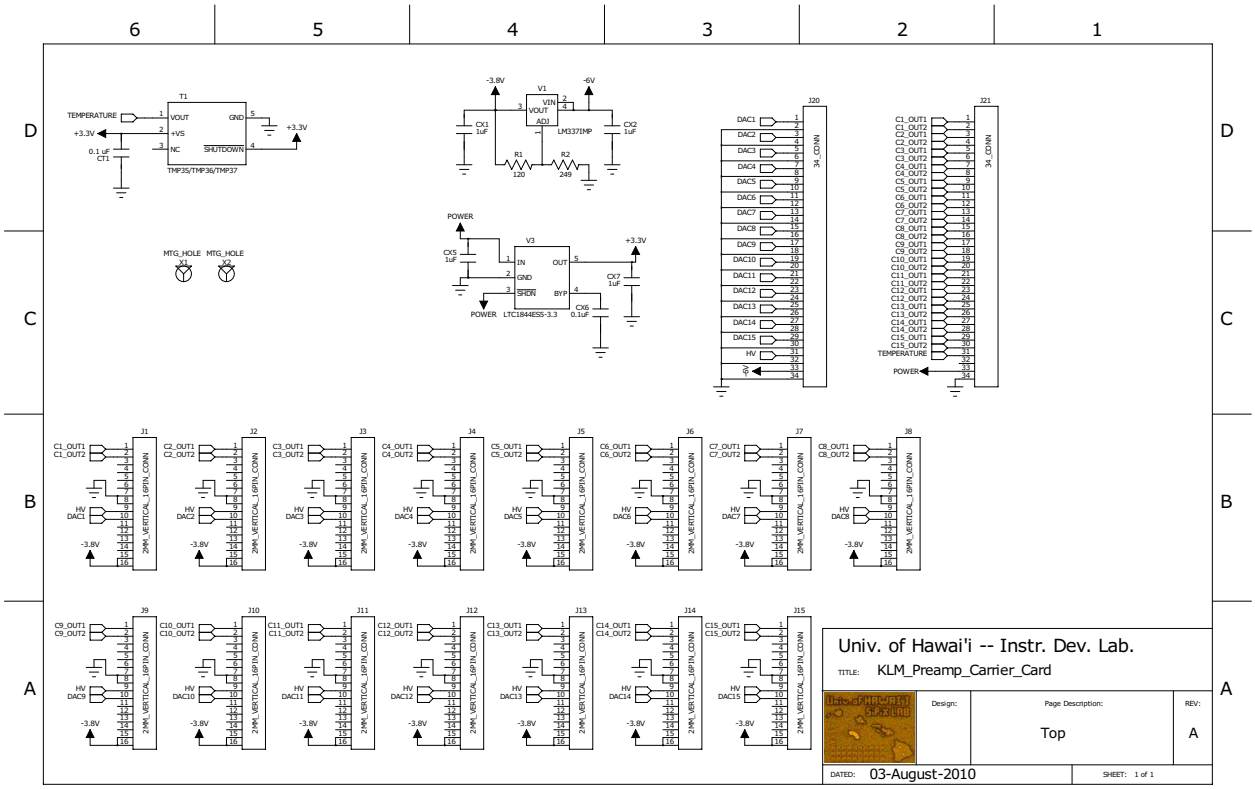

Figure 74: *Schematic of the MPPC-preamplifier carrier card.*

C KLM Technical Drawings

Figures 74 and 75 show the schematic and layout dimensions, respectively, of the MPPC-preamplifier carrier card. One such card holds 15 independent preamplifiers whose schematic is shown in Fig. 76.

The layout of one standard-size detector module in layer 0 of the barrel KLM is shown in Fig. 77. This module contains 54 short z-measuring strips and 37 long ϕ-measuring strips, powered and read out by the preamplifiers on seven carrier cards along the module's perimeter.

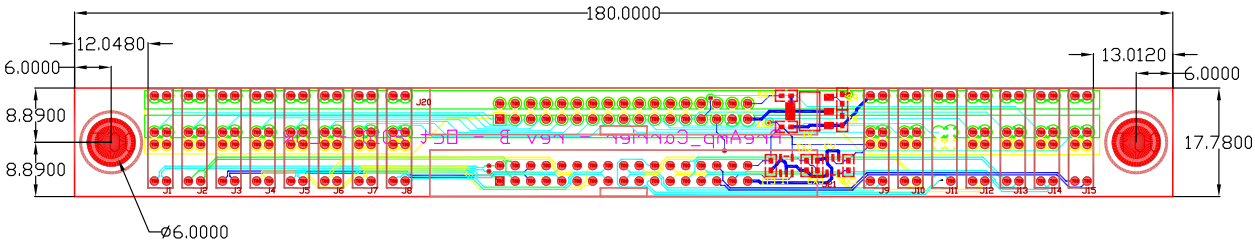

Figure 75: *Dimensions of the MPPC-preamplifier carrier card (in mm). The 15 preamplifiers are oriented perpendicular to this view.*

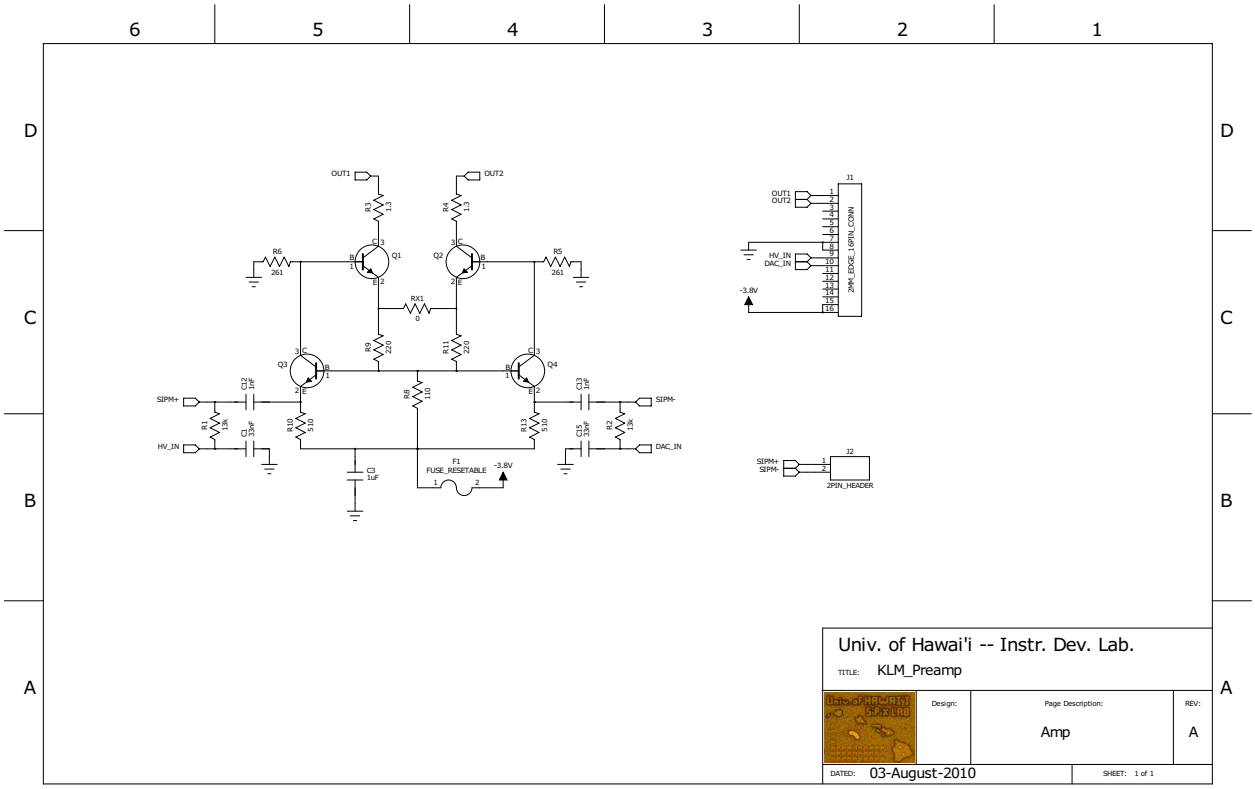

Figure 76: *Schematic of the MPPC preamplifier and power controller (including fine control on the MPPC supply voltage).*

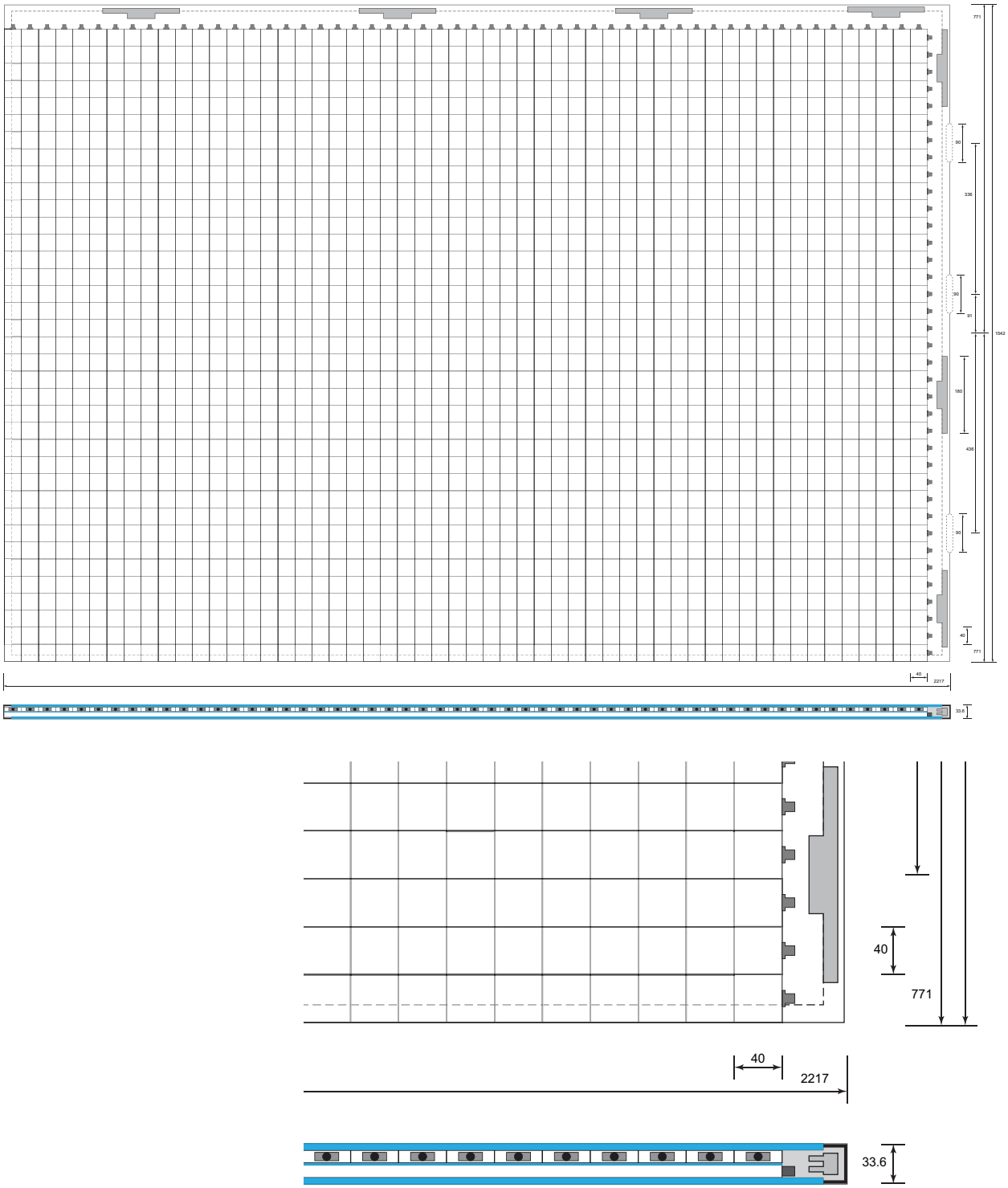

Figure 77: *Top: Layout (plan and elevation) of one standard-size barrel KLM detector module in layer 0. Bottom: Detail showing lower-left corner.*

D SuperKEKB Commissioning Detector

This appendix contains supplementary information relevant to the commissioning detector, such as results from simulation studies, which guided the design of the commissioning detector in general and TPC system in particular, a more detailed discussion of the US contribution, and a description of contributions from non-US institutions.

D.1 VXD Group Plans and Requirements

D.1.1 Introduction

In the Belle experiment the synchrotron and neutron backgrounds were unexpectedly high (figure 78) and the silicon detector system close the interaction point was damaged in few weeks time.

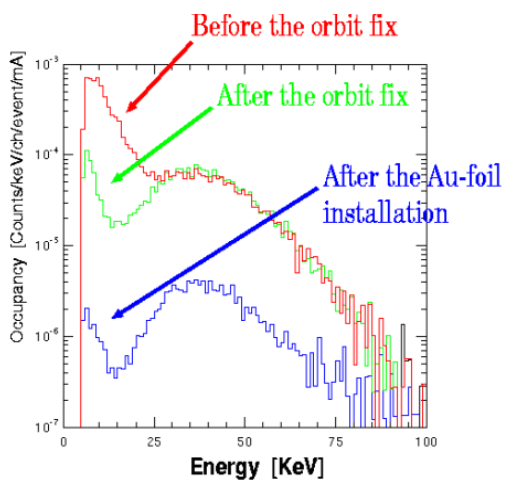

Figure 78: The synchrotron radiation in the Belle experiment was higher than expected, and damaged the SVD front end electronics within two months. The counter-measures added to protect the new detector included a better machine tuning and also a gold foil around the beam pipe near the interaction point.

The main purpose of the BEAST II experiment from the vertex detector (VXD) point of view is to determine when it is safe for the silicon sensors to be installed in the Belle II detector. The generation of the different types of background as a function of the settings in the collimator system, beam size at the interaction point, luminosity and vacuum pressure have to be determined using a set of sub-detectors at the final position of the silicon systems. In addition BEAST II is the perfect venue to perform extra measurements like temperature, humidity, vibrations, and also to exercise the final detector installation. Finally, during the BEAST II phase, the injection abort and the beam loss abort should be exercised, in addition to the study of the machine injection noise.

D.1.2 VXD proposal for BEAST II

The different set of sub-detectors proposed to be installed in the inner BEAST II will be introduced to perform the measurements mentioned in the introduction.

Temperature and humidity

The proper environmental conditions inside the VXD chamber are vital to ensure the safe operation of the detectors. During the BEAST II operation, the chamber will be instrumented with several temperature and humidity sensors, complemented with calibrated Bragg fibers for cross checking. These small devices, shown in Figure 79, will be attached directly onto the beam pipe, the PXD cooling blocks and on the inner and outer surfaces of the thermal enclosure (TE). Several studies are planned, including:

- Influence of the beam current on the beam pipe temperature
- Performance of the beam pipe cooling
- Temperature gradient across the TE wall
- Mass flow and time needed to achieve temperature/humidity stable conditions

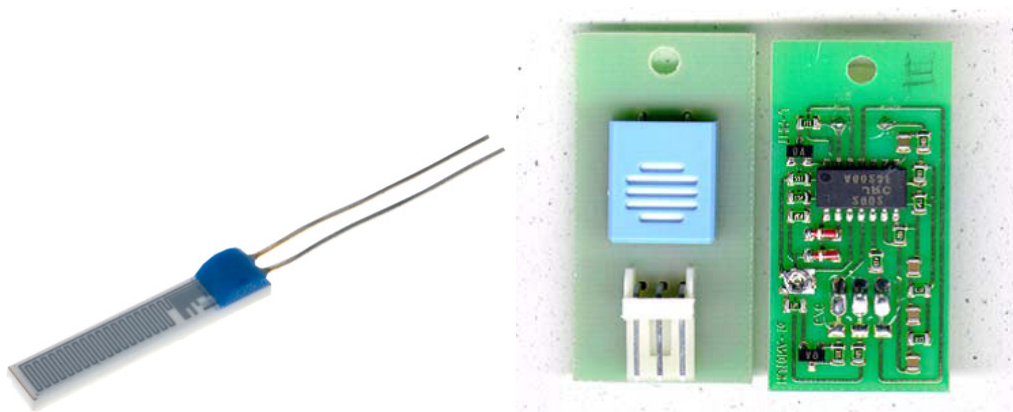

Figure 79: Example of one of the Pt100 temperature (left) and humidity sensors (right) under study.

Several humidity sensors have been irradiated with 20 MeV electrons in the ELSA accelerator in Bonn up to a total integrated dose of 2 Mrad [1]. Several devices were found to be operational after the irradiation, but the commercial readout electronics, integrated in the sensor housing, was found to be not radiation tolerant. Therefore a new readout Arduino-based readout with additional conditioning circuitry is under design phase and, once tested, will replace the current system.

Photon Energy Spectrum

[1] The expected TID during the commissioning phase is still unknown.

As already mentioned in the introduction, the precise determination of the synchrotron radiation, both energy spectrum and rate, is critical. The rate is proportional to $E^2 \cdot B^2$, and therefore the larger contribution is expected to come from the HER.

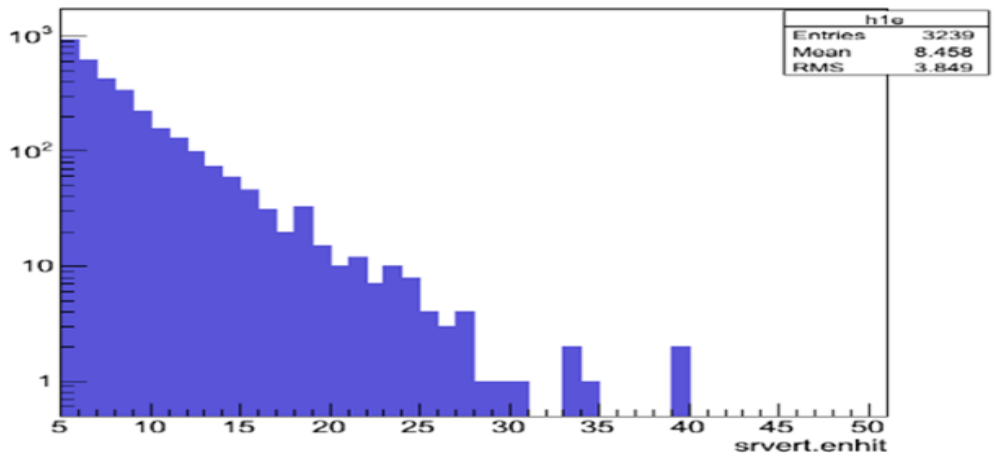

Figure 80: Rate versus energy (keV) spectrum of the simulated LER synchrotron radiation photons that will hit the Be part of the beam pipe at $\phi \sim 0$ per bunch.

The photon energy spectrum has to be measured with high resolution in order to understand in detail the damage the impinging synchrotron radiation may cause in the detector. Although the impact of the synchrotron radiation, shown in Figure 80, is expected to be more benign than in the original Belle experiment due to the lack of strong beam bending downstream, the larger crossing angle, the gold coated beam pipe and the saw-tooth geometry in the tantalum part of the beam pipe to avoid reflections, it is mandatory to study the rates and energies of the photons that will reach the pixel detector.

Figure 80 shows that the requirements the detectors should fulfill include a dynamic range from few keV up to tens of keV and be able to cope with kHz rates. Although the final decision concerning the detector is not taken, two technologies are under consideration: silicon drift detectors (SDD) and hybrid planar silicon sensors with FE-I4 readout.

A Silicon Drift Detector is a device which functionality is similar to a p-i-n diode, but with an unique electrode structure and extremely small anode capacitance. The main feature of these devices is the extremely high energy resolution at short peaking times. In Figure 81 the overlapping spectra of Fe55 and Am241 is visible, on top of additional peaks due to the fluorescence of the material of the collimator (Zr). The device shows good energy resolution, 1% in the 5.9 keV peak, within the expected dynamic range.

Nevertheless, there are at the moment some aspects that need more investigation, since the radiation hardness of the device is still unknown and also pile-up was observed with high activity sources.

A completely different approach to the SR problem is to use a hybrid planar silicon pixel sensor with FE-I4 readout shown in Figure 82). Although the energy resolution is coarse, see

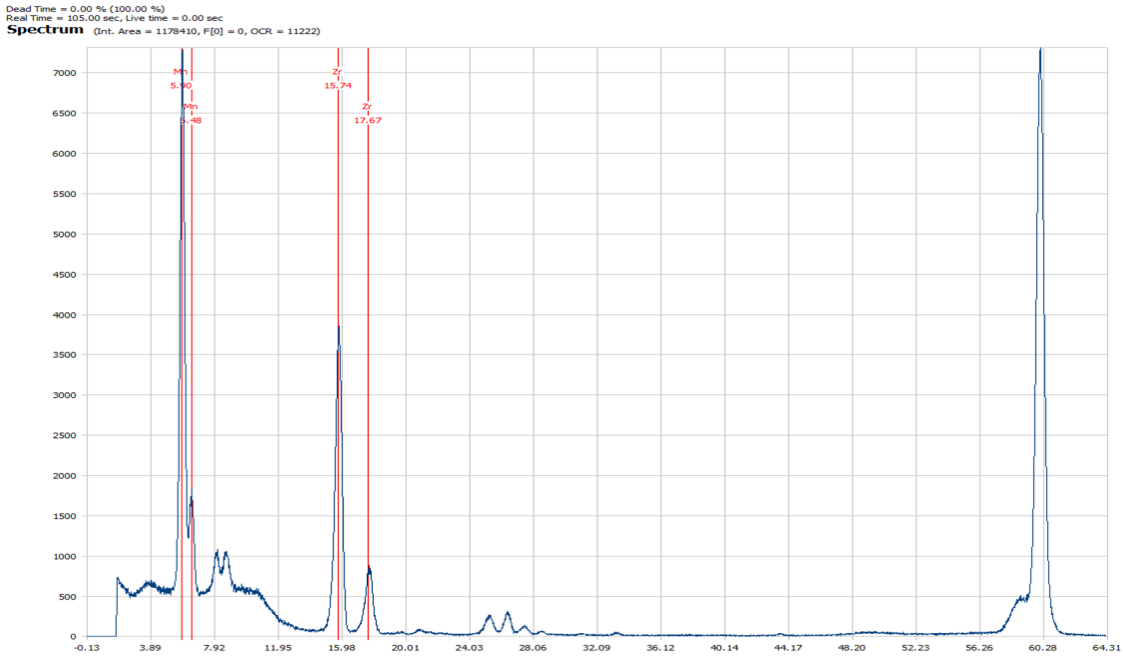

Figure 81: Silicon Drift Detectors allow the determination of the photon energy spectrum with high accuracy in the low (from keV up to tens of keV) range expected in Belle II.

Figure 83), the detector is radiation hard, up to 300 Mrad, and has a hit trigger association resolution of 20 ns.

Beam loss monitor

Experience shows that beam accidents can happen and such beam losses can be potentially dangerous to the Belle II inner detectors. Therefore beam loss abort systems with short time constants are a must in the experiment, to take a fast action and dump the beam in time and prevent accidents.

The first proposal, still under review, is to develop a radiation monitor focused on radiative Bhabha events, making use of polycrystal single channel diamond sensors placed up and downstream of the interaction point as shown in Figure 84). This process represents the major background source via particle loss near the IP and the radiation monitor should abort beams on large current spikes or prolonged radiation doses.

One readout style could consist of the measurement of the DC current of a diamond detector produced by the particle flux, also called slow readout. The readout can be kept quite simple, and this system was already used in experiments like Belle, BaBar or currently in CMS.

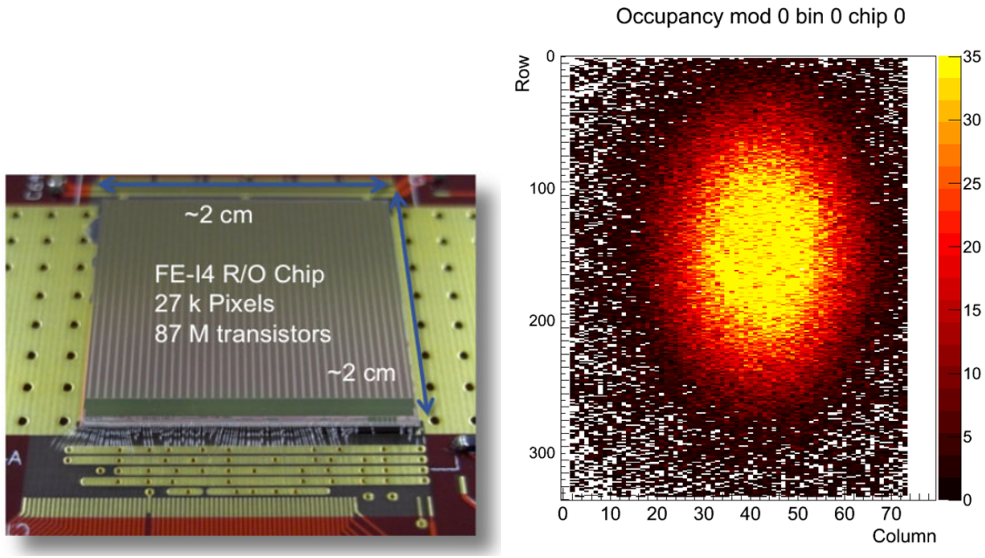

Figure 82: (Left) Photography of the FE-I4 chip. This chip covers an area of 2×2 cm^2, reading almost 30000 pixels of 50×250 μm^2 pitch. (Right) Hitmap recorded while the sensor is illuminated with a copper source (∼8 keV photons).

D.1.3 BEAST II PXD

The final test to ensure the safety installation of the silicon detectors will consist on the installation of two DEPFET half ladders, Figure 85), in their final position. The ladders have to be operated under the final conditions and with the full services that will be later used for the real PXD. These have to be ready and operational by the BEAST II period. These services include data transmission, DAQ, power supplies, the CO_2 cooling plant, the cooling and support structures around the beam pipe, capillaries for air cooling, and the thermal enclosure for the SVD and PXD.

Alternative scenarios Another interesting possibility is the study of shower creation by the Toushek effect. The use of a MAPS detectors along the beam pipe and close to the IP is under investigation. The sensor under consideration corresponds to Mimosa26 sensors with low material budget and excellent single point resolution. Feasibility investigations are ongoing since the long integration time, 112 μs, and poor radiation hardness, 300 krad, of these CMOS sensors could make them not viable in the BEAST II experiment.

D.2 Commissioning Detector Luminosity Monitoring Device

Introduction

Members from the National Taiwan University High Energy Physics Group (NTUHEP), including YuTan Chen, GuanBo Lin, and FaHui Lin, led by Professor Min-Zu Wang and Dr. Jing-Ge Shiu, will contribute to the luminosity monitoring device for BEAST II. FaHui Lin and Yutan Chen will install this device in the summer of 2014. Some other members

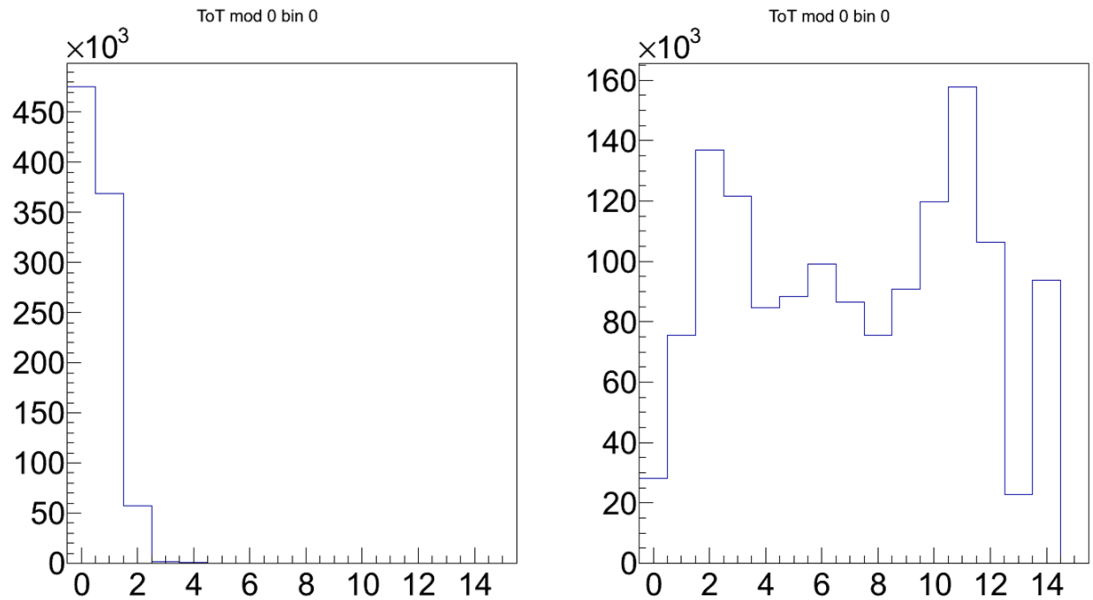

Figure 83: (Left) Fe55 spectra recorded with a planar silicon hybrid pixel detector with FE-I4 readout. The chip was tunned to operate at a threshold of ∼600 electrons. (Right) On the upper edge of the dynamic range, the spectrum of Am241 is also visible. The FE-I4 option can access the energies of the X-rays expected during the BEAST II phase, although with a coarse energy resolution.

in the NTUHEP will operate it after that. The luminosity monitor can provide luminosity information using coincidence signals from the back-to-back feature of candidate Bhabha events, and background intensity via the accumulated charge as a function of time.

Detecting System

This monitor consists of 8 sets of BGO (Bismuth Germanate) scintillation crystals fixed around the interaction point. A full ring version of this device has been used at Belle for the luminosity monitoring of KEK-B, and is radiation hard, up to an accumulated dosage of 100 Mrad. The scintillation light from each BGO crystal is imaged through an array of optical fibers onto photomultiplier tubes in the readout system.

There are different commissioning scenarios for BEAST2. In T0 and T1 scenarios, the BGO luminosity monitor is not very useful since there is no collisions. However, this device can function as another background monitor, with background current measurement circuits, and can be located at places other than the VXD volume if necessary. In T2 scenario, with no SVD nor PXD installed, the BGO luminosity monitor is installed inside the VXD volume, right near the interaction point. These 8 BGO crystals are mounted on 2 aluminum rings, with 4 crystals each, which are fixed to the inner tube in VXD volume. The 4 forward crystals are located at at an angle of 11.5° from the symmetry axis, while other 4 backward crystals are located at an angle of 20° by the symmetric axis as shown in Figures 86 and 87 and a single crystal in Figure 88.

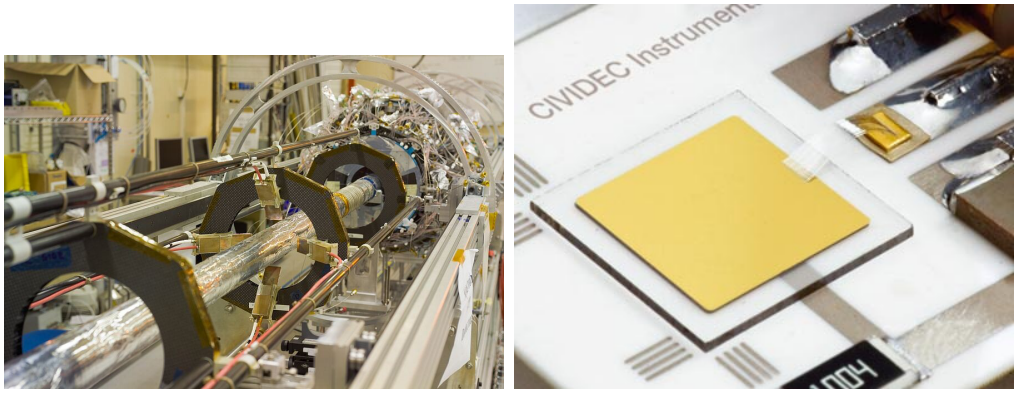

Figure 84: (Left) The beam abort system in Belle II will be geometrically implemented like the diamond system used in many high energy physics experiments. ATLAS is shown in the figure. (Right) As an illustration, four single channel CVD diamond modules close to the beam pipe facing the interaction point will be in charge of a fast pulse delivery to the accelerator for beam dump.

Readout System

One multi-anode photomultiplier tube (MAPMT) is used, to receive scintillation lights from the 8 BGO crystals. The MAPMT needs $900V$ high voltage and it is expected that KEK will provide the HV power supply. Between the crystals and the MAPMT, there are 8 optical fibers. The fiber length is roughly 25 m. The fibers are put into a flexible black hose with a diameter of ~ 1 cm. The required length is to connect the crystal in the VXD volume to the MAPMT at the readout system zone. The space needed in the readout system zone is about 1 m^3 .

The MAPMT outputs charge signals. After the front-end circuit, the signals become digitized charge information. The signal frequency should be kept under 100 Hz with proper threshold settings. The characteristic time or decay time for BGO scintillation is about 300 ns.

The 8 logic signals will go through a logic circuit, implemented with an FPGA as shown in Figure 89 to obtain the coincident signals via the back-to-back feature of Bhabha event. After subtracting the signals from random coincidence, the signal rate gives the luminosity information.

The first version of the readout circuit is in production during the summer 2013, and the final version will be produced in the end of 2013.

Figure 85: Half DEPFET ladder after being cut from the wafer. One full ladder will be obtained by gluing two half pieces as the one shown here.

Simulation
A simulation of the BGO luminosity monitors using GEANT4, the geometry is shown in Figure 90, is underway in order to get the conversion factor between the rate of triggered events and the instant luminosity. An energy threshold 0.5 GeV is required to get rid of background. This energy threshold corresponds to the threshold of input signals. From simulations of Bhabha scattering, the luminosity required for one particle detected per second is estimated to be about 10^{30} cm^{-2} s^{-1}. Example GEANT events are shown in Figure 91.

System Test
The device response will be checked before its installation at KEK in the spring of 2014. NTUHEP members will use a radiation testing facility with a 10^4 Curie Co-60 source in northern Taiwan to get the conversion factor between the accumulated charge and the received radiation dose. It will be important to have some ideas about the effect of radiation damage or annealing behavior of this monitor in the same test.

D.3 micro-TPC Simulation & Design Optimization

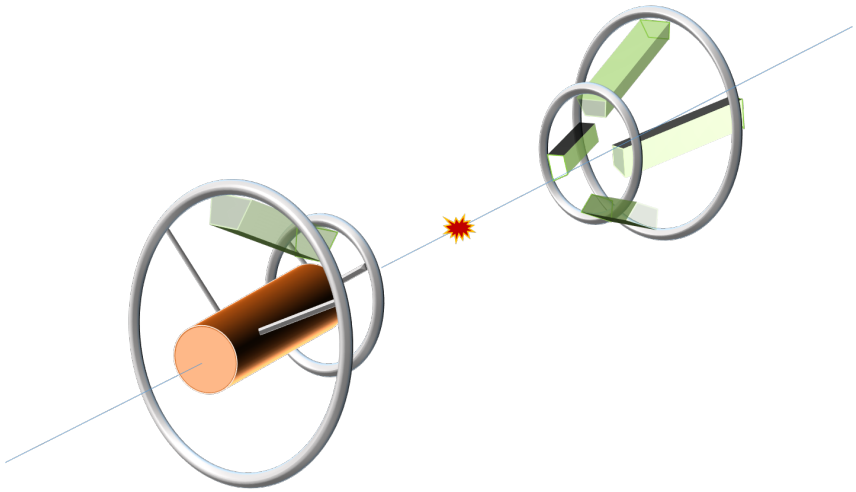

Figure 86: A 3-D conceptual drawing for BGO crystals, green, mounted on the aluminum rings, metallic, near the interaction point inside the VXD volume. The brown cylinder shows the inner tube inside the VXD volume where the rings can be fixed with screws and support beams.

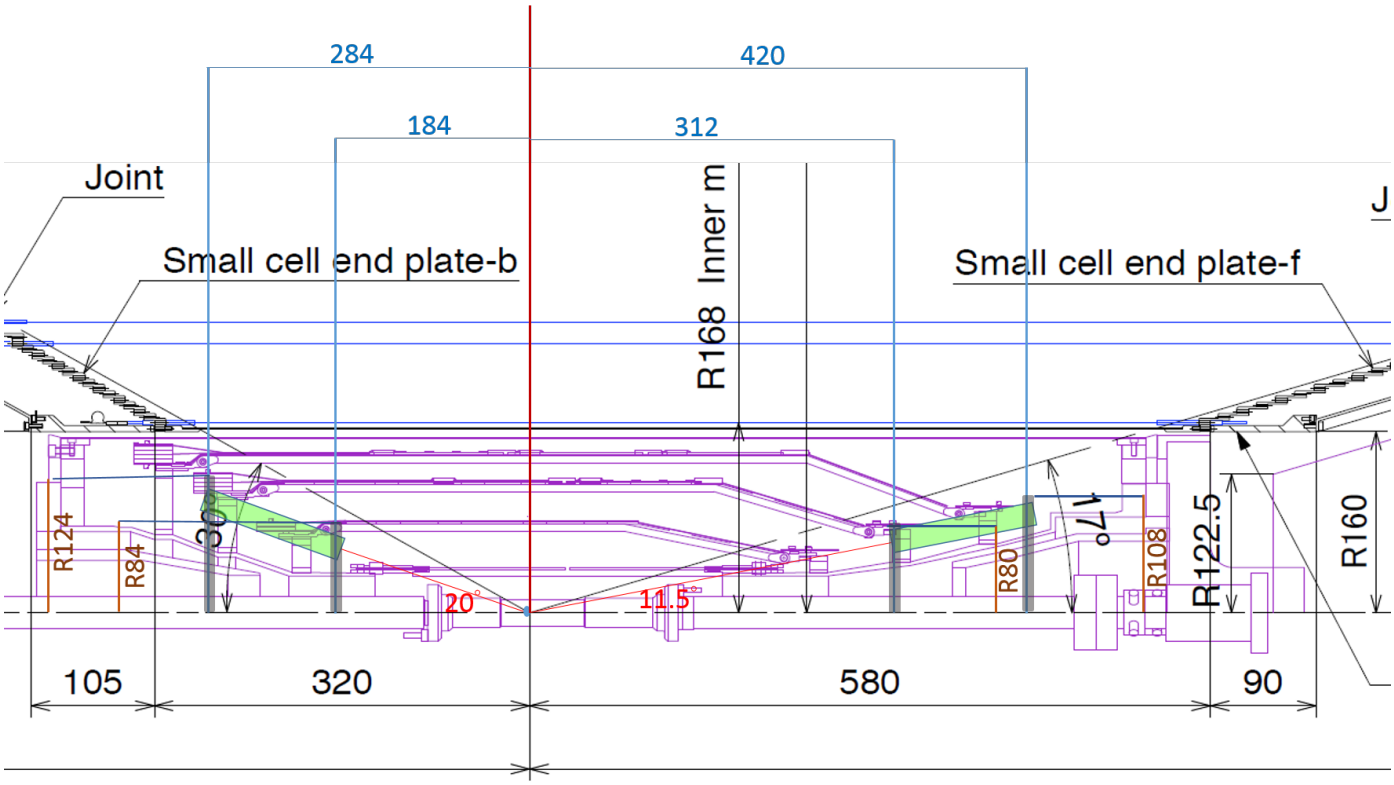

Figure 87: A partial sub-detector installation blueprint focusing on the VXD, showing locations of BGH crystals, in green, and aluminum rings, in gray.

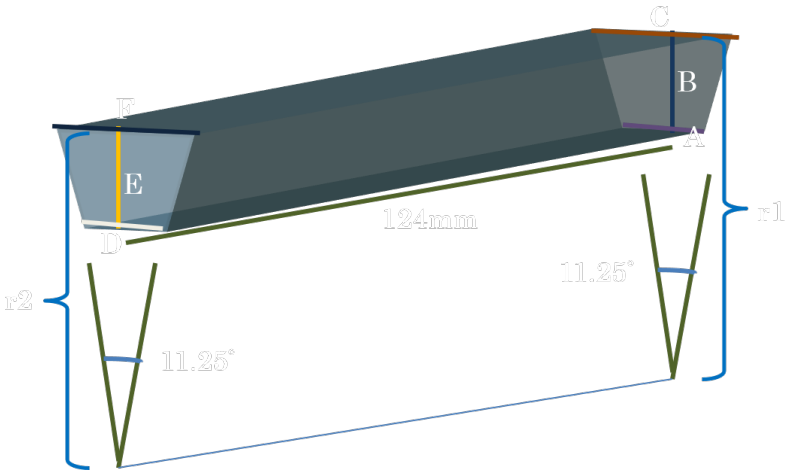

Figure 88: Dimensions of a single BGO crystal.

type	A	B	C	D	E	F	r1	r2
B5 (mm)	22.938	12.280	25.356	30.828	19.616	34.692	130.48	177.87

Figure 89: The Xilinx vertex V4 FPGA board

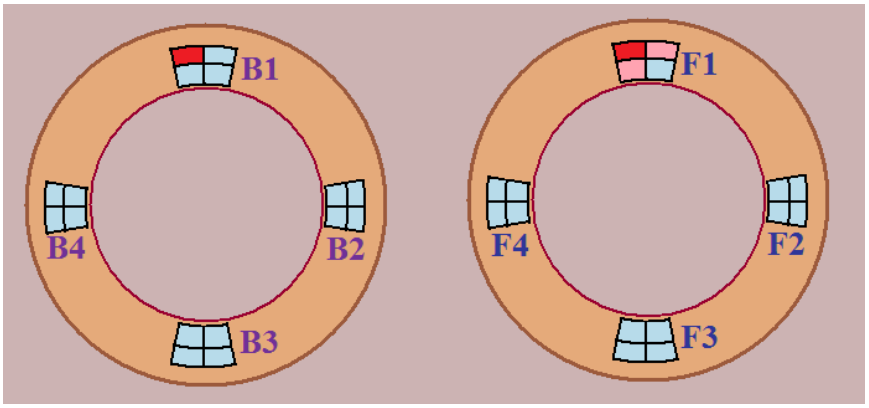

Figure 90: Geometry of BGO Luminosity Monitor, made up of 8 BGO crystals, plotted with GEANT4 in BASF2

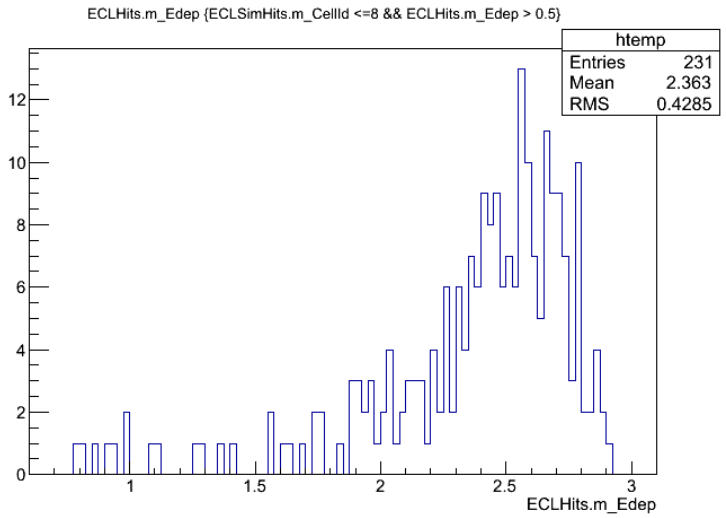

Figure 91: Simulation of 1000 events (e^+, e^-, γ) with energy 4 GeV at $\theta = 10.5°$ to $12.5°$, and full range of ϕ.

In this section, Monte Carlo simulations studies of the micro-BEAST-TPCs are described. These studies were performed in order to design and optimize the micro-BEAST-TPCs to be able to distinguish the different beam-induced backgrounds (Touschek, Radiative Bhabha and Coulomb) by measuring the angular distributions of the nuclear recoils procured when neutrons scatter elastically off the nuclei of the gas-target.

These section is divided into three parts: the **simulation framework** is introduced, the **design optimization** and the neutron **detection efficiency** are presented.

D.3.1 Simulation framework

Our Monte Carlo study of micro-BEAST-TPC performance is based on two detector simulators: BASF2 and CYGNUS (our TPC-simulator). BASF2 and CYGNUS are both a full detector simulator based on GEANT4 but also on a Fast Monte Carlo or Full simulation for CYGNUS. Our Fast Monte Carlo is based on MAGBOLTZ. Our Full simulation is based on SRIM and GARFIELD. At the moment, both simulators are separated but work is underway to combine the GEANT4 part of CYGNUS into BASF2.

Simulation strategy

A two steps simulation strategy is adopted to enhance the recoil number due to the low neutron cross section and also because GEANT4 is not simulating the electrons drift under the influence of an electric field.

- first step: BASF2 simulation of the different beam-induced backgrounds. This step is used to determine the types, origins, energy and angular distributions of the particles passing through the micro-BEAST-TPCs ie the beam-induced particles background profiles.
- second step: beam-induced particles background profiles served as an event generator for CYGNUS

BASF2

BASF2 tracks particles due to the beam-induced background from the interaction points through various Belle2 detector components, taking into account their various interactions with detector materials. There are three types of beam-induced background: Radiative Bhabha (RBB), Coulomb and Touschek. These beam-induced backgrounds are producing mostly electromagnetic particles and neutrons. The plan is to produce beam-induced background simulation corresponding to phase 2 stage. Phase 1 stage can not be used to test the beam-induced background simulation at the designed luminosity so there is no interest to simulate this stage. All our studies are based on the 5th compaign of beam-induced background simulation produced by Nakayama-San at the designed luminosity and with the full Belle2 setup. The luminosity at the end of phase 2 should be 100 smaller than the one at designed luminosity. All rates originating from RBB, Touschek and Coulomb bacground

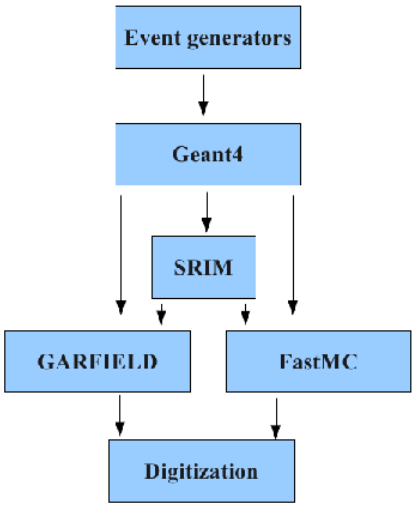

Figure 92: Flow chart showing the simulation steps.

presented below have been scaled by a factor 1/100. It should be noted only RBB background is scaling with luminosity. Touschek and Coulomb backgrounds are not scaling with the luminosity and only require one beam. Touschek background is scaling with the particles density per beam bunch. Coulomb or beam-gas bakcground is scaling with the Pressure. So in principal in phase 2, the Touschek and Coulomb background rates can be increased by the accelerator people by increasing respectively the beam bunch density and the pressure in the beam pipe.

TPC-simulator (CYGNUS)

The TPC-simulator aka CYGNUS is done in two steps:

- first step: beam-induced particles background profiles served as an event generator for the GEANT4 part of CYGNUS.
- second step: Fast Monte Carlo for
  - electron drift parameterization (using v_{drift}, D_l and D_t)
  - GEMs or avalanche-charge parameterization
  - digitization into pixel hit

Figure D.3.1 shows a flow chart of CYGNUS. There is the possibility to use a full simulation for the electron drift and also to use SRIM transport model instead of SRIM-like GEANT4 transport model.

Figure D.3.1-left shows a G4 drawing of a single micro-BEAST-TPC and a G4 drawing of eight micro-BEAST- TPCs located in the dock space (Figure D.3.1-right).

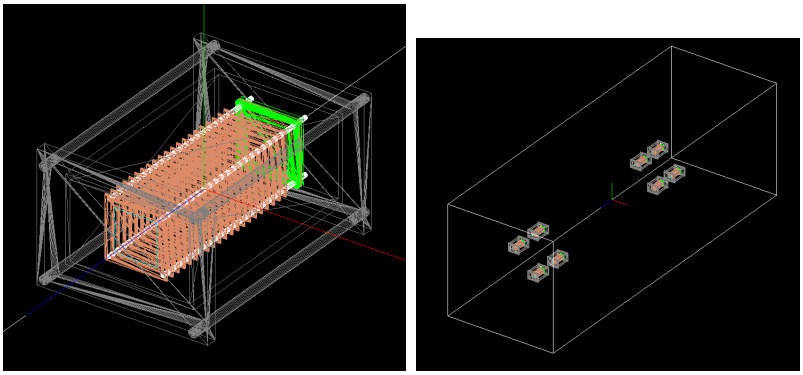

Figure 93: Left: G4 drawing of a single micro-BEAST-TPC. Right: G4 drawing of eight micro-BEAST-TPCs located in the dock space.

Table 15: TPC positions in the dock spaces at phase 2.

TPC #	1	2	3	4	5	6	7	8
r [cm]	37	37	37	37	32	32	32	32
z [cm]	-122	-122	-122	-122	190	190	190	190
ϕ [^{o}]	-90	0	90	180	-90	0	90	180

D.3.2 Design optimization

TPC position

At this stage, the optimum position for the T1 phase cannot be determined. For the phase 2 phase, the TPCs will be located in the dock space. Figures D.3.2 and D.3.2 represent two section views: a top view and r-phi views for the backward and forward dock spaces. The rectangular red boxes show the possible TPC positions. Figure D.3.2 gives also the TPC numbering. The TPCs can be located at different z positions in the backward and forward dock spaces: -210 $\leq$ z $\leq$ -105 cm and 155 $\leq$ z $\leq$ 212 cm respectively.

The rates at phase 2 for the different beam-induced backgrounds are shown in Figure D.3.2 at the locations corresponding to the full red line box of Figure D.3.2-top-left and Table D.3.2. Figure D.3.2(-top-right and bottom) show also the rates at alternative locations corresponding to the dashed red line boxes of Figure D.3.2-top-right and -bottom. The neutron rates amount of 10 % of lower to the total rate. The rates at phase 2 phase will be 100 smaller than the rates at designed luminosity. The rates of reconstructible events that the TPCs can measure will be at least 1000 smaller. So all together at phase 2 phase should be around few 10's Hz at best.

The neutron rates summed for the backward and forward TPCs traversing the TPCs was estimated at phase 2 as function of the neutron kinetic energy, neutron polar and azimuthal angles as seen in Figures D.3.2-top-row and D.3.2-top-row and corresponding to the positions

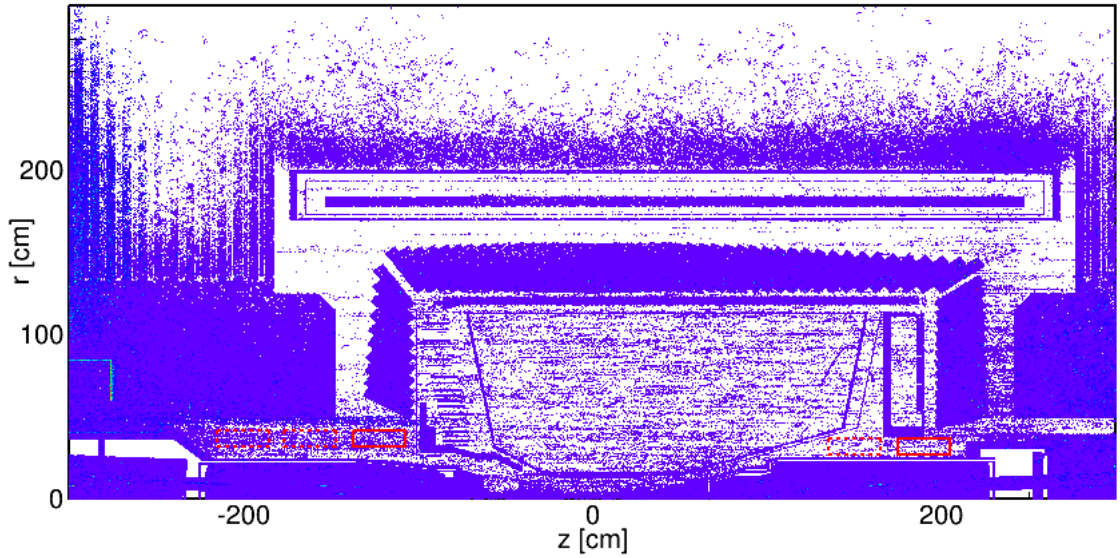

Figure 94: Top view. Distribution for the particle decay points in the radial plane r = $\sqrt{x^2 + y^2}$ versus z-axis.

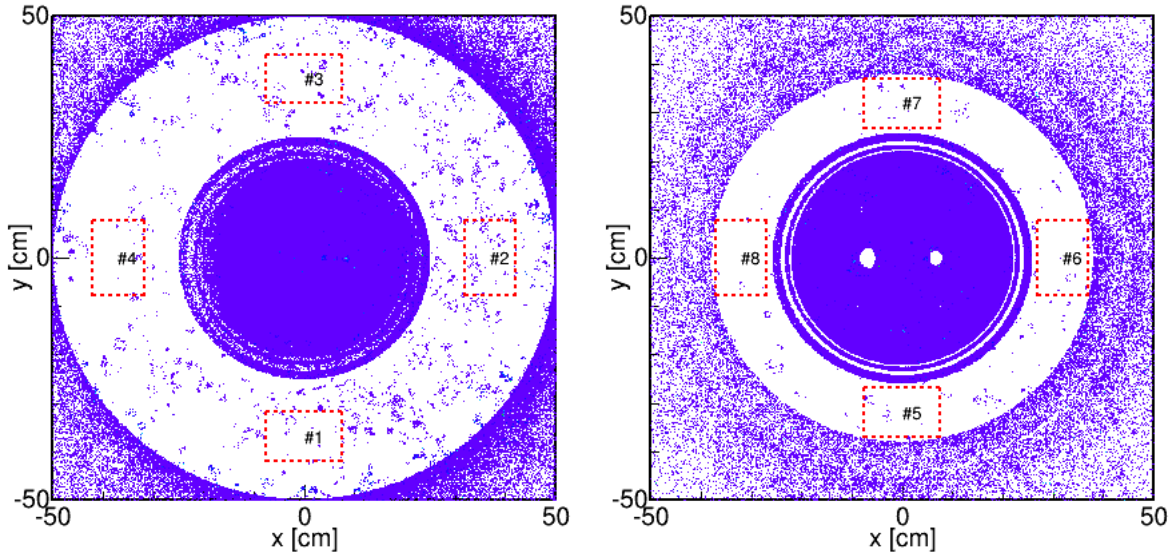

Figure 95: R-phi view. Distribution for the particle decay points in the plane perpendicular to the z-axis. Left: for -210 $\leq$ z $\leq$ -105 cm ie backward dock space. Right: for 155 $\leq$ z $\leq$ 212 cm ie forward dock space.

Table 16: Iso-butane optimized drift velocity and field.

chip	time resolution [ns]	pixel size [μm]	v_{drift} [μm/ns]	E [kV/cm]	D_t [$\mu m/\sqrt{cm}$]
FE-I3	25	400	16	0.5	130.5
FE-I4	25	250	10	0.3	148

Table 17: He:CO_2:70:30 optimized drift velocity and field.

chip	time resolution [ns]	pixel size [μm]	v_{drift} [μm/ns]	E [kV/cm]	D_t [$\mu m/\sqrt{cm}$]
FE-I3	25	400	16	0.84	124.5
FE-I4	25	250	10	0.53	124.3

of Table D.3.2. The (proton) recoil rates expected was calculated by a Fast Monte Carlo simulation using the two-body kinematic and considering a neutron detection efficiency of 0.1 % in average.

The dominant beam-induced background are RBB LER and HER and Touschek LER. As function of z the RBB LER and HER rates are more or less constant, while the Touschek LER is decreasing in the backward dock space for negative z because they are further away from the QCS. Although the rates emanating from the tunnel increased for smaller z (labeled far in Figure D.3.2), the rates will be most likely of the same level than the internal irreducible TPC background.

Gas choice

The gas choice depends of several factors. It should be composed of a light gas-nucleus in order to have a good neutron elastic cross section and also to have recoil with enough energy to produce long enough track that can be detected and still have directionality. In addition, the gas or the gas-mixture should have a drift velocity high enough to clear the chamber volume rapidly but no too high to have a good 3D hit resolution. The drift velocity will be limited in our case by the pixel size 250 μm for the FE-I4 and 400 μm for the FE-I3: v_{drift} x FE-I3/4 time resolution $\leq$ pixel size. For FE-I3: v_{drift}(E/P) $\leq \frac{400\mu m}{25ns} = 16$ μm/ns and for FE-I4: v_{drift}(E/P) $\leq \frac{250\mu m}{25ns} = 10$ μm/ns. Tables D.3.2 and D.3.2 show the maximum values of v_{drift}(E/P) for the lowest D_l at low drift field to keep drift voltage reasonably low and cage field simple for iso-butane and the gas mixture He:CO_2:70:30.

The attachment coefficient should also be low. The gas gain should stable and on the order of 100 for each GEMs. Several gas and gas mixture: iC_4H_{10} (flammable and explosive), Ar:CO_2, He:CO_2, He:CF_4 and He:CH_4 (flammable, but not explosive), have been investigate with GEANT4 and MAGBOLTZ to determine the neutron probability of interaction per centimeter (Figure D.3.2), the gas parameters respectively and the mixture composition in case of a gas mixture all at 1 atm. Isobutane has the highest neutron cross section 7 to 9

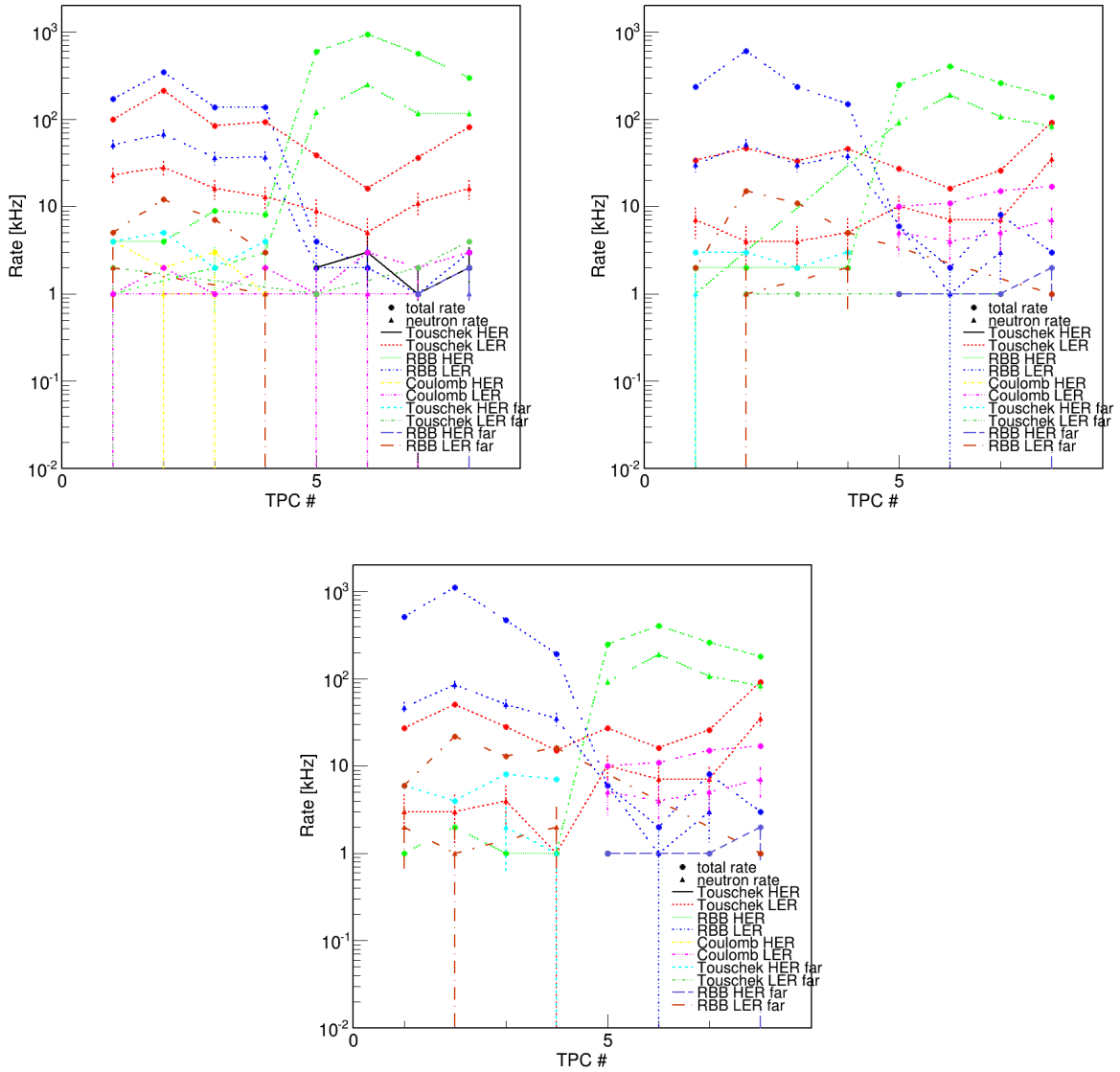

Figure 96: Rates at phase 2 of the different beam-induced backgrounds inside each TPC at different dock space locations. The numbering corresponds to Figure D.3.2. Left top: rate corresponding to the full red line box in Figure D.3.2. Right top and bottom: rates corresponding to the dashed red line boxes in Figure D.3.2. Point symbol total rate. Triangle symbol neutron rate.

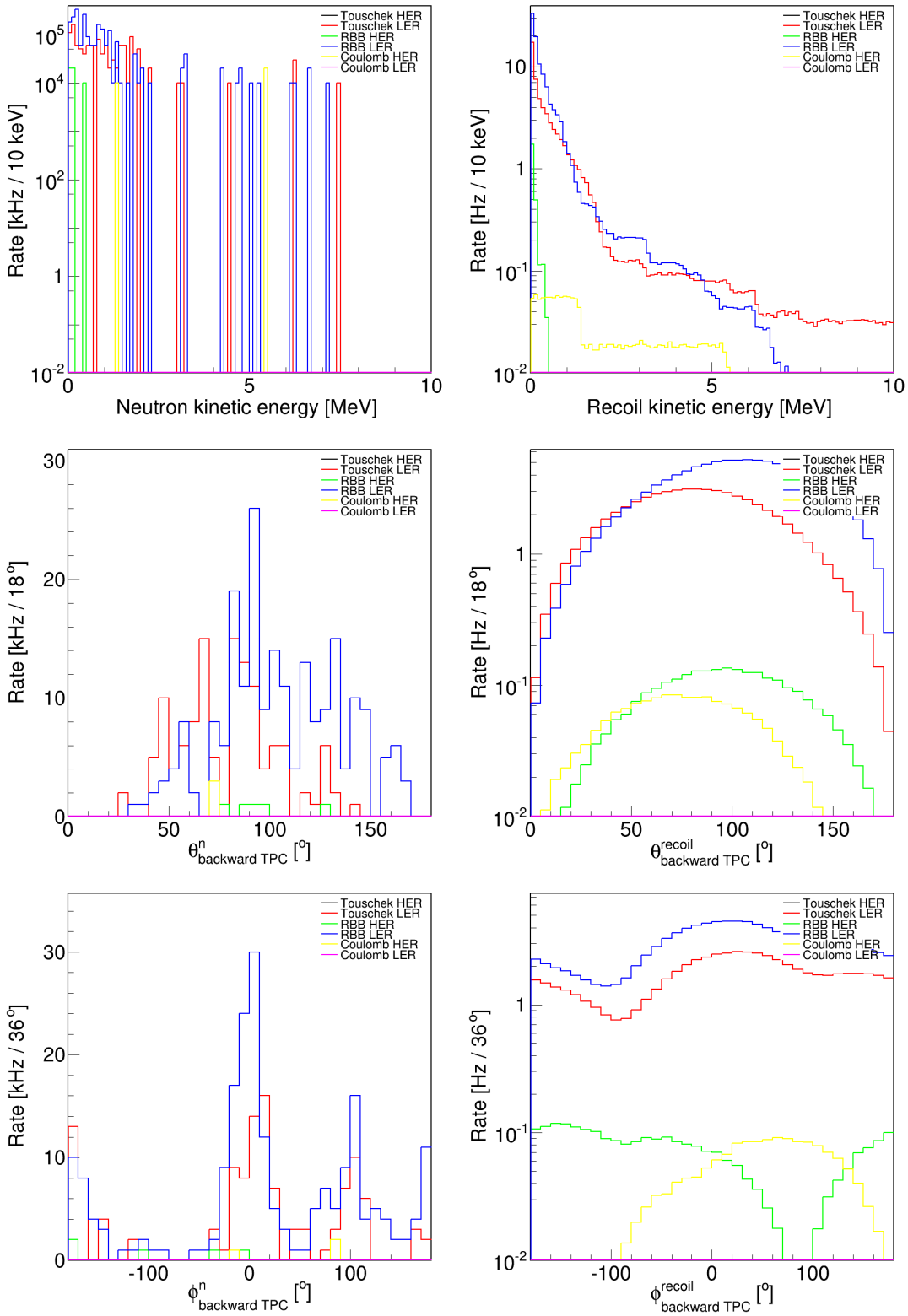

Figure 97: Rates at phase 2 for the beam-induced backgrounds traversing or expected to be measured by the TPCs located in the backward dock-space. Left column: neutron. Right column: proton recoils. Top row: versus kinetic energy. Middle row: versus polar angle. Bottom row: versus azimuthal angle.

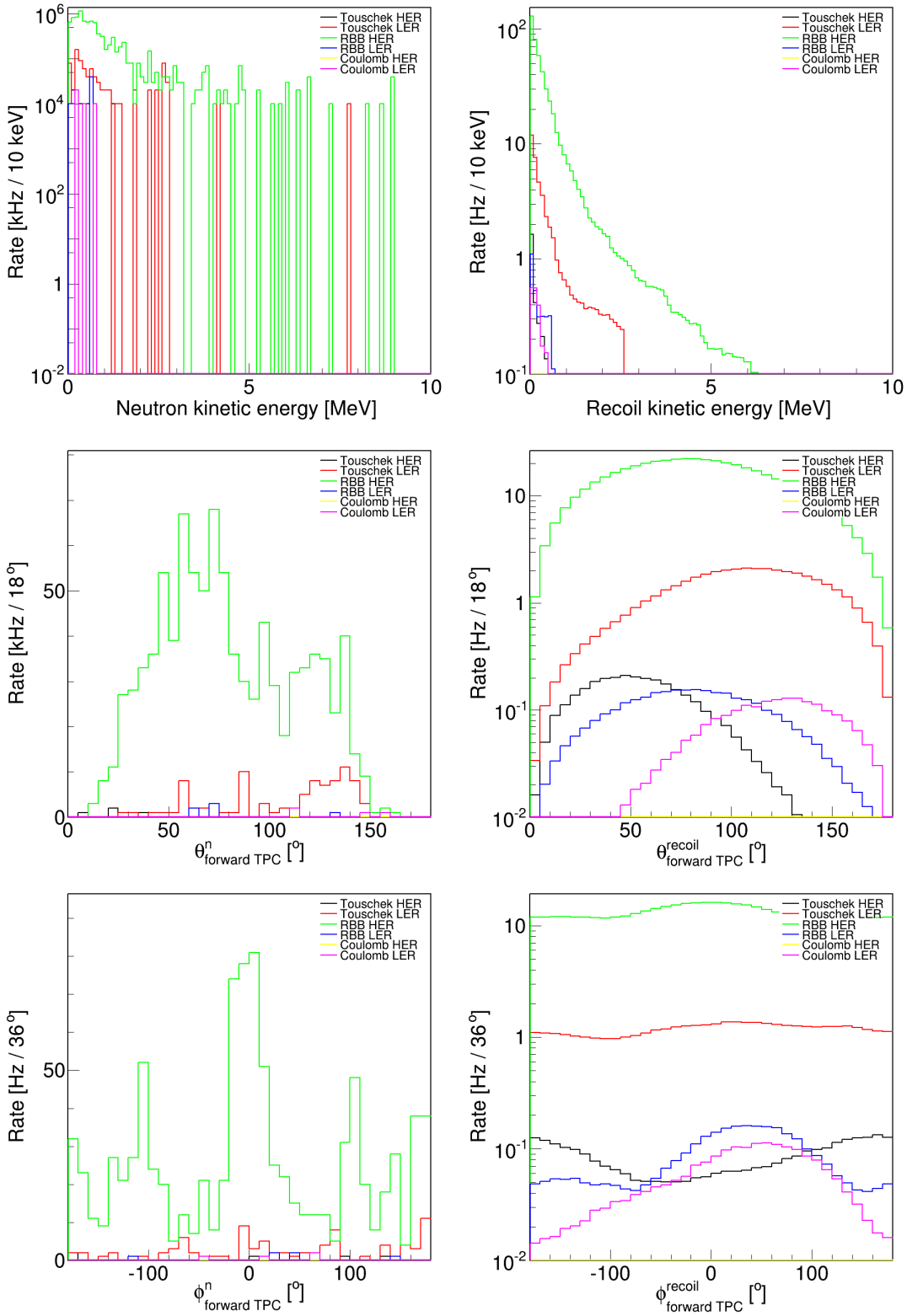

Figure 98: Rates at phase 2 for the beam-induced backgrounds traversing or expected to be measured by the TPCs located in the forward dock-space. Left column: neutron. Right column: proton recoils. Top row: versus kinetic energy. Middle row: versus polar angle. Bottom row: versus azimuthal angle.

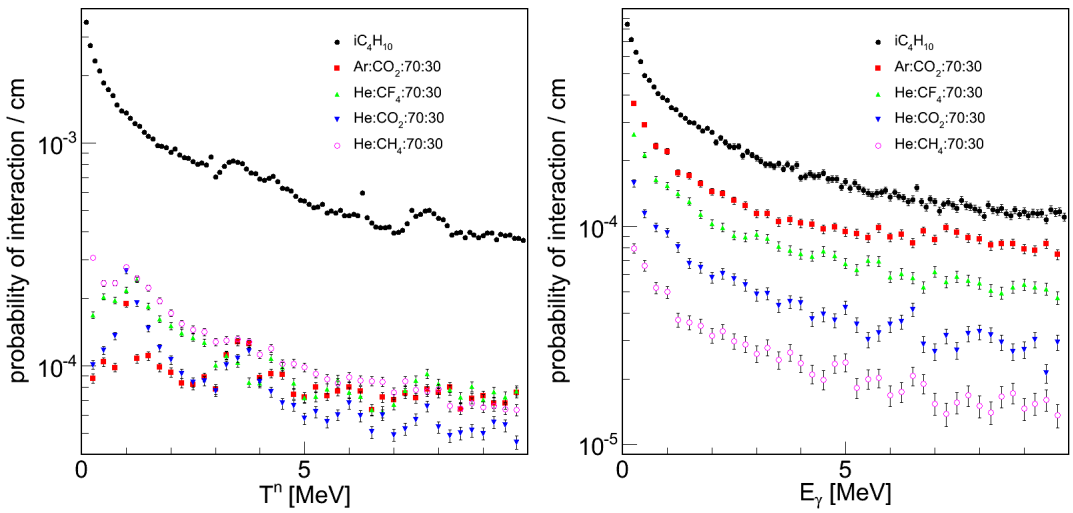

Figure 99: Interaction probability per centimeter as function of kinetic energy for various gas and gas mixtures. Left: neutron. Right: photons.

times higher than He:CO_2:70:30.

Figure D.3.2 shows gas parameters: the drift velocity and the diffusion (transverse and longitudinal), for the different gas or gas mixture studied, as function of the electric and pressure (with the pressure at 1 atm) ratio. Figure D.3.2 also illustrates the influence of gases: CH_4, CO_2 and CF_4, which allow depending of the proportion of it compared to Helium to vary the drift velocity for approximately similar diffusions. The evolution of the gas parameters for different proportion of He and CO_2 is shown in Figure D.3.2. The introduction of CO_2 in higher proportion decreases the drift velocity and also lowered the optimal field needed to be applied in the drift region. The influence of the magnetic has also been studies as an illustration, Figure D.3.2 shows the magnetic field influence on He:CO_2:70:30 and iso-butane. In general if the magnetic and the electric field are parallel, the influence of the magnetic field has small effect on gases with small drift velocity. If the magnetic and the electric field are not aligned, the drift velocity and the diffusion parameters expression will be more complicate since for example the diffusion will become tensorial and the drift velocity will have components in all direction.

The gas that offers the best trade off between neutron interaction probability, good gas properties and easy to use is He:CO_2:70:30. Iso-butane is the best gas in general but because its dangerosity make its more challenging but KEK has experience with this type of gas.

Field cage

To minimize the internal background due to natural radioactivity and the neutron probability of interaction with the field cage different width of rectangular rings have been studied using COMSOL. Figure 103 shows the electric field streamlines calculated by COMSOL. Figure D.3.2 shows the radial diffusion as function of the ring width at different transverse

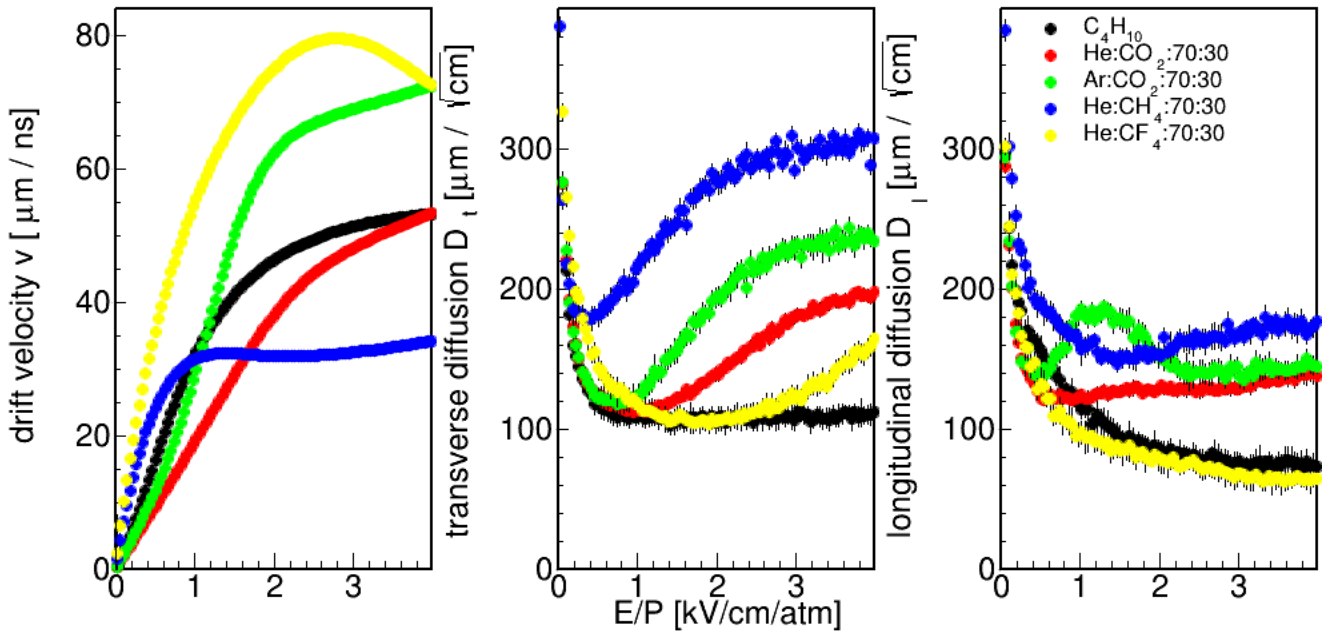

Figure 100: Gas parameters calculated by MAGBOLTZ as function of electric field and pressure (P = 1 atm) ratio for the different gas or gas mixture candidates studied.

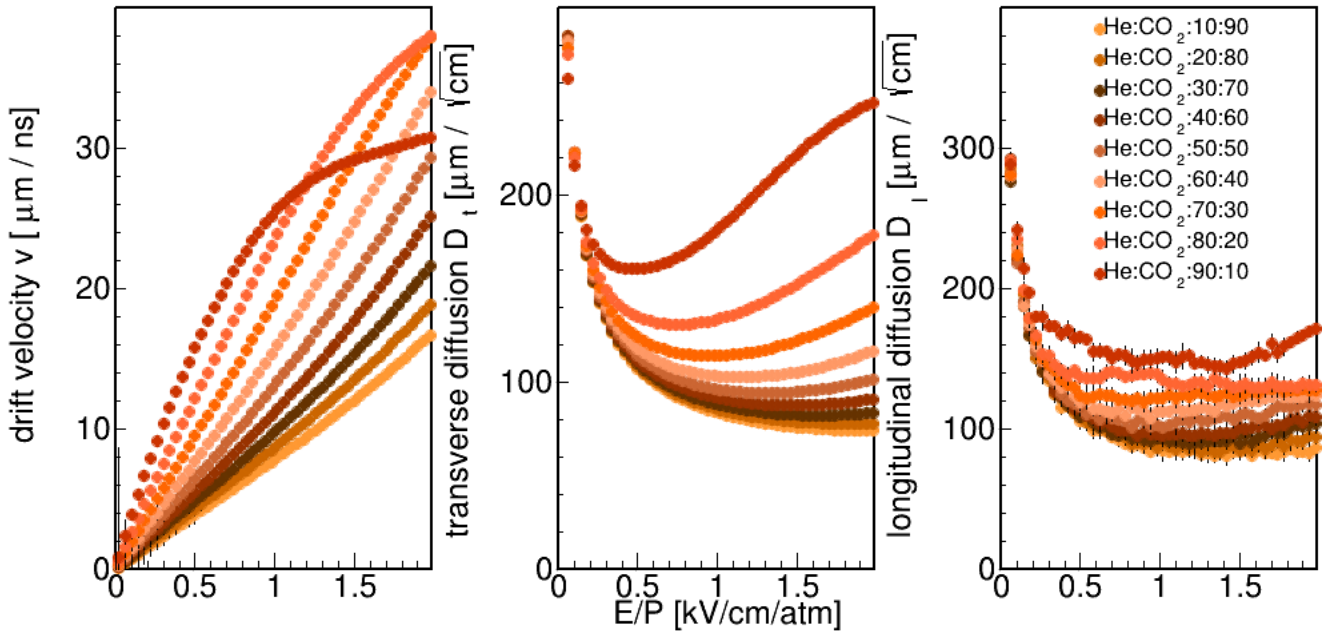

Figure 101: Gas parameters calculated by MAGBOLTZ as function of electric field and pressure (P = 1 atm) ratio for the different percentage of Helium and carbon di-oxygen.

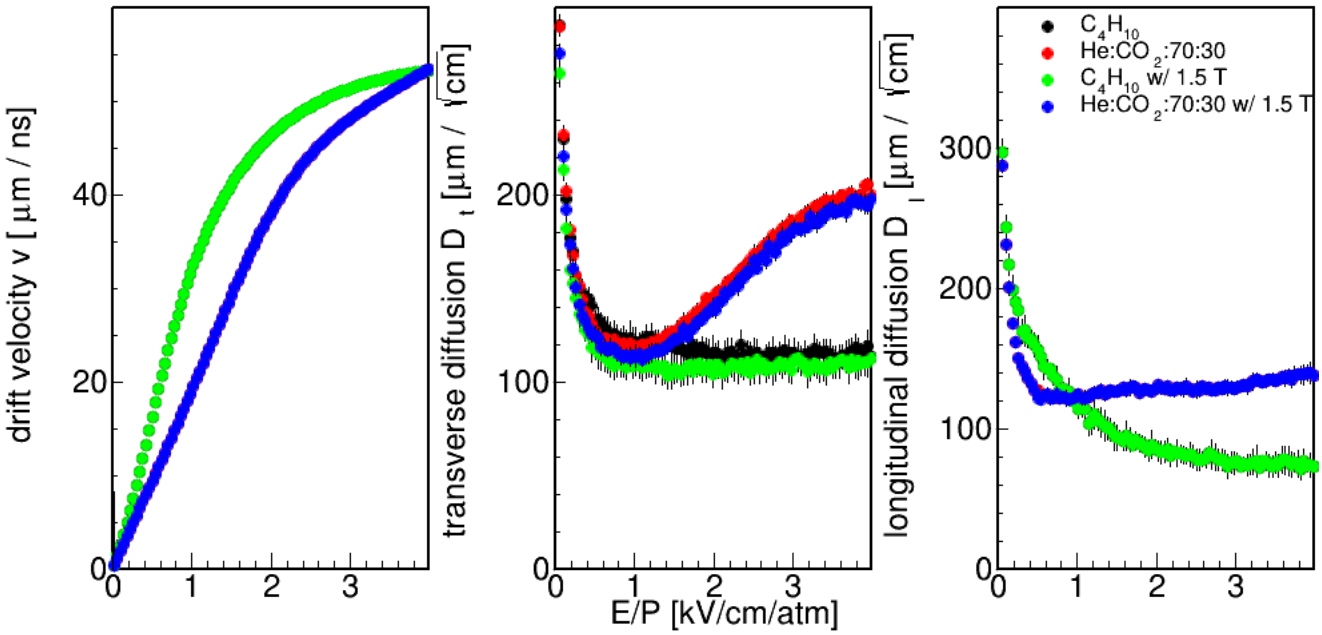

Figure 102: Gas parameters calculated by MAGBOLTZ as function of electric field and pressure (P = 1 atm) ratio for the He:CO_2:70:30 and iso-butane without and with 1.5 T magnetic field.

positions. The radial distance an electron can drift is below 40 μm ie below the pixel height (50 μm). A mm width can be used for the field cage.

Gain choice

To achieve the highest possible detection of the primary ionization, Gas-Electron-Multipliers (GEMs) are used to amplify the signal. The GEMs have very good rate capability and intrinsic ion feedback suppression. GEMs are also gate-less and can operate continuously. Each GEM has a gain of the order of 100 in a gas chosen adequately. The gain has to be adapted to the amount of ionization losses. The electronic energy loss to the gas electron per centimeter can be calculated by using SRIM as illustrated in Figure D.3.2. From this curve, an average number of electrons that can reach a GEM hole can be calculated.

Since roughly a pixel is in front of two GEM holes, the optimal gain necessary to be above the pixel threshold can be deduced. A figure-of-merit, Figure D.3.2, can be constructed that takes into account pressure, diffusion, pixel threshold and range. Table D.3.2 summarizes the results.

Pixel chip choice

There are two version of the pixel chip: FE-I3 and FE-I4. A short description can be find below.

- FE-I3

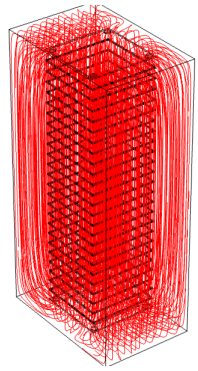

Figure 103: Electric field streamlines calculated by COMSOL.

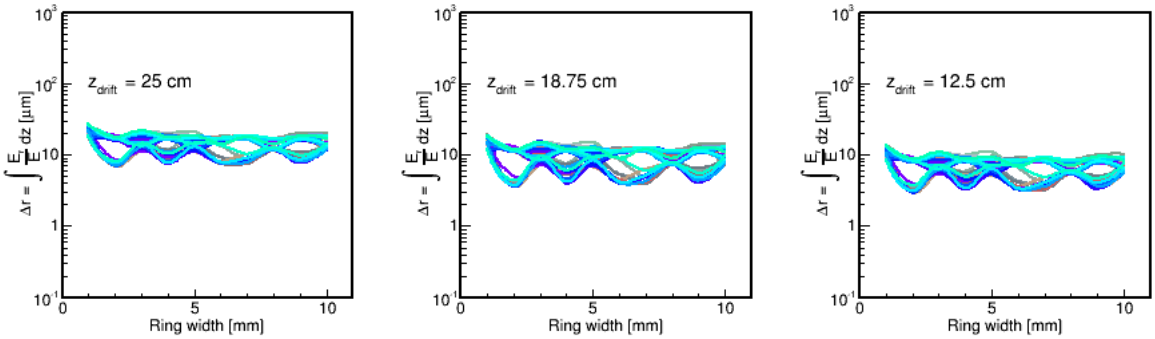

Figure 104: Radial distance an electron drifts from different drift distance to the bottom of the field cage. Left: from top to bottom. Middle: from 18.75 cm to bottom. Right: from 12.5 cm to bottom.

Table 18: Average electron number per pixel and optimal gain for He:CO_2:70:30 and C_4H_{10} at 1 atm.

gas	He in He:CO_2:70:30	H in C_4H_{10}
electron number per pixel	171	1294
optimal gain	2800	400

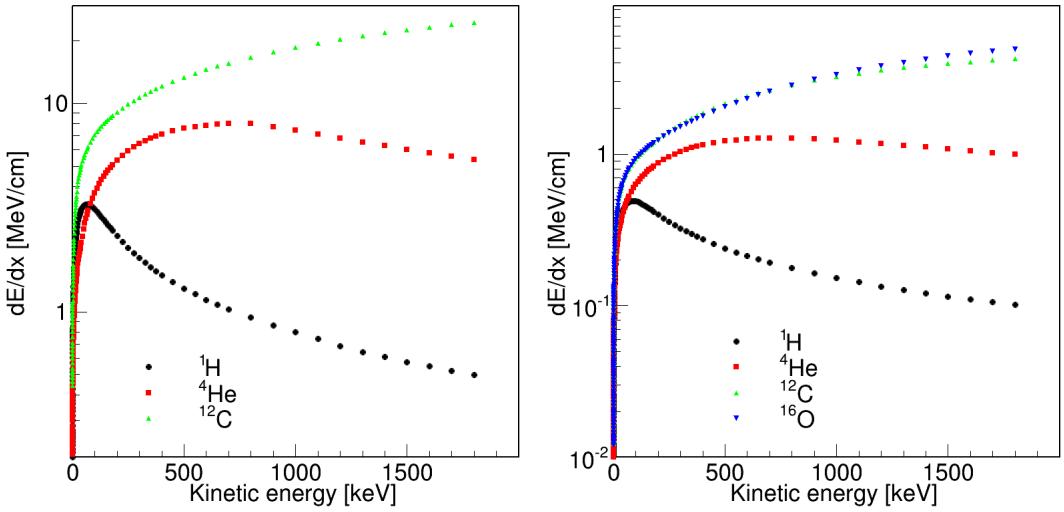

Figure 105: SRIM calculation of electronic energy loss to the gas electron per centimeter versus recoil kinetic energy. Left: Black point H. Red square He, Green triangle C in C_4H_{10} at 1 atm. Right: Black point H. Red square He, Green triangle C and Blue triangle down O in He:CO_2:70:30 at 1 atm.

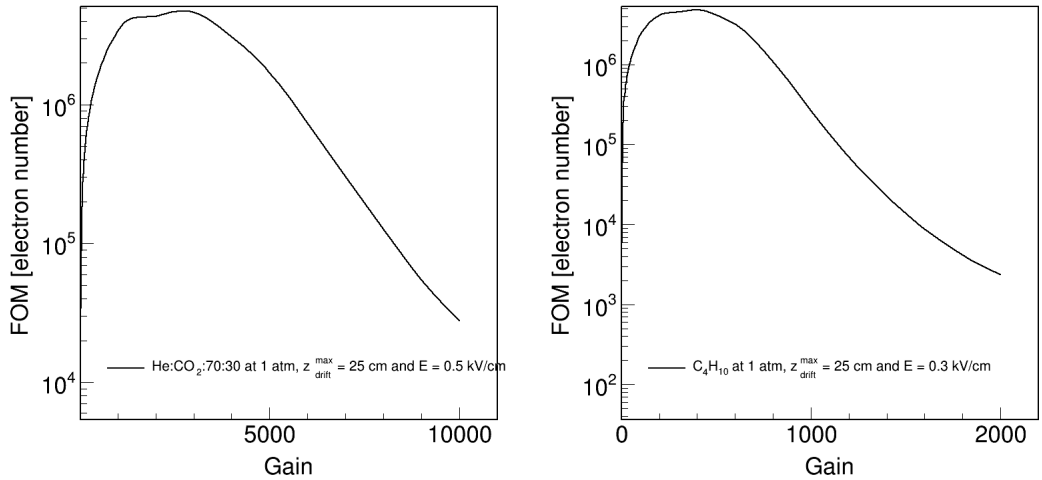

Figure 106: Gain figure-of-merit for 25 cm drift distance, 1 atm and 200 μm pixel size. Left: for He in He:CO_2:70:30. Right: for H in C_4H_{10}.

Table 19: Work function and mean ionization energy recorded per FE-I4 pixel for He:CO_2:70:30 and C_4H_{10} at 1 atm.

gas	He in He:CO_2:70:30	H in C_4H_{10}
Work function [eV/ion-electron-pair]	35.075	23.4
ionization energy per pixel [keV]	4.6	22

  - chip size 0.84 cm x 0.76 cm
  - pixel size 50 μm x 400 μm
  - 18 column x 160 row
  - 400 ns time range with 16 graduation
  - threshold 2215 electrons
  - 100k e^- charge range with 128 graduation

- FE-I4
  - chip size 2 cm x 1.68 cm
  - pixel size 50 μm x 250 μm
  - 80 column x 336 row
  - 1600 ns time range with 64 graduation
  - threshold 1384 electrons
  - 100k e^- charge range with 16 graduation

Table D.3.2 can be converted into Table D.3.2 which highlights the ionization energy each (FE-I4) pixel should record for He:CO_2:70:30 or/and C_4H_{10} (both at 1 atm). Even if the FE-I4 has much less charge graduation than the FE-I3 if the GEMs gain is properly chosen, the FE-I4 can reach an intrasic energy resolution of 290 eV and 1.38 keV tuned respectively for He in He:CO_2:70:30 and H in C_4H_{10}. The GEM and gas intrasic energy resolutions, roughly 20 % for both, should be added in quadrature ie total $\Delta E = 1.33$ and 6.4 keV respectively for He in He:CO_2:70:30 and H in C_4H_{10}.

If the TPC is correctly optimized the angular resolution should be dominated by the straggling as illustrated in Figures D.3.2 and D.3.2

Pressure and drift length choices

The pressures as well as the drift length can be optimized by determining a figure-of-merit shown in Fig. D.3.2. The pressure and the drift length figure-of-merits take into account the recoil energy spectrum due to the neutron and the directionality by considering that the diffusion effect is dominating the directionality: $L > 6.\sigma_{diffusion}(z)$ ie HT is not taken into account.

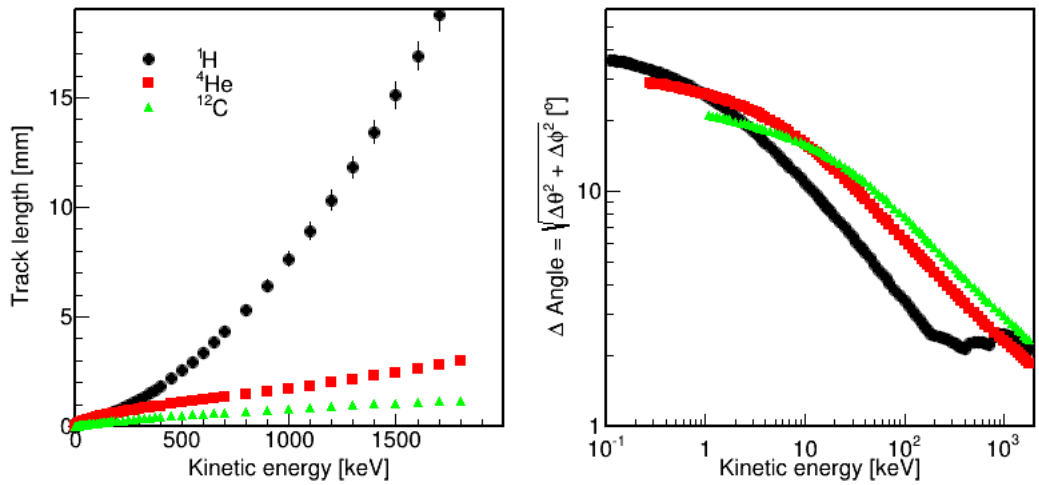

Figure 107: Left: track length versus recoil kinetic energy in C_4H_{10}. Right: angular resolution due the longitudinal and transverse straggling versus recoil kinetic energy in C_4H_{10}.

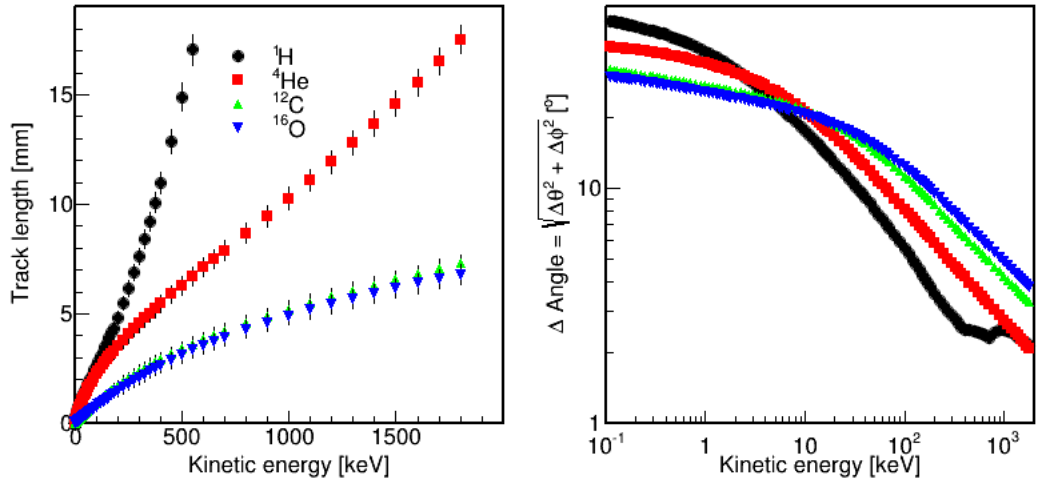

Figure 108: Left: track length versus recoil kinetic energy in He:CO_2:70:30. Right: angular resolution due the longitudinal and transverse straggling versus recoil kinetic energy in He:CO_2:70:30.

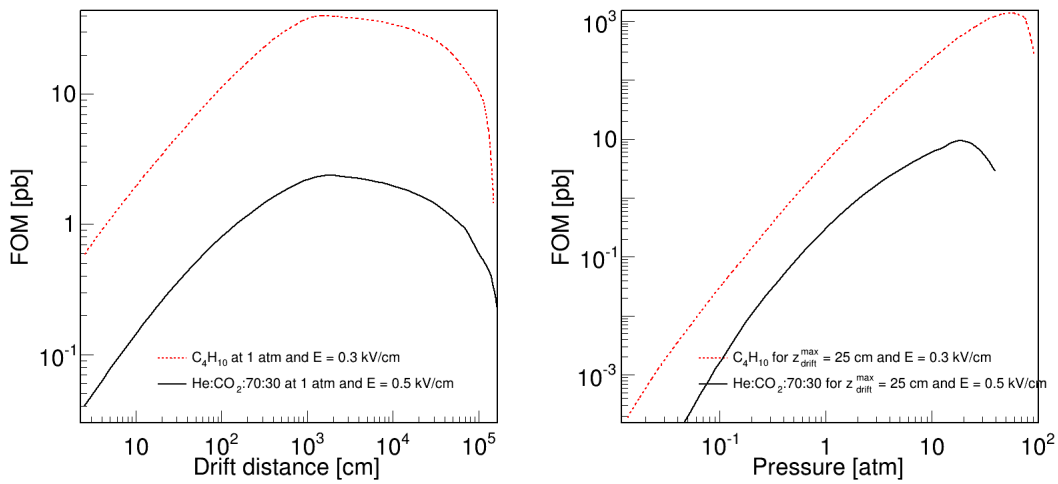

Figure 109: Left: drift distance figure-of-merit. Right: pressure figure-of-merit.

The fact that the optimum drift distance is well above 25 cm can be explained by the increase of the target volume and the long tail in the recoil energy spectrum see Figure D.3.2-bottom-left.

The iso-butane start to be liquid above 2 atm but the He:CO_2:70:30 can operate in principal at higher pressure. It should be noted that He:CO_2:70:30 $\sim$ 8 atm has the same figure-of-merit than iso-butane at 1 atm. For He:CO_2:70:30 at 8 atm, the optimum gain is 90 implying that one GEM might be enough.

D.3.3 Rates and Detection efficiency

Several conditions are imposed on the track to ensure that the projection of the track, with a length L, on the two-dimensionally segmented pixel chip readout plane can be exploited to extract the directionality:

- L $> 6\ \sigma_{xy}$ where σ_{xy} is the transverse diffusion
- L $> 3 \times$ GEM holes spacing
- $\Delta E_{HT} > 6\ .\ \Delta E$(E) where ΔE_{HT} is the difference in energy between the head (E_H) and the tale (E_T) and ΔE(E) the energy resolution

A so-called edge cut (Figure-right 110) is also applied to remove alpha-particle coming from natural radiation contained in the detector material and which are located outside of the sensitive volume. This background is critical particularly for He:CO_2:70:30 gas-mixture, since one cannot distinguish an alpha-particle recoiling due to a neutron scattering elastically on it to an alpha-particle coming from a Radon decay chain for example. The current irreducible

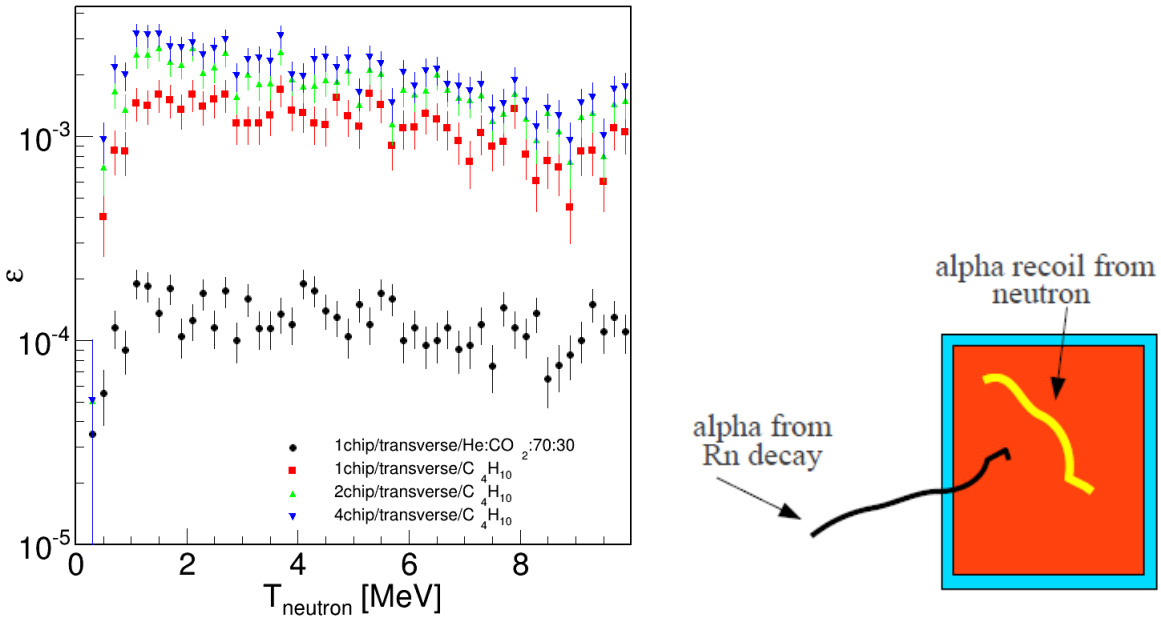

Figure 110: Left: Neutron detection efficiency as function of the neutron kinetic energy and number of pixel chip used. Right: edge cut drawing. Edge represented by the blue aera.

background rate in the sensitive volume after an edge cut with the micro-DCube prototype, which used the FE-I3 pixel chip, is around 0.2 per minute. So if one considers that the irreducible background will scale with the surface then 0.2 x A(4 FE-I4) x A(1 FE-I3) ie 4.2 per minute ie roughly 0.1 Hz for the micro-BEAST-TPCs. The irreducible background is represented by a black line at 0.1 Hz in Figure 111 or by a line at 0.044 Hz (0.1 Hz x 8 TPC / 18°) in the TPC angular plot rates: Figures 112, 113 and 114. Figure 111 shows the neutron rates with recoil exploitable directionality per TPC compared to the total rates in the TPCs.

Figures 112, 113 and 114 show the angular neutron rates for all TPCs combined with recoil exploitable directionality for the gas-mixture He:CO_2:70:30 and iso-butane both at 1 atm for the different beam-induced backgrounds.

The neutron detection efficiency as function of the neutron kinetic energy for iso-butane and the gas-mixture He:CO_2:70:30 (both 1 atm) for one, two and four FE-I4 pixel chips, Figure-left 110-left. Between one chip with gas-mixture He:CO_2:70:30 at 1 atm and four chips with iso-butane at 1 atm there is a factor ~ 8 improvement.

The neutron detection efficiency is also compared to the electron/positron and muons detection efficiencies in Figure 115.

The relatively large rates due to electromagnetic particles will not be a problem as shown in Figure 116 since it can rejected during the data analysis by applying a cut on the quantity L / E where L is the track length and E the ionization energy.

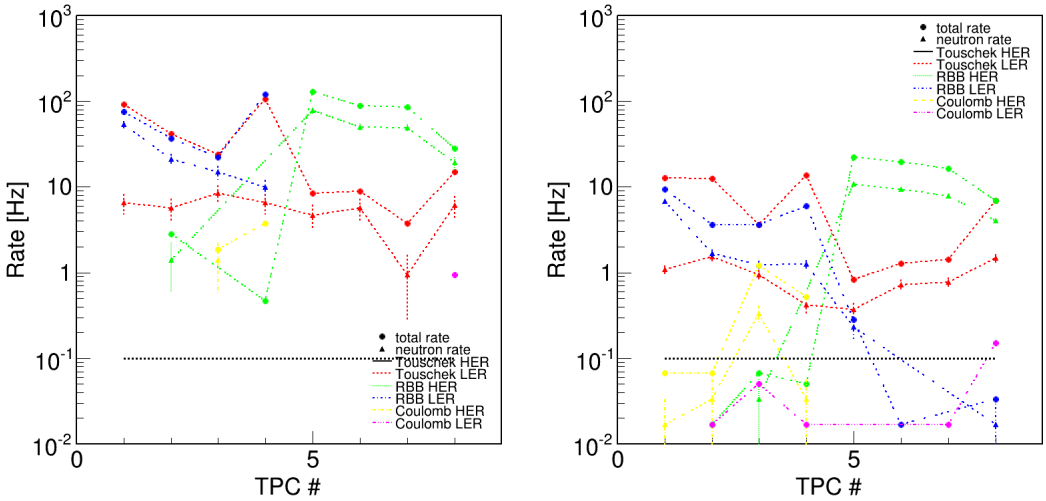

Figure 111: Rate at phase 2-phase recorded by four FE-I4 pixel chips in each TPC for the different beam-induced backgrounds. Left for C_4H_{10} at 1 atm. Right for He:CO_2:70:30 at 1 atm. The neutron rates correspond to the rate of recoil with directionality and edge cut. The total rates include all particles seen all hits recorded by the pixel chips. The black line represents the irreducible background expected.

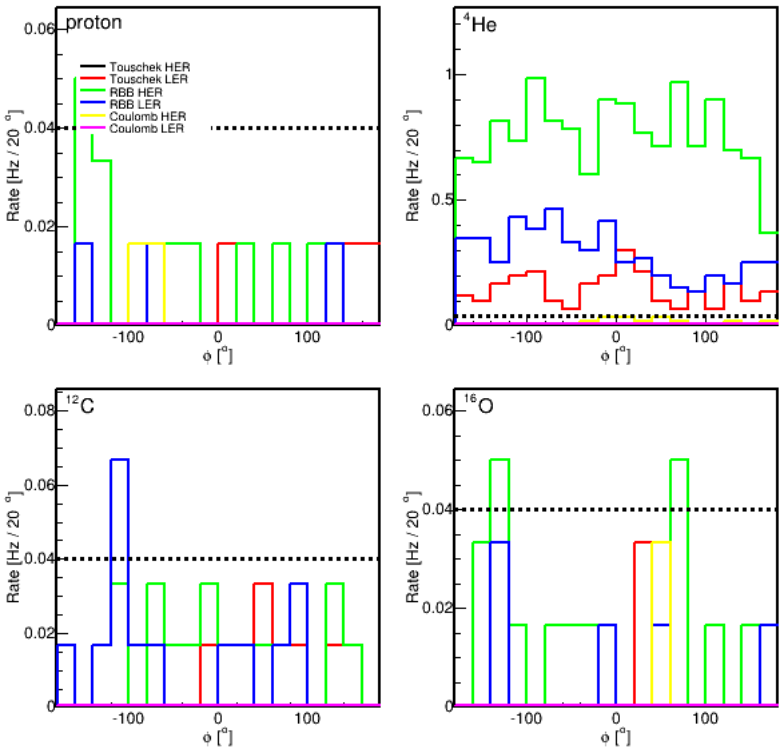

Figure 112: Rate of recoils (with directionality) versus azimuthal angle in He:CO_2:70:30 at 1 atm for the different beam-induced backgrounds at phase 2 and for all TPCs combined. Top-left: proton knock off from the detector materials. Top-right: He recoil. Bottom-left: carbon recoil. Bottom-right: oxygen recoil.

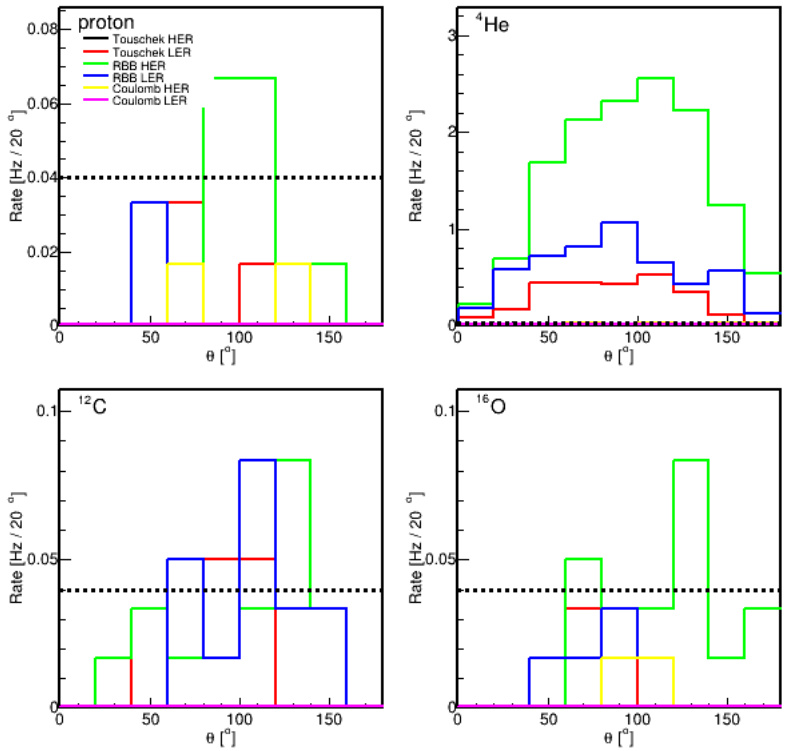

Figure 113: Rate of recoils (with directionality) versus polar angle in He:CO_2:70:30 at 1 atm for the different beam-induced backgrounds at phase 2 and for all TPCs combined. Top-left: proton knock off from the detector materials. Top-right: He recoil. Bottom-left: carbon recoil. Bottom-right: oxygen recoil.

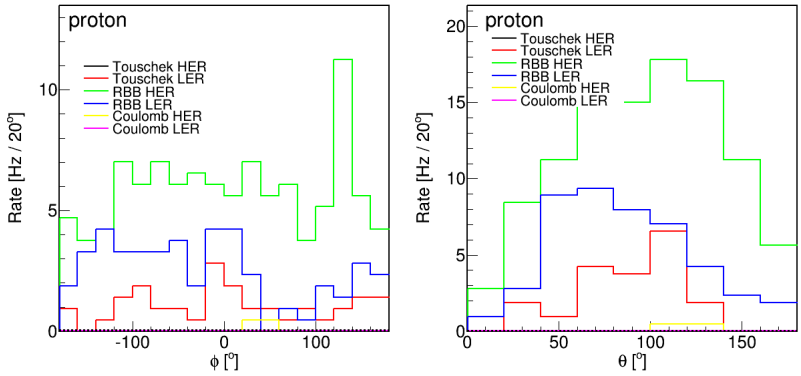

Figure 114: Rate of proton recoils (with directionality) in C_4H_{10} at 1 atm for the different beam-induced backgrounds at phase 2 and for all TPCs combined. Left: rate versus azimuthal angle. Right: rate versus polar angle.

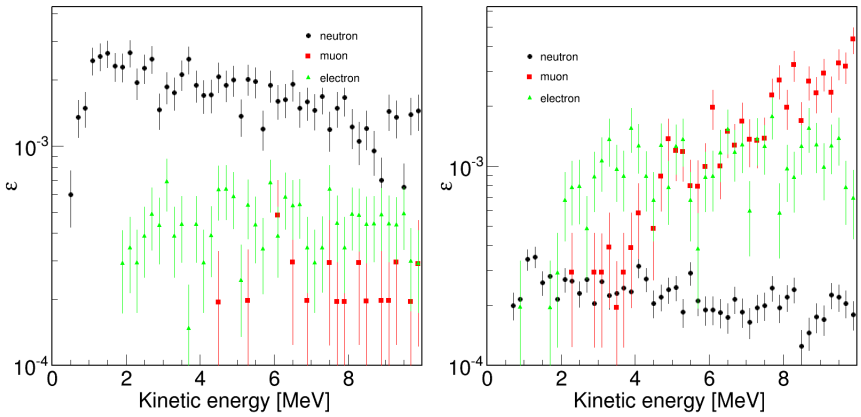

Figure 115: Detection efficiency of neutron, electron/positron and muons as function of the kinetic energy and number of pixel chip used. Left: for He:CO_2:70:30 at 1 atm. Right: for C_4H_{10} at 1 atm.

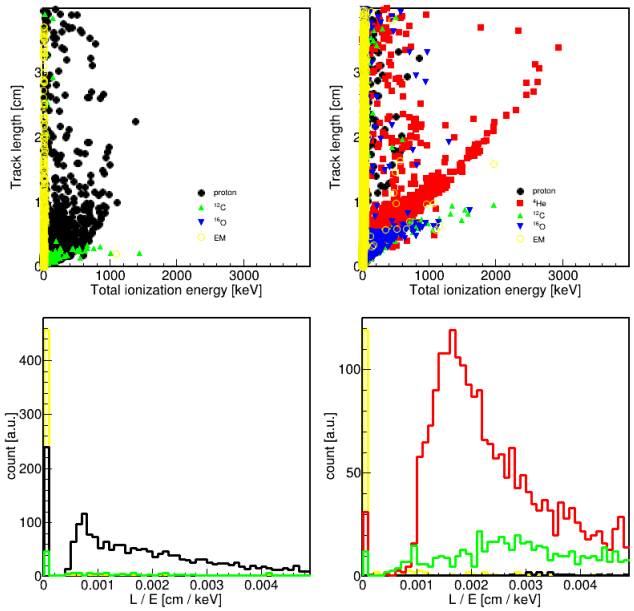

Figure 116: Top row: track length versus total ionization energy. Bottom row: L / E. Left column: C_4H_{10} at 1 atm. Right column: He:CO_2:70:30 at 1 atm.

D.4 Older Simulation Studies

D.4.1 Beam Background Dose Estimates

	Total Dose (rad)	EM Dose (rad)	Neutron Dose (rad)
CoulombHER	0	0	0
CoulombLER	0.027	0.026	0.0010
RBBHER	0.384	0.375	0.0081
RBBLER	0.076	0.070	0.0024
TouschekHER	0.044	0.043	0.0007
TouschekLER	0.121	0.118	0.0029
Total	0.649	0.633	0.0151

Table 20: *Expected dose in the electromagnetic calorimeter from beam backgrounds, per month of running at SuperKEKB design luminosity, at a vacuum pressure of* $10^{-}9$ *Torr (simulation). In the 20* μs *simulated there was no ECL dose from beam-gas Coulomb events originating in the HER.*

D.4.2 Commissioning Detector: Neutron Simulations

	Rate in backward TPCs (MHz)	Rate in forward TPCs (MHz)
Touschek LER	0.8	0.35
Touschek HER	0.3	0.01
Coulomb LER	0.75	0.15
Radiative Bhabha LER	0.25	2.35
Radiative Bhabha HER	2.7	0.3

Table 21: *Predicted rate of neutrons traversing the backward and forward micro-TPC arrays, at design luminosity.*

D.4.3 Commissioning Detector: Micro-TPC Simulations

Candidate target gases for the micro-TPCs are: $He : CF_4$, $He : CO_2$ and iso-C_4H_{10}, and $He : CH_4$. Helium and Hydrogen-based target gases are best for neutron detection, and the light target atoms maximize energy transfer during elastic scattering. In addition, typically $Ar : CO_2$ is used for prototype studies and calibration. This section summarizes they key

gas mixture	Ar:CO2 (70:30)	He:CF4 (70:30)	He:CO2 (70:30)	iso-C4H10 (100)	He:CH4 (70:30)
field strength simulated (V/cm)	1.0	1.0	1.0	2.0	1.0
drift velocity (μm/ns)	8.9	85	8.7	46.4	71.3
transverse diffusion ($\mu m/\sqrt{(cm)}$)	86.3	57	86.2	107	218.8
longitudinal diffusion ($\mu m/\sqrt{(cm)}$)	86.3	76	87.3	86	141.5

Table 22: Key parameters of candidate TPC gas mixtures.

performance parameters of these candidate gases, which were used to arrive at the micro-TPC specification in the commissioning detector CDR.

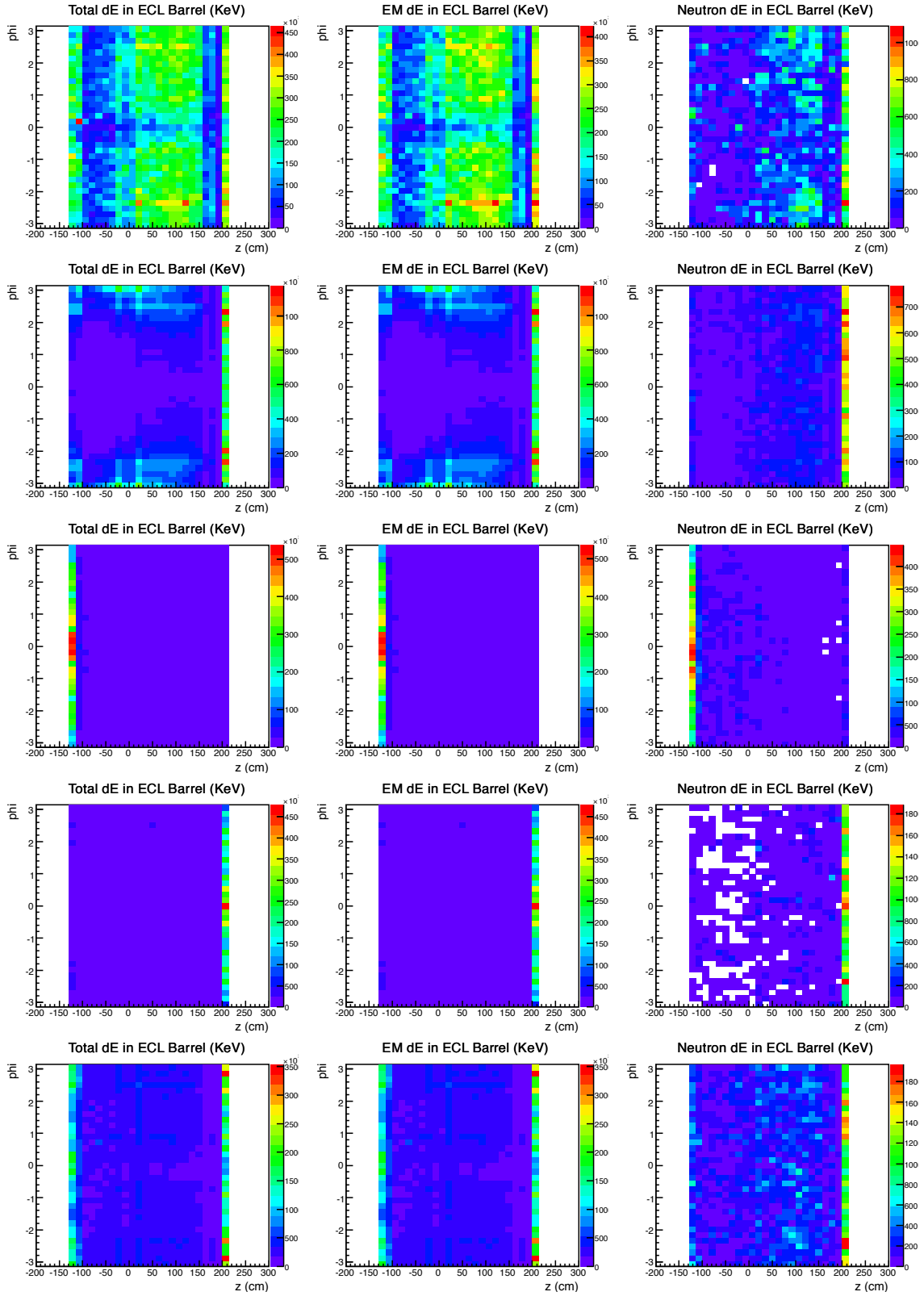

Figure 117: *Distribution of energy deposited in the electromagnetic calorimeter (ECL) from Radiative Bhabha Events, Beam-Gas Coulomb Events, and Touschek Scattering in 20 μs at SuperKEKB design luminosity (simulation). Backgrounds originating from the positron low-energy ring (LER) and electron high-energy ring (HER) were simulated and are hence plotted separately. In the 20 μ simulated there was no ECL dose from Beam-Gas Coulomb*

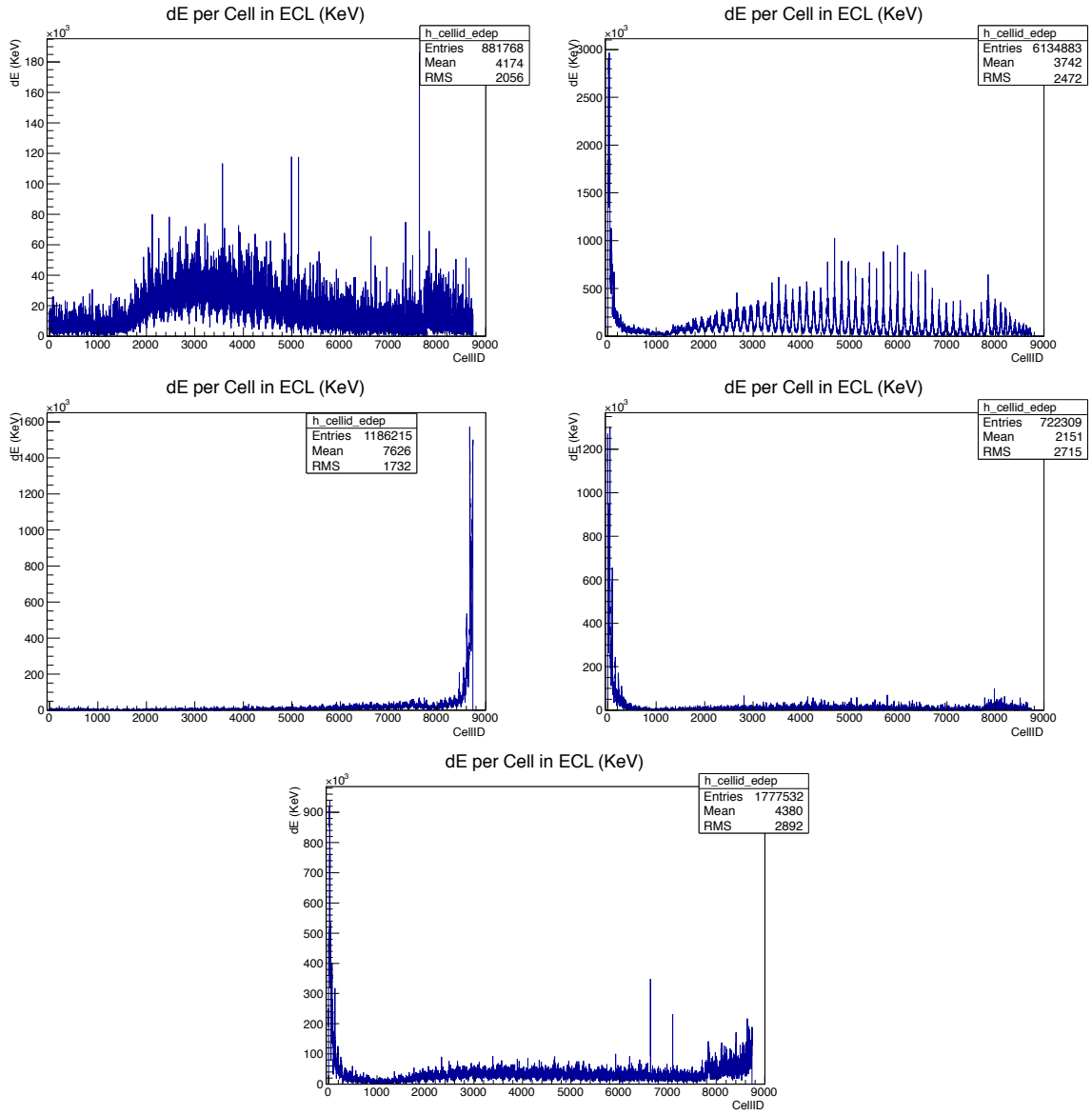

Figure 118: *Energy deposited versus electromagnetic calorimeter (ECL) crystal ID number, for Radiative Bhabha Events, Beam-Gas Coulomb Events, and Touschek Scattering, in 20 μs at SuperKEKB design luminosity (simulation). Backgrounds originating from the positron low-energy ring (LER) and electron high-energy ring (HER) were simulated and are hence plotted separately. In the 20 μ simulated there was no ECL dose from Beam-Gas Coulomb Events originating in the HER.*

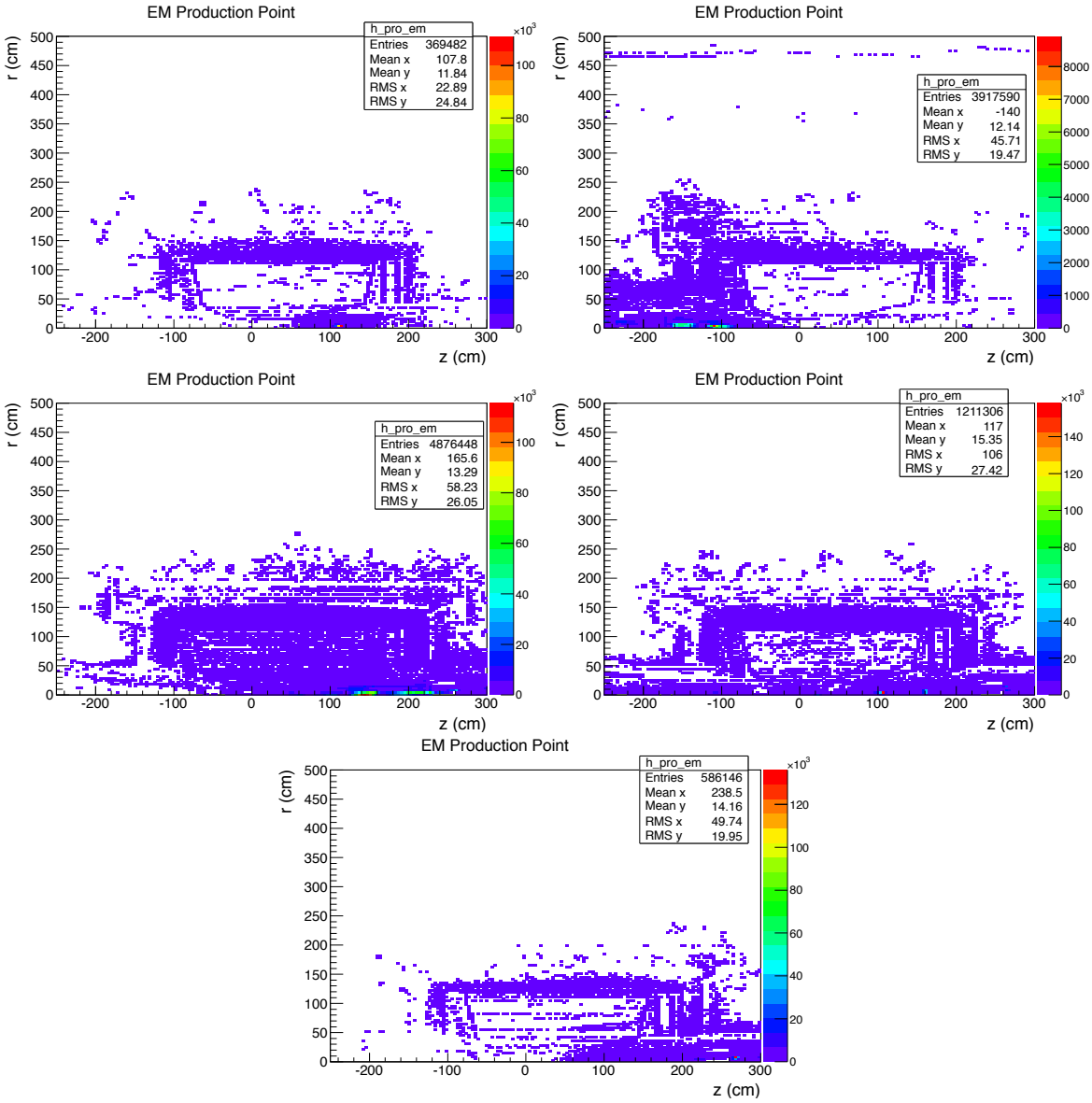

Figure 119: *Production point of EM radition for Radiative Bhabha Events, Beam-Gas Coulomb Events, and Touschek Scattering, in 1 μs at SuperKEKB design luminosity (simulation). Backgrounds originating from the positron low-energy ring (LER) and electron high-energy ring (HER) were simulated and are hence plotted separately. In the 1 μ simulated there was no ECL dose from Beam-Gas Coulomb Events originating in the HER.*

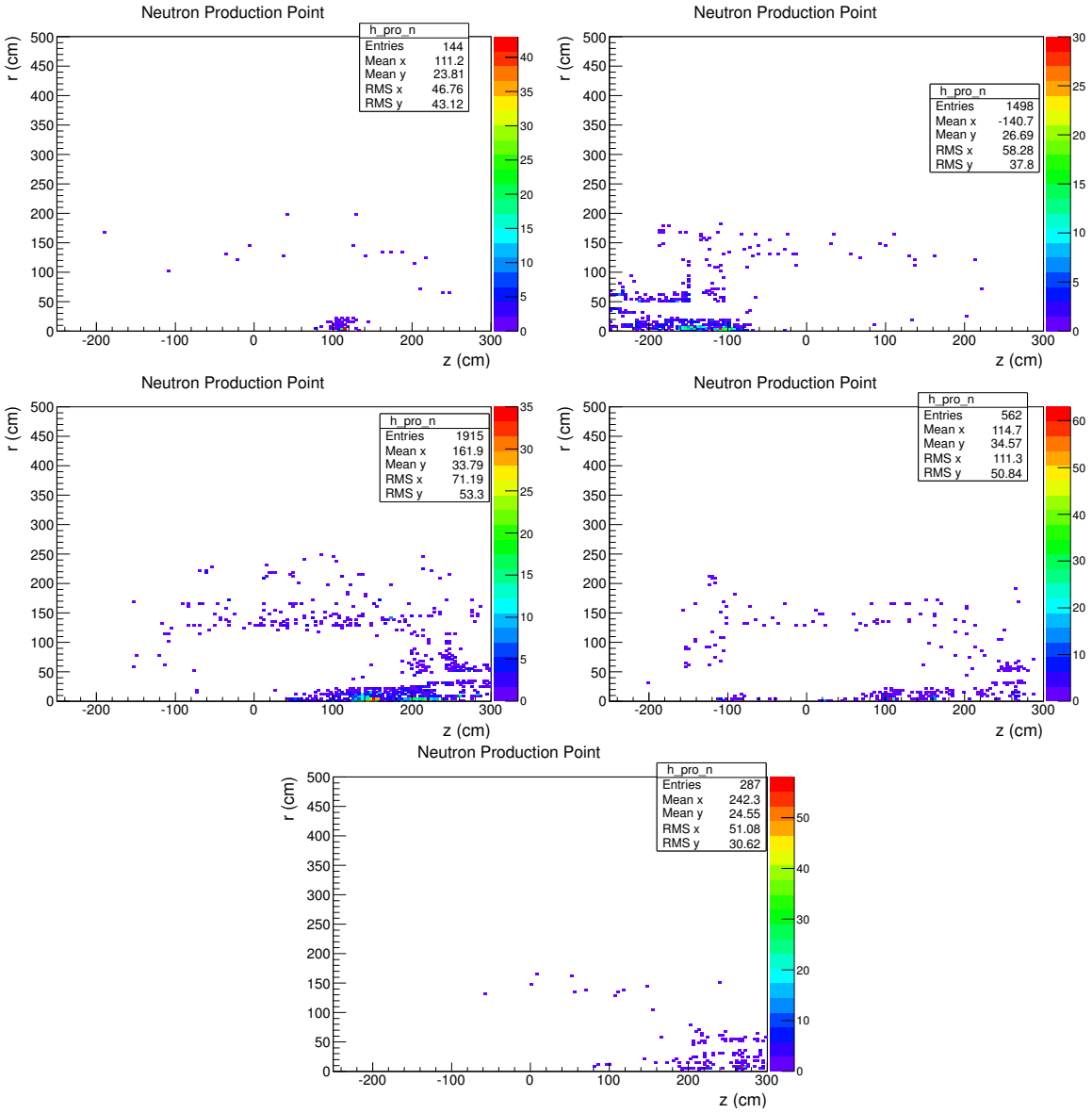

Figure 120: *Production point of neutrons for Radiative Bhabha Events, Beam-Gas Coulomb Events, and Touschek Scattering, in 1 μs at SuperKEKB design luminosity (simulation). Backgrounds originating from the positron low-energy ring (LER) and electron high-energy ring (HER) were simulated and are hence plotted separately. In the 1 μ simulated there was no ECL dose from Beam-Gas Coulomb Events originating in the HER.*

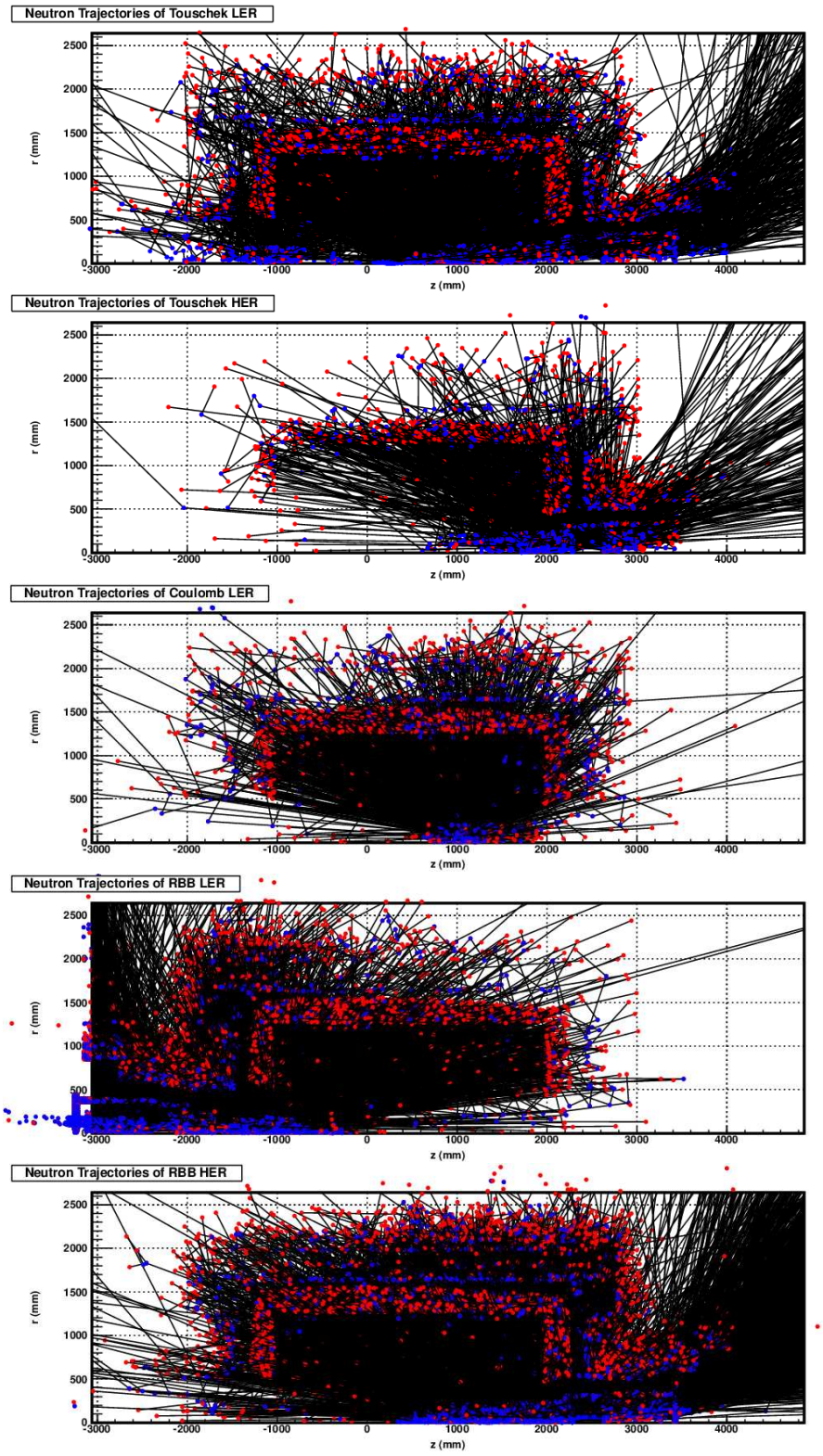

Figure 121: *GEANT production points (blue), GEANT decay points (red), and trajectories (black) of neutrons that deposit energy in the Calorimeter.*

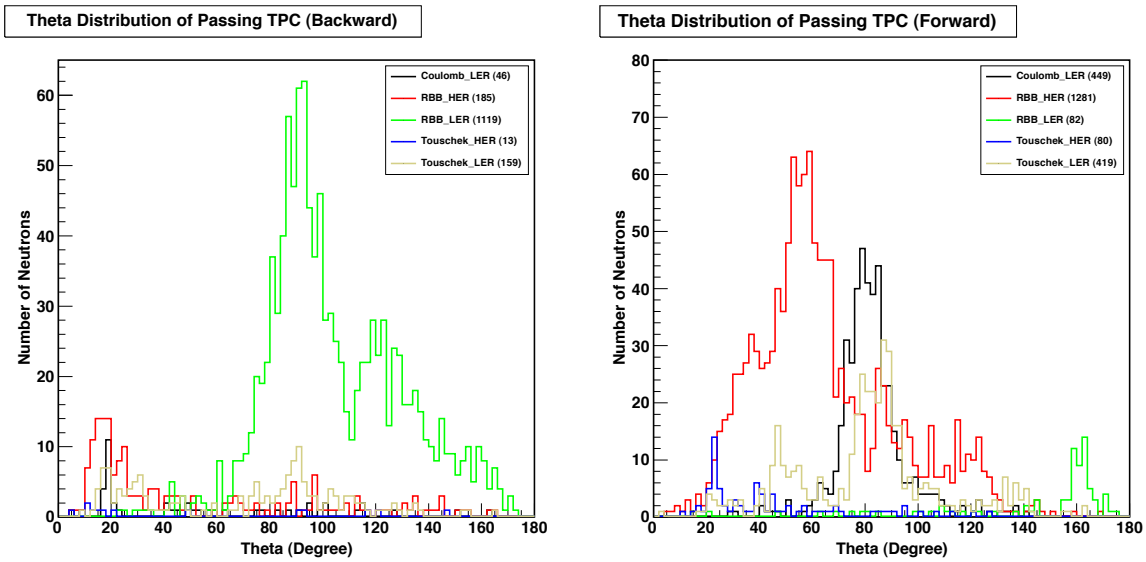

Figure 122: *Polar angle of neutrons that pass through the backward (left) and forward (right) array of microTPCs. The angle plotted is the polar angle of the incoming neutron neutron direction, as seen by each microTPC.*

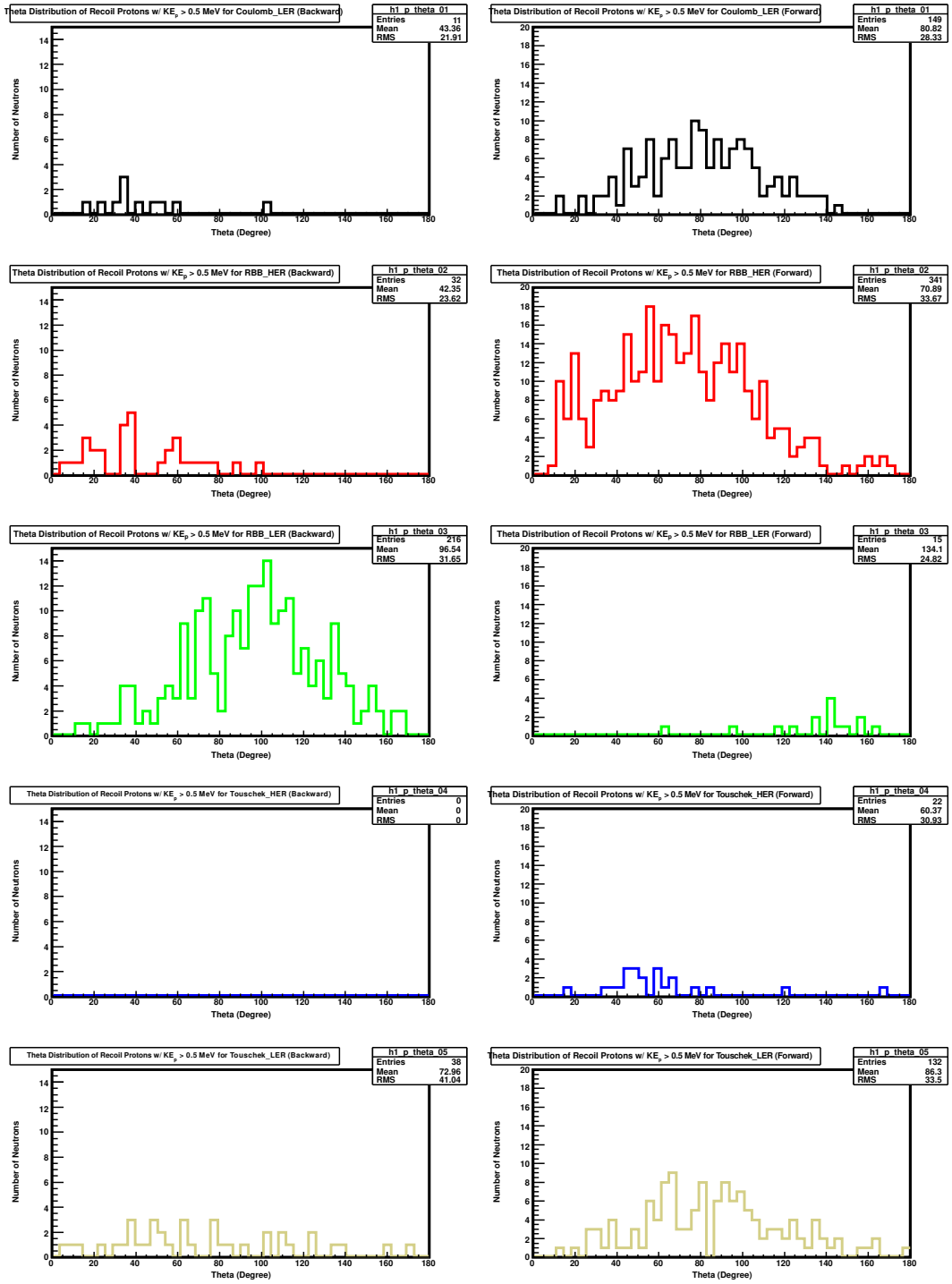

Figure 123: *Polar angle of proton recoils with $E > 500$ keV, from elastic neutron scattering in the backward (left) and forward (right) array of microTPCs - s expected to be observed in the detector with a Hydrogen-based target gas.*

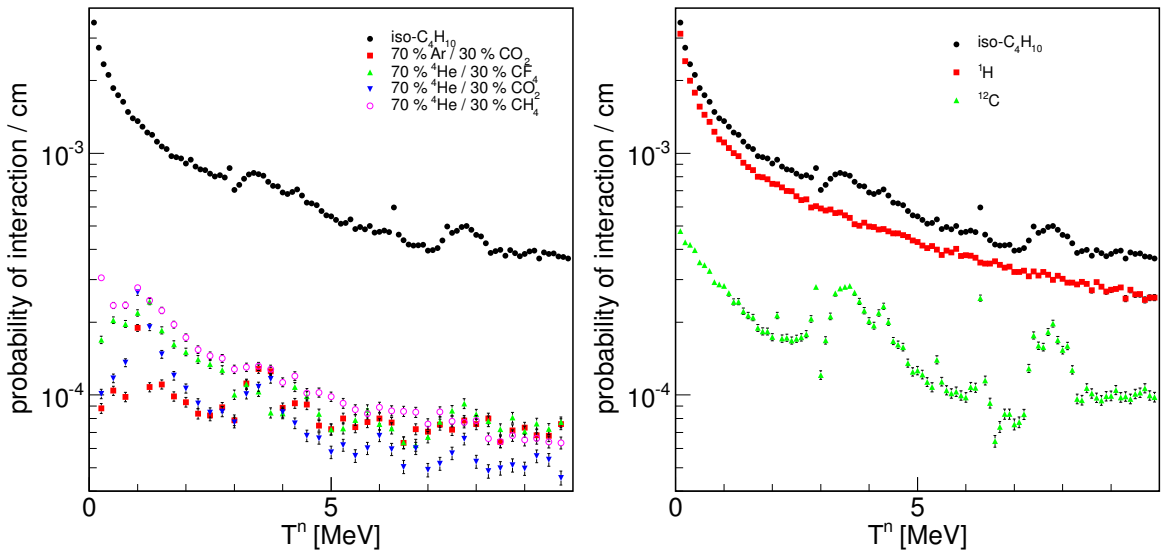

Figure 124: *Probability of neutron scattering per cm of target gas, at atmospheric pressure and room temperature. Below 2-MeV, the scattering is almost exclusively elastic. The effiency of iso-C4H10 is an order of magnitude higher than that of other candidate gases, simply because there are 10 hydrogen atoms per molecule. Hydrogen is also better than Helium for maximizing energy exchange during scattering, and in that the scattering probability for the target nucleus (Hydrogen) is significantly higher than that of other nuclei in the gas. The drawback of working with hydrogen-based gas mixtures is safety - they tend to be flammable.*

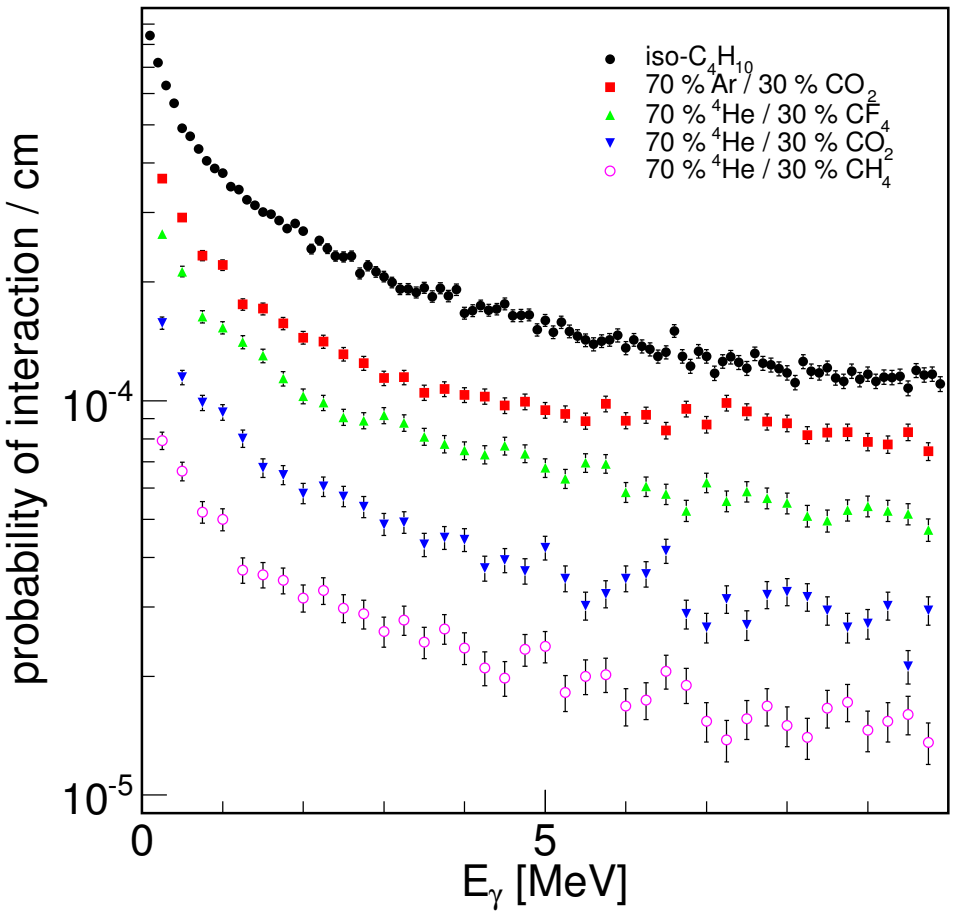

Figure 125: *Probability of gamma-ray scattering per cm of target gas, at atmospheric pressure and room temperature.*

E.1 Work Breakdown Structure Dictionary – WBS 1.01

1. Project Title: Belle-II	**2. WBS Element No.** 1.01	**3. WBS Owner:** Jim Fast
4. WBS Element Title: Project Integration and Support		
5. Task/Element Description: Integrated management and support services for the Belle-II project. Provides resources for general management and PNNL subject matter expert support to ensure the technical, cost, and schedule objectives of the project are met. Substantial work packages within this WBS include general management, project controls implementation and risk management, financial and procurement systems support, ES&H program support and participation with the Belle collaboration.		

A. Technical Objective:

The objective of this WBS element is to

This WBS element will deliver resources for general management, project integration and support services for the development and assembly of detector systems for installation in the Belle II detector upgrade at the SuperKEKB accelerator at the KEK laboratory in Tsukuba, Japan. This includes establishing and maintaining effective working relationships between the Federal Project Director (FPD) and the Director, PNNL. The resources within this task will direct and support the efforts required to successfully support design, analysis, fabrication, testing, and delivery of detector system elements. This scope includes identifying/assessing all vulnerabilities and assuring managerial action is taken to prevent adverse consequences to the Belle-II project.

B. Assumption(s):

Major assumptions for this WBS include:

- Battelle, as the M&O contractor for PNNL, will use DOE Capital Acquisition Orders as a framework for managing the Belle-II Major Item of Equipment (MIE). Project management requirements essential for compliance with DOE Order 413.3 will be flowed down into appropriate PNNL subcontracts to ensure project management expectations are maintained.

C. Scope of Work Statement:

This WBS element involves the following activities:

<u>WBS 1.01.01 – Project Management and Business System Integration</u>
The primary elements of work and goals of this element are to integrate PNNL project and business management systems to provide effective management direction, administrative planning and control for the project. This includes activities involving project operations, project planning and controls, business support, communications, records and documentation management, quality assurance, and chief scientist support.

WBS 1.01.02 – Project Reviews
The primary elements of work and goals of this WBS element are to coordinate the assembly of the various Critical Decision documents, submit the packages, and prepare for external project reviews. This includes Critical Decision assessment and tracking.

WBS 1.01.03 – Contracts and Procurement
The primary elements of work and goals of this WBS element are to provide management for the contract, procurement and support services needed to plan/place/administer the contracts planned for the Belle-II Project. These general management and support services include support of Pre-bid, Bid/Solicitation and award, Contract Administration and Close-out activities.

WBS 1.01.04 – Environmental Safety & Health
The objective of this WBS element is to manage the Environmental, Safety, and Health support to the Belle-II project in accordance with the applicable requirements of DOE Order 413.3 and PNNL management systems/procedures. This element will establish the high level ES&H project objectives, coordinate ES&H subject matter experts to support these processes, and provide status/reporting of ES&H activities throughout the life of the project.

WBS 1.01.05 – Belle-II Meetings
The objective of this WBS element is to attend and participate in the various Belle-II review meetings, specifically attendance at the Belle Physics Advisory Committee and Belle-II General Meeting.

D. Deliverables/Schedule:

Activity ID	Activity Name	Baseline Date	Milestone Level
1.1.3.1-210	CD-0 Approval	7/28/2011	Level 1
1.1.3.1-110	CD-1 or Equivalent	9/18/2012	Level 1
1.3-470	L1 MS CD-2a/3a Approval (KLM)	11/8/2012	Level 1
1.1.3.2-310	L1 MS CD-2/3 or Equivalent	5/27/2014	Level 1
A1010	L1 MS CD-4 or Equivalent	6/15/2016	Level 1
1.1.1.2-160	DOE FY12 Funding Received - $650K - MIE	4/2/2012	Level 2
1.1.1.2-40	DOE FY13 Funding Received - (CD-2b/3b)	12/31/2012	Level 2
1.1.1.2-50	DOE FY13 Funding Received (CD-3b) OPC Only	5/10/2013	Level 2
1.1.1.2-60	DOE FY14 Funding Received	12/30/2013	Level 2
1.1.1.2-70	DOE FY15 Funding Received	12/29/2014	Level 2
1.1.1.2-10	JFY11 Nichibei Funding Received - $781K	8/1/2011	Level 3
1.1.1.2-30	DOE FY12 Funding Received - $450K OPC	10/3/2011	Level 3
1.1.1.2-20	JFY12 Nichibei Funding Received - $781K	8/1/2012	Level 3
1.1.3.2-170	L3-M - CD-2/3 or Equivalent	4/21/2014	Level 3
A0990	Project Complete - Start Project Closeout	2/13/2015	Level 3

E. Relationships/Interfaces to Other WBS Elements:

Key inputs/outputs from/to other project WBS are as follows:

This activity has direct day-to-day interface and management interactions with all Belle-II project WBS managers, the FPD, and PNNL Director.

Inputs

E.2 Work Breakdown Structure Dictionary – WBS 1.02

1. Project Title: Belle-II	**2. WBS Element No.** 1.02	**3. WBS Owner:** Jim Fast
4. WBS Element Title: iTOP Optics		
5. Task/Element Description: The element provides for the development of design specifications and procurement actions for the barrel particle identification system. This element includes the design and specification of the iTOP fused silica optics, and procurement and delivery of the optics to KEK. This task includes simulation, prototyping, test beam and cosmic ray test of prototypes, software, and associated administration.		

A. Technical Objective:

The objective of this WBS element is to

Fused silica optical component specifications will be developed based on prototype studies conducted to date, followed by procurement of the preproduction and production bars, mirrors and prisms. Procurement will be managed by PNNL. Prior to shipping, metrology will be done by vendor(s) with the results being reviewed by physicists at PNNL and at Cincinnati and upon approval the vendor will ship to KEK. Acceptance testing will be performed at KEK on receipt of optics. This WBS will provide engineering and fabrication support for the bar boxes to ensure integration with electronic systems in WBS 1.3. A calibration system and cosmic ray test system for the iTOP will be developed and will be used as part of the testing prior to installation. This WBS element also includes Cosmic Ray and beam test of prototype and preproduction iTOP modules. Integration, installation and commissioning of the iTOP modules is not included in this WBS as the system integration is reliant on photodetectors and bar boxes that are to be supplied by Japanese collaborators.

B. Assumption(s):

Major assumptions for this WBS include:

- Other Belle-II collaborators will provide photodetectors and bar boxes.
- The support structure for the barrel particle identification system is being designed and built as part of the KEK upgrade.

C. Scope of Work Statement:

This WBS element involves the following activities:

<u>WBS 1.02.01 – iTOP Optics</u>
The primary elements of work and goals of this element are to develop quartz component specifications based on prototype studies conducted to date and quartz bars, mirrors and wedges will be procured. Procurement will be managed by PNNL. QA will be done by vendor prior to shipment; results will be reviewed by physicists at PNNL and at Cincinnati; and, upon approval, the

vendor will ship to KEK for assembly. At KEK the optical components will be tested to verify no damage occurred during shipment. Once all quartz material has been tested the project is complete.

Additional OPC prototyping/testing was added to the iTOP WBS with two prototype quartz bars, mirrors and prisms being procured and support for optical testing and analysis.

WBS 1.02.02 – Software Development
The primary elements of work and goals of this WBS element are to conduct simulations to determine probability density functions for pion and kaon tracks in order to quantify detector performance. Results from previous GEANT-3-based Monte Carlo will be evaluated and new simulations using GEANT-4 code will be performed

WBS 1.02.03 – Mechanical Systems
The primary elements of work within this WBS are to provide engineering support to the design and fabrication of the bar boxes and the support frame for the iTOP modules. This element does not include any procurement. Oversight and design reviews of the bar boxes and support frame being designed and fabricated by KEK. KEK is the design authority. Effort is to ensure integration with electronic systems, WBS 1.3.02.

WBS 1.02.04 – iTOP Calibration System
The primary elements of work of this WBS element are the design, engineering, procurement, and assembly of the calibration system using a light source to measure/test iTOP modules. Light source will be provided by KEK. System needs to be ready for testing, WBS 1.2.06 once the optics are delivered.

WBS 1.02.05 – iTOP Prototype Testing
The objective of this WBS element is to certify the performance of the iTOP detector under realistic beam conditions. Using a full-size prototype module, tests in a test beam will be conducted and the results analyzed to support development of final specifications for the optic material.

WBS 1.02.06 – Quartz Acceptance Testing
The primary elements of work of this WBS element are to develop test plans and conduct testing of the quartz material after it has been shipped and received at KEK.

D. Deliverables/Schedule:

Activity ID	Activity Name	Baseline Date	Milestone Level
1.2.1.1-250	L2 MS Complete Initial Beam Test Analysis	2/28/2012	Level 2
1.2.1.2.2-150	Begin Bar Production	5/3/2012	Level 2
1.2.1.1-320	L2 MS Complete Initial Beam Test Analysis at LEPS	2/22/2013	Level 2
1.2.6-280	L2 MS Pre-Production iTOP Beam Test Complete	6/14/2013	Level 2
1.2.01.05-280	L2 MS Lot 1 Optics Arrival at KEK	3/27/2014	Level 2
1.2.1.2.2-810	Begin TEC Bars 1-4 Production	4/28/2014	Level 2
1.2.01.05-290	L2 MS Lot 2 Optics Arrival at KEK	6/20/2014	Level 2

1.2.1.2.2-820	Begin TEC Bars 9-12 Production	11/13/2014	Level 2
1.2.3-240	All iTOP Mechanical Assemblies at KEK	1/22/2015	Level 2
1.2.1.2.2-830	Begin TEC Bars 21-24 Production	5/7/2015	Level 2
1.2.01.05-300	L2 MS Lot 5 Optics Shipment Arrives at KEK	5/21/2015	Level 2
1.2.01.05-270	L2 MS Last Optics Shipment Arrives at KEK	12/10/2015	Level 2
1.2.1.2.2-240	L2 MS Quartz Bar Production Completed	1/12/2016	Level 2
1.2.1.1-230	Initial Beam Test Analysis (1/16 Prototype)	1/31/2012	Level 3
1.2.2-290	Full GEANT Simulation of iTOP	3/30/2012	Level 3
1.2.1.1-290	Initial Beam Test Analysis (1/16 Prototype) at LEPS	12/4/2012	Level 3
1.2.2-110	Pre-Production Photodetectors Available (64 SL10s)	12/26/2012	Level 3
1.2.1.2.2-230	Received Bars 1&2 (2)	1/25/2013	Level 3
1.2.3-230	Pre-production Units Received	3/4/2013	Level 3
1.2.6-220	Pre-Production iTOP Module Complete	4/1/2013	Level 3
1.2.6-260	Pre-Production iTOP Beam Test Complete	6/14/2013	Level 3
1.2.2-300	Completed Alignment Calibration Algorithm	6/18/2013	Level 3
1.2.3-150	Final Design Complete	8/20/2013	Level 3
1.2.01.05-230	Lot 1 Optics Arrival at KEK	2/13/2014	Level 3
1.2.01.05-240	Lot 2 Optics Arrival at KEK	3/27/2014	Level 3
1.2.04-150	iTOP Calibration System Engineering Completed	6/23/2014	Level 3
1.2.1.2.2-210	Complete Production TEC Bars 1-4	10/16/2014	Level 3
1.2.01.05-250	Lot 3 Optics Arrival at KEK	11/13/2014	Level 3
1.2.04-160	iTOP Calibration System Assembled and Tested	12/10/2014	Level 3
1.2.1.2.2-220	Complete Production TEC Bars 5-8	12/15/2014	Level 3
1.2.01.05-340	Lot 4 Optics Arrival at KEK	12/31/2014	Level 3
1.2.1.2.2-300	Complete Production of TEC Bars 9-12	2/12/2015	Level 3
1.2.01.05-360	Lot 5 Optics Arrival at KEK	2/26/2015	Level 3
1.2.1.2.2-330	Complete Production of TEC Bars 13-16	4/9/2015	Level 3
1.2.01.05-380	Lot 6 Optics Arrival at KEK	5/21/2015	Level 3
1.2.1.2.2-360	Complete Production of TEC Bars 17-20	6/5/2015	Level 3
1.2.01.05-400	Lot 7 Optics Arrival at KEK	6/19/2015	Level 3
1.2.1.2.2-390	Complete Production of TEC Bars 21-24	8/3/2015	Level 3
1.2.01.05-420	Lot 8 Optics Arrival at KEK	8/17/2015	Level 3
1.2.01.05-440	Lot 9 Optics Arrival at KEK	9/15/2015	Level 3
1.2.1.2.2-420	Complete Production of TEC Bars 25-28	9/29/2015	Level 3
1.2.6-340	Complete Production Optics Testing	10/13/2015	Level 3
1.2.1.2.2-460	Complete Production of TEC Bars 29-32	11/24/2015	Level 3

E. Relationships/Interfaces to Other WBS Elements:

Key inputs/outputs from/to other project WBS are as follows:

Inputs

Deliverable	**Date Needed**	**From WBS**
CD-2/3	4/21/2014	1.01
1/16th iTOP Readout System	10/15/2012	1.03

Outputs

Deliverable	Date Completed	To WBS
Ship iTOP Assemblies to KEK	02/2013-11/2015	2.02

E.3 Work Breakdown Structure Dictionary – WBS 1.03

1. Project Title: Belle-II	**2. WBS Element No.** 1.03	**3. WBS Owner:** Gary Varner
4. WBS Element Title: Readout Systems		
5. Task/Element Description: This WBS element covers the design, procurement, assembly and testing of the iTOP and KLM readout systems in the US and shipment to KEK. This includes developing, fabricating and testing custom ASICs as well as circuit boards. This element includes developing firmware, software, and associated administration.		

A. Technical Objective:

The objective of this WBS element is to

Readout systems for the iTOP and KLM systems are included in this WBS element. The iTOP readout system includes Application Specific Integrated Circuits (ASICs) used to digitize the signals from the MCP-PMTs, a local board stack at the end of each iTOP module which houses the ASICs, ASIC controllers (FPGAs), HV distribution etc. Two different readout systems will be used by the KLM systems. The first is an updated system for the resistive plate chambers (RPCs) that will be retained from the existing Belle system. This updated readout system will provide signal digitization and faster readout required to meet the demands of the Belle II environment. The rest of the KLM system (inner barrel layers and the full end cap systems) will have new plastic scintillator detectors requiring completely new readout. That system will include amplifiers within the new modules with ASIC digitizers located on VME boards in crates outside the detector.

First generation R&D prototypes of iTOP and KLM readout have been produced. The remaining R&D/prototyping work consists of 2 more phases. In Rev. B, the final form-factors of the readout PCBs and ASICs will be fabricated and evaluated. In Rev. C, pre-production prototypes will be assembled, using candidate final versions of all commercial and custom components, and evaluated versus all final engineering specifications. Successful completion of Phase C prototyping is necessary prior to commitment for production fabrication. Due to the use of Ball Grid Array and other difficult to assemble parts (for space reasons), all production boards will be assembled in industry and checked/debugged at Belle II member institute laboratories. Subcomponents will be individually tested and characterized prior to integration into Sub-detector Readout Modules (SRMs). SRMs are the units that are directly integrated with opto-detector front-ends to form the (iTOP or eKLM) detector instrumentation.

Integration of the SRMs and backend readout (FINESSE/COPPER) into fully-assembled detector sub-modules, wherein cosmic ray calibration data can be taken completes this WBS element.

B. Assumption(s):

Major assumptions for this WBS include:

- ASIC foundries will maintain a consistent production schedule.
- Estimates for electromechanical development depend upon maintaining current detector envelope.

C. Scope of Work Statement:

This WBS element involves the following activities:

WBS 1.03.01 – iTOP Readout System
This WBS element includes finalizing specifications for production boards to be fabricated for the iTOP front-end and back-end electronics and the procurement of electronic components, assembly of boards and testing the boards prior to and after delivery to KEK.

WBS 1.03.02 – Common Electronics
This WBS element includes finalizing specifications for production to be fabricated for both the iTOP and KLM detectors; and the procurement of electronic components, assembly of boards and testing the boards prior to and after delivery to KEK.

WBS 1.03.03 – Barrel KLM (B-KLM) and Endcap KLM (E-KLM) Readout System
This WBS element includes finalizing specifications for production boards to be fabricated for the barrel and end-cap KLM and the procurement of electronic components, assembly of boards and testing the boards prior to and after delivery to KEK.

D. Deliverables/Schedule:

Activity ID	Activity Name	Baseline Date	Milestone Level
1.3.1.3-160	L2 MS - Complete iTOP Readout Pre-Production Prototyping	3/28/2014	Level 2
1.3.2.3-100	L2 MS - Complete KLM Readout Pre-Production Prototyping	4/7/2014	Level 2
1.4.2.5-70	L2 MS E-KLM HV Electronics Arrive at KEK	5/2/2014	Level 2
1.3.5-80	L2 MS - Complete Production of KLM Readout Modules	2/19/2015	Level 2
1.3.4-80	L2 MS - Complete Production of iTOP Readout Modules	3/20/2015	Level 2
1.3.1.2-60	ASIC Ordered	6/25/2012	Level 3
1.3.2.2-40	TARGET Chip Ordered	12/21/2012	Level 3
1.3.2.3-960	Complete Pre-Production of Pre-Amps and Carrier Boards for EKLM	3/22/2013	Level 3
1.3.5-50	Complete Production of Pre-Amps and Carrier Boards for BKLM	6/3/2013	Level 3
1.3.2.2-120	TARGET 7 Chip Ordered for Pre-Production Run	1/13/2014	Level 3
1.3.1.3-140	Complete iTOP Readout Pre-Production Prototyping	2/14/2014	Level 3
1.4.2.5-50	EKLM HV Electronics Arrive at KEK	3/21/2014	Level 3
1.5.1.7.4-40	B-KLM HV Electronics Arrive at KEK	3/21/2014	Level 3

1.3.1.3-370	Complete iTOP Readout 1/4 Scale Pre-Production Prototyping	3/21/2014	Level 3
1.3.2.3-80	Complete KLM Readout Pre-Production Prototyping	3/24/2014	Level 3
1.3.5-110	Complete Production of Pre-Amps and Carrier Boards for EKLM	6/24/2014	Level 3
1.3.6-120	Complete Production of 1/16th of the RPC for KLM	7/16/2014	Level 3
1.3.2.3-400	HV board Production Complete	8/13/2014	Level 3
1.3.2.3-540	Front board: PMT-to-ASIC electromechanical interface Production Complete	8/13/2014	Level 3
1.3.2.2-80	ASIC Production (TARGET) Complete	8/27/2014	Level 3
1.3.4-50	Complete Production of iTOP Readout Modules For Lot 2	8/27/2014	Level 3
1.3.1.2-80	ASIC Production Complete (BLAB)	9/4/2014	Level 3
1.3.2.3-860	SCROD control and data collection module Production Complete	9/11/2014	Level 3
1.3.4-90	Complete Production of iTOP Readout Modules For Lot 3	10/10/2014	Level 3
1.3.4-100	Complete Production of iTOP Readout Modules For Lot 4	10/17/2014	Level 3
1.3.2.3-670	Carrier Boards Production Complete	10/30/2014	Level 3
1.3.2.3-730	Interface Boards Production Complete	10/30/2014	Level 3
1.3.4-110	Complete Production of iTOP Readout Modules For Lot 5	11/7/2014	Level 3
1.3.4-120	Complete Production of iTOP Readout Modules For Lot 6	11/14/2014	Level 3
1.3.5-60	Complete Production of KLM Readout Modules	11/20/2014	Level 3
1.3.2.3-410	Complete Production of Readout Mother Boards for KLM	11/20/2014	Level 3
1.3.2.3-420	Complete Production of TARGET Daughter Card	11/20/2014	Level 3
1.3.4-130	Complete Production of iTOP Readout Modules For Lot 7	12/9/2014	Level 3
1.3.4-140	Complete Production of iTOP Readout Modules For Lot 8	12/16/2014	Level 3
1.3.4-60	Complete Production of iTOP Readout Modules For Lot 9	12/23/2014	Level 3

E. Relationships/Interfaces to Other WBS Elements:

Key inputs/outputs from/to other project WBS are as follows:

Inputs

Deliverable	Date Needed	From WBS
CD-2/3	4/21/2014	1.01
Final iTOP Quartz Bar Box Mechanics	01/2014	1.02

Outputs

Deliverable	Date Completed	To WBS
iTOP SRMs	11/6/2014	2.02
KLM Readout Modules	10/30/2014	2.04
1/16th RPCs for KLM	6/2/2014	2.04

E.4 Work Breakdown Structure Dictionary – WBS 1.04

1. Project Title: Belle-II	**2. WBS Element No.** 1.04	**3. WBS Owner:** Leo Piilonen
4. WBS Element Title: KLM Systems		
5. Task/Element Description: This WBS element entails the design, procurements, fabrication and assembly of new plastic scintillator modules for the two innermost layers (numbered 0 and 1) of the barrel KLM. This element will also develop software and firmware for the readout and high voltage systems. The modules will be fully assembled[1] and tested prior to shipping to KEK and acceptance tests performed on receipt at KEK.		

A. Technical Objective:

The objective of this WBS element is to

This WBS element will construct muon panels to replace the RPCs in the inner layers of the barrel portion of Belle. This element includes the design and specification of the scintillator panels, wave-length shifting fiber, power supplies and photodetectors, procurement of all components, assembly and integration of electronics from WBS 1.03, testing in the US, and shipment to KEK. Specification and procurement of high voltage systems for both KLM subsystems is also included in this element. This element includes simulation, software, and associated administration.

B. Assumption(s):

Major assumptions for this WBS include:

- Scintillator will be procured from Fermilab's Scintillator extrusion facility.
- Wave length fiber will be procured from Kuraruay.
- Scintillator mass: 23800 kg x 1.133 (FNAL wastage factor) = 27000 kg for Layers 0-14 (2700 kg for Layers 0-1)
- WLS fiber length: 57,000 m x 1.10 (ITEP wastage factor) = 62700 m for Layers 0-14 (6270 m for Layers 0-1)
- SiPM count: (55 x 15 + 800) x 2 x 8 = 26000 x 1.05 (VT wastage factor) = 27300 for Layers 0-14 (3200 for Layers 0-1)

C. Scope of Work Statement:

This WBS element involves the following activities:

<u>WBS 1.04.01 – Endcap KLM Detector</u>
This WBS element includes developing specifications for high voltage electronics based on prototype studies conducted to date and procuring the electronics. Procurement will be managed by

[1] This task relies on in-kind contribution of the component materials: scintillator strips, wavelength shifting fibers, photosensors, and HV supplies.

PNNL. Material will be received at VT and will be tested prior to shipment to KEK for assembly. Work scope is complete once electronics are received and accepted at KEK.

WBS 1.04.02 – Barrel KLM (Layers 0 and 1)

This WBS element includes the following:

- Design of the layout and mechanical structure for the scintillator detector modules in each of the two innermost layers (numbered 0 and 1) of the barrel KLM.
- Procurement of the component materials: scintillators, optical fibers, photosensors, signal cables and connectors, HV cables and connectors, HV electronics, and module frames. Upon delivery, apply QA/QC tests.
- Procure material and build/test prototype modules.
- Prepare a dedicated assembly area.
- Machine and assemble the frames that hold each module.
- Install optical fiber in each scintillator. Attach photosensor to optical fiber. Install scintillators in module. Install preamplifier board (WBS 1.3.0.3) in module. Attach module's exterior. Apply QA/QC to module.
- Arrange for international shipping permit with multiple shipments to KEK via land/sea. Place module in shipping container; when full, ship to KEK in Japan. At KEK, prepare a dedicated storage area for delivered modules. Apply QA/QC to modules.
- Development of simulation software.

D. Deliverables/Schedule:

Activity ID	Activity Name	Baseline Date	Milestone Level
1.5.1.5-250	L2 MS Complete Assembly of B-KLM Scintillator Modules	7/24/2013	Level 2
1.4.2.2-30	Complete Procurement of E-KLM HV Electronics	12/30/2011	Level 3
1.5.1.1-130	Complete Procurement of B-KLM Fibers	2/24/2012	Level 3
1.5.1.2-20	Issue RFP to Hamamatsu	8/6/2012	Level 3
1.5.1.3-060	Issue RFP to FNAL Scint Extrusion Facility	8/20/2012	Level 3
1.5.1.3-170	Complete Procurement of B-KLM Scintillator	11/16/2012	Level 3
1.5.1.7.2-30	Complete Procurement of B-KLM HV Electronics	1/7/2013	Level 3
1.5.1.2-80	Complete Procurement of B-KLM Photosensors	1/18/2013	Level 3
1.5.1.5-230	Complete Assembly of B-KLM Scintillator Modules	7/24/2013	Level 3

E. Relationships/Interfaces to Other WBS Elements:

Key inputs/outputs from/to other project WBS are as follows:

Inputs

Deliverable	Date Needed	From WBS
CD-3a (KLM)	4/21/2014	1.01
Pre-Amps From Hawaii	01/11/2013	1.03

Outputs

Deliverable	Date Completed	To WBS
E-KLM HV Electronics Arrive at KEK	3/21/2014	2.05
B-KLM HV Electronics Arrive at KEK	3/21/2014	2.05
KLM Modules Received at KEK	09/30/2013	2.05

E.5 Work Breakdown Structure Dictionary – WBS 1.05

1. Project Title: Belle-II	**2. WBS Element No.** 1.05	**3. WBS Owner:** Sven Vahsen
4. WBS Element Title: Commissioning Detectors		
5. Task/Element Description: This WBS element provides micro-Time Projection Chamber (micro-TPC) detectors for monitoring rates and radiation levels in the Belle II detector volume during SuperKEKB commissioning prior to installation of the inner detectors for Belle II. This task includes the design and prototyping, gas system, support structure, electronics, testing, software and associated administration.		

A. Technical Objective:

The objective of this WBS element is to

This WBS element will install the commissioning detector system for Belle II in place of the inner detector systems (silicon, drift chamber and iTOP) during initial accelerator commissioning to measure the particle rates in the detector space. This system will need to operate in the harsh environment anticipated during bake-out of the beam vacuum system and is vital for ensuring that the electromagnetic calorimeter is not damaged during beam commissioning. This task includes the design, fabrication, and delivery of the support structure and micro time projection chambers (micro-TPCs) that will monitor charged particle and neutron rates. This task includes the electronics and data acquisition system required for the micro-TPCs. Equipment will undergo acceptance tests on receipt at KEK. Installation and commissioning with the beams will occur during operations and is not included in this WBS.

B. Assumption(s):

Major assumptions for this WBS include:

- Design is funded off-project utilizing combination of funding sources.
- US project will design the calorimeter shielding. KEK will provide the material and construct.
- Berkeley National Lab will provide FE-I4 chips prior to TPC prototyping.
- SLAC will deliver Reconfigurable Cluster Element (RCE) Pixel DAQ System.

C. Scope of Work Statement:

This WBS element involves the following activities:

<u>WBS 1.05.01 – Commissioning Detector Design</u>
This WBS element includes design of the support structure for the entire commissioning system, calorimeter shielding, micro TPCs, readout electronics and data acquisition system for the micro

TPCs and readout diodes and development of the placement locations for the subsystems on the support structure.

WBS 1.05.02 – Micro TPC Prototyping
This WBS element includes constructing two prototype micro TPCs with readout electronics and data acquisition system for testing with radioactive sources and beams. In addition, a prototype diode readout system circuit will be developed and tested through irradiation studies.

WBS 1.05.03 – Fabrication / Construction
This WBS element includes fabrication and assembly of the support structure, micro TPCs and Diode readout system. Support structure will be assembled, tested, and disassembled and shipped to KEK. Materials for the TPCs will be procured, assembled and tested. The TPCs will be mounted to the support structure for verification and removal prior to shipment to KEK. Circuit boards and components for the Diodes will be procured, assembled and tested prior to shipment to KEK.

WBS 1.05.04 – TPC Acceptance Testing
The primary elements of work of this WBS element are to develop test plans and conduct testing of the commissioning detector after it has been shipped and received at KEK. Planned tests consist of testing the pixel electronics, inspection and other quality testing of the TPCs.

D. Deliverables/Schedule:

Activity ID	Activity Name	Baseline Date	Milestone Level
1.7.1.3-50	L2 MS Complete Commissioning Detector Design	5/24/2013	Level 2
1.7.3-100	L2 MS Commissioning Detector TPCs to KEK	12/31/2014	Level 2
1.7.1.3-20	Finalize Choice of Pixel Chip	1/25/2013	Level 3
1.7.1.2-30	Complete Commissioning Detector Support Structure Design	5/24/2013	Level 3
1.7.2.1-40	Complete Commissioning Detector TPC Readout Electronics Prototype	7/26/2013	Level 3
1.7.2-80	Complete Testing of Commissioning Detector TPC Prototype	5/1/2014	Level 3
1.7.3-90	Complete Fabrication/Construction Commissioning Detector TPCs	10/29/2014	Level 3
1.7.3-120	Support Structure, TPCs, All Needed Supports Arrive at KEK	11/13/2014	Level 3
1.7.3-140	TPCs and Support Systems (HV, LV, Gas) Arrive at KEK	11/13/2014	Level 3
1.2.6-370	Complete TPC Testing	12/05/2014	Level 3

E. Relationships/Interfaces to Other WBS Elements:

Key inputs/outputs from/to other project WBS are as follows:

Inputs

Deliverable	Date Needed	From WBS
CD-2/3	10/13/2013	1.01
Demonstration of Neutron Detection with Pixel TPC	11/2012	Off Project
SLAC Deliver Reconfigurable Cluster Element (RCE) Pixel DAQ System	09/01/2012	Off Project

Outputs

Deliverable	Date Completed	To WBS
TPCs and Support Systems (HV, LV, Gas) Shipped to KEK	7/24/2014	2.06
Complete TPC testing	7/1/2014	2.06